SIMULATION OF CHLORIDE TRANSPORT IN CONCRETE WITH STRESS INDUCED DAMAGE

BY

WALID ABUBAKER SALEM AL-KUTTI

A Dissertation Presented to the

DEANSHIP OF GRADUATE STUDIES

KING FAHD UNIVERSITY OF PETROLEUM & MINERALS

DHAHRAN, SAUDI ARABIA

In Partial Fulfillment of the

Requirements for the Degree of

DOCTOR OF PHILOSOPHY

In

CIVIL ENGINEERING

JUNE 2011

KING FAHD UNIVERSITY OF PETROLEUM AND MINERALS

DHAHRAN 31261, SAUDI ARABIA

DEANSHIP OF GRADUATE STUDIES

This dissertation, written by **WALID ABUBAKER SALEM AL-KUTTI** under the direction of his thesis advisor and approval by his thesis committee, has been presented to and accepted by the Dean of Graduate Studies, in the partial fulfillment of the requirement for the degree **OF DOCTOR OF PHILOSOPHY IN CIVIL ENGINEERING.**

Dissertation Committee

Dr. Mohammed H. Baluch
Dissertation Advisor

Dr. Muhammad K. Rahman
Dissertation Co-Advisor

Dr. Mohammed A. Shazali
Member

Dr. Omar S. B. Al-Amoudi
Member

Dr. Ali H. Al-Gadhib
Member

13 JUN 2011

Dr. Nedal T. Al-Ratrout
Chairman, Civil Engineering

Dr. Salam A. Zummo
Dean of Graduate Studies

عمادة الدراسات العليا
DEANSHIP OF GRADUATE STUDIES

Date: 15/6/11

In the Name of Allah, Most Gracious, Most Merciful

Dedication

To:

My beloved parents, wife and children

For their love, sacrifices and prayers

ACKNOWLEGEMENTS

All praises and thanks are due to Allah (subhanaho wa taala) for bestowing me with health, knowledge and patience to complete this work. May the peace and blessings of Allah be upon Prophet Muhammad (PBUH), his family, and his companions. Thereafter, acknowledgement is due to KFUPM and the Deanship of Scientific Research for support under the FT090004 project and for providing me the opportunity to pursue PhD studies with financial support.

I acknowledge, with deep gratitude and appreciation the guidance give to me by my committee chairman, Dr. Mohammed H. Baluch, special thanks are due to my committee co-chairman, Dr. Muhammad K. Rahman and for the committee member Dr. Mohammed A. Shazali, who took care and showed great interest in the work by assisting and giving constructive comments with patients. Special thanks are extended to the committee members, Dr. Omar B. Al-Amoudi and Dr. Ali H. Al-Gadhib for their valuable comments to improve my work.

Special thanks are due to Eng. Omer Ahmed in the department of civil engineering, Center of Engineering Research, and extended to industrial companies, PRAINSA and Saudi Ready-Mix for supplying materials and the assistance in conducting the experimental program.

TABLE OF CONTENTS

LIST OF TABLES

LIST OF FIGURES

DISSERTATION ABSTRACT

Full name : **Walid Abubaker Salem Al-Kutti**

Title of study : **Simulation of Chloride Transport in Concrete with Stress Induced Damage**

Major Field : **Civil Engineering**

Date of degree : **June 2011**

Durability of reinforced concrete structures in Arabian Gulf region is a major problem which results from corrosion of the reinforcement occurring as a consequence of chloride transport in concrete. Although chloride-induced corrosion is directly influenced by the chloride diffusivity property of the concrete, the diffusivity itself is affected by a number of other factors like mix parameters, stress level leading to damage, moisture content, chloride binding capacity and ambient temperature. There is a need to simulate the chloride transport in concrete with regard to the coupled impact of stress level leading to damage, binding capacity and the effect of crack widths which reflects the actual mechanism of chloride transport in concrete structures.

This research presents experimental and numerical results using COMSOL multi-physics finite element model used to simulate the chloride transport in damaged concrete samples. The electrochemical transport of chloride in concrete was evaluated using NT BULD 492 test for chloride migration in concrete subjected to different levels of compressive-induced damage. Besides, eight reinforced concrete beams of 1200 mm span were subjected to 40%, 60% 75% and 90 % of its ultimate flexural strength and loaded back to back using steel frames and subjected to 8% of NaCl solution for three months to simulate the coupled problem of chloride diffusion and mechanical loads leads to induced damage.

It was found that there is a significant increase in the chloride diffusivity with the increase of tensile stress in the RC beams subjected to flexural loading and a good correlation was established between effective chloride diffusion coefficient and the level of the damage in RC beams. A crack influencing function F_w was developed to correlate the crack width (w) and the ratio of chloride diffusion coefficient in the crack D_{cr} to the chloride diffusion coefficients in sound concrete D_o and two configuration were used in the RC beams which matches consistently the chloride diffusion: the first one when the diffusion relates as a function of distributed damage and second one when it is govern by the crack width. Finite Element model using COMSOL was matching well the experimental results of the mechanical behavior as well as the transport of the chloride in damaged RC beams.

ملخص بحث
درجة الدكتوراه في الفلسفة

الأسم : وليد أبوبكر سالم القطي
عنوان الرسالة : محاكاة انتقال الكلوريدات الى الخرسانة المعرضة للأجهادات المسببه للضرر
التخصص: الهندسة المدنية
تاريخ التخرج : مايو 2011

تعتبر ديمومة المنشاءات الخرسانية المسلحة مشكلة رئيسية في منطقة الخليج العربي والناتجة من صدأ حديد التسليح نتيجة نفاذية أملاح الكلوريدات للخرسانة. بالرغم من أن صدأ حديد التسليح يتأثر مباشرة بخواص النفاذية للكوريدات في الخرسانة, فان خواص النفاذية نفسها تأتأثر بعدد من العوامل مثل محددات الخلطة الخرسانية, مستوى الأجهادات الميكانية المؤدية للضرر,محتوى الرطوبة, المقدرة على استيعاب الكلوريدات ودرجة الحرارة المحيطة. هناك حاجة لنمذجة نفاذية الكلوريدات في الخرسانة مع الأخذ بالأعتبار اثرمستوى الأجهادات الميكانيكة الموذية للضرر مترابطا مع قابلية استيعاب الكلوريدات وكذلك عرض شرخ الخرسانة والتي تعكس مجتمعة الطريقة الفعلية لنفاذية الكلوريدات في تالمنشئات الخرسانية.

يعرض هذا البحث دراسة معملية وعددية باستخدام برنامج COMSOL بطريقة العناصر المحددة لنمذجة نفااذية الكلوريدات في الخرسانة المتضررة. تم تقييم نفاذية الخرسانة المنتقلة بالطريقة الكيموكهربائية باستخدام الأختبار القياسي NT BULD 492 للخرسانة المعرضة للضرر عن طريقة مستويات مختلفة من اجهادات الضغط المحورية. بالأضافة, تم استخدام ثمانية عينات من جسور الخرسانة المسلحة وبحر مقداره 1200 مليمتر لتقييم نفاذية الكلوريدات في الخرسانة المسلحة. تم تعريض الجسور لاحمال بنسب 40% , 60%, 75% و 90% من كامل مقاومتها القصوى للأنحناء. بعد ذلك تم تحميل الجسور باستخدام قطاعات حديدة وتعريضها لمحلول كلوريدات الصوديوم وبنسبة 8% ولمدة تسعون يوما وذلك لنمذجة نفاذية الكلوريدات في الخرسانة مع الأخذ بالأعتبار اثرمستوى الأجهادات الميكانيكة الموذية للضرر مترابطا مع قابلية استيعاب الكلوريدات وكذلك عرض شرخ الخرسانة والتي تعكس مجتمعة الطريقة الفعلية لنفاذية الكلوريدات في تالمنشئات الخرسانية.

لوحظ ان هناك زيادة مقدرة لنفاذية الكلوريدات في الجسور الخرسانية المعرضة لاجهادات الشد الميكانيكية , وتم تطوير علاقة احصائية لمعامل النفاذية للكلوريدات في الخرسانة مع معامل الضرر الميكانيكي. بالأضافة لذلك, تم تطوير علاقة احصائية بين عرض الشرخ في الخرسانة مع معامل النفاذية في الخرسانة المعرضة للشروخ الكبيرة. تم تقسيم الجسر الخرساني الى منطقتين: أحداهما يقع تحت تأثير معامل الضرر الميكانيكي والثانية تقع تحت تأثير عرض الشرخ الخرساني. تم مقارنة نتائج النمذجة العددية مع النتائج المعملية ووجد تطابق ممتاز بين النذجة العددية والأختبارات المعملية.

CHAPTER 1

INTRODUCTION

1.1 General

Durability of concrete is a major concern in reinforced concrete structures in the Arabian Gulf region. During the service life of a reinforced concrete structure, several external and internal factors play major roles in the reduction of the service life of the structures. Wearing due to traffic loading, chemical reactions, weathering, sulfate attacks and penetration of salts tend to reduce the structure's durability.

Among the above causes of the deterioration of concrete structures, the reinforcement corrosion is a major problem in many parts of the world. In the Arabian Gulf region, the climate is characterized by high temperature and humidity. Further, there are large fluctuations in the diurnal and seasonal temperature and humidity. The temperature can vary by as much as 20 ºC during a summer day and the relative humidity ranges from 40 to 100% over 24 hours. These sudden and continuous variations in temperature and humidity initiate cycles of expansion/contraction and hydration/dehydration, which result in cracking of concrete (Baluch et al., 2002). The damage to concrete due to these cycles is reflected by micro-cracking and enhanced permeability, which results in an increase in the diffusion of chloride, oxygen, carbon dioxide and moisture, into concrete. Moreover,

concrete construction in the coastal areas of the Arabian Gulf and the Red Sea is exposed to ground and atmosphere contaminated with salts. Aided by capillary action and high humidity conditions, the salt-contaminated groundwater and the salt-laden airborne moisture and dew find an easy ingress into the concrete matrix causing severe corrosion of reinforcing steel.

For the several decades over which concrete material has been in existence, a vast array of reinforced concrete infrastructures has been constructed, much of which remains to this day. At the present rate, it is estimated that about two billion tons of reinforced concrete, representing about 1500 square kilometer, is being built each year (Alexander,2003). However, material deterioration significantly affects the performance of reinforced concrete constructed facilities and systems. Decay and deterioration of concrete constructed infrastructures directly affect on everyday life in terms of safety and economy. Of the massive tonnages of concrete produced around the world each year, a significant fraction is increasingly being used for repair and rehabilitation rather than for new construction. Rehabilitation is a highly labor-intensive and time-consuming process, and it imposes a substantial economic burden on society.

The study of concrete durability or its resistance to deterioration is, however, considerably complex. Deterioration of concrete under combined environmental and mechanical loading involves different mechanisms acting over a broad range of scales, from the nanometer to the meter level. Research in this field requires an interdisciplinary approach

based on qualitative understanding of both governing microscopic chemo-physical processes and coupling with the macroscopic observable materials behavior.

A good resolution would require a holistic approach relating transport and strength to durability. Holistic modeling of deterioration of concrete requires sound scientific knowledge based on physical chemistry, material sciences, and mechanics of the constituent concrete materials as well as knowledge of the concrete built environment in addition to experimental research.

According to the ACI Committee 201 on Durability of Concrete (ACI.2R-01, 2001), durability of concrete is defined as "its ability to resist weathering action, chemical attack, abrasion, or any other process of deterioration". Serviceability is viewed as the capacity of the above to perform the function(s) for which they are designed and constructed." The latter definition particularly made a subtle distinction with service life, defined as the "period of time after installation during which all properties exceed the minimum acceptable values when routinely maintained."

Regardless of the aforementioned definitions, it is understood that all "durable" concrete should maintain its original form, quality, and serviceability when exposed to the deleterious action of the elements. Possible significant deterioration processes for concrete structures include ingress of chlorides, sulfates attack, carbonation process, wetting/drying cycles, stress corrosion, and rebar corrosion, alkali-aggregate reactions, concrete leaching, and salt crystallization, among others. The influence of environmental

factors on exacerbating the various deterioration mechanisms occurring in concrete with discontinuous microcracks will cause the microcracks to propagate until they become continuous and subsequent increase in transport properties are responsible for increased rate of damage. Thereafter, crack growth, which depends on the concrete fracture strength, accelerates the penetration of the deleterious substances involved into the concrete and thereby the spiral of deterioration continues downwards.

A detail of a holistic approach to modeling inherent synergism of factors involved in concrete deterioration has been expounded (Basheer et al., 1984). The mutual synergism or interdependence of all these factors and the importance of transport properties and strength is included (Long et al., 2000).

For nearly all the physico-chemically induced processes affecting concrete durability, two parameters that play dominant roles are transport and strength or mechanical properties. It shows that the chemical influence of transport mechanisms on transport properties has a direct link to influence of stresses arising from mechanical loadings on strength properties of the concrete.

It is obvious that the durability of field concrete is greatly dictated by the synergism that dynamically subsists between its material (transport and mechanical) properties and the exposure environment. It becomes of vital importance to consider this mutual interdependence when field concrete is assessed to predict its service life.

Thus, against the commonly held view that concrete is a durable and maintenance-free construction material, there is now a distinct realization of the challenge posed by degradation mechanisms induced by the time variant environmental and mechanical loading processes. In order to predict or model the durability of concrete, accurate information must be obtained on the condition of the concrete and these major environmental stressors and degradation factors. Adequate account must be taken of the synergetic influence of such discrete chemo-mechanical agents, which when collectively taken considerably cause concrete durability level to be lower than expected, with the total effect being greater than the sum of the effects of the individual factors (Saetta et al., 1998). Although the holistic model for an integrated approach to evaluating concrete durability in complete synergy with its built environment is becoming well recognized, the complexity of tackling transport phenomena in concrete is ever presenting a great challenge to achieving it.

1.2 Need for the Research

Chloride-induced corrosion is one of the major causes affecting the corrosion of reinforcement in concrete. In the Arabian Gulf region, the hot and arid environment has resulted in premature deterioration of concrete structures, requiring extensive repairs. It is estimated that repair and maintenance of concrete structures in Saudi Arabia would run into billions in the coming few decades (Rasheeduzzafar et.al, 1990). Therefore, the resistance to the chloride ion penetration into concrete is one of the most important properties of concrete and becomes more important in the design and construction of concrete structures exposed to chloride-bearing exposures.

The main parameters affecting the chloride diffusivity of undamaged concrete including mix parameters, moisture contents and environment conditions in concrete have been investigated in many researches. This approach is used to evaluate the chloride transport properties of undamaged concrete but it could not be used for cracked or damaged concrete because, in undamaged concrete transport properties is related to the porosity, while in damaged concrete it is related to the cracks . Therefore, no prediction on the behavior of damaged concrete can be made based on the data for undamaged concrete and there is a need to study the chloride transport in concrete with stress-induced damage.

Moreover, chloride binding isotherms which describe the relationship between free and bound chloride needs to be established to estimate the chloride binding capacity in locally produced concrete. A major feature of this research is that the coupled problem of chloride transport and stress related damage due to mechanical loading was simulated using multiphysics finite element models. This model could be used for predicting the service life of concrete structures.

1.3 Objectives and Scope

The primary objective of this study was to investigate the chloride diffusion in ordinary Portland concretes samples subjected to different mechanical loading levels leading to damage.

The specific scopes of this study objective are as follows:

1- To investigate the effect of mechanical damage levels on the transport of chloride in concrete specimens.

2- To develop chloride binding isotherms that describe the relationship between the free and bound chloride for locally produced concrete.

3- To investigate the effect of crack width on chloride diffusivity in concrete.

4- To develop multiphysics finite element model for prediction of chloride diffusion in damaged concrete using two models:

- Damage Mechanics.
- Diffusion of Chloride.

1.4 Dissertation Organization

Chapter 1 presents a brief introduction on durability problems in concrete structures and the ongoing research regarding coupling between environmental and mechanical loads with the transport properties on concrete. Need for the research and the objective were presented in this chapter.

In Chapter 2, a comprehensive literature survey is presented on chloride induced corrosion, mechanism of chloride transport in concrete, the modeling of chloride diffusivity in concrete and the use of electrochemical migration test on evaluation of chloride transport in concrete. Mathematical modeling of the diffusivity using Fick's second law and the migration modeling using Nernst–Planck equation is presented in this chapter. All related influencing factors on chloride diffusivity such as the chloride binding

capacity isotherms, the influence of the mechanical damage on the transport of the chloride in concrete are presented. Moreover, literature review on research conducted to correlate the chloride migration test and the salt ponding test and numerical simulation techniques for the simulation of the chloride transport coupled with mechanical loading leading to damage is noted.

Chapter 3 describes the modeling and the assumptions used for this present study. Two approaches are presented to describe the transport of chloride into concrete subjected to stress-induced damage. First, chloride diffusion problem using Fick's law coupled with two influence functions used in this study which are: (a) the chloride binding and (b) the mechanical damage influencing functions. Second, chloride migration problem using Nernst-Planck equation coupled with same influence functions is presented. Besides, phenomenological continuum damage mechanics is presented to describe the scalar damage parameter to be used to model cracking effects that are induced due to the mechanical loads.

Chapter 4 contains a description of the experimental works and the deferent experimental procedure carried out in this study, The tested specimens consists of reinforced concrete beams (RC beams) and concrete cylinders both of which were subjected to different levels of mechanical loading leading to damage. Details of material parameters used in this study, testing procedures and specifications are discussed in this chapter.

The experimental results and the COMSOL numerical simulation of chloride migration in concrete subjected to compressive stress-induced damage are presented in Chapter 5. This

chapter describes the results of the experimental works; the results are presented in figures and tables, followed by discussion. Discussed in particular are measured chloride profiles obtained from experimental results, chloride migration coefficient estimated from measured chloride profile for damaged and undamaged concrete.

In Chapter 6, experiential results and finite element analysis of chloride diffusion in reinforced concrete beams coupled with flexure damage and chloride binding capacity are presented. Calibration of the finite element model with the experimental data obtained from test results and parametric studies is presented.

Chapter 7 gives the conclusions and recommendations for further study.

CHAPTER 2

LITERATURE REVIEW

2.1 Introduction

Concrete has once been considered as a maintenance-free material and sound enough to resist all weather and exposure conditions. Unfortunately, this assumption has been proven to be untrue when durability problems were reported from many parts of the world. The Arabian Gulf region, as a typical example, is faced with major concrete durability problems caused by one or a combination of many factors: its adverse climate, concentrated salt-laden ground and atmosphere, poor quality of aggregates available in this region and the adverse geomorphic and exposure conditions [Rasheeduzzafar et.al, (1989), Al-Amoudi et.al, (1992)].

Many researchers studied the durability problems in the Arabian Gulf in the last three decades. Al-Gahtani, (1981) conducted condition surveys accompanied by comprehensive recordings and photographic documentation on 42 framed reinforced structures 15 to 20 years old located in the Eastern Province of Saudi Arabia and showed that the main causal factors for concrete deterioration, in decreasing order of importance, are the following:

1. Reinforcement corrosion;
2. Sulfate attack and salt weathering; and
3. Cracking due to environmental factors.

Although concrete deterioration due to other factors, namely alkali-silica reactivity and carbonation, may occur, the nature of the distresses due to the above three factors, reinforcement corrosion in particular, is very large. Field and laboratory studies have confirmed that the major cause of concrete deterioration, cracking and spalling in this region is the corrosion of reinforcing steel bars (Saricimen, 1993).

Corrosion of reinforcement may occur if the following components surround the reinforcing steel: moisture, oxygen and chloride ions. Once reinforcement corrosion is initiated, the passive film formed on the surface of rebar, due to high alkalinity of concrete pore solution (pH > 13), is destroyed or disrupted either by the ingress of chloride ions to the steel surface or by carbonation. Once the passive film is destroyed, active corrosion takes place ultimately leading to the formation of hydrated red rust on the surface of the rebar. Corrosion of reinforcing steel has the following two major detrimental effects on the durability of reinforced concrete structures:

1. Since the red rust produced as a result of corrosion has a volume 2 to 8 times than that of steel (Mehta, 1986), it causes volume expansion thereby developing tensile stresses of the order of 27.5 MPa, which is about 10 times the tensile strength of normal concrete, thereby causing cracking and spalling of the cover concrete. Due to the loss of cover

concrete, there may be a significant reduction in the load-carrying capacity of the structure and, besides this; steel may be more accessible to the aggressive agents leading to further corrosion at an accelerated rate.

2. Corrosion ultimately reduces the cross-section of the steel bars and thereby endangering the load-carrying capacity of the structure. Pitting (i.e., localized) corrosion of the rebar is more dangerous than uniform corrosion because it progressively reduces the cross-sectional area of the rebar to a point where the rebar can no longer withstand the applied load leading to a catastrophic failure of the structure.

In the Arabian Gulf, the service life of the concrete structures is found to be very short, mainly due to reinforcement corrosion caused by the chloride ingress in concrete and exposure to the harsh environmental conditions that are highly conducive to corrosion. The major cause of chloride-induced reinforcement corrosion is the presence of chloride ions at the concrete-steel interface.

There are various reasons to the presence of chloride in concrete. Chloride can be incorporated into concrete either by the use of contaminated ingredients of concrete like aggregate and water or by the penetration of the chloride ions from the surrounding aggressive environment causing presence of chloride in concrete in the form of (Yunping and Nakhi, 2005):

- Free chloride ions dissolved in the pore solution;

- Bound chloride either chemically combined with the hydration compound of the cement or physically absorbed on cement gel.

2.2 Chloride Induced Corrosion

The performance of concrete structures in chloride-invaded environments, such as seawater where also a maze of interwoven mechanisms or deterioration synergies are at work, is of great importance. The importance of chloride ions to concrete durability is reflected in the tremendous amount of literature devoted to its study in terms of its role in inducing corrosion of reinforcing steel in concrete.

In Portland cement concrete, the presence of abundant amount of calcium hydroxide (portlandite) and relatively small amount of alkali elements such as sodium and potassium, gives concrete a very high alkalinity of pH in the range 13 to 14. It is widely accepted that at the early age of the reinforced concrete, this high alkalinity results in the transformation of a surface layer of the embedded steel to a tightly adhering film and as long as this film remains passive and is not disturbed, it will keep the steel passive and protected from active corrosion.

A concrete structure is often exposed to chloride sources comprising deicing salts, salt splashes, slat spray, seawater, or chloride contaminated concrete making constituents. The amount of salt introduced by mixing and curing waters may be generally small, but in arid areas where amount of desalinated water is scarce, concrete is often mixed and cured with brackish water. Chloride ions from external sources will slowly penetrate into the concrete through the pores of the hydrated cement paste in the concrete and will

eventually reach the steel. When the penetrated chloride ions at the face of the steel accumulates beyond a certain threshold concentration level, the protective film is destroyed leaving the steel to corrode in as much as oxygen and moisture are present at the steel-concrete interface. In this regard, chloride ions have been identified as the unique and specific destroyer of passivity of the reinforcing steel (Rasheeduzzafar et.al, 1991).

In most diffusion-based studies, only the effect of chloride ions on the initiation period has often been considered. This is reasonable if rapid corrosion is assumed following the end of the initiation period. Nonetheless, the general approach in service life modeling associated with reinforcement corrosion has been with focus on two strategies as reported by Tuutti, (1982) and shown in Figure 2.1. These are namely: (i) the initiation stage when considering the design life of new structures in order to ensure the longest possible service period before steel depassivates, and (ii) the propagation stage when assessing residual service life of existing structures, whose reinforcing steel may already have depassivated, in order to evaluate different strategies for maintenance, repair or even replacement. For chloride-induced corrosion, the length of the initiation period depends on the rate of penetration of chloride ions in the concrete, the depth of the concrete cover, and by the threshold concentration required to jump-start the corrosion process.

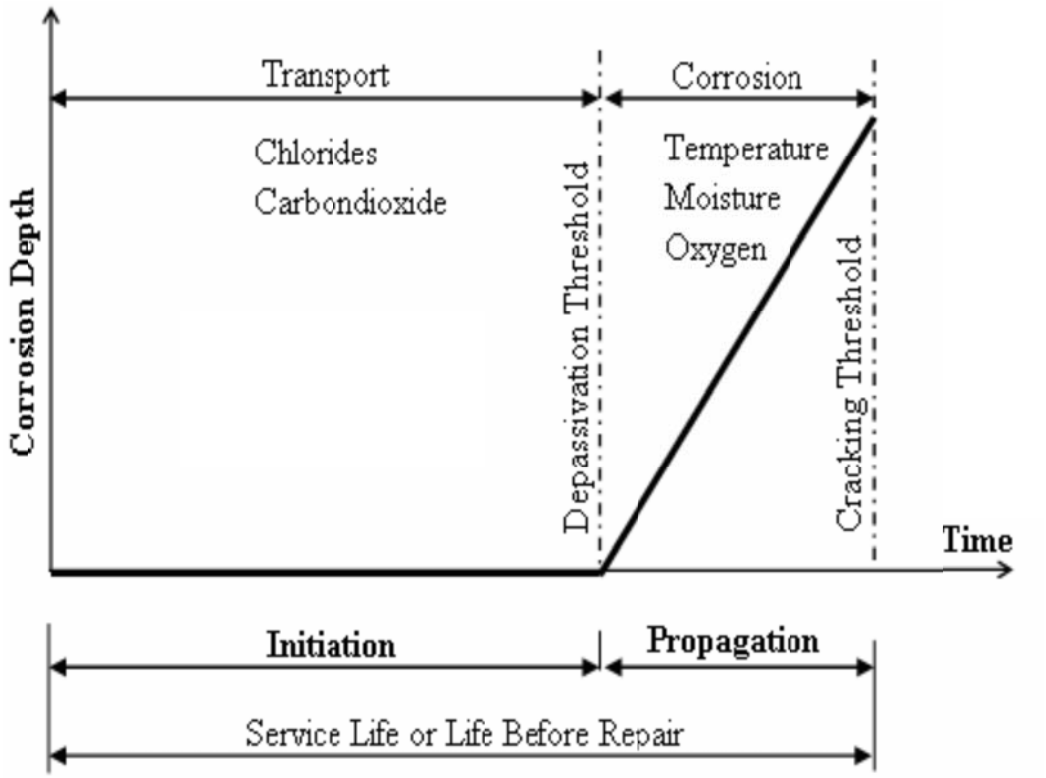

Figure 2.1: Conceptual corrosion sequence in concrete (Tuutti, 1982).

2.3 Mechanisms of Chloride Transport into Concrete

Figure 2.2 shows different chloride transport mechanism according to the surrounding conditions. In saturated concrete and with some limitation, it can be assumed that the main transport mechanism for the penetration of the chloride is the diffusion, while the capillary suction driving force could be ignored and this usually occurred for marine structures (Raharinaivo et.al 1986). While for partially submerged or saturated concrete structures, the chlorides are absorbed into the unfilled pores and the capillary suction is the main transport mechanism and this is usually happened when the structure is subjected to cycles of drying and wetting. Concrete transport properties play a key role in the concrete durability aspect. Increasing deleterious fluid and/or gas transportation inside concrete would result in an accelerated deterioration of the concrete structures. Chlorides can usually move inside concrete mainly by one or the combination of the following transport mechanisms:

2.3.1 Permeability of Chloride into Concrete

The permeability of chloride into concrete is the transport process in which the chloride ions are drawn into the concrete under the hydrostatic head. Its relevance to concrete structure in service is limited to such cases where the element is under a hydrostatic head, such as ground water flow. For a marine structure, this condition most commonly occurs in sections of structures submerged in seawater (Richardson 2002). Permeability can be defined as the ease through which fluids or gases flow through concrete. The higher the

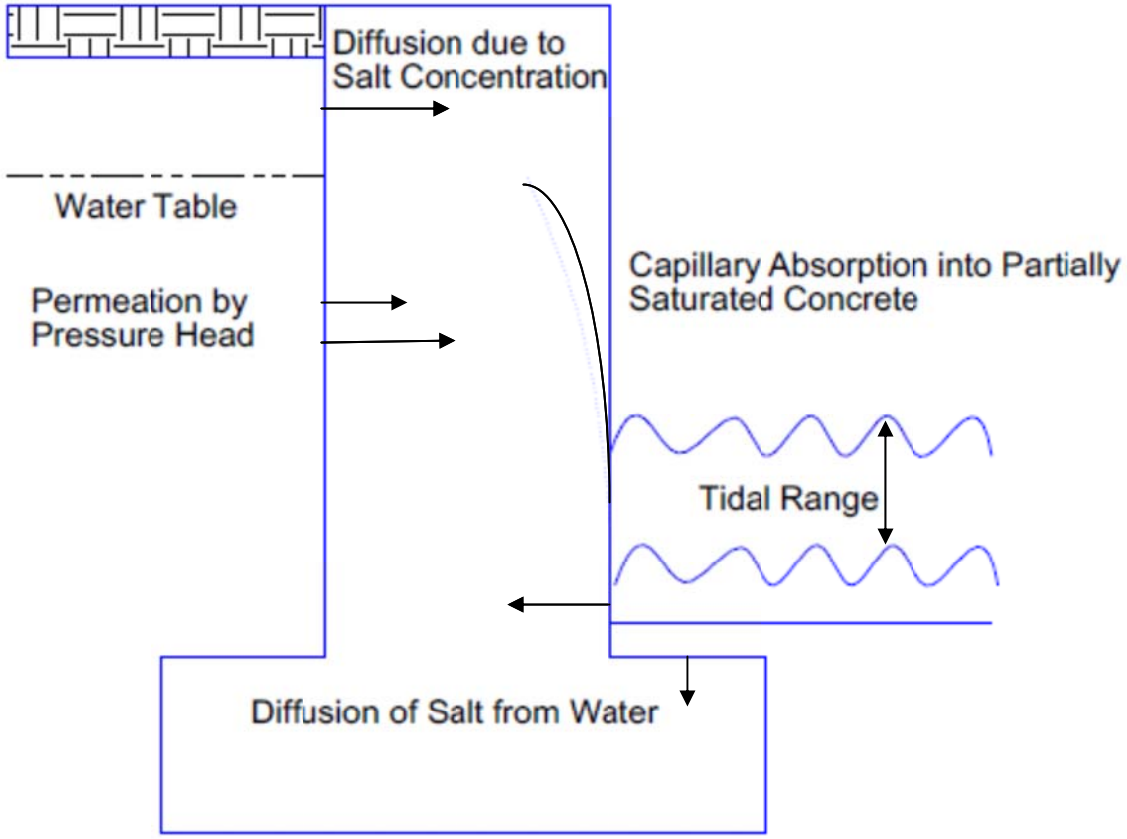

Figure 2.2: Mechanisms of chloride transport into concrete (Concrete Society, 1996).

permeability of the concrete, the less durable the structure would be. The concrete coefficient of permeability can be found experimentally by Darcy's law (Neville, 1995).

2.3.2 Capillary Suction of Chloride into Concrete

Capillary suction is a process in which fluid or chloride containing water is taken into the concrete pores due to surface tension acting in capillaries. For all concrete elements that may be dried out to some extent in the near surface regions, the ingress of chlorides into the concrete is supported by capillary absorption of the seawater upon direct contact (Kropp 1995). Capillary suction can take place only in partially dry concrete, so this mechanism will not be taken place in completely dry or in fully saturated concrete (Neville 1995).

Capillary suction may be significant in concrete structure subjected to alternating wetting and drying cycles. The extent of absorbed chloride depends on the length of the wetting and drying period, as the degree of drying between the individual period increases so does the chloride absorption (Kropp 1995). During wetting period, the near surface concrete layer readily absorbs the chloride solution. During the drying period, the water will evaporate and the salt remains in the pore system of the near surface region. The next cycle of wetting will bring more chloride present in solution into the capillary pores. Depending on the relative humidity and duration of the drying period, it is possible for most of the water in the outer zone of the concrete to evaporate so that water remaining in the interior will become saturated with salt. Thus, repeated wetting and drying cycles

increase the salt concentration in the pore system, which may become even higher than the concentration of the chloride solution at the surface. (Kropp, 1995; Neville 1995).

2.3.3 Diffusivity of Chloride into Concrete

Diffusion occurs when there is a concentration difference. Diffusion of chloride ions into concrete takes place when the concentration of chloride ions in the external environment is higher than the concentration of chloride ions in the pores of concrete. It is this difference in concentration that provides the driving force for the diffusion. Chlorides can only diffuse as ions in the solution.

Thus, the penetration of chloride into concrete can take place only through the pore water solution within the concrete. It is in the pore water that reactions with hydrated cement paste take place, so chloride diffusion sometimes also refers as ionic diffusion. In this diffusion process, the degree of pore saturation in concrete pores plays an important role; the ionic diffusion is most effective when concrete is under saturated condition, although it can also take place when the concrete is partially saturated.

Diffusion is usually described by Fick's second law of diffusion equation [2.1] and in certain conditions can be represented by the error function solution of Crank (1975):

$$\frac{\partial(\theta C)}{\partial t} = \frac{\partial}{\partial x}\left\{D_C \frac{\partial(\theta C)}{\partial x}\right\} + \frac{\partial}{\partial y}\left\{D_C \frac{\partial(\theta C)}{\partial y}\right\} + Q_C \qquad [2.1]$$

in which C is the free chloride content in g of chloride per g of concrete; θ is the volumetric moisture content in mm^3 of solution per mm^3 of concrete; t is the time in second; D_C is the chloride diffusivity in mm^2/s; x, y are Cartesian coordinates at a particular point in the concrete; and Q_C is the rate of internal chloride evolution function per unit area of the concrete.

When concrete is saturated ($\partial\theta = \theta_{sat}$ = constant) and chloride binding and other effects embodied by the internal chloride evolution function are neglected ($Q_C = 0$), then the one-dimensional form of equation [2.1] will reduce to the commonly written Fick's Law:

$$\frac{\partial C}{\partial t} = \frac{\partial}{\partial x}\left\{D_C \frac{\partial C}{\partial x}\right\} \qquad [2.2]$$

Equation [2.2] can be solved if an initial and two boundary conditions are known for the following initial condition C (x > 0, t = 0) = 0 and boundary condition C(x = 0, t > 0) = Cs, a close-form solution of Equation [2.2] for a semi-infinite medium (i.e. from x = 0 to x = L) was obtained by Crank (1975) as:

$$C(x.t) = Cs\left[1 - erf\left(\frac{x}{\sqrt{4D_C t}}\right)\right] \qquad [2.3]$$

Where $C(x,t)$ is the concentration of free chlorides at depth x after time t, Cs is the chloride concentration at the surface x=0; and erf( ) is the error function of the embraced argument. This solution is only valid when both the diffusion coefficient D_C and the

surface concentration *Cs* are assumed constant in space and time. However, this is a simplification since it is known that D_C varies with space and time due to variation in concentration of the chloride itself, temperature, moisture, concrete quality, and exposure conditions. To find the chloride diffusivity in concrete, the salt ponding test (also called natural diffusion test) is used.

Several investigations on the parameters affecting the chloride diffusivity were conducted in the last three decades (Andrade, 1993; Antoni, 2003; Azad, 1997 and Dhir, 1994). These parameters vary from mix ingredients, porosity, and degree of hydration, aggregate size, temperature, humidity and local chloride concentration.

It is well known that binder type and w/c ratio significantly affect chloride transport due to their effect on pore structure. Bentz et al. (1996) and Bamforth (1999) showed that the diffusion coefficient *D* for the concrete with w/c = 0.66 was about one order greater than the D with w/c = 0.40. Same conclusions were noted by Azad et al. (1997).

Christenen (1979) developed a composite model for diffusivity based on a three-phase model depends on the volume fraction of aggregates; the transition zone and the cement paste and he reported that the effective diffusivity of concrete is increasing with the volume fraction of aggregate. The same conclusion was reported by Winslow et.al, (1994), in addition to the composition effect, the interface transition zone (ITZ) between the aggregate and the surrounding cement paste has been considered to be very important

for all kinds of properties of concrete. The ITZ has a higher porosity and, thus, a higher diffusivity than the bulk cement paste.

Experimental results presented by Sujata et al. (1996) and Neubauer et al. (1997) showed that the thickness of high porosity zone or ITZ varies randomly around the perimeters of aggregates and it depends on the aggregate size, average spacing between aggregates and surface condition of aggregate particles.

The reduction in chloride diffusion in silica fume and fly ash concretes over normal concrete has been reported by several researchers. Maage (1996) has reported that the chloride diffusion coefficients of silica fume cement concrete were less than that of normal concrete. Chloride diffusion tests conducted by Byfors (1987) on 10 and 20 % microsilica cements showed that the chloride diffusion of these cements to be 2 to 11 times less than that of normal concrete. Page et al. (1995) reported that the chloride diffusion coefficients of normal concrete decreased by a factor of 10 when 30% fly ash cement was used.

Thomas and Bamforth (1999) concluded that the differences in chloride penetration rates between plain Portland cement concrete and concrete containing either fly ash or slag became much more marked with the duration of exposure. They reported that the diffusion coefficients for fly ash or slag concretes are likely to decrease to one or two orders of magnitude less than similar grade Portland cement concrete during a 100-year service life. The use of fly ash or slag will considerably increase the service life of structures exposed to chloride environments.

The significant reduction in the chloride diffusion in silica fume and fly ash cement concretes may be attributed to the development of secondary calcium silicate hydrate by the pozzolanic reaction which reduces the pore sizes, leading to a dense micro-structure which decreased the diffusion of chloride ions compared to normal concrete. The significantly reduced chloride diffusion in blended cements would be reflected in delayed corrosion initiation times of steel imbedded in the concrete.

2.4 Chloride Migration in Concrete

The salt ponding test is a common method for measuring the penetration of chloride into concrete. For the salt ponding test, chloride ions require considerable time to penetrate the concrete specimen. Several accelerated chloride ions diffusion test methods by the application of an electrical field were developed to accelerate the movement of chloride ions (Tang and Nilson 1992; Andrade, 1993).

In recent years, migration testing has been widely used for accelerated testing to evaluate the chloride diffusivity in concrete. Figure 2.3 shows the experimental setup proposed by Andrade (1993), that could be considered as a modified version of the ASTM C 1202 (Rapid Chloride Penetration Test). For this purpose, a disk, 50 mm thick, will be cut from the center of the cylindrical (76 x 152 mm) specimens. The disk specimens will be vacuum saturated in a 300 mmol/L NaOH solution prior to testing. The disks will be then glued to plastic rims that fit between the upstream and downstream cell (see Figure 2.3), leaving an exposed diameter of 76 mm. Two chambers are separated by the concrete disk,

with one containing a known chloride ion concentration (cathode chamber, upstream) and the other chamber containing a distilled or lime water (anode chamber, downstream).

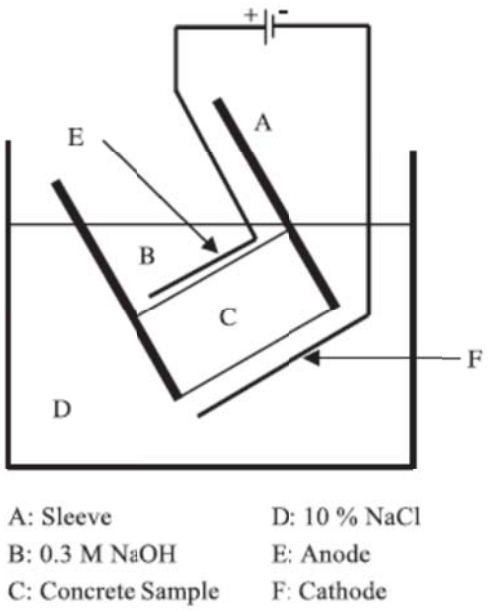

Figure 2.3: Chloride migration test setup (Andrade, 1993).

The transport of ions through the sample is accelerated by applying an electrical potential (usually 500 V/m) across the two surfaces of the sample. The current passing through the system and the chloride concentration of the downstream chamber will be monitored during approximately 120 h. Tang and Nilson (1992) and Andrade (1993) developed a theoretical model based on Nernst Planck equation to calculate the chloride effective diffusivity coefficient through concrete (D_{eff}), which states:

Nernst-Planck: Total flow = Diffusion + Migration + Convection.

$$-J(x) = D_{eff}\frac{\partial C(x)}{\partial x} + \frac{zF}{RT}D_{eff}C\frac{\partial U(x)}{\partial x} + cv(x) \qquad [2.4]$$

where:

For fully saturated concrete specimens, the convection term in the Nernest-Planck equation- equation [2.4] vanish as v(x) = 0, and becomes:

$$-J(x) = D_{eff}\frac{\partial C(x)}{\partial x} + \frac{zF}{RT}D_{eff}C\frac{\partial U(x)}{\partial x} \qquad [2.5]$$

The effective Diffusion Coefficient could be calculated by solving equation [2.5] and after finding the chloride flux *J(x)*.

The electrochemical approach to accelerate the chloride diffusion into concrete was under investigation in the last decade. Marsavian et al. (2008) used the migration test NT BUILD 492 and the numerical simulation to investigate the influence of artificial cracks with different crack widths and crack depths on the chloride penetration in concrete. Frederiksen et al. (1997) used 2 D simulation software to model the effect of transverse

cracks on chloride penetration into concrete cover. Calculations were performed for various depths and crack densities which define the number of cracks in a specific area of the concrete assuming unlimited chloride supply. The results were evaluated in terms of an equivalent cover thickness when the cover contains cracks. The result indicated that a single crack does not significantly reduces the equivalent cover thickness until the depth of the crack reach over 50% of the actual cover, however, the higher the crack density, the smaller the equivalent cover thickness.

Samson and Marchand (2007) used a constant electrical current used in the chloride migration test to simulate the chloride diffusion in concrete using the Nernst- Planck equation. Their proposed approach was based on the non-steady state analysis of the migration test using the extended Nernst-Planck/Poisson set of equations. The chemical reactions were neglected from the analysis and the numerical simulation was based on the current measurements of the migration test and their method calculates the diffusion coefficient of different ions in the material. Persson (2004) conducted laboratory and analytical studies to determine the chloride migration coefficient (D_m) in self compacting concrete (SCC) using Nernst-Plank equation and the results were compared with normal concrete. He noted that the D_m in SCC was somewhat 60% larger than normal concrete when using limestone filler. He also reported that D_m at 90 days was about 60% that of 28 days. In order to determine the uncertainty of the measured values for chloride diffusion coefficient, a round-robin test was carried out by Tang and Sorensen (2001). The NT BUILD 443 test provides satisfactory precision. Of the different methods tested in that research, the chloride migration test provides the best precision for measurements of the

chloride diffusion coefficient. Its repeatability (COV) is in a range of 5-9%. They concluded that the migration test is, therefore, a good alternative method compared to natural diffusion test due to its simplicity, rapidity, and good precision and fairly comparable results with other tests.

Baroghel et al. (2007) investigated the feasibility of colorimetric techniques on saturated specimens cast in laboratory. Colorimetric methods have been applied to determine the average penetration depth and used to calculate the apparent and effective chloride diffusion coefficients from non-steady-state diffusion and migration tests. Baroghel et al. (2007) concluded that the chloride diffusion coefficients from migration test D_m is in the same order of magnitude with the chloride diffusion coefficients D from non-steady-state diffusion test and in most of cases $D_m > D$. the finding seems consistent with the results reported by Tan and Nelson (2001).

Chiang and Yang (2007) noted a good experimental linear correlation between the diffusion coefficient measured by ponding test and the migration coefficient obtained from colourimetric method after accelerated chloride migration test was investigated. They concluded that the 90-day salt ponding test is a long-term test for measuring the penetration of chloride into concrete. By using the migration test, it would be the easy way to obtain the transport property of concrete in suitable time. Same objective was also investigated by Friedmann et al. (2004) where a phenomenological model of the chloride migration in steady state was developed. Based on the electroneutrality and on the

Nernst–Planck equation, the model leads to simple equations which are easy to solve. They showed that the migration test is enough to calculate the chloride diffusion coefficient. Thus, chloride titration, a heavy and time-consuming operation, may be avoided.

2.5 Chloride Binding Mechanism

When chloride ions from environmental solutions penetrate into the concrete, some of them are captured by the hydration products. This is called chloride binding (Qian et.al, 2009). Chloride binding is significant to the study of the service life of concrete structures for the following four reasons: (1) it is only the free chloride (water soluble chloride) that is responsible for corrosion of reinforcement (Elsener et.al. 1995; Collepardi 1995); (2) reduction of the free chloride concentration in the vicinity of the reinforcing steel will reduce the chance of corrosion; (3) removal of chloride from the diffusion flux, thus retarding the penetration of chloride to the level of the steel (McGrath, 1996); and (4) formation of Friedel's salt, which results in a less porous structure and slows down the transport of chloride ions. Thus, due to the retardation effect of bound chlorides, the free and bound chlorides must be distinguished from each other in service life prediction models.

The mass transport through the solid portion of the matrix is negligible when compared to that through the pores. Chlorides can exist either in the pore solution, chemically bound to hydration products, or physically held to the surface of hydration products (Berman,

1972). While physical binding is due to the adsorption of chloride ion to the C–S–H surfaces, chemical binding is generally the result of reaction between chlorides and C_3A to form Friedel's salt or the reaction with C_4AF to form a Friedel's salt analogue. As shown in equations [2.5] and [2.6].

$$Ca(OH)_2 + 2NaCl = CaCl_2 + 2Na^+ \ 2OH^- \quad [2.5]$$

$$C_3A + CaCl_2 + 10H_2O \rightarrow C_3A.CaCl_2.10H_2O \quad [2.6]$$

2.5.1 Factors effecting Chloride Binding in Concrete

Several investigations were conducted to find out the factors affecting the chloride binding capacity in concrete and mortar (Qiang et. al, 2009). The binding of chloride ion by cementitious materials is very complicated, and is influenced by many factors including chloride concentration, cement composition, hydroxyl concentration, cation of chloride salt, temperature, supplementary cementing materials, electrical field, etc. Tang (1996) found that the rate of chloride binding changes the shape of chloride profile, although it does not remarkably change the penetration depth, as shown in Figure 2.4, where k represents the binding rate, and C/Cs represents the ratio of the chloride concentration at the point of interest to the surface chloride concentration.

Chloride concentration

Chloride concentration is probably one of the most important factors affecting the chloride binding. Several studies have confirmed that a higher concentration of external chloride results in a higher chloride concentration in the pore solution and, consequently,

a high level of chloride binding (Blunk et al. 1986, Dhir et al. 1994). For given cement, a maximum binding capacity exists for chloride ion. Under this limit, the higher the chloride concentration in the pore solution is, the more chloride ion has the chance to access to the binding sites, and the higher the chloride binding will be. The relationship between free chloride and bound chloride is known as binding isotherm, which will be discussed in details in Section 2.5.3.

Cement Content

Racheeduzzafar et al. (1990) found a substantial reduction in water-soluble chloride content with increased C_3A content. Blunk et al. (1986) noticed that a pure C_3A-gypsum mixture bound more chlorides than an ordinary Portland cement and C_3S paste when they were treated with chloride solutions of varying concentrations. Arya et al. (1990) stored

Supplementary Cementitious Materials

Several studies have been carried out to study the effect of supplementary cementitious materials such as silica fume and fly ash on binding chloride in concrete. Each cementitious material has a different chemical composition and physical properties, which result in different effects on chloride binding isotherms. Arya et al. (1990) studied the chloride binding behavior of cement paste with 15% silica fume by exposing the cement paste to 0.56 M NaCl solution, and found that partial replacement of cement with silica fume decreased chloride binding

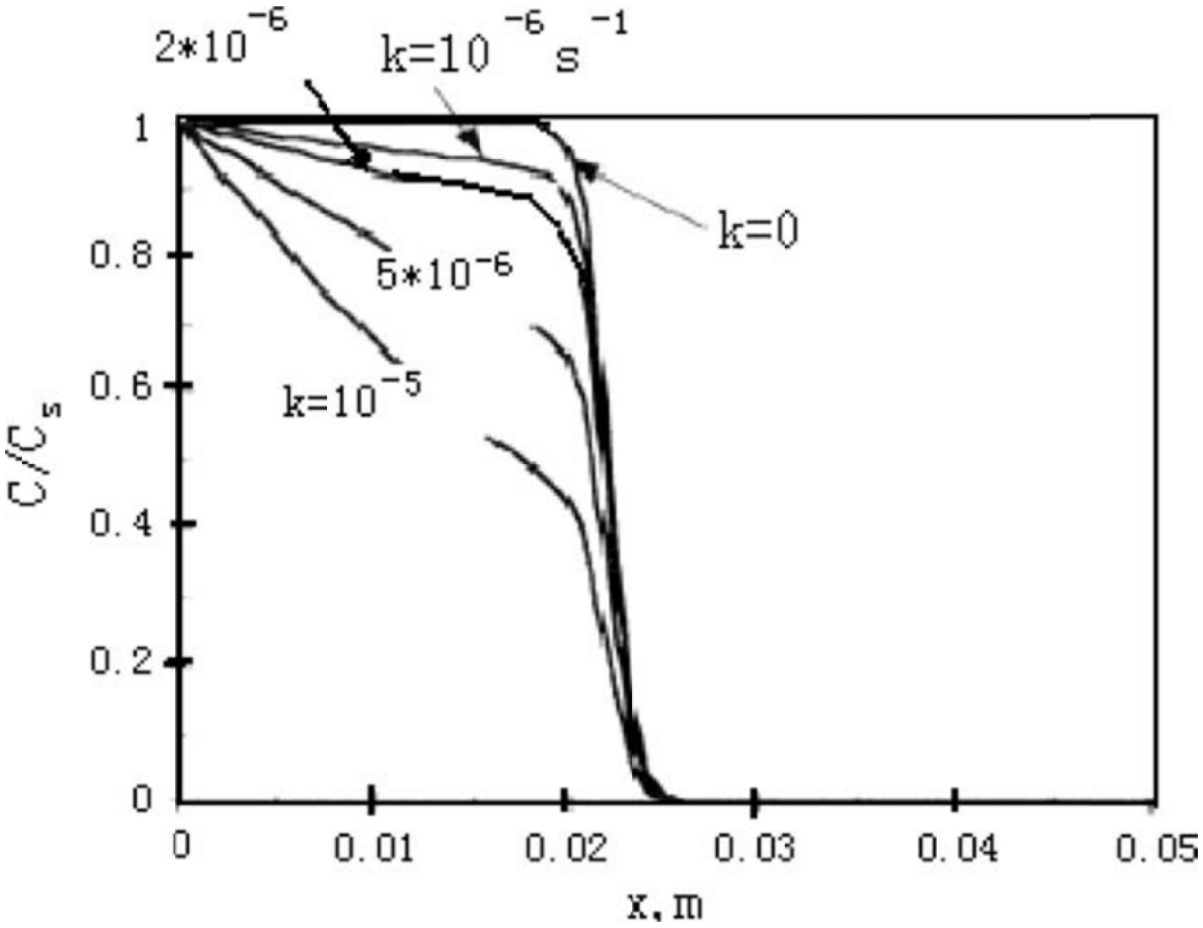

Figure 2.4: Chloride profiles with different values of chloride binding rate, Tang (1996).

ordinary Portland cement (OPC) and sulfate resistant Portland cement (SRPC) in a 20 g/l NaCl solution, and found that SRPC bound considerably less chloride than OPC, because of its lower C_3A content. The same conclusion was reported by Zibara, (2001), Sandberg and Larsson (1993), where silica fume decreased chloride binding in the case of external chlorides. The decreasing of chloride binding capacity in silica fume concrete could be explained by the decreasing of the quantity of C_3A content in the concrete.

The effect of fly ash replacement in concrete on the chloride binding capacity is not clear. Dhir et al. (1997) used the equilibrium method and found that the chloride binding capacity of cement paste increases with the increase in fly ash replacement level up to 50%, and then declines at 67%. Many other researchers [Arya (1990), Wiens and Schiessl (1997)] also found that partial replacement of cement with fly ash has a positive effect on the chloride binding when the cement paste was exposed to a chloride environment. However, Nagataki et al. (1993) found that the replacement of 30% cement with fly ash reduced the chloride binding capacity of cementious material in the case of external chlorides. The controversy of these researches highlighted on the need to further research in this subject to study the affect of curing methods and other factors on the chloride binding capacity of concrete with mineral admixtures.

The Hydroxyl Concentration (pH values)

Tritthart (1989) immersed cement pastes in chloride solutions with different pH values, and found that the chloride binding increased with decreased pH value. Many researchers (Page et.al ,1991, Sandberg and Larsson,1993) also found that the hydroxyl concentration

in the external environment has a significant influence on chloride binding. The general tendency is that the higher the hydroxyl concentration is, the lower the amount of bound chloride would be. As pointed out by Tritthart (1989), a competition exists between hydroxyl and chloride ions for adsorption sites on cement surface.

Cation of Chloride Salt

Delagrave et al. (1997) has found that the cations of chloride salts affect the chloride binding. He noted that $CaCl_2$ resulted in more bound chlorides than NaCl, as shown in Figure 2.5. The presence of Na+ in hardened concrete results in a higher pH value than that of Ca^{2+} and Mg^{2+}. Thus, the degree of competition offered by OH^- in NaCl solution is higher than that in $CaCl_2$ and $MgCl_2$ solution.

Temperature

Larsson (1995) and Roberts (1962) found that the amount of bound chloride decreased as temperature increases. Indeed, for a physical adsorption, an elevated temperature increases the thermal vibration of absorbents, resulting in more unbound chloride. Zibara (2001) found that at a low chloride concentration (0.1 M, 1.0 M), an increased temperature resulted in a decreased binding; while at high chloride concentration (3.0 M), an increased temperature results in an increased binding.

Electrical Field

It is very common now to use an applied voltage to accelerate the chloride transport and to shorten test duration during the measurement of resistance of concrete to chloride

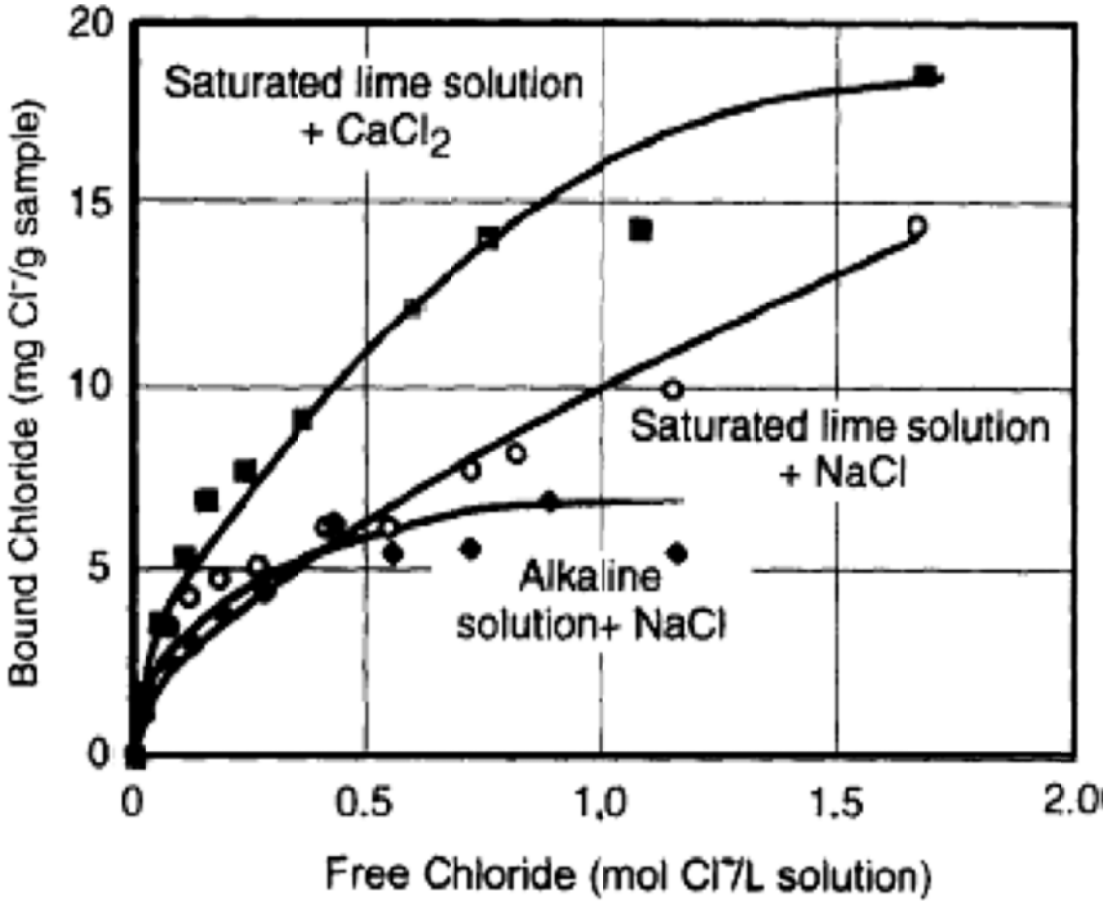

Figure 2.5: Influence of cation of chloride Salt on the chloride binding isotherms, Delagrave et al, (1997).

transport. Ollivier et al. (1997) examined the chloride binding after a migration test and found no difference in binding capacity over an applied voltage range of 2 to 30 V.

Castellote et al. (1999) also examined the effect of electrical potential on chloride binding after a non-steady state migration experiment. They found that no binding occurs as long as the total chloride concentration remains below 0.14%. Above this level, the amount of bound chlorides is less than what would be expected in a natural diffusion experiment.

2.5.2 Chloride Binding Isotherms

The relationship between free and bound chloride ions over a range of chloride concentrations at a given temperature are known as the chloride binding isotherms. Until now, three types of binding isotherm (i.e., linear, Langmuir, and Freundlich binding isotherms) have been proposed to describe the relationship, which are described in the following sections. As mentioned before, there actually exist two types of chloride in concrete. One is the free chloride C_f, (g of chloride per g of concrete), which is dissolved in the pore solution and can diffuse through concrete; the other is the bound chloride C_b, (g of chloride per g of concrete), which is chemically and physically bound to the cement hydrates and cannot move. The total chloride content C_t, (g of chloride per g of concrete) can be expressed as the sum of the bound and free chlorides:

$$C_t = C_b + C_f \qquad [2.7]$$

The relationship between free chlorides and bound chlorides is described in the literature using empirical isotherms. Following Martin-Perez et al. (2000), three established chloride binding isotherm models: linear, Langmuir, and Freundlich as follows:

1) Linear isotherm model:

$$C_b = \alpha_{cl} C_f \quad [2.8]$$

2) Langmuir isotherm model:

$$C_b = (\alpha_{cl} C_f)/ (1+ \beta_{cl} C_f) \quad [2.9]$$

3) Freundlich isotherm model:

$$C_b = \alpha_{cl} C_f^{\beta cl} \quad [2.10]$$

The three chloride binding isotherm models in equations [2.8] to [2.10] are illustrated in Figure 2.6 and these models depend on two parameters α, β that could be found using experimental tests. Several numerical simulations were conducted using the above binding isotherms models (Shazali et al. 2009, Chen, 2006).

2.6 Transport of Chloride in Concrete Subjected to Mechanical Loading

The modeling of transport phenomena in concrete and the coupling between environment and mechanical damages has gained the attention of the concrete research community in recent years. As Leung et al. (2000) noted, the field of durability mechanics presents research with great opportunities and challenges and is certainly in its infancy in its attempts to resolve very difficult but extremely important problems ascribed to concrete durability. The growth of research in the field is expected to make design life, service life, or residual life prediction a reality in engineering design and analysis of concrete.

The core of concrete durability research is the study of deterioration mechanisms. Materials deterioration can be due to mechanical effects (such as external loads leading to cracking), coupled chemical/mechanical effects (such as chemical reaction resulting in expansion and softening that induce cracking and strength loss). It can also be due to coupled physical/mechanical effects (such as water wetting/drying cycles in concrete, resulting in drying shrinkage that induces cracking), or thermal/mechanical effects (such as cooling/heating cycles in concrete resulting in thermal shrinkage that induced thermal cracking). Thus, deterioration of concrete is induced by the synergy between the concrete materials and environmental factors [Rahman et.al, (1999), Baluch et al (2002), and Page

and Venneslan, (1983)]. These factors include temperature, humidity, and various types of aggressive chemical reactions, such as those involving chlorides, sulfates and carbonation. Clearly coupled transport processes (heat conduction, moisture diffusion, and mass transfer) govern the interaction and thus the deterioration of the concrete materials. Research in this field of multiple interactive phenomena requires an interdisciplinary approach based on the qualitative understanding of both the governing microscopic chemo-physical processes and their link to macroscopic materials behavior.

In most cases, deterioration is initiated by chemical reactions, which may lead to either demolish of materials, thus increasing the porosity, or creation of new phases that are expansive, leading to the generation of disruptive internal stresses. On the other hand, damages induced by mechanical loading interact with the environmental factors and accelerate the deterioration process. To quantify degradation under such conditions,

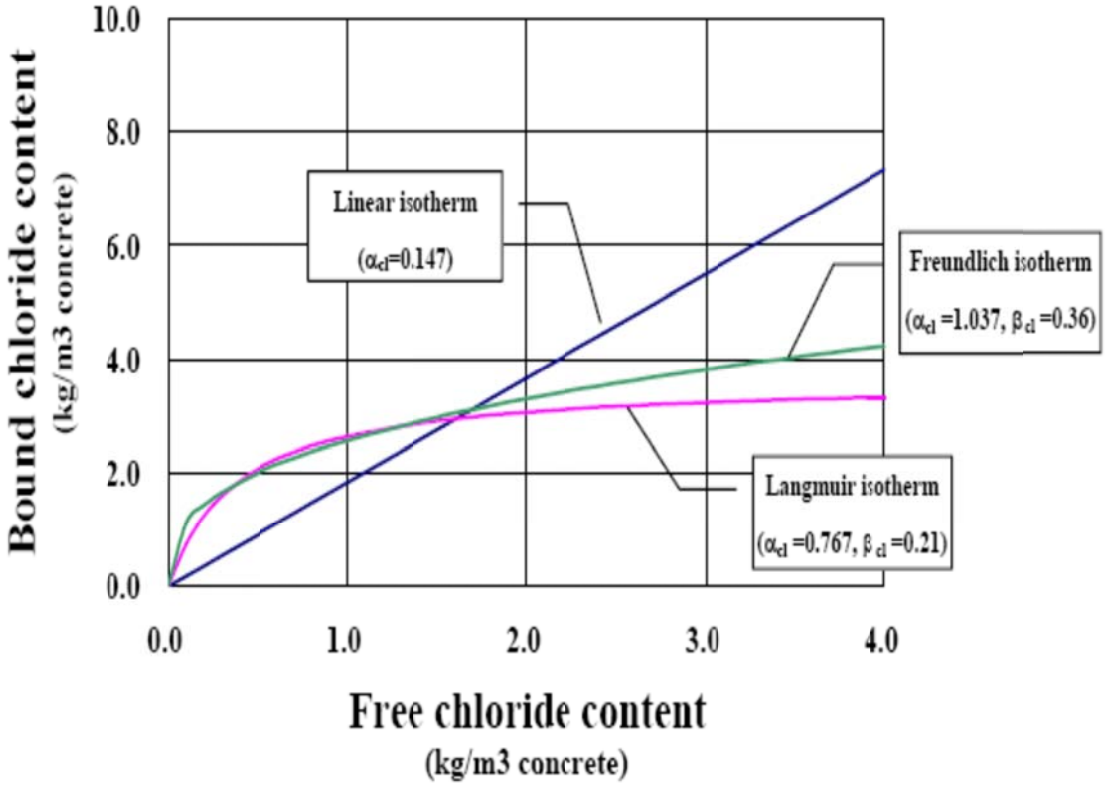

Figure 2.6: Chloride binding isotherm models (Chen, 2006).

methods of damage mechanics and fracture mechanics are employed to follow the inherent logic of the transport phenomena involved. The presence of cracks can significantly modify the transport properties of concrete. For instance, an increase of permeability as a direct result of cracking can be of several orders of magnitude, while diffusivity is much less affected by cracks and, regardless of the transport mechanisms, properties of cracks become more important in cracked concrete than the properties of concrete itself, (Gerard and Marchand, 2000).

Breysse and Gerard (1997) presented a review on the most important problems associated with the prediction of the transport properties of cementitious materials, namely permeability. Both cracked and uncracked materials were considered. They pointed out that concrete response to permeation cannot be deduced from that of cement paste or mortar due to a greater degree of inhomogeneity. They also concluded that the main parameters for describing flow in damaged and sound materials are different, in uncracked concrete, the transport properties is related to the porosity, while in cracked concrete it is related to the crack properties. Therefore, no prediction on the behavior of cracked concrete can be made based on the data for uncracked concrete.

Gerard and Marchand (2000) studied the influence of traversing cracks (caused by cycles of freezing and thawing) on the steady-state diffusion properties of concrete. The effect of both anisotropic and isotropic crack networks was first theoretically assessed using an analytical approach where the cracks were assumed to be of uniform size and evenly distributed on a one- or two-dimensional grid. Results of the theoretical analysis were

then compared to experimental data. Both series of results indicated that cracking can markedly alter the diffusion properties of the materials and a simple method to predict the effect of cracking on the concrete diffusivity is proposed. Further research on modeling the diffusivity of distressed materials was conducted by Yunping and Nakhi (2005) who considered the distressed material as a two–phase composite material with the distressed areas as one phase and the original material as the other phase. They developed a parallel diffusion model in which the damaged phase and the original phase were arranged parallel to the direction of diffusion. The parallel model is associated with the isogradient principle in that the concentration gradients in the damaged phase and in the original phase are the same.

A serial diffusion model was developed in which the two phases are arranged perpendicular to the direction of diffusion. The serial model is associated with the isoflux principle in that the fluxes in the two phases are the same. The two-phase composite models were further extended into general multiphase composite models to evaluate the effect of multilevel damage on the effective diffusivity of distressed materials. A principle of minimum complementary "chemical-flux energy" and a principle of minimum "potential chemical energy" were established similar to the commonly used principles of minimum complementary energy and minimum potential energy. Based on the two new minimum energy principles, it was shown that the parallel model is the lower bound and the serial model is the upper bound for effective diffusivity of distressed materials. Diffusivity of distressed concrete subjected to fatigue cyclic loading was used as an

example and the experimental data agreed quite well with predictions of the theoretical models.

Antoni (2003) investigated the effect of loading, and air content on the chloride penetration into fiber reinforced concrete. In the research, he concluded that the chloride penetration increases when concrete is subjected to loading and the increase was more pronounced when concrete was subjected to tensile and cyclic loading. The results showed that an increase in the air content in fiber reinforced concrete does not lead to an increase in chloride penetration.

2.7 Effect of Cracks on Chloride Transport into Concrete

Several researches were conducted to study the effect of cracks on the transport of chloride into concrete. Sahraman (2007) studies the relationship between the crack width and the effective diffusion coefficient of chloride. Mortar specimens about 355.6 x 50.8 x 76.2 mm prisms were produced for salt ponding test, at the age of 42 days, the prisms were pre-cracked using 4-point bending test to obtain different crack widths and exposed to 30 days NaCl solution.

Sahraman (2007) observed, as seen from Figure 2.7, two different trends. The effective diffusion coefficient increased with increases in the crack width and was almost constant when the crack width was between 29.4 and 102.9 μm. As shown in Figure 2.7, a critical crack width occurs at approximately 135 μm. The effective diffusion coefficient is significantly increased when the crack width was larger than 135 μm as illustrated in

Figure 2.7. He also concluded that the effective diffusion coefficient of mortar has the form of power function of the crack width. The relationship between crack width and chloride diffusivity was also examined by other researchers. Some authors found some increase of the diffusivity in the range of 1–10 higher than uncracked concrete [Raharinaivo et,al (1986), Tognazzi et, al (1998). Others found no effect or a decrease of the diffusion, but in that work the influence of the

artificially created, roughly constant width cracks on chloride ingress into concrete was studied Rodriguez and Hooton (2003). However, in real field condition, cracks generally are not constant in widths on the inside as on the surface and the shape of the crack is generally V-shaped. The experimental methods to create cracks, the methods used to measure chloride transport properties, the methods used to measure chloride contents and the reactivity of the chemical elements with the solid body are the main reasons of diversity obtained from different studies (Gerard et al. 1997).

The self-healing of cracks should also be taken into account when crack width is small. Based on experimental results, Reinhardt and Jooss (2003) proposed that cracks with width below 0.1 mm can be closed by a self healing process. Castel et al. (1999) studied the effect of loading on the transport of CO_2 in reinforced concrete beams; the samples used for this study were two reinforced concrete beams with 15 x 28-cm cross section and 300-cm length with two different concrete covers. The beams were loaded in three point's flexural test by coupling the beams back to back and loading rates were kept constant by means of an adequate device.

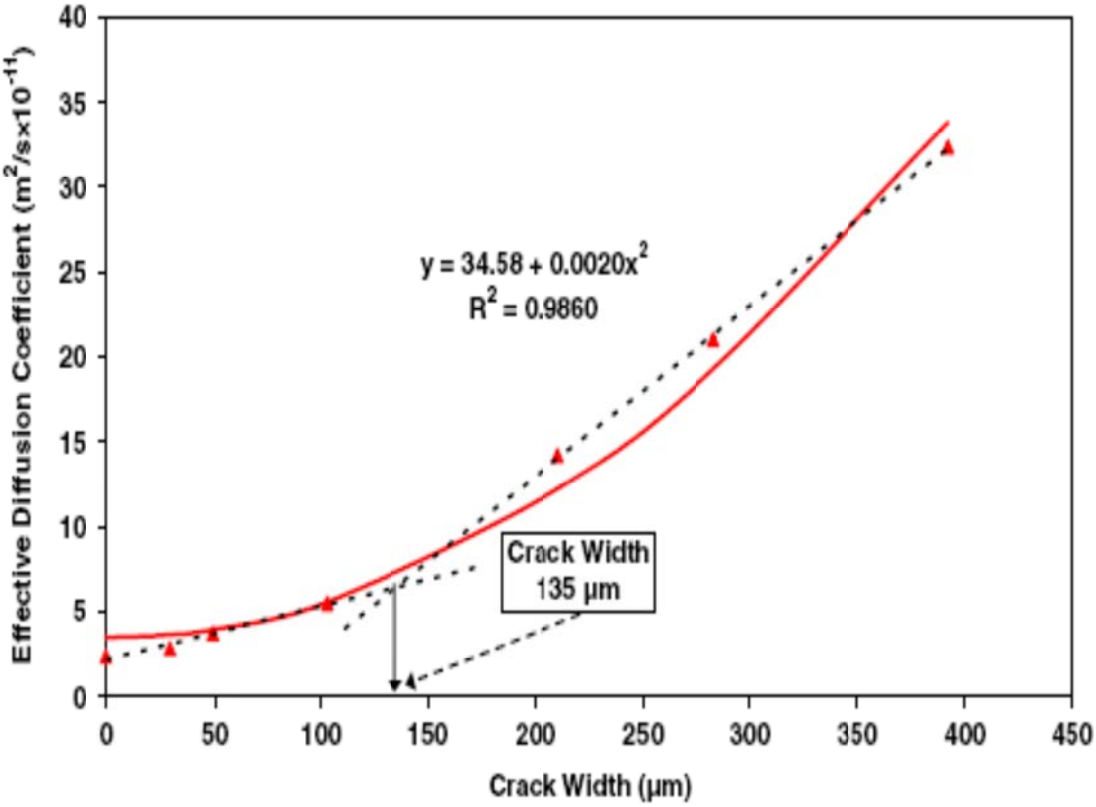

Figure 2.7: Diffusion coefficient vs. crack width for mortar deformed under bending load (Sahmaran, 2007).

As shown in Figure 2.8, the load applied to a reinforced concrete beam and its intensity play a significant role in the penetration of the CO_2 because of the increase of the tensile concrete microcracking mainly located at the paste-aggregate interface. A power relationship was established to correlate the carbonation depth with the applied tensile steel stress criterion (σs).

Pijaudier-Cabot et al. (2009) investigated the effect of the mechanical damage on the permeability in concrete. A formula describing the evolution of permeability with damage has been proposed. It matches consistently the following two extreme configurations: In the first one, permeability is an exponential function of distributed diffuse damage as shown in Figure 2.9:

$$k\,(D) = k_0 \exp(\alpha D^{\beta}) \qquad [2.13]$$

Where k is the permeability coefficient in Darcy's law and D is a scalar damage parameter, α and β are experimental parameters. And in the second, a relationship between the crack opening [u] and the crack roughness [ξ] was established with the permeability coefficient as shown in Figure 2.9 and equation [2.14]:

$$k_p = 1/12\ \xi\ [u]^2 \qquad [2.14]$$

From Figure 2.10, it can be noted that with higher deformation there is an increase of the permeability in concrete with about 10000 times the initial permeability. Similar

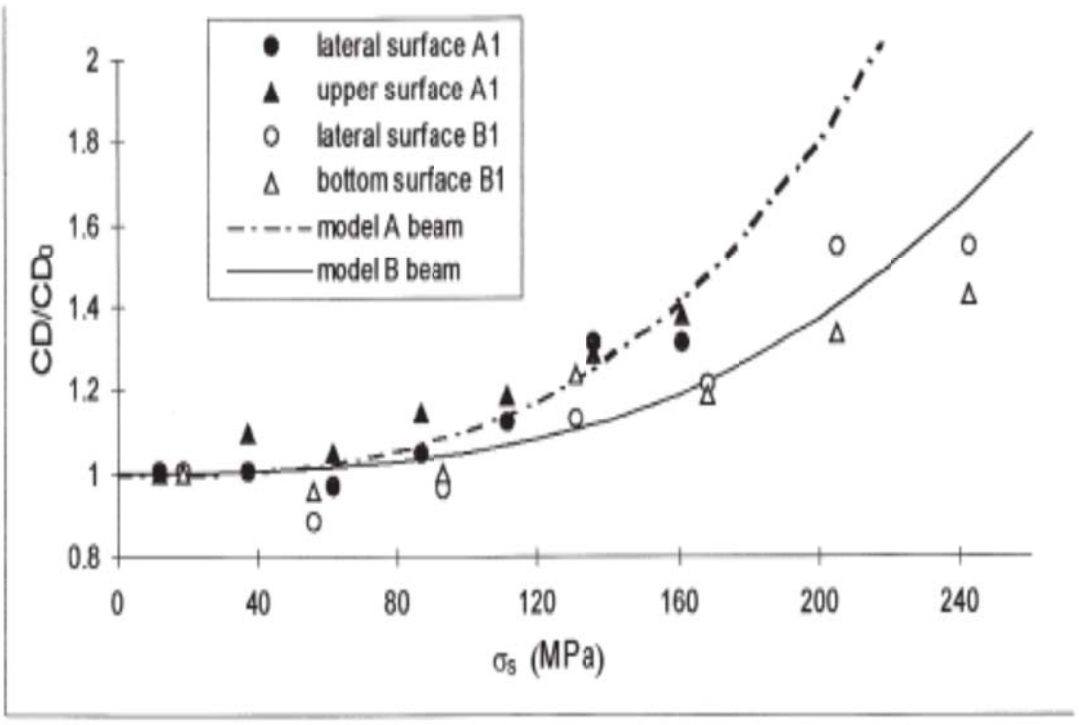

Figure 2.8: Evaluation of carbonation depth in relation with steel tensile stress (Castel et al, 1999).

conclusions were noted by Choinska et al (2007), where they investigated the damage-temperature-stress level-permeability interactions in structural concrete.

The tests were performed on hollow cylindrical concrete specimens, subjected to compressive loading and temperature up to 150 °C. As shown in Figure 2.11, at stress levels lower than 80% of the peak stress, the variation of permeability is small and it is slightly influenced by the stress. As a matter of fact, the permeability under load is smaller than the permeability

measured after unloading. As the load exceeds 80% of the peak stress, microcracking increases rapidly, causing an increase of the permeability and a greater sensitivity to the applied load, i.e. a noticeable difference between the permeability measured under load and after unloading, the first becoming greater than the latter. In the post-peak phase, the increase of permeability is much larger due to significant crack width growth.

The increase of permeability with the applied load seems to be greater with temperature, inducing further alterations of concrete and dilation of the porous structure of the material (Choinska et al. 2007).

2.8 Numerical Simulation of Chloride Transport in Concrete Coupled with Mechanical Loading

Numerical simulation is a powerful tool in studying the transport properties of concrete. Bringing the existing theoretical knowledge and experimental evidence together,

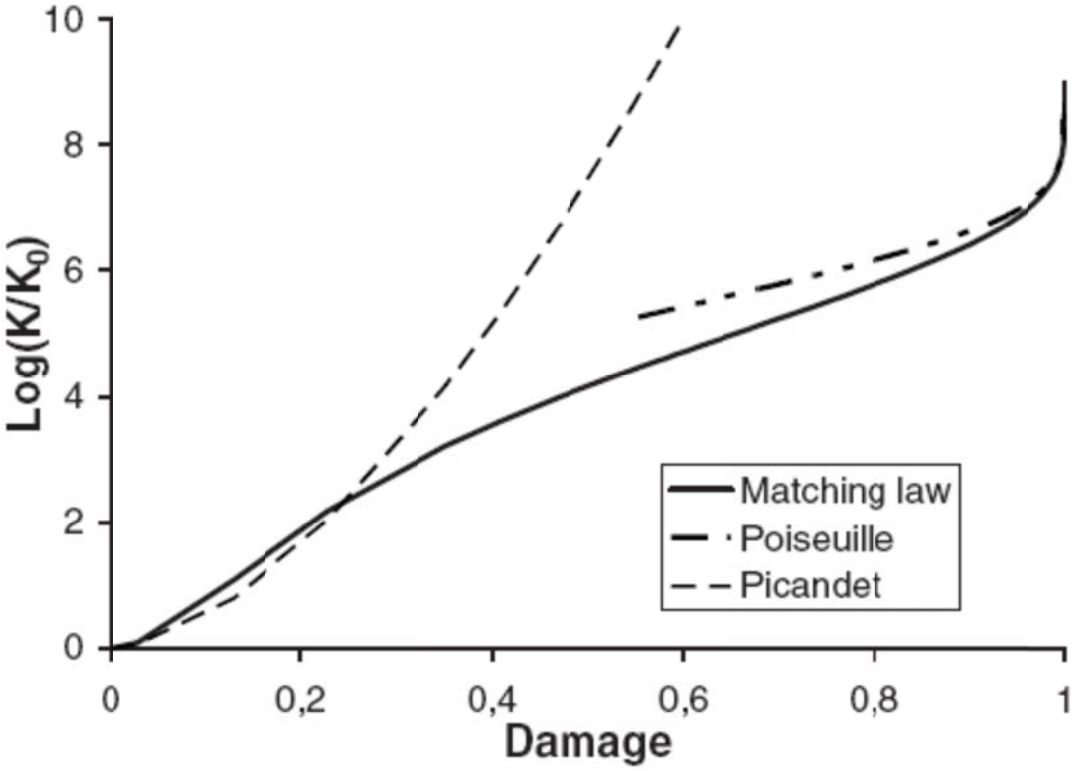

Figure 2.9: Permeability related to mechanical damage
(Pijaudier-Cabot et al., 2009).

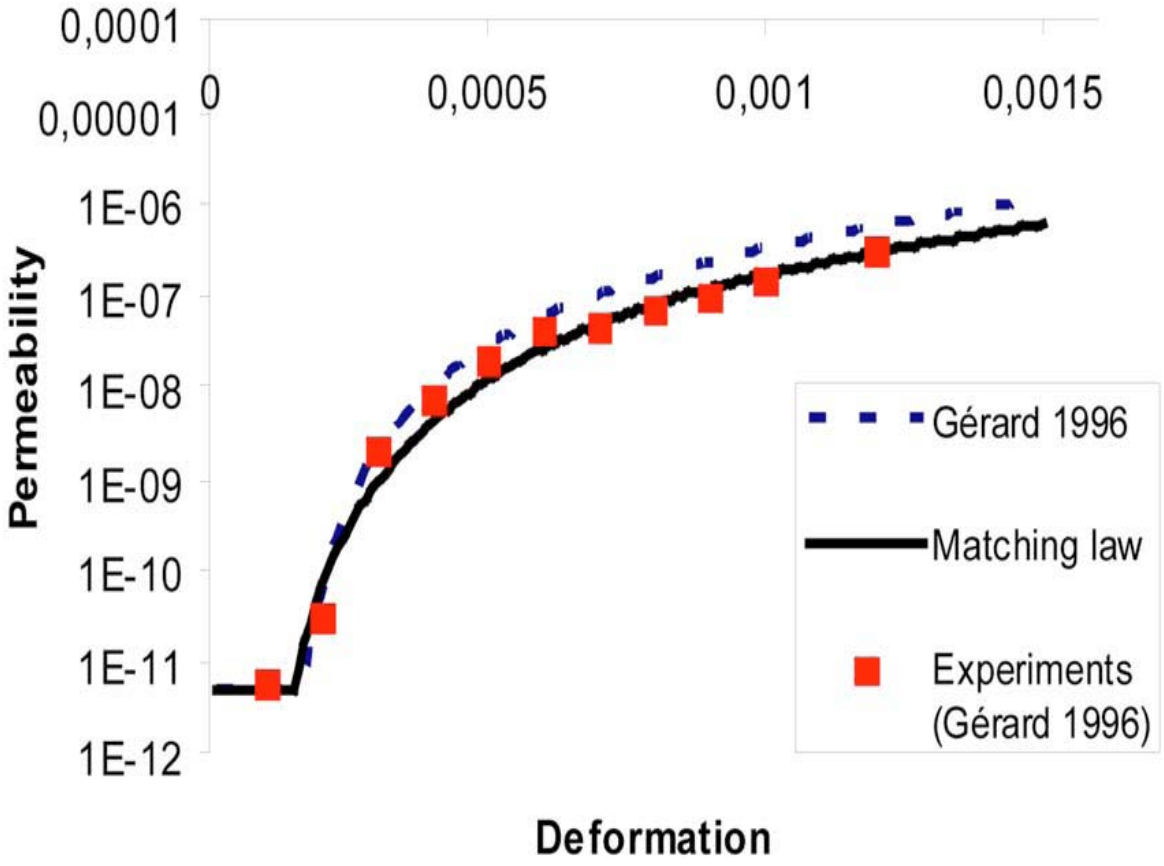

Figure 2.10: Permeability related to mechanical deformation (Pijaudier-Cabot et al., 2009).

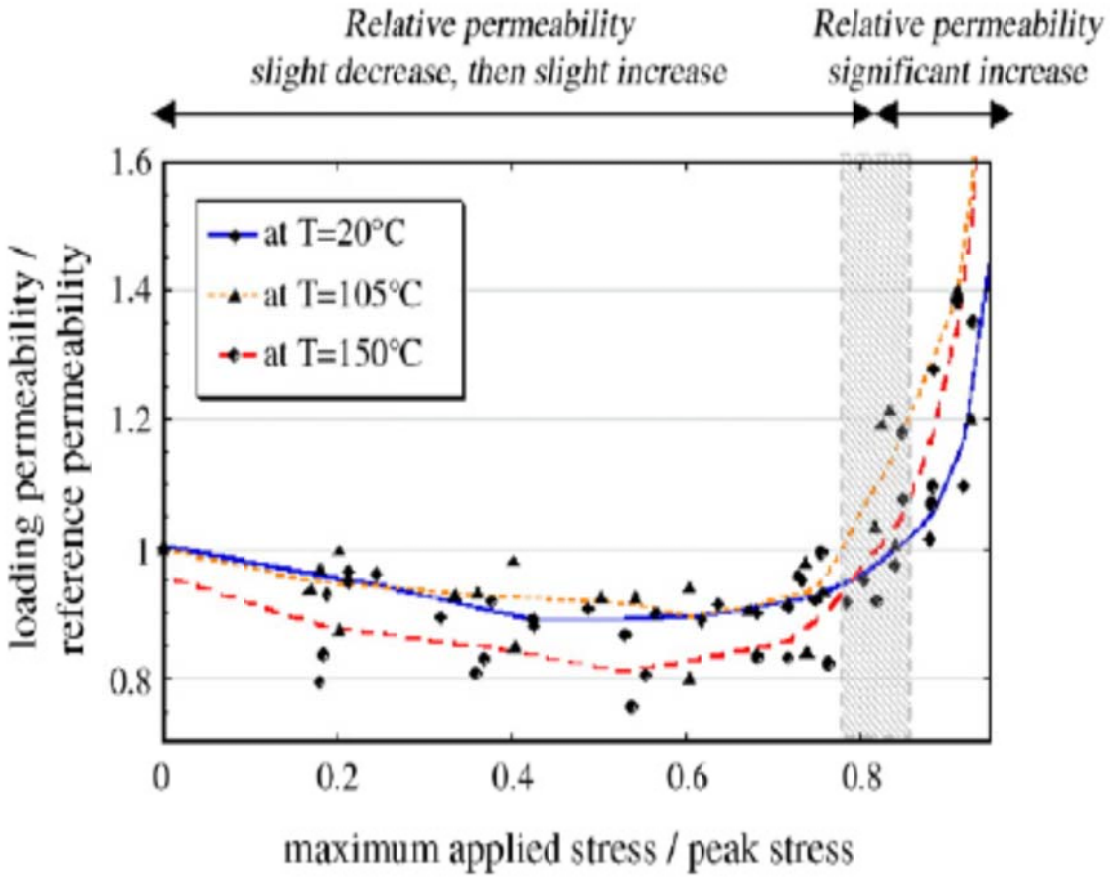

Figure 2.11: Permeability related to mechanical stress (Choinska et al. 2007).

numerical models offer a great flexibility and, precision, as they allow examination of the relationships among different parameters and thereby, predictable of general trends in the material properties. The predictive ability and accuracy of these models depend on the choice of the theoretical approach, relevant materials properties and assumptions made.

Marsavian et al. (2008) used transient finite element analysis for the second Fick's low to determine the diffusion coefficient in cracked concrete. The research investigated the influence of artificial cracks, with different crack widths and crack depths on the chloride penetration in concrete. The chloride penetration was determined using the migration test NT BUILD 492. The numerical results agree fairly well with the experimental results.

Frederiksen et al. (1997) used 2-D simulation software to model the effect of transverse cracks on chloride penetration into concrete cover. Calculations were performed for various depths and crack densities assuming unlimited chloride supply. The results were evaluated in terms of an equivalent cover thickness when cover contains cracks. The result indicated that a single crack does not significantly reduces the equivalent cover thickness until the depth of the crack reachs over 50% of the actual cover, however, the higher the crack densities, the smaller the equivalent cover thickness would be.

CHAPTER 3

MODELING OF CHLORIDE TRANSPORT IN SATURATED CONCRETE SUBJECTED TO STRESS INDUCED DAMAGE

3.1 Chloride Diffusion in Coupled with Mechanical Damage and Chloride Binding

As mentioned in Section 2.3.3, the chloride diffusion in saturated concrete is mathematically expressed in two dimension model using Fick's law as mentioned in equation [2.2]. In order o find out the influence of chloride binding capacity, substitution of equation [2.7] in equation [2.2] leads to the following derivatives:

$$\frac{\partial C_a}{\partial t} = \frac{\partial C_f}{\partial t} + \frac{\partial C_b}{\partial t} = D_d \frac{\partial^2 C_f}{\partial^2 x} + D_d \frac{\partial^2 C_f}{\partial^2 y} \qquad [3.1]$$

where C_f is the free chloride concentration in gm chloride per gm of concrete, C_b is the bound chloride concentration in gm chloride per gm of concrete, and D_d is the chloride diffusion coefficient in mm^2/s. Applying the chain rule leads to:

$$\frac{\partial C_a}{\partial t} = \frac{\partial C_f}{\partial t} + \frac{\partial C_b}{\partial C_f} \cdot \frac{\partial C_f}{\partial t} = D_d \frac{\partial^2 C_f}{\partial^2 x} + D_d \frac{\partial^2 C_f}{\partial^2 y} \qquad [3.2]$$

The governing equation [3.2] can be reduced further to:

$$\frac{\partial C_f}{\partial t} = D_{effd}\frac{\partial^2 C_f}{\partial^2 x} + D_{effd}\frac{\partial^2 C_f}{\partial^2 y} \qquad [3.3]$$

Where D_{effd} is the effective chloride diffusion coefficient, which can be measured experimentally. To consider the effect of mechanical damage and chloride binding capacity on the diffusivity of chloride in concrete we can adopt a form of multivariate law proposed by Bazant et al. (1972) and used by Saetta et al. (1998) in which the effective chloride diffusion coefficient D_{effd} is introduced as

$$D_{effd} = D_d \,.F_{cb} \,.F_d \qquad [3.4]$$

Where D_d may be regarded as the reference or nominal diffusion coefficient when all influence factors assume values of unity. F_d represents the influence of the mechanical damage on chloride transport into concrete. F_{cb} denotes the influence of the chloride binding capacity.

3.2 Chloride Migration Coupled With Mechanical Damage and Chloride Binding.

Same principals applied in Section 3.1 could be applied in the electrochemical transport of chloride in concrete based on the electro-diffusion of ions in the pore electrolyte solutions under the influence of an electrical field. This transport may be modeled using the Nernst-Planck equation [2.4] for fully saturated concrete specimens (Andrade, 1993).

$$\frac{-\partial J(x)}{\partial t} = \frac{\partial C_a}{\partial t} = D_m \frac{\partial^2 C_f}{\partial^2 x} + D_m \frac{zFE}{RTL} \frac{\partial C_f}{\partial x} \quad [3.5]$$

where C_f is the free chloride concentration in gm chloride per gm of concrete, C_b is the bound chloride concentration in gm chloride per gm of concrete, z is the valence of chloride ions (z=1), F is Faraday's constant (F = 96480 J.V^{-1}. mol^{-1}), R is the ideal gas constant (R = 8.3144 J mol^{-1} K^{-1}), T is the absolute temperature (K), E is the electric potential in Volts, L is the length of the specimen in mm, and D_m is the chloride migration coefficient in mm^2/s. In order to solve the above equation, the relationship between the total C_a, bound C_b and free C_f chloride contents in equation [2.7] will be used as follows:

$$\frac{\partial C_a}{\partial t} = \frac{\partial C_f}{\partial t} + \frac{\partial C_b}{\partial t} = D_m \frac{\partial^2 C_f}{\partial^2 x} + D_m \frac{zFE}{RTL} \frac{\partial C_f}{\partial x} \quad [3.6]$$

$$\frac{\partial C_a}{\partial t} = \frac{\partial C_f}{\partial t} + \frac{\partial C_b}{\partial C_f} \cdot \frac{\partial C_f}{\partial t} = D_m \frac{\partial^2 C_f}{\partial^2 x} + D_m \frac{zFE}{RTL} \frac{\partial C_f}{\partial x} \quad [3.7]$$

$$\frac{\partial C_a}{\partial t} = \frac{\partial C_f}{\partial t} \left[1 + \frac{\partial C_b}{\partial C_f} \right] = D_m \frac{\partial^2 C_f}{\partial^2 x} + D_m \frac{zFE}{RTL} \frac{\partial C_f}{\partial x} \quad [3.8]$$

The governing equation equation [3.8] can be reduced further to:

$$\frac{\partial C_f}{\partial t} = D_{effm} \frac{\partial^2 C_f}{\partial^2 x} + D_{effm} \frac{zFE}{RTL} \frac{\partial C_f}{\partial x} \quad [3.9]$$

Where D_{effm} is the effective chloride migration coefficient, which can be measured experimentally. To consider the effect of mechanical damage and chloride binding capacity on the diffusivity of chloride in concrete we can adopt a form of multivariate law proposed by Bazant et al. (1972) and used by Saetta et al. (1998) in which the effective chloride migration coefficient D_{effm} is introduced as

$$D_{effm} = D_m .F_{cb} .F_d \qquad [3.10]$$

Where D_m may be regarded as the reference or nominal migration coefficient when all influence functions have values of unity. F_d represents the influence of the mechanical damage on chloride transport into concrete. F_{cb} denotes the influence of the chloride binding capacity.

3.3 Chloride Binding Capacity Influence Function F_{cb}

From equation [3.8], it can be noted that the chloride binding influence function would be as follows:

$$F_{cb} = \frac{1}{1 + \frac{\partial C_b}{\partial C_f}} \qquad [3.11]$$

Where $\frac{\partial C_b}{\partial C_f}$ has been referred to as the chloride "binding capacity" of concrete by Tang and Nilsson (1993) and can be computed based on any appropriate chloride binding isotherm model. The chloride binding isotherm characterizes the relationship between

bound and free chlorides in concrete. Following Martin-Perez et al. (2000), three established chloride binding isotherm models (linear, Langmuir, and Freundlich as presented in equations [2.8], [2.9] and [2.10]) could be used to calculated the corresponding chloride binding capacity and the associated influencing function F_{cb} , are given as follows:

1- Linear isotherm model:

$$C_b = \alpha C_f \rightarrow \frac{\partial C_b}{\partial C_f} = \alpha \rightarrow F_{cb} = \frac{1}{1+\alpha} \qquad [3.12]$$

2- Langmuir isotherm model:

$$C_b = \frac{\alpha C_f}{1+\beta C_f} \rightarrow \frac{\partial C_b}{\partial C_f} = \frac{\alpha}{\left(1+\beta C_f\right)^2} \rightarrow F_{cb} = \frac{1}{\left(1+\frac{\alpha}{\left(1+\beta C_f\right)^2}\right)} \qquad [3.13]$$

3- Freundlich isotherm model:

$$C_b = \alpha C_f{}^{\beta} \rightarrow \frac{\partial C_b}{\partial C_f} = \alpha\beta C_f{}^{\beta-1} \rightarrow F_{cb} = \frac{1}{\left(1+\alpha\beta C_f{}^{\beta-1}\right)} \qquad [3.14]$$

3.4 Mechanical Damage Influence Function F_d

The term damage mechanics has been conventionally used to refer to constitutive models that are characterized by a loss of stiffness or a reduction of the secant modulus. It was first introduced by Kachanov (1958) for creep-related problems and later applied to the description of progressive failure of metals and composites and to represent the material behavior under fatigue. Damage models are used to describe the strain-softening behavior

of concrete. Researchers have developed damage models of varying degrees of sophistication to represent concrete damage (Mazars et al. 1982; Taher et al. 1994; Khan et al. 1998; Voyiadjis et al. 1993). Of the several damage formulations, the phenomenological approach suggested by Mazars et al. (1982), in which the influence of damage on the response of material due to degradation of its elastic stiffness is used to evaluate a scalar damage parameter (*d)*. Based on this, the uniaxial stress-strain relationship is given by

$$\sigma = E\varepsilon \qquad [3.15]$$

$$E = (1-d)E_o \qquad [3.16]$$

Where E_o and E are the secant (undamaged) and (damaged) modulus, and d is a scalar damage variable. Taher et al. (1994) developed an elasto-damage model for concrete using a constitutive law proposed by Popovics [16] for stress-total strain relation of plain concrete subjected to uniaxial tensile and compressive stress in the form of :

$$\frac{\sigma}{\sigma_u} = \frac{m\left(\frac{\varepsilon}{\varepsilon_u}\right)}{m-1+\left(\frac{\varepsilon}{\varepsilon_u}\right)^m} \qquad [3.17]$$

Where σ_u and ε_u are peak stress and strain, respectively, and m is a parameter dependent on σ_u. Using equation [3.17], a relationship between the moduli and damage variable could be obtained as shown in Figures 3.1 and 3.2 as the following:

$$E = \frac{\sigma}{\varepsilon} = \frac{m\frac{\sigma_u}{\varepsilon_u}}{m-1+\left(\frac{\varepsilon}{\varepsilon_u}\right)m} \qquad [3.18]$$

$$E_o = E(\varepsilon = 0) = \frac{m\sigma_u}{(m-1)\varepsilon_u} \qquad [3.19]$$

The scalar damage becomes:

$$d_c = 1 - \frac{E}{E_c} = 1 - \frac{m_c - 1}{m_c - 1 + \left(\frac{\varepsilon_x}{\varepsilon_u}\right)^{m_c}} \quad \text{for} \quad \varepsilon_x < 0 \text{ (Compression)} \qquad [3.20]$$

$$d_t = 1 - \frac{E}{E_t} = 1 - \frac{m_t - 1}{m_t - 1 + \left(\frac{\varepsilon_x}{\varepsilon_{cr}}\right)^{m_t}} \quad \text{for} \quad \varepsilon_x > 0 \text{ (Tension)} \qquad [3.21]$$

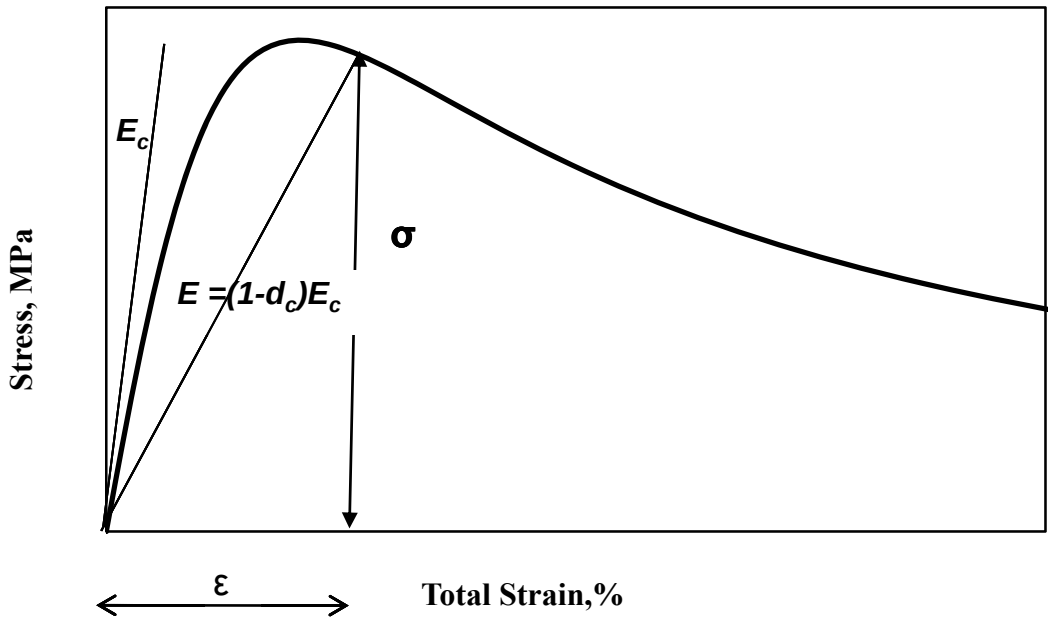

Figure 3.1: The Relationship between scalar damage and uniaxial compressive Stress-Total Strain Curve.

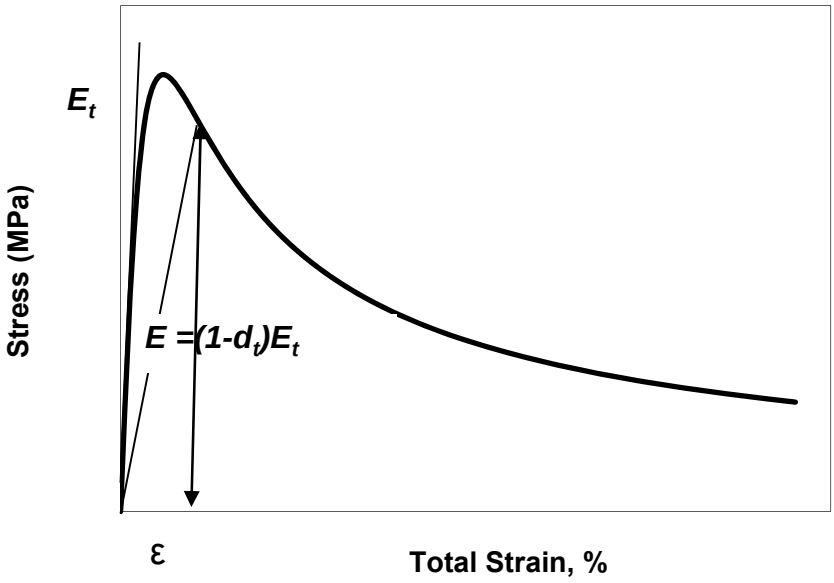

Figure 3.2: The Relationship between scalar damage and uniaxial tensile Stress-Total Strain Curve.

CHAPTER 4

EXPERIMENTAL PROGRAM

4.1 Testing Plan

Most of the researches conducted to study the chloride diffusion in concrete did not consider the mechanical loading leading to damage as well as the transport properties of concrete simultaneously which simulates the actual process of chloride diffusion in existing concrete structures under service.

The **first** objective of this study is to investigate the effect of the mechanical damage on the transport of the chloride in concrete. In order to achieve this objective different concrete samples including reinforced concrete (RC) beams and concrete cylinders will be used. Four levels of mechanical loading were applied on the concrete samples as a percentage of the compressive strength of the concrete after 28 days of curing. The concrete samples were tested for chloride ponding test according to AASHTO T259 for 90 days. After that, chemical analysis was conducted to find the chloride profile for each sample. This experimental procedure simulated the chloride diffusion in concrete under mechanical loading and natural chloride diffusion.

To achieve the **second** and **third** objectives of this study, which are the development of a relationship between free and bound chloride in both chloride migration test and the chloride ponding test, and the development of chloride binding isotherms for locally-produced concrete, total and free chloride contents were measured for all samples at different depths and the results of both tests were used to establish the chloride binding isotherms in both tests. Using the experimental results, numerical simulation of the coupled problem of chloride transport of concrete subjected to mechanical loading leading to damage, would be achieved.

4.2 Cement, Aggregates and Mix Design

ASTM C 150 Type I Portland cement was utilized in all the concrete mixes. The coarse aggregates used in this study were crushed limestone procured from Riyadh region. The fine aggregate was dune sand. The specific gravity and absorption of the coarse and fine aggregates are shown in Table 3.1.

The fine and coarse aggregates were combined such that the coarse aggregate constituted 62% of the total aggregates. The grading of coarse aggregates was selected conforming to ASTM C 33 and is shown in Table 3.2. Potable water was used for casting and curing all the concrete specimens and the water to cement ratio was 0.40. Details of the mix ingredients are shown in Table 3.3.

Table 3.1: Absorption and specific gravity of the coarse and fine aggregates.

Aggregate	**Absorption (%)**	**Bulk Specific Gravity**
Coarse Aggregate	2.5	2.54
Fine aggregate	0.5	2.64

Table 3.2: Grading of coarse aggregates.

SIZE (mm)	% Retained	Cumulative (% Retained)	Cumulative (% Passing)	ASTM C 33 (No.7 Grading)
¾ in	0	0	100	100
½ in	35	35	90	90-100
3/8 in	35	70	65	40-70
3/16 in	20	90	10	0-15
3/32 in	10	100	0	0-5

Table 3.3: Mixes ingredients.

Concrete Type	**Cement Content (kg/m^3)**	**w/c**	**Admixture (kg/m^3)**	**Aggregate (kg/m^3)**
OPC	480	0.40	3.25 (Conplast SP-440)	1725
SCC	490	0.40	(4.5) Viscocrete	1722

4.3 Specimens

In this study, the experimental program consisted of the following parameters: Ordinary Portland Concrete (**OPC**), Self–Compacting Concrete (**SCC**) and five levels of mechanical loading leading to damage applied on the concrete beams and cylinders as a percentage of compressive strength of concrete after 28 days of curing. The following concrete specimens were cast from each concrete mix:

(i) 12 reinforced concrete (RC) beams (150 x 150 x 1200 mm) for the determination of the effect of mechanical damage on the chloride diffusivity using salt ponding test. Figure 4.1 shows the cross section details for the RC beams. Besides, strain gauges were used to monitor the mechanical behavior of the RC beams when subjected to the four point flexural test and to find the losses in the forces when the beam were loaded back to back by steel frames. Figures 4.2 through 4.6 shows different stages to produce the RC beams.

(ii) 24 damaged concrete cylinders (75 x 150 mm) for the determination of the chloride migration coefficient. The concrete cylinders were damaged in compressive with 40%, 75% and 90% of its ultimate compressive strength.

(iii) 6 cylindrical concrete specimens (76 x 150) mm for the determination of compressive strength.

4.4 Curing

After casting, the RC concrete beams were covered with a wet towel for 24 hours and cured in the laboratory under dry conditions for one month, while the cylindrical concrete specimens were demolded and cured in water tanks for 28 days.

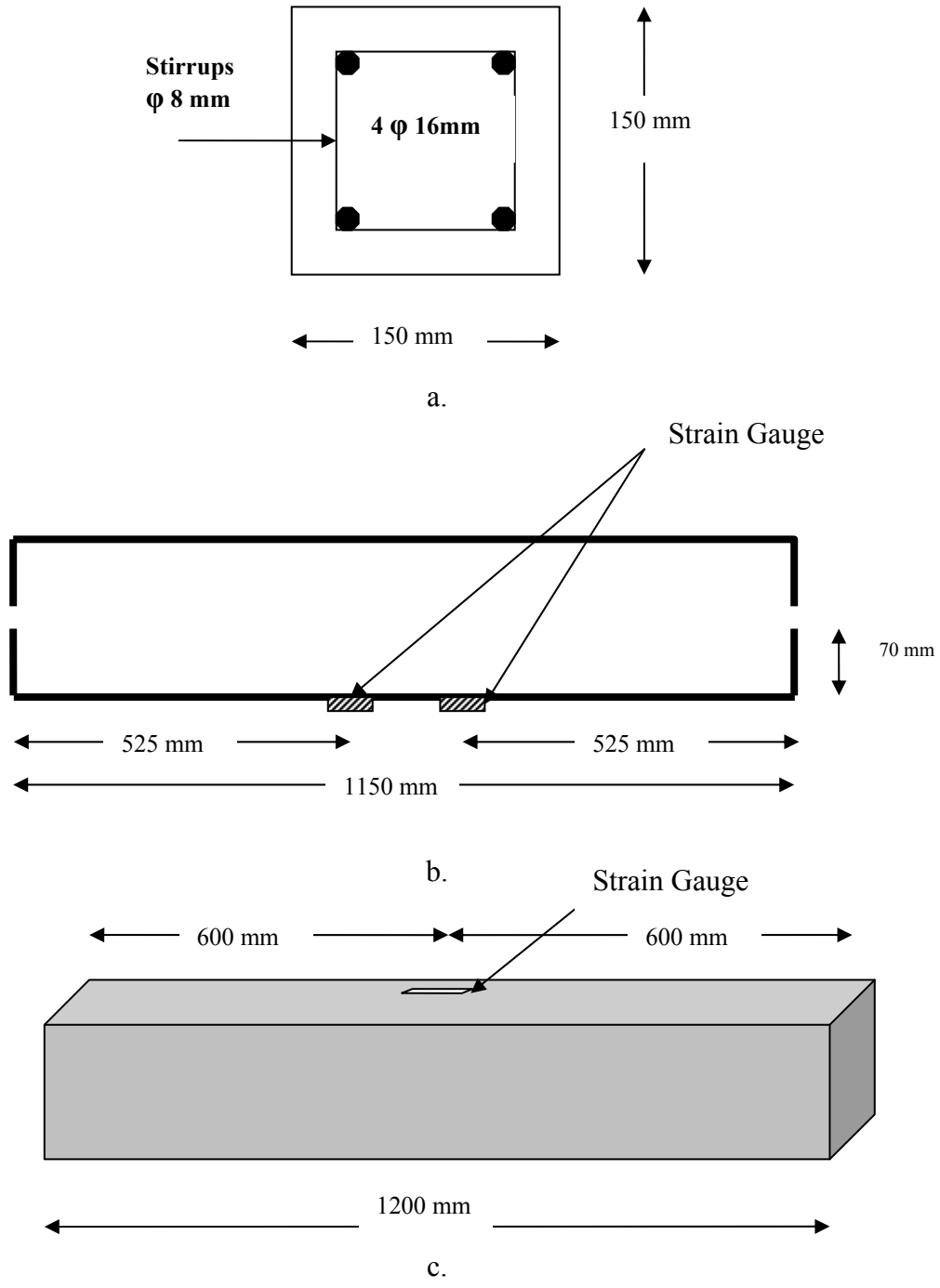

Figure 4.1: a- RC beam cross section details; b-arrangement for strain gauges in reinforcement bars; c- arrangement of strain gauge in concrete.

Figure 4.2: Mould preparation for the Rc beams.

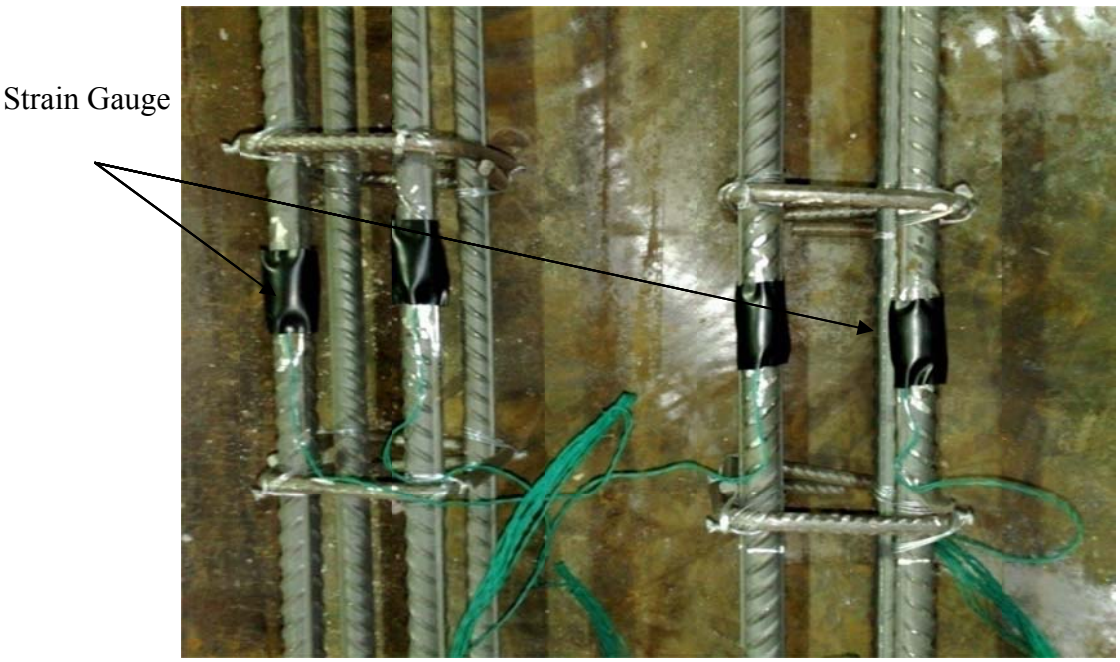

Figure 4.3: Strain gauges arrangement in reinforcement bars.

Figure 4.4: Fixing the strain gauges in the moulds.

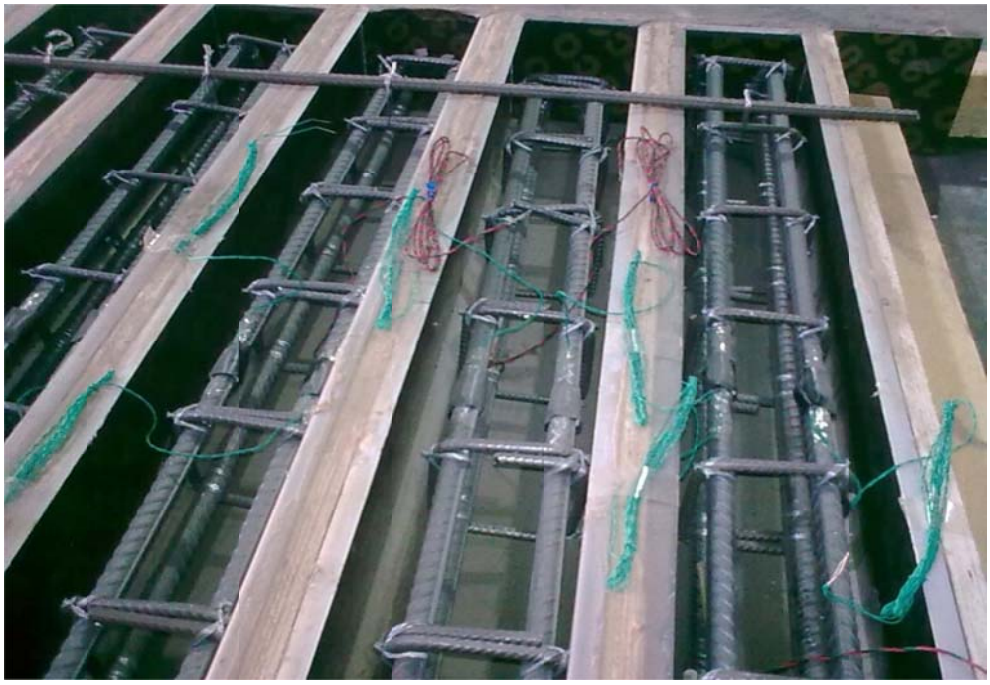

Figure 4.5: Reinforcement details and the strain gauges in the RC beams.

Figure 4.6: RC beams.

4.5 Laboratory Tests

The following tests were carried out to assess the mechanical properties and to investigate the chloride transport in damaged and undamaged concrete:

4.5.1 Compressive strength

The concrete specimens were tested for compressive strength after 28 days of water curing. The specimens were capped with a sulfur compound. Prior to capping, the diameter and height of the specimens were measured. The capped specimens were then placed in a compression testing machine of 3000 kN capacity. The compressive strength was determined according to ASTM C 39.

4.5.2 Flexural Test

After the beams were cured for 28 days under dry laboratory condition, two RC beams were loaded by four point's flexural loading test up to the failure to find the ultimate bending moment capacity as shown in Figure 4.7 through 4.9. During the loading, the strain in the reinforcement bars at the bottom of the RC beams were monitored as well as the strain in concrete in the compressive zone. Besides, the deflection at the mid span of the beams was measured using linear variable differential transformer (LVDT). To create mechanical induced damage, eight RC beams were then loaded at 40%, 60%, 75% and 90% of the ultimate loading capacity of the beams. After cracks had been induced for all test beams, the beams were arranged in pairs and loaded back to back by steel frames on both ends of the paired beams to maintain the crack width, as shown in Figures 4.10 and 4.11. Finally crack widths of loaded beams were measured.

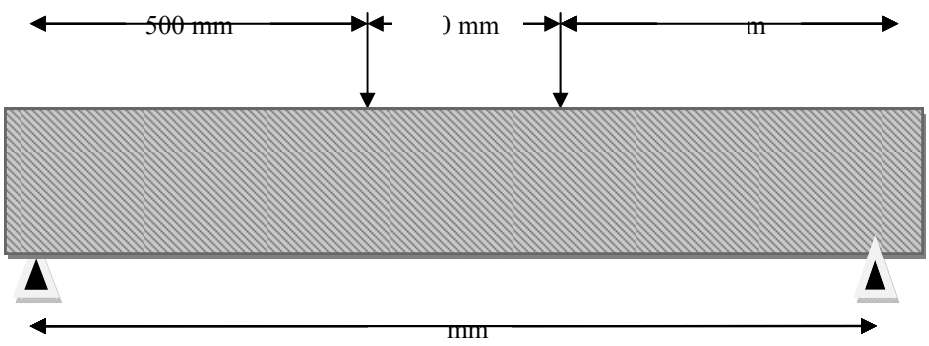

Figure 4.7: Four point flexural loading.

Figure 4.8: LVDT arrangement for mid span deflection measurement.

Figure 4.9: Measurements of the strains in reinforcing bars and the deflection at mid span using data logger.

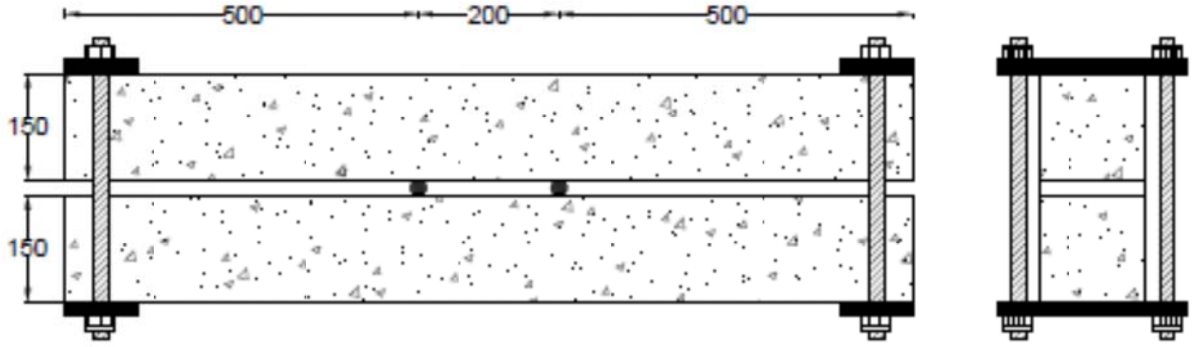

Figure 4.10: Arrangement for the pairs of the RC beams loaded back to back using steel frames at both ends.

Figure 4.11: RC beams loaded back to back using steel frames at both ends.

4.5.3 Salt Ponding Test according to AASHTO T 259

To find the effect of mechanical-induced damage on the chloride diffusion into concrete, a total of four pairs of damaged beams and two control (uncracked) beams were prepared for this study. Left and right surfaces of the beams were coated with epoxy, so that chloride only make possible to penetrate from tension and compression surfaces. As shown in Figure 4.12, two large water tanks were constructed for immersing the beams and the tanks were filled with 8% NaCl solution to simulate marine exposure condition for 90 days. After this period, the specimens were cleaned and dried to remove the surface moisture and drilled at depths of 5, 15, 35, 50 and 75 mm. In order to determine the water-soluble chloride concentration, and the acid–soluble chloride concatenations, three grams of the powder was tested using rapid chloride test RCT and rapid chloride water test RCTW equipment shown in Figure 4.13,in which rapid chloride determination could be measured according to AASHTO -260.

4.5.4 Chloride Migration Test

Chloride migration test was conducted according to NT BUILD 492 as suggested by Tang and Nilson (1992) and as shown in Figure 4.14. A small disc of 50 mm from the middle of the concrete cylinder was cut and cured according to the test procedure in which specimens are placed on plastic supports in the catholyte reservoir (10% NaC1) and the sleeve was filled with 300 ml anolyte (0.3 M NaOH) and a power supply at 60 V was applied to specimens for 24 h. The specimens were then split into two pieces and silver nitrate solution $AgNO_3$ sprayed on the samples and the chloride concentration measured with an accuracy of 0.1 mm. Details are shown in Figures 4.15 through 4.19.

Figure 4.12: Pairs of RC beams in the tanks for chloride ponding test.

Figure 4.13: RCT and RCTW chloride measurement instrument.

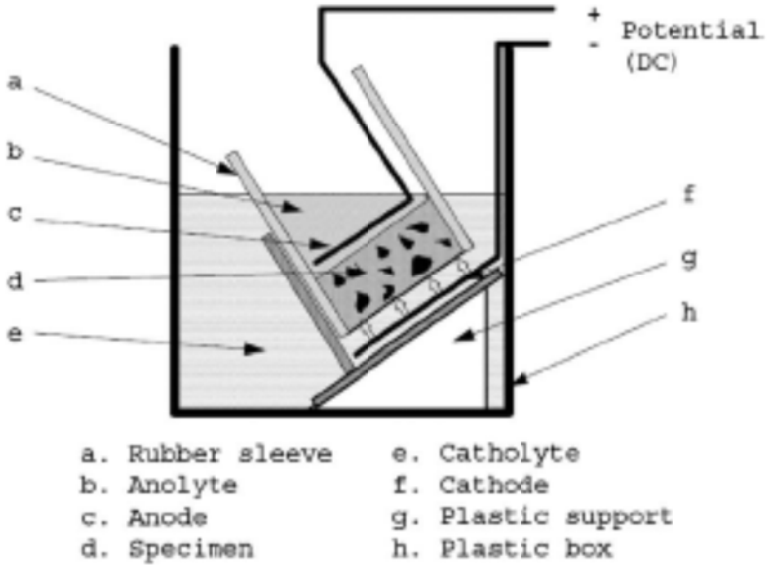

Figure 4.14: Typical schematic arrangement for NT Build 492 test.

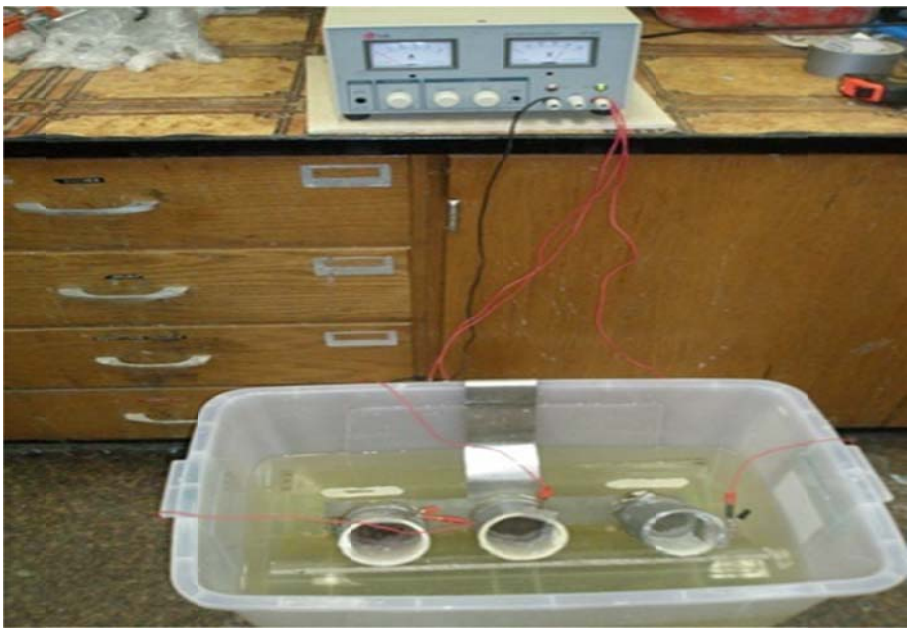

Figure 4.15: Chloride migration test set up.

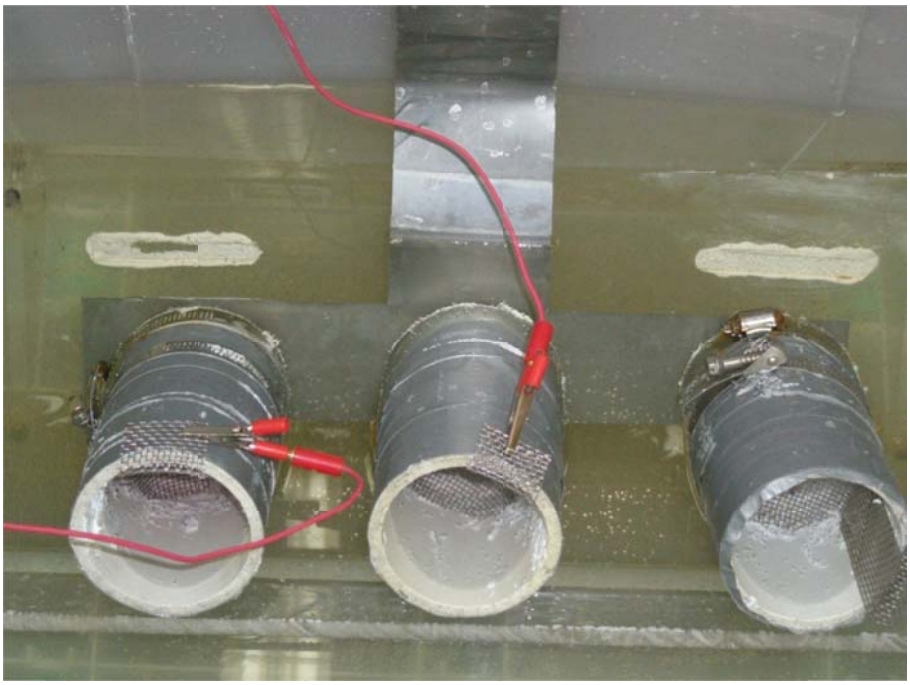

Figure 4.16: Chloride migration test cells.

Figure 4.17: Samples under vacuum.

Figure 4.18: Chloride migration test samples.

Figure 4.19: Samples split in compression.

CHAPTER 5

CHLORIDE MIGRARTION IN CONCRETE SUBJECTED TO COMPRESSIVE INDUCED DAMAGE

5.1 Experimental Results Chloride Migration in Concrete Subjected to Compressive Induced Damage

5.1.1 Effect of Compressive Stress on Chloride Migration in Concrete

Figure 5.1 and Tables 5.1 and 5.2 show the average chloride penetration depths and chloride contents in all concrete samples. From Figure 5.1, it can be noted that with more applied compressive stress there is increasing in chloride penetration depth. For undamaged samples, the penetration depth was 16.7 mm and for the damaged concrete corresponding to stress levels of 40%, 75% and 90% of the compressive strength of the concrete, the chloride penetration depths were 17.5, 25 and 40.8 mm, respectively. The effective migration coefficient D_{effm} was obtained for different damaged samples using NT BUILD 492. For undamaged concrete, D_{effm} (D_d F_{cb}) was 4×10^{-5} mm^2/s which is of a similar order of magnitude when compared with the experimental results obtained by Persson (2004) (2x 10^{-5} mm^2/s).

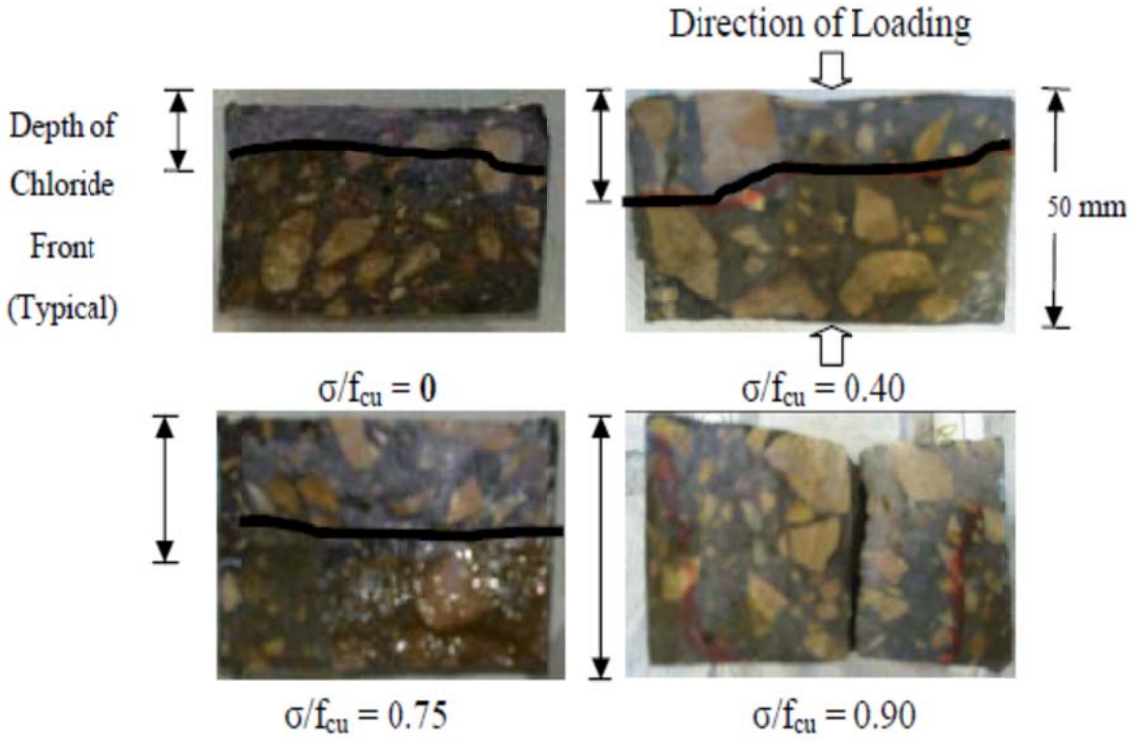

Figure 5.1: Chloride penetration depths at 24 hours in damaged and sound concrete.

Table 5.1: Free chloride content (C_f %) by weight of concrete at various compressive stress levels

Level of Compressive Stress, % of f_{cu}	**Depth in mm**					**Average Depth of Chloride Front in mm**
	2.25	**7.25**	**12.25**	**17.25**	**22.25**	
0%	0.24	0.21	0.07	0.01	0.005	16.7
40%	0.255	0.235	0.09	0.015	0.005	17.5
75%	0.26	0.24	0.18	0.125	0.035	25
90%	0.26	0.242	0.24	0.239	0.24	40.8

Table 5.2: Total chloride content (C_t %) by weight of concrete at various compressive stress levels

Level of Compressive Stress, % of f_{cu}	**Depth in mm**				
	2.25	**7.25**	**12.25**	**17.25**	**22.25**
0%	0.30	0.262	0.082	0.011	0.006
40%	0.32	0.295	0.114	0.0153	0.006
75%	0.33	0.30	0.23	0.185	0.09
90%	0.32	0.29	0.29	0.291	0.285

More details could be found in Figures 5.2 through 5.5 in which chloride profiles for total, free and bound chloride are presented for sound and damaged concrete samples. Figure 5.2 shows the chloride profiles for sound concrete after 24 hours of NT Build migration test. From Figure 5.2, it can be noted that the total chloride was found to be 0.3% by weight of concrete while it was about 0.24% and 0.06% by weight of concrete for free and bound chloride, respectively.

As shown in Figures 5.3 through 5.7, the chloride penetration depths tend to increase with the increase of the applied compressive stress on the concrete samples. However, from the data in these figures, it can be observed that the bound chloride tends to have a maximum value of 0.05% by weight of concrete, and this value didn't change although there was an increase in the free chloride content, which suggests an upper bound limit of bound chloride as reported by Tang and Nilsson (1995).

Comparison of free chloride profiles of undamaged and damaged self compacting concrete samples are shown in Figure 5.6. From these results it can be noted that up to 40% of ultimate compressive strength, no significant increase in the free chloride content was noted where the value range between 0.04% and 0.24% by weight of concrete. Upon increasing the load up to 75% of compressive strength, the penetration depth increase as well as the free chloride content and these values increase in concrete samples subjected to 90% compressive stress loading.

The same trend could be found in total chloride content profiles presented in Figure 5.7, where the total chloride content range was from 0.034% to 0.05% by weight of concrete.

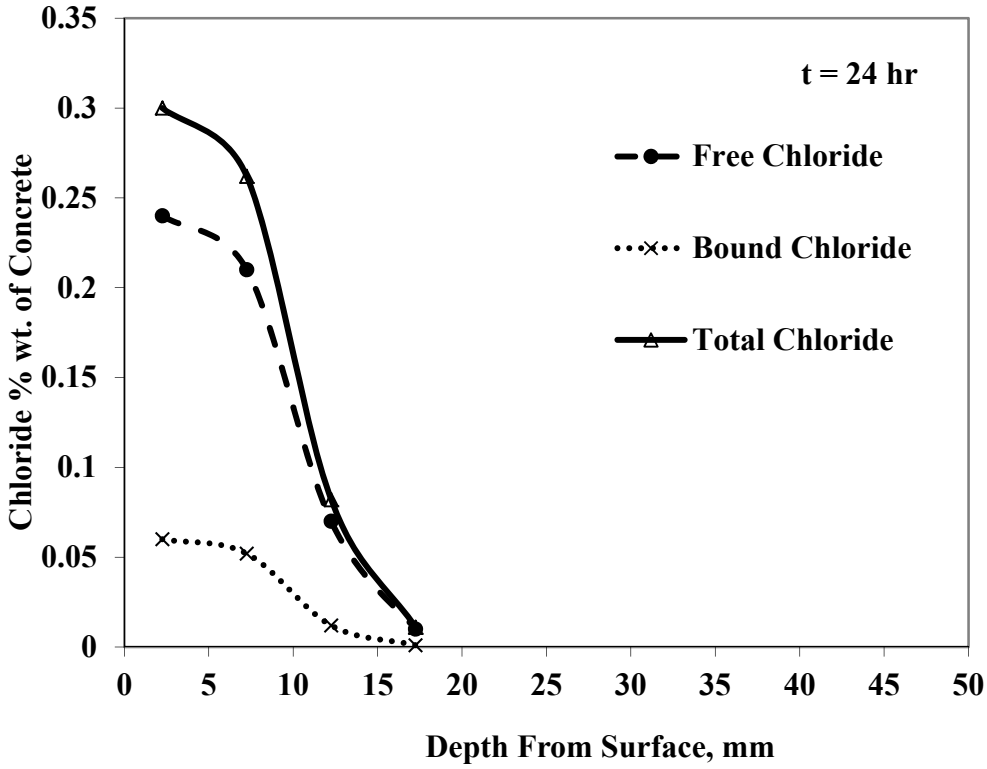

Figure 5.2: Total, bound and free chloride penetration in undamaged concrete.

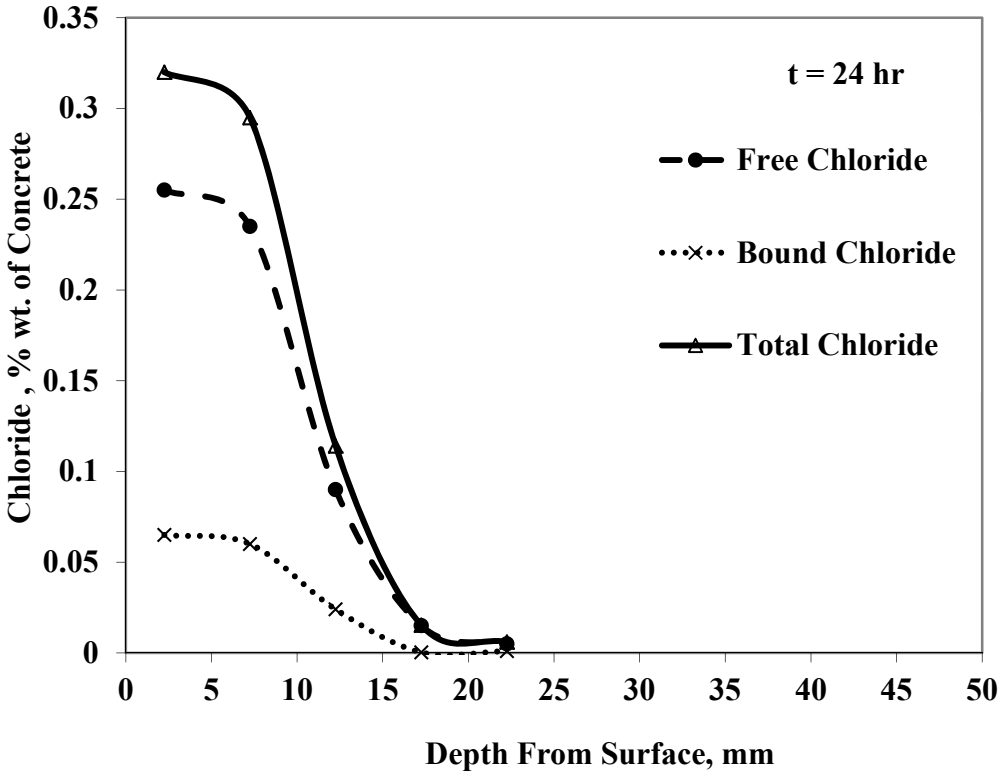

Figure 5.3: Total, bound and free chloride penetration in 40% f_{cu} damaged concrete.

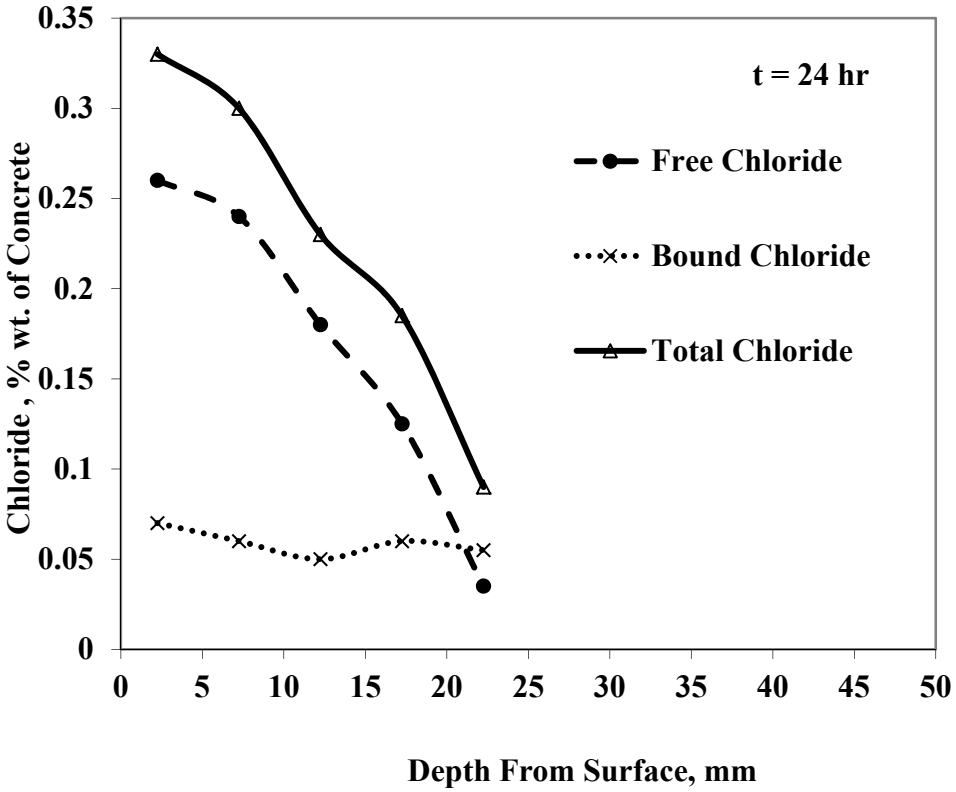

Figure 5.4: Total, bound and free chloride penetration in 75% f_{cu} damaged concrete.

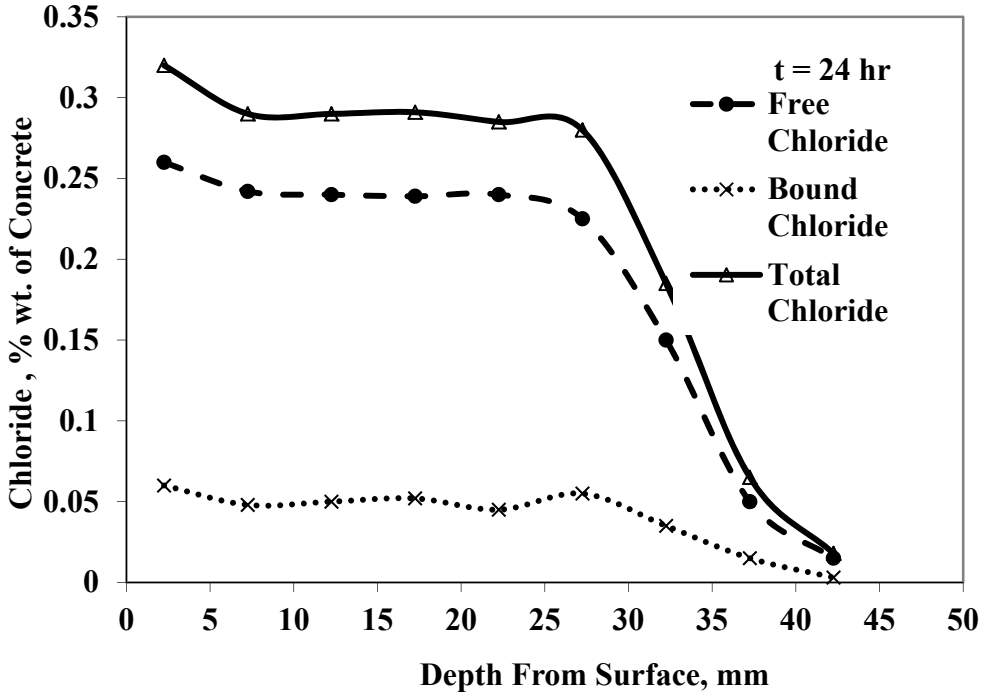

Figure 5.5: Total, Bound and Free Chloride Penetration in 90% f_{cu} Damaged Concrete.

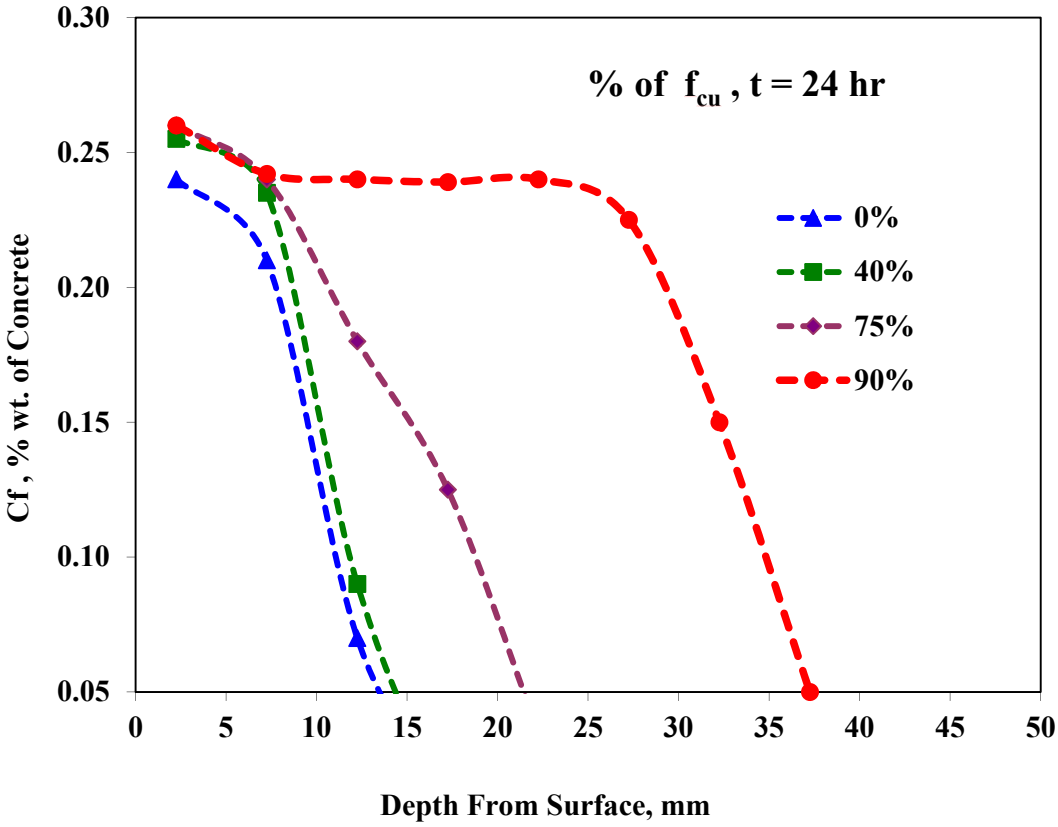

Figure 5.6: Experimental free chloride penetration depth in damaged and undamaged concrete.

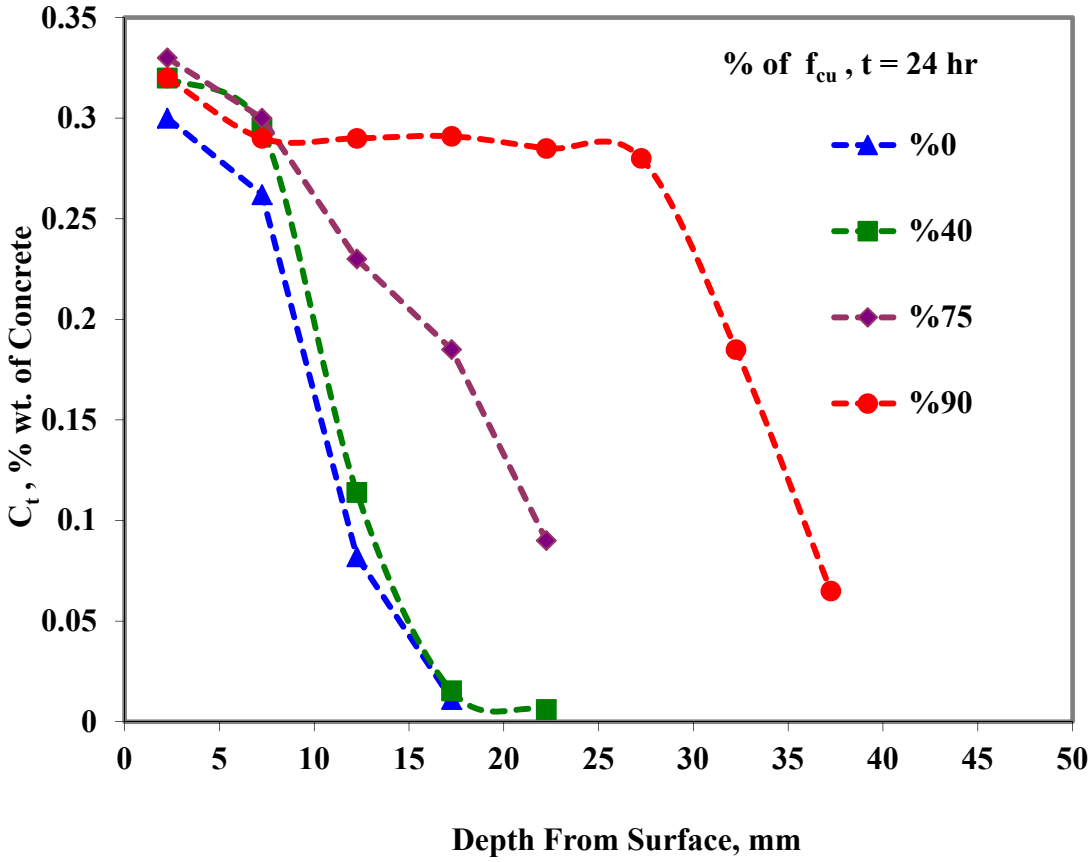

Figure 5.7: Experimental total chloride penetration depth in damaged and undamaged concrete.

Table 5.3 and Figure 5.8 show the results of effective chloride migration coefficient for undamaged and damaged self compacting concrete samples. For the damaged concrete corresponding to stress levels of 40%, 75% and 90% of the compressive strength of the concrete, the effective migration coefficient D_{effm} was computed as 4.5, 7.5 and 12×10^{-5} mm^2/s, respectively. This indicates significant increase of diffusivity of up to three times in damaged concrete subjected to a stress level corresponding to 90% of compressive strength.

Based on the damage model and the ratio of migration coefficient of damaged and undamaged samples ($D_{effm}/ D_d. F_{cb}$), the damage influence function (F_d) was established as follows (see Figure 5.8):

$$F_d = D_{effm}/ (D_d . F_{cb}) = 0.18d + 1 \quad [5.1]$$

Similar experimental observations have been reported by several researchers. Antoni and Saekin (2003) studied the effect of stress on chloride penetration into plain and fiber reinforced concrete using non-steady state chloride migration test and showed that there was a significant increase in the chloride penetration into concrete at higher levels of compressive stress. Wang et al. (2008) concluded that the chloride diffusivity of concrete under compression and tension increases rapidly when the applied stress surpasses a certain threshold value. Sakoi and Horiguchi (2006) studied the loading effects on chloride penetration in fiber reinforced concrete and they reported that for concrete samples subjected to compressive stress up to 80% of ultimate strength, there was about 70% increase in the chloride diffusion coefficient compared to sound concrete samples.

Table 5.3: Correlation between damage function (F_d) and chloride diffusivity at various dtress levels

Stress Level (% f_{cu})	**Damage** (*d*%)	**Depth** (mm)	D_{effm} 10^{-5} mm^2/s	$F_d = D_{effm}/(D_d . F_{cb})$
0	0	16.7	4	1.00
40	0.9	17.5	4.5	1.11
75	3.75	25	7.5	1.85
90	12	40.8	12	3.00

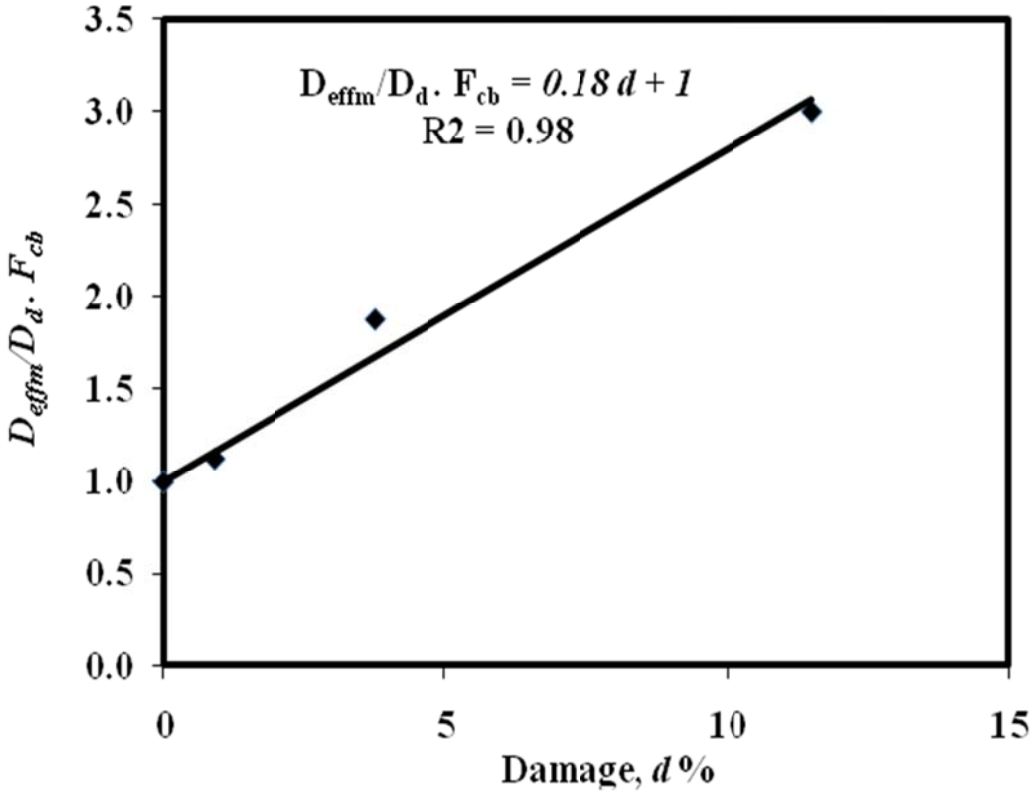

Figure 5.8: Relationship between Mechanical Damage and D_{effm}.

5.1.2 Effect of Chloride Binding Capacity on Chloride Migration in Concrete

As mentioned previously, chlorides exist in concrete in two forms: free and bound. While, free chlorides exist in the pores solution and can diffuse freely through the concrete, some chloride will be bound to the internal surfaces of cement paste and aggregate. Figure 5.9 shows the results of free and bound chloride for damaged and undamaged self compacting concrete samples. From Figure 5.9, it can be observed that a linear relationship could be established as chloride binding isotherm as follows:

$$C_b = 0.236\, C_f \qquad [5.2]$$

Mohammed and Hamadea (2003) reported that linear chloride binding isotherm could be established for concrete subjected to low to medium external chloride concentrations. Same linear relationship was reported by Tuutti (1982). From equation 5.2, it can be observed that the bound chloride is about 24% of free chloride; this low bound chloride compared to the free part was explained by Castellote et al (1999) where they mentioned that in migration test, the transport rate of chloride is so rapid that the binding does not occur in the same extension with normal diffusion test. Solving equation [5.2] with equation [3.8], it can be noted that the chloride binding influencing function would be as follows:

$$F_{cb} = \frac{1}{1 + 0.236} = 0.81 \qquad [5.3]$$

Which means the chloride binding influencing function will reduce the effective chloride migration coefficient by about 20%.

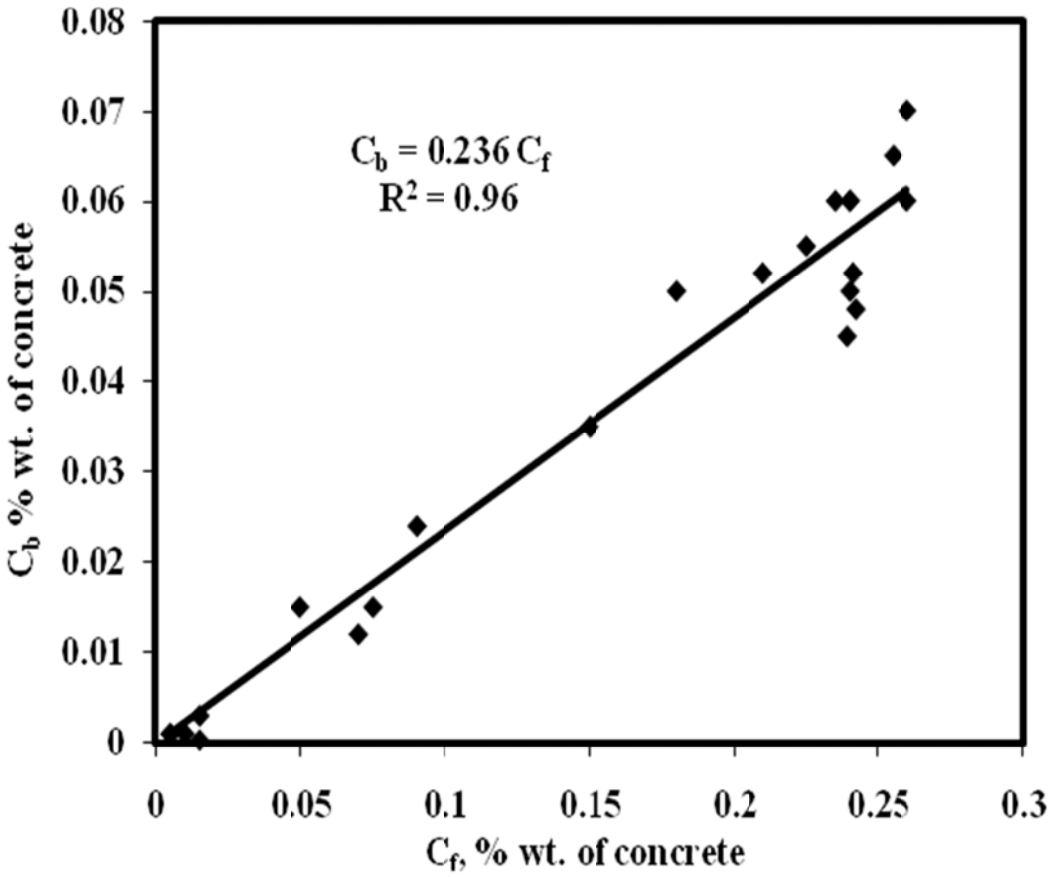

Figure 5.9: Relationship between free and bound chloride for damaged and undamaged samples.

5.2 COMSOL Simulation of Chloride Migration in Concrete Subjected to Uniaxial Compressive Damage

5.2.1 COMSOL Modeling, Subdomain Physics and Boundary Conditions

Based on the model used by Shazali et al. (2009) and Narsilio et al. (2007) where COMSOL finite element software was used to simulate chloride diffusion in undamaged concrete taking into consideration, the effect of binding capacity of concrete, (equations [3.12] to [3.14]) and the effect of damage as described in equation [3.20]. The axisymmetric structural mechanics boundary value problem (BVP) can be used to simulate the degradation of the stiffness of the concrete cylinder corresponding to the appropriate state of loading. The differential equation governing diffusion was then used to solve the coupled problem of mechanical damage and migration of chloride in one way interaction. Figure 5.10 shows the boundary and initial conditions used in COMSOL in concrete.

Table 5.4 shows the parameters used in COMSOL model, in which the coefficient of chloride migration parameter *(D_d)* was taken as 5×10^{-5} mm^2/s, the free chloride concentration (C_f) at the boundary was 0.25% per weight of concrete and the material parameter for the linear binding capacity isotherm (α) was 0.236. Initial chloride content in the sample, C_i, was assumed to be zero. Using the Nernst Planck equation [3.5] coupled with the influence functions F_d and F_{cb}, a numerical simulation was carried out to simulate

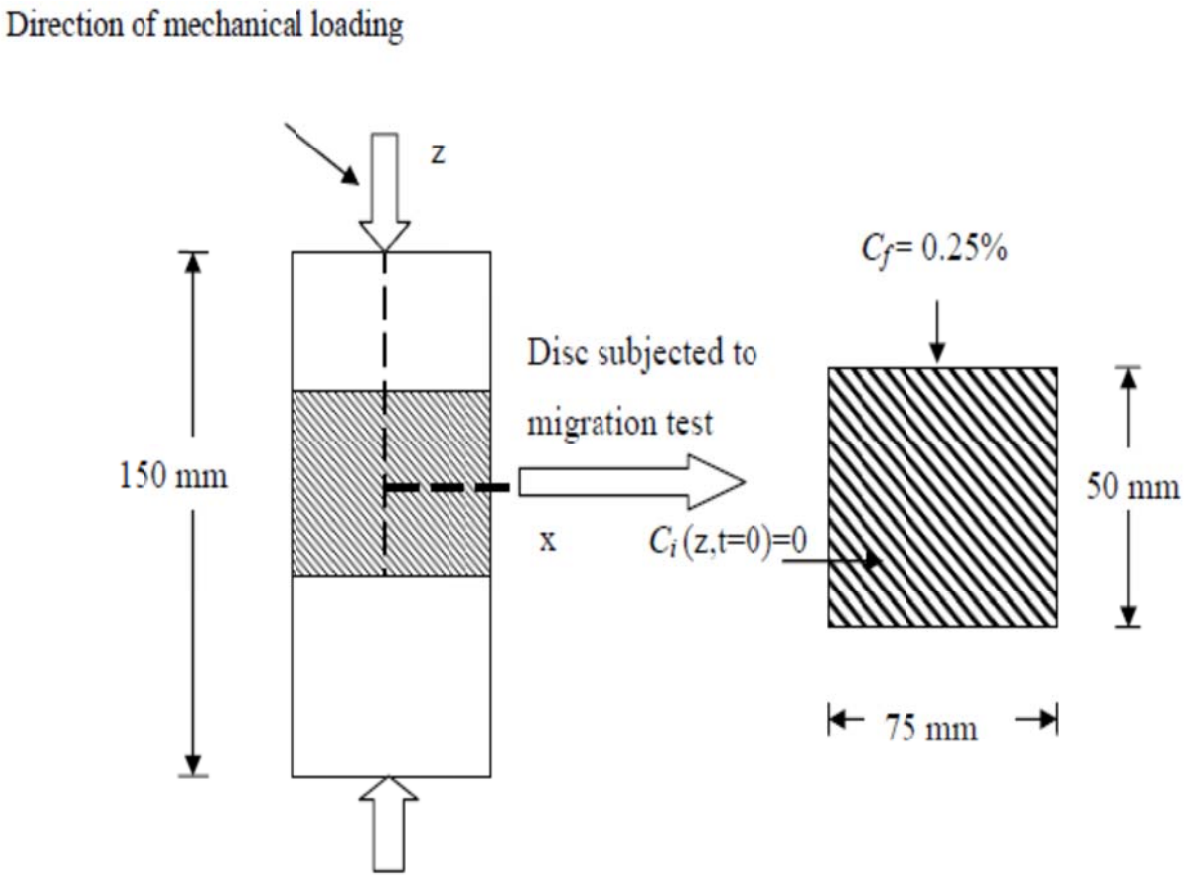

Figure 5.10: Finite element modeling

Table 5.4: COMSOL model parameters

COMSOL commands	COMSOL expression/parameters	Value
Subdomain setting	$\delta_{ts}\frac{\partial C}{\partial t}+\nabla.(-D\nabla C)=R-u\nabla C$	$\frac{\partial C_f}{\partial t}=D_{effm}\frac{\partial^2 C_f}{\partial x^2}+D_{effm}\frac{zFV}{RTL}\frac{\partial C_f}{\partial x}$
	δ_{ts}	1
	D	$D_{effm}=D_d*F_{cb}*F_d$
	u	$D_{effm}=D_d*F_{cb}*F_d$ *a
Scalar expression	a	$\frac{zFV}{LRT}$
Boundary setting	C_o	C_f=0.25% by weight. of concrete
Constant	D_d	5x10^{-5} mm^2/s
	z	1
	F	9.648x 10^{-4} J.V^{-1}.mol^{-1}
	V	–40 volt
	R	8.3144 J.mol^{-1}.K^{-1}
	T	297 K
	L	50 mm
	α	0.236
Scalar expression	F_d	0.18*d+1
	F_{cb}	1/(1+ α)
	C_b	α C
	C_t	C_b+C

chloride diffusion in both damaged and sound specimens for different levels of compressive stress.

5.2.2 Finite Element Simulation of Concrete Subjected to Compressive-Induced Damage

To verify the damage model suggested in equation [3.20], a numerical simulation was conducted for concrete with low, normal and high compressive strength. The numerical solution was compared to results of complete stress-strain curves for concrete subjected to uniaxial compressive stress as reported by Wischers (1978). Figure 5.11 shows the stress-strain relationships of concrete with different compressive strength using the damage model. It can be noted that the damage model is representing well the data of stress-strain curves for concrete subjected to uniaxial compressive stress from Wischers (1978).

Although it seems that the damage model is over-estimated the stress in the concrete with 48 MPa compressive strength at strain more than 2 times the peak strain (~ ε_p=0.004). Figure 5.11 shows that before reaching the peak stress, a linear behavior of concrete with higher compressive strength could be observed at higher stress, while after the peak stress, the higher the compressive strength of concrete the more brittle behavior of concrete. More details could be found in Figure 5.12 in which, the rate of the damage in concrete which represent the degradation of the stiffness due to microcracks in the concrete is calculated up to the peak stress. It is observed from Figure 5.12 that the lower the compressive strength of concrete the higher the degradation in the stiffness in the concrete at the peak strain. For concrete with 15MPa compressive strength, the damage reaches to

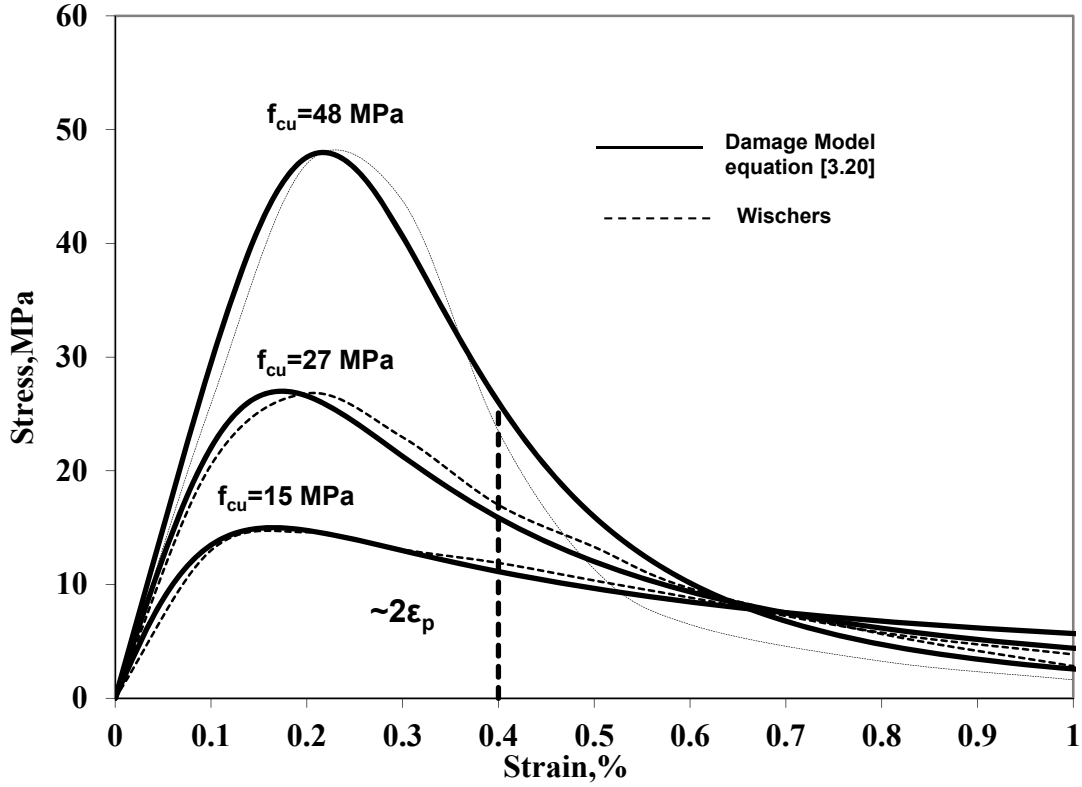

Figure 5.11: Complete compressive stress-strain using damage model.

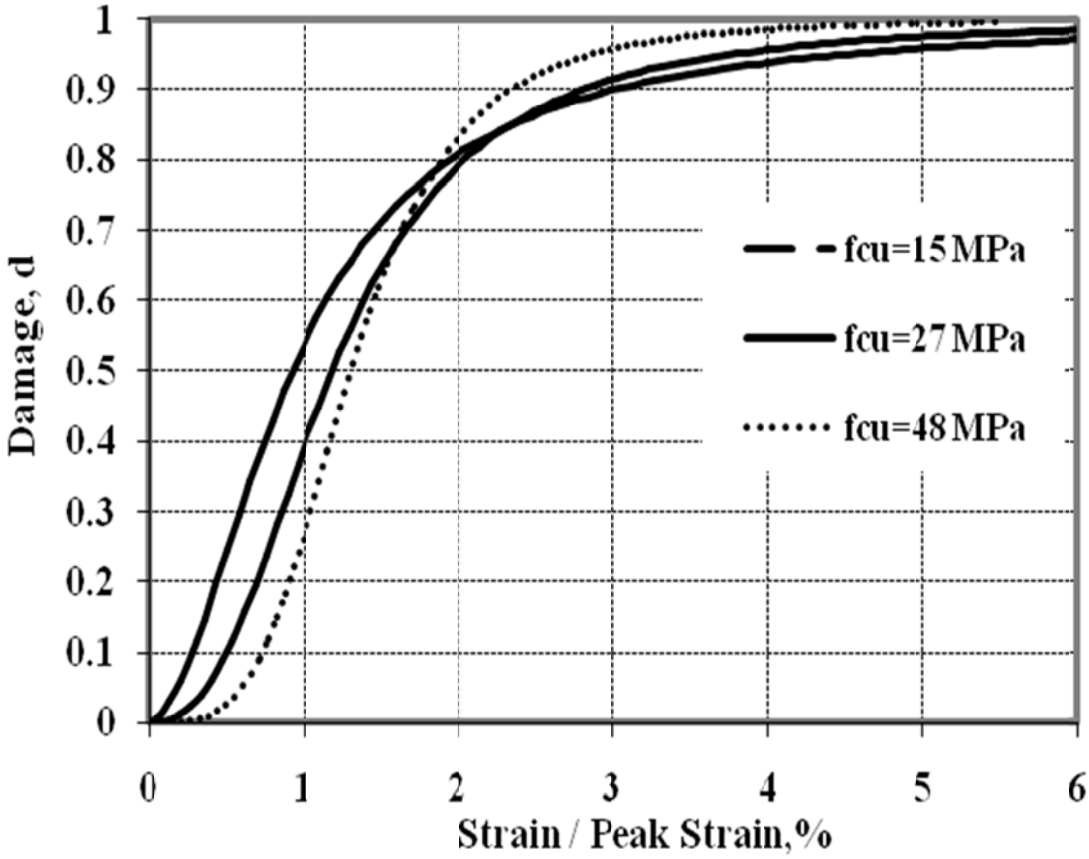

Figure 5.12: Rate of the damage in concrete subjected to different compressive stresses.

54% at the peak strain, while it is about 40% and 25% for concrete with 27 MPa and 48 MPa compressive strength, respectively.

Besides, no damage was found at early state of loading up to 30% of peak stress for concrete with 48 MPa compressive strength while the degradation of the stiffness of concrete starts at 10% and 20% of peak strain for concrete with 15 MPa and 27 MPa compressive strength. After reaching the peak strain, it can be observed from Fig. 3 that in the region of the strain of concrete between the peak strain ε_p and $2\varepsilon_p$, the rate of the damage increases with increasing the compressive strength of concrete. It starts to be higher for axial strain more than $2\varepsilon_p$ which reflect the brittle behavior of concrete as the compressive strength of concrete increases. The damage values could be more as the damage model suggested in this study overestimated the stress in high- strength concrete when the strain is more than $2\varepsilon_p$.

5.2.3 Finite Element Simulation of Chloride Migration in Concrete Subjected to Compressive-Induced Damage

Figure 5.13 shows a comparison between the experimental results of the free chloride profiles for damaged and sound concrete conducted in this study. Based on the numerical solution using COMSOL model, it can be observed that the numerical solution shows good correlation with the experimental results. No significant increase in both free chloride content and penetration depth for concrete subjected to compressive stress up to 40% of ultimate compressive strength, where after that the chloride penetration depth

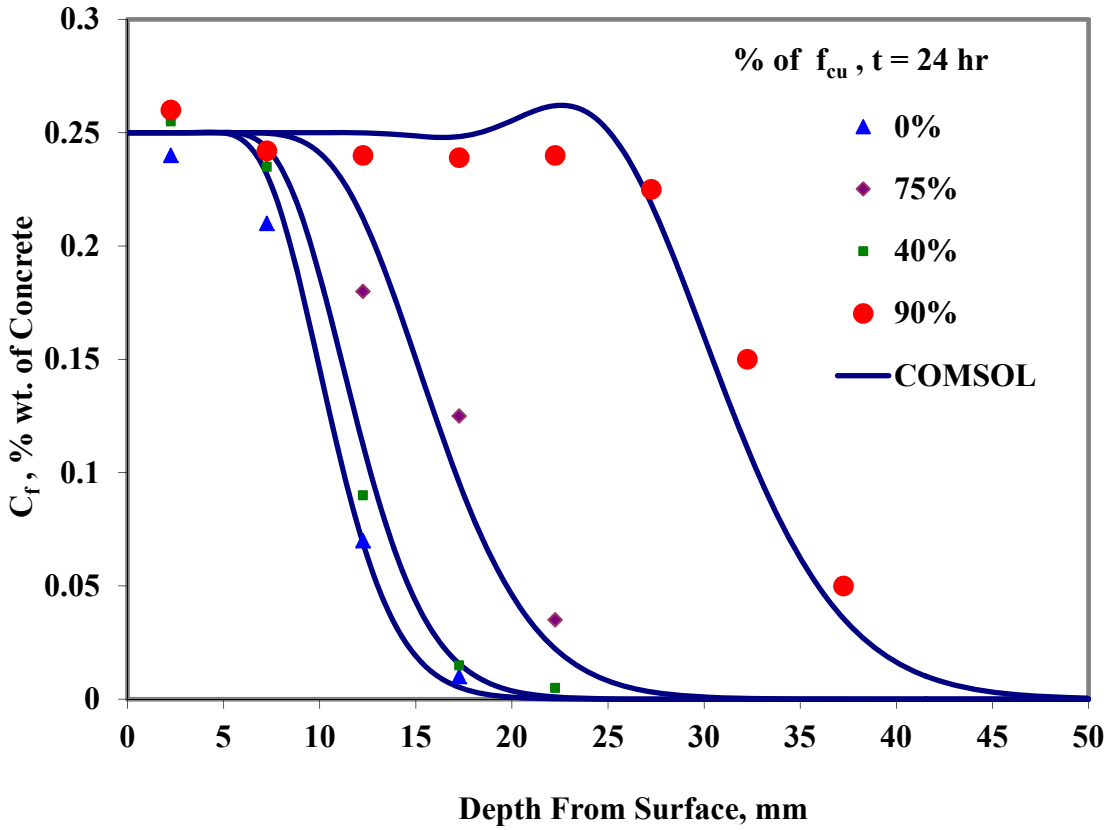

Figure 5.13: Experimental vs COMSOL simulation for free chloride penetration depth in damaged and undamaged concrete.

increase to about 38 and 45 mm for concrete subjected to 75% and 90% of ultimate compressive strength.

The same trend was found in Figure 5.14 where the comparison between COMSOL simulation and experimental results of total chloride contents in all specimens. From Table 5.3 and Figure 5.13 and Figure 5.14, it can be shown that at higher levels of stress, there is a significant increase of chloride migration in concrete up to about three times that of the migration coefficient in undamaged concrete, while the effect of damage is insignificant for concrete subjected to level of compressive stress less than 40% of its compressive strength. While the mechanical damage was noted to increase the chloride migration in concrete significantly, the phenomenon of chloride binding was found to decrease the chloride migration diffusivity by about 20%.

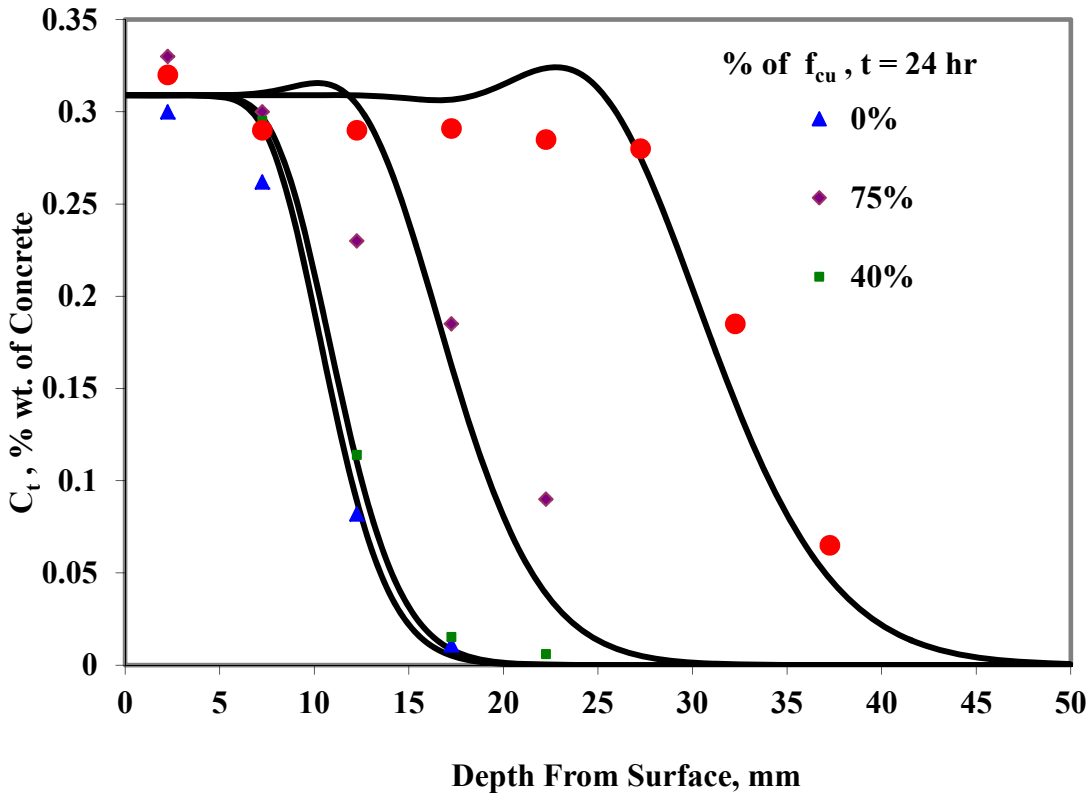

Figure 5.14: Experimental vs COMSOL simulation for total chloride penetration depth in damaged and undamaged concrete.

CHAPTER 6

CHLORIDE DIFFUSION IN RC BEAMS SUBJETED TO FLEXURE

6.1 Experimental Results of the Mechanical Behavior of the RC Beams under Flexural Loading

Table 6.1 shows the details of the cracking loads, deflection and strains in the reinforcement for different damaged RC beams. More details could be found in Figures 6.1 through 6.6 that show the experimental results of load-deflection curves up to failure loading. From Figure 6.1 through 6.6, it can be noted the three zones of the flexural behavior of reinforced concrete beams which are: (I) the elastic zone ended at the first cracking loads which was found vary between 6.5 to 8 kN with an average of 7.5 kN, (II) the cracking section zone and, (III) the steel yielding zone where the reinforced concrete beam approaches to average ultimate load of 95 kN. These results match well with the cracking load calculated using ACI approach (ACI 224R-01, 2001) where it was found about 7.25 kN. Although ACI shows more stiffened behavior than the experimental results after the cracking load, all ACI calculation is presented in Appendix A.

Table 6.1: Details of Cracking and Maximum Flexural Loading, Mid Span deflection and Strains in Reinforcement for Damaged RC Beams.

RC Beams Code	First Crack Load, P_{cr} (kN)	Maximum Load, P (kN)	Mid Span Deflection (mm)	Strain in Reinforcement Steel at Mid Span (μm)
B40	7.5	38	2.5	1500
B60	6.5	62	4.5	2350
B75	7.5	75	5.5	2600
B90	7.5	84	7.0	3400
B100	8	98	9.0	3750

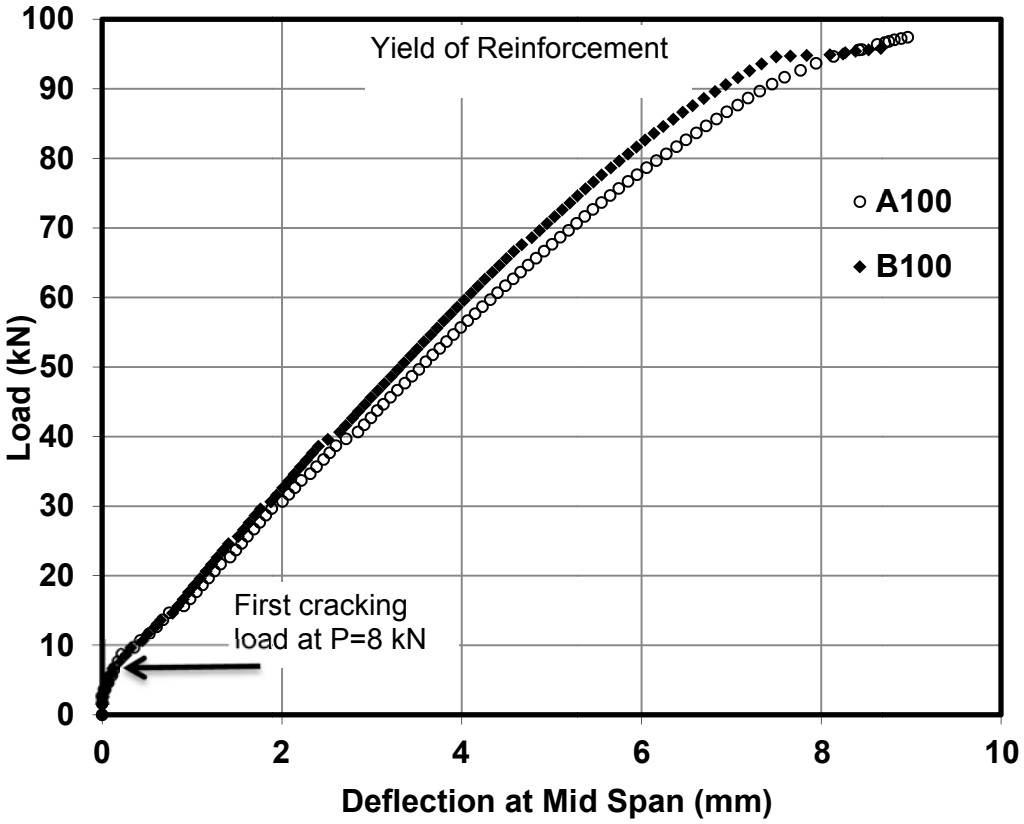

Figure 6.1: Load – mid span deflection curve for A100 and B100 beams.

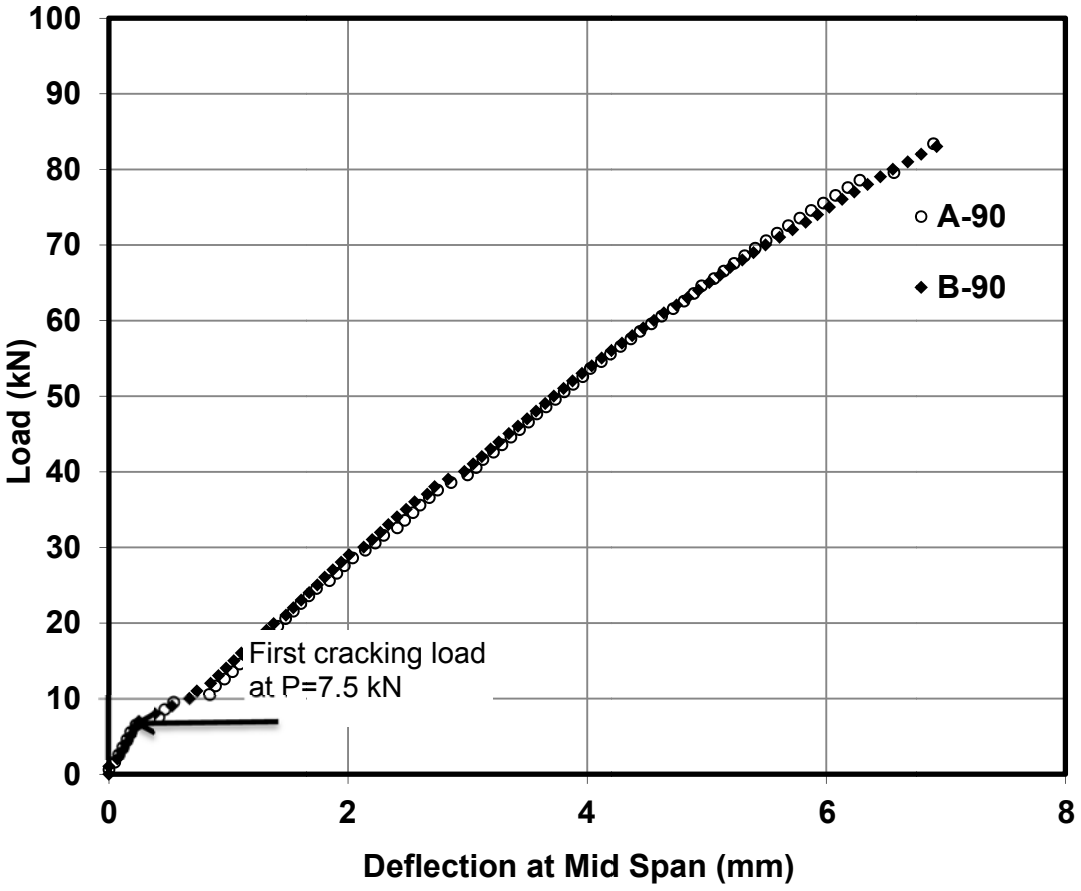

Figure 6.2: Load – mid span deflection curve for A90 and B90 beams.

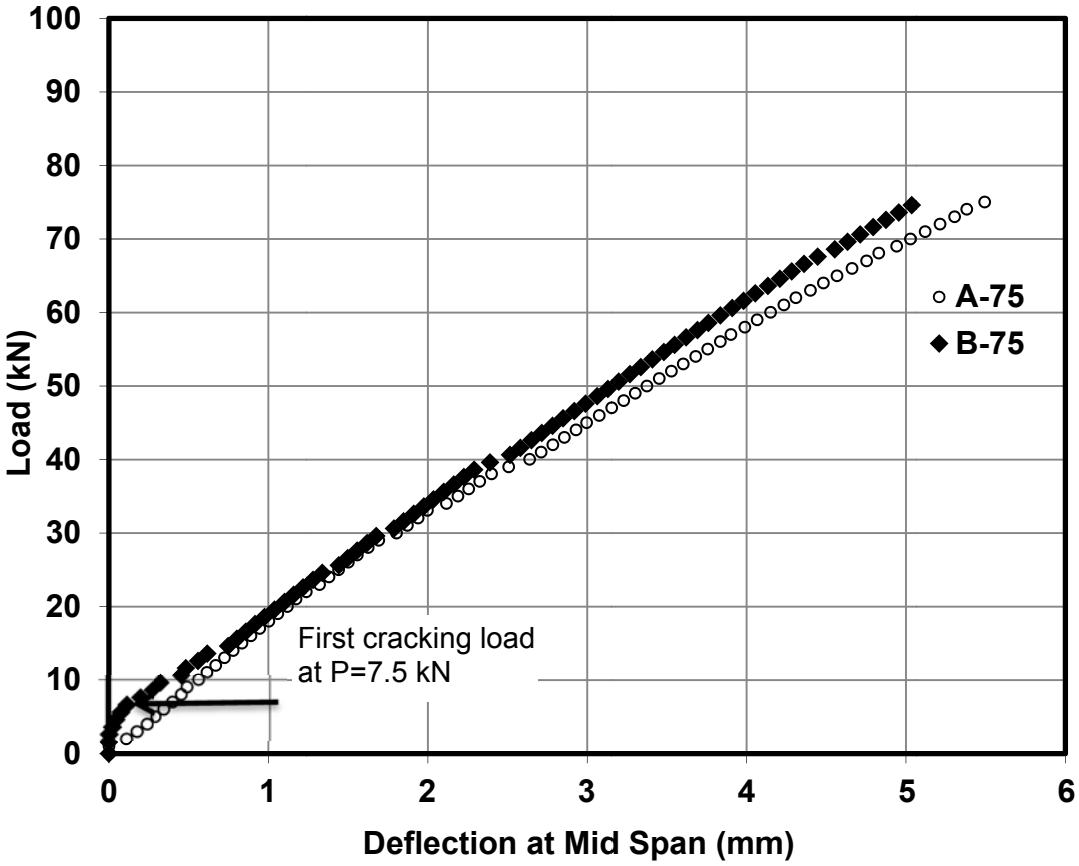

Figure 6.3: Load – mid span deflection curve for A75 and B75 beams.

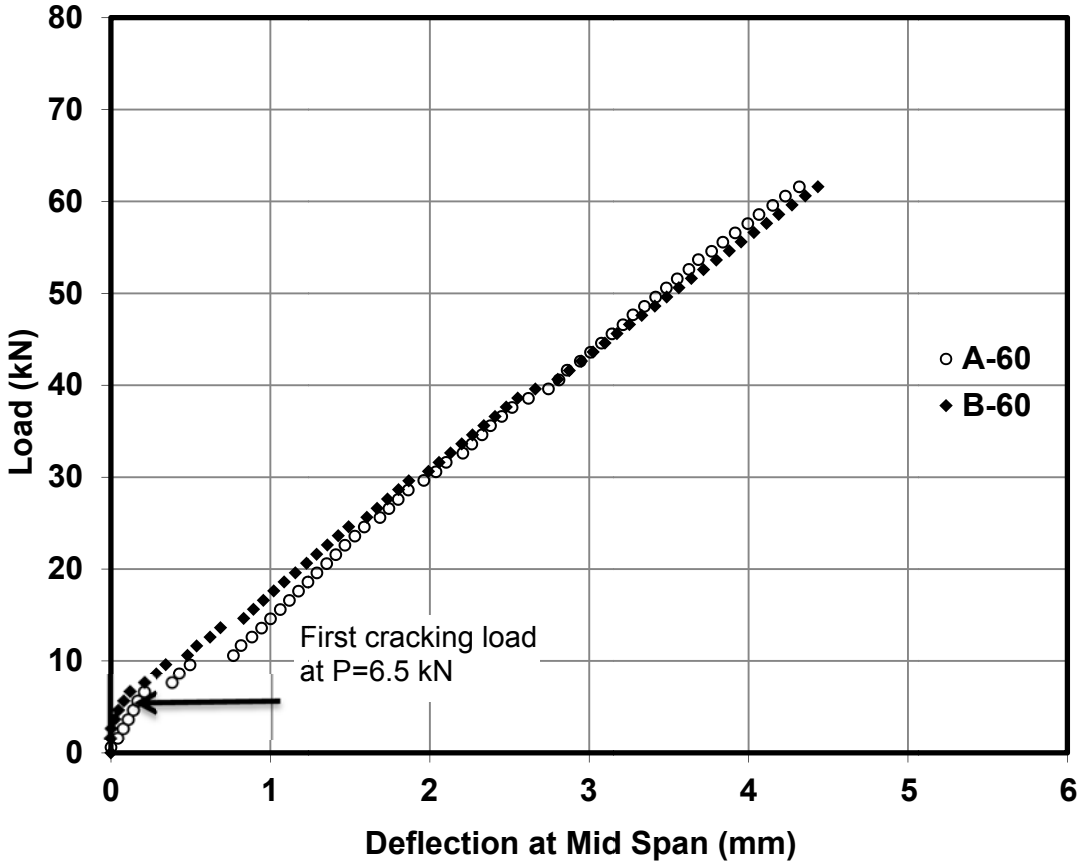

Figure 6.4: Load – mid span deflection curve for A60 and B60 beams.

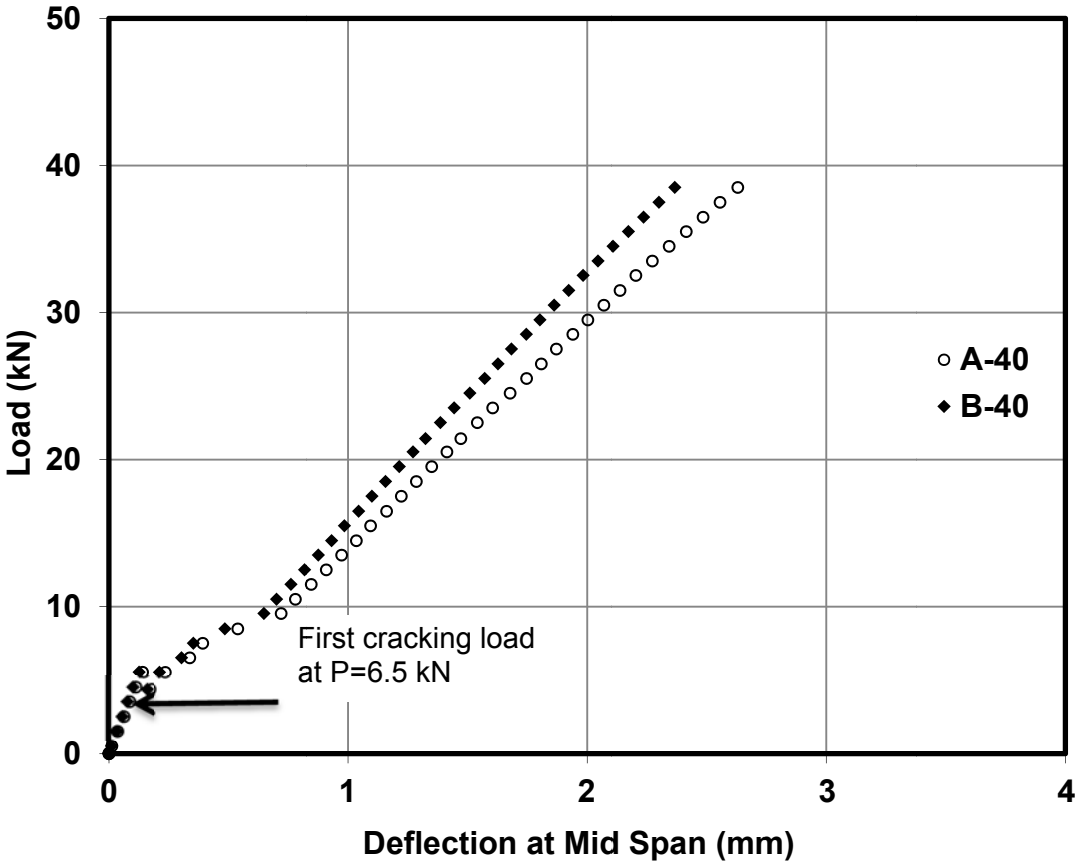

Figure 6.5: Load – mid span deflection curve for A40 and B40 beams.

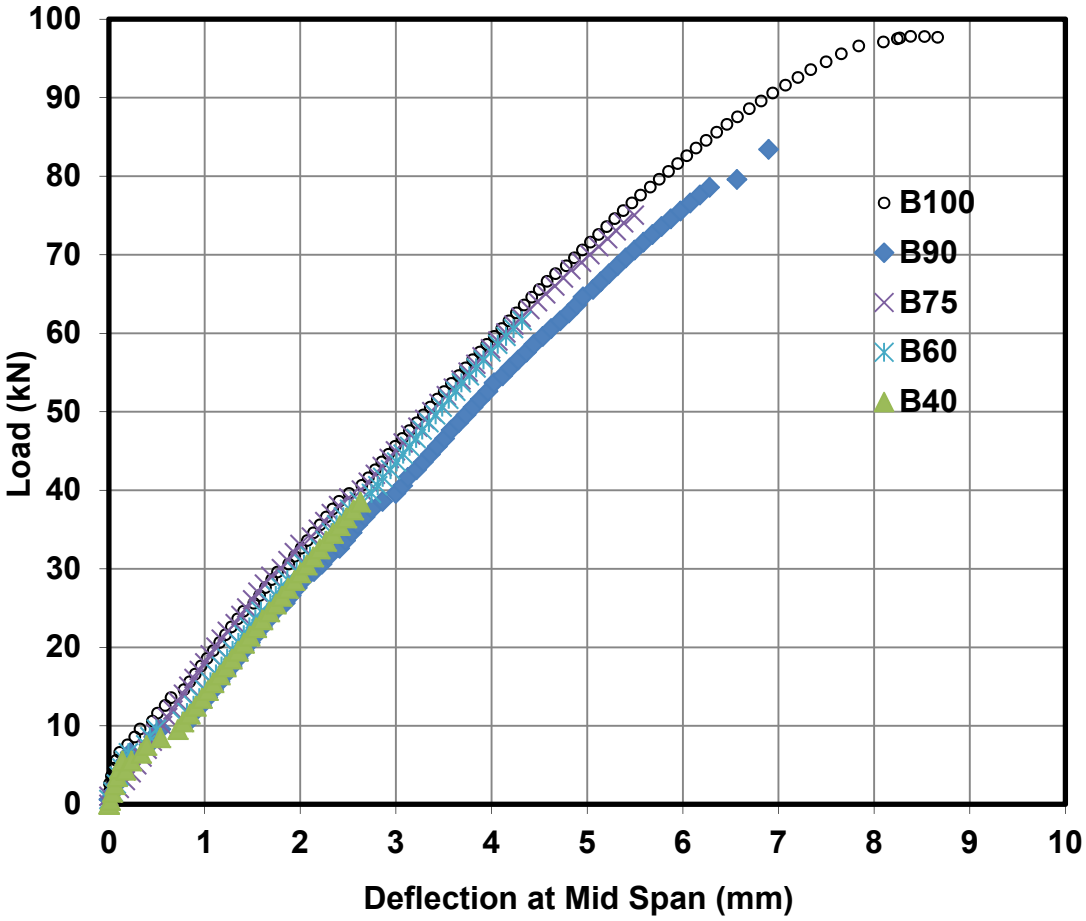

Figure 6.6: Load – mid span deflection curve for 40%, 60%, 75%, 90% and 100% loading.

Figure 6.7 through 6.12 shows the experimental results of reinforcement strain vs. mid span deflection up to failure loading. The strain measurements were measured in the constant moment zone about 500 mm from the support. From the figures, it can be noted that the steel yielding strain in tensile reinforcement was 3500 μm at the maximum mid-span deflection of about 8 mm. Figure 6.13 shows the cracking map of up to failure loading. It can be noted that the maximum cracking depth was found to be about 90 mm These results match with the calculated value of z using ACI procedures (ACI 224R-01, 2001) as shown in Appendix A in which z was found about 92.4 mm from bottom of the beam.

6.2 Experimental Results of Free and Total Chloride Contents in RC Beams Subjected to Stress-Induced Damage

6.2.1 Effect of Tensile Stresses on Chloride Diffusion in RC Beams

Figures 6.14 through 6.20 show the total, free and bound chloride profiles in sound and damaged RC beams subjected to different flexural loading after 90 days of exposure to 0.3% of free chloride at a distance of 120 mm and 550 mm from the edge of the beam and from the bottom of the RC beams. All experimental results for chloride content in the tensile zone for different damaged beams are presented in Table 6.2. Figure 6.14 and Table 6.2 show the total, bound and free chloride profiles for undamaged RC beam after 90 days of exposure to 8% of NaCl where, the free chloride in undamaged RC beam was found to be 0.18% by weight of concrete, while the total and bound chloride were 0.3% and 0.12% by weight of concrete, respectively.

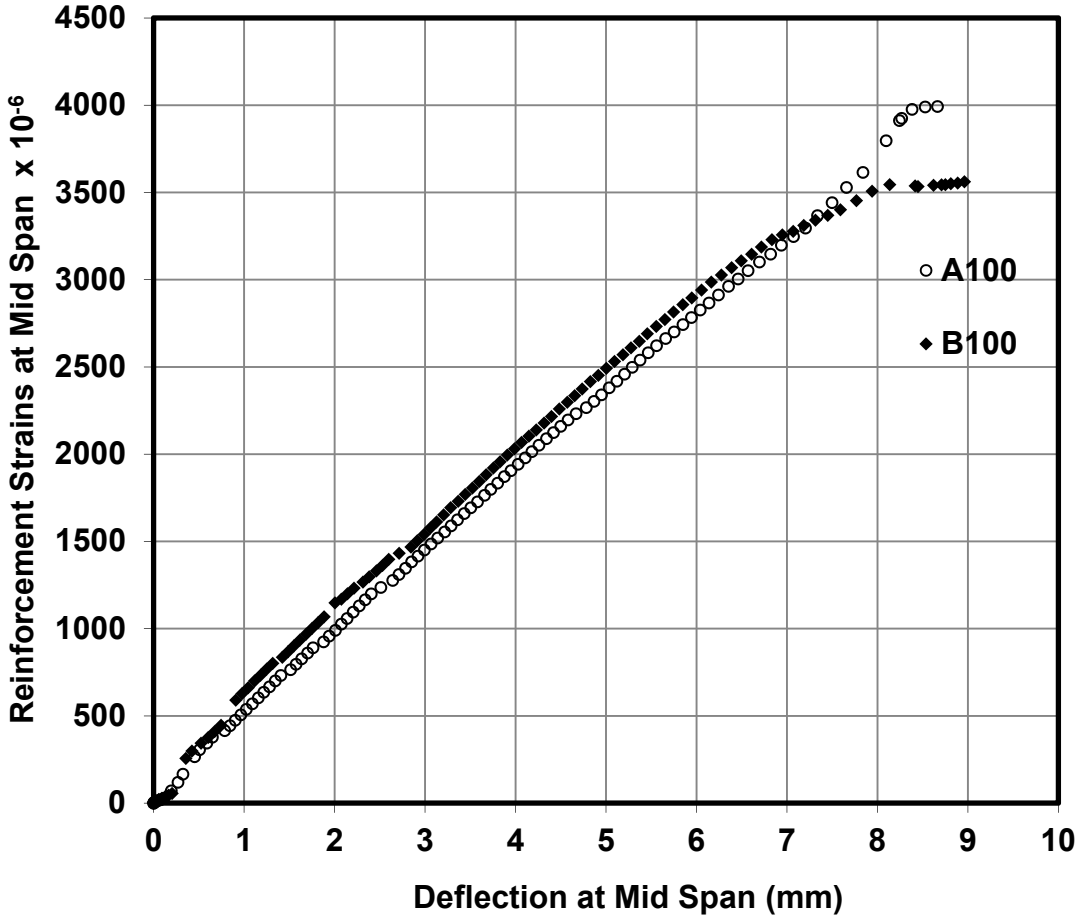

Figure 6.7: Strain in tensile reinforcement at mid span vs mid span deflection curve for A100 and B100 beams.

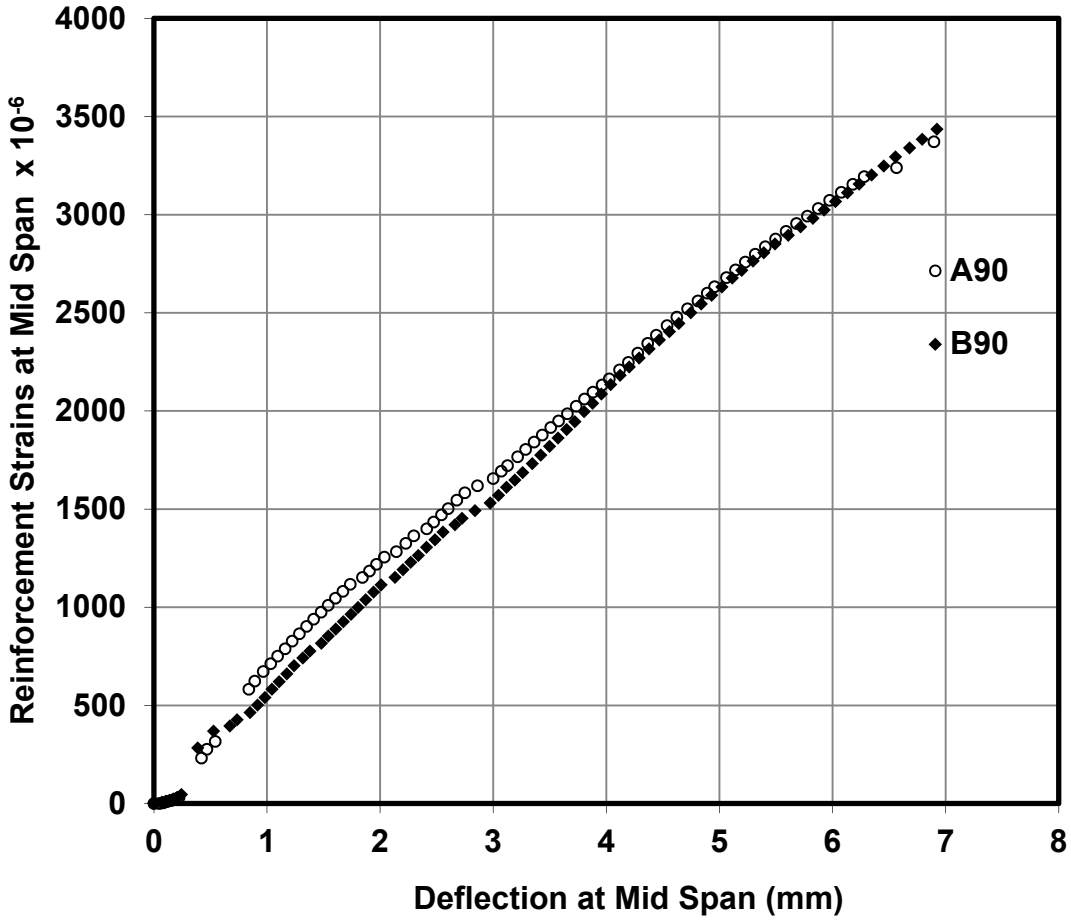

Figure 6.8: Strain in tensile reinforcement at mid span vs mid span deflection curve for A90 and B90 beams.

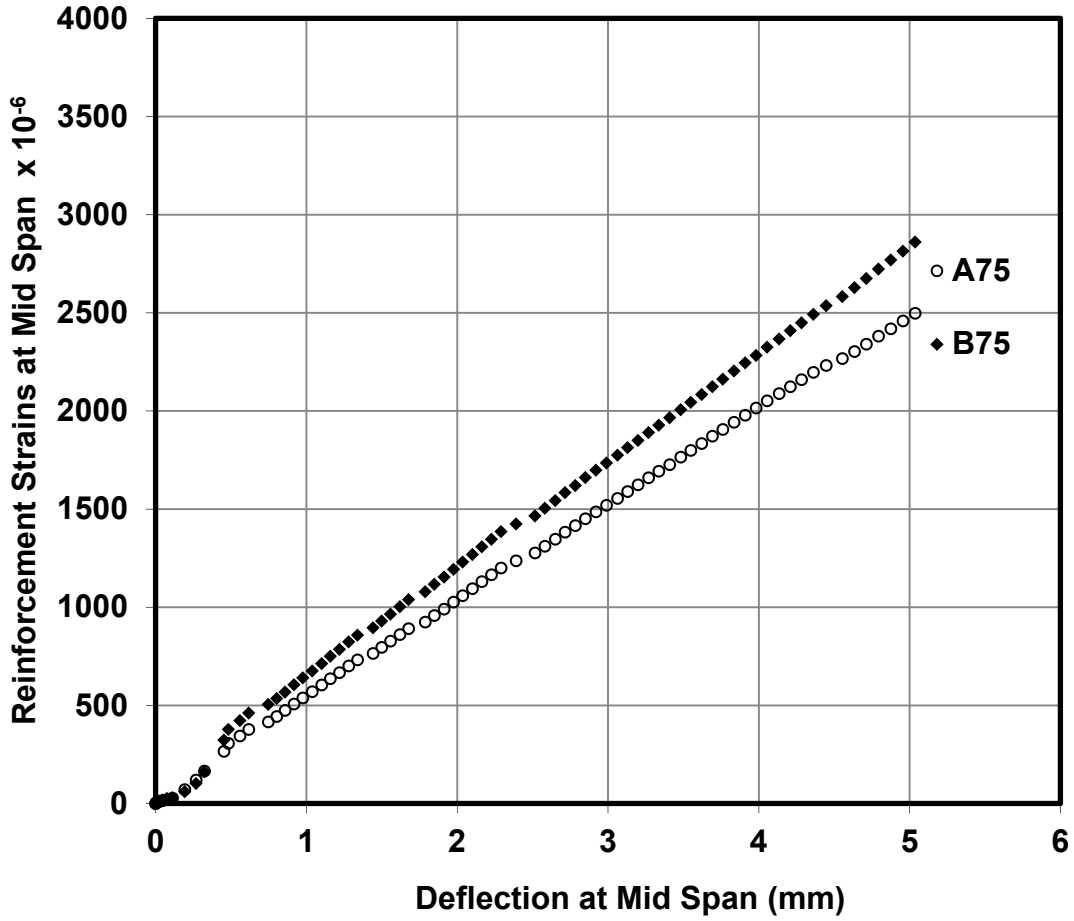

Figure 6.9: Strain in tensile reinforcement at mid span vs mid span deflection curve for A75 and B75 beams.

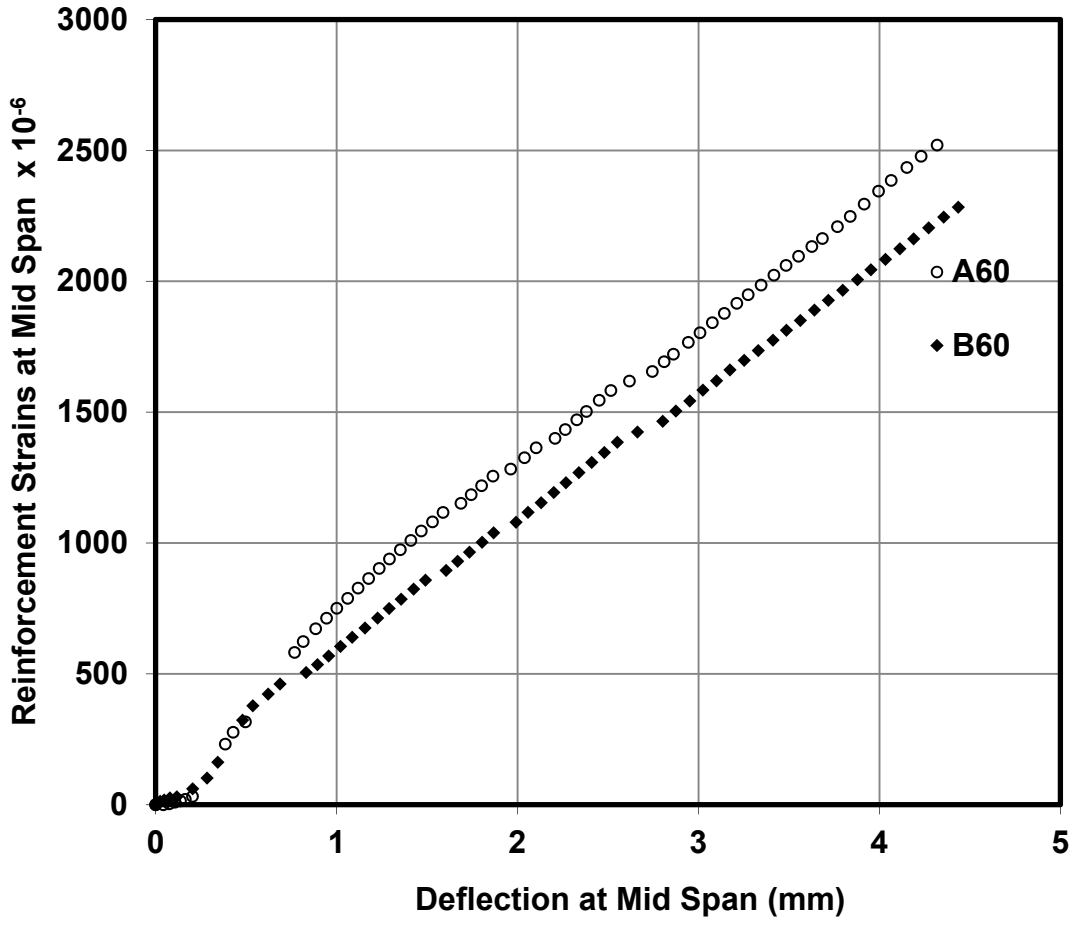

Figure 6.10: Strain in tensile reinforcement at mid span vs mid span deflection curve for A60 and B60 beams.

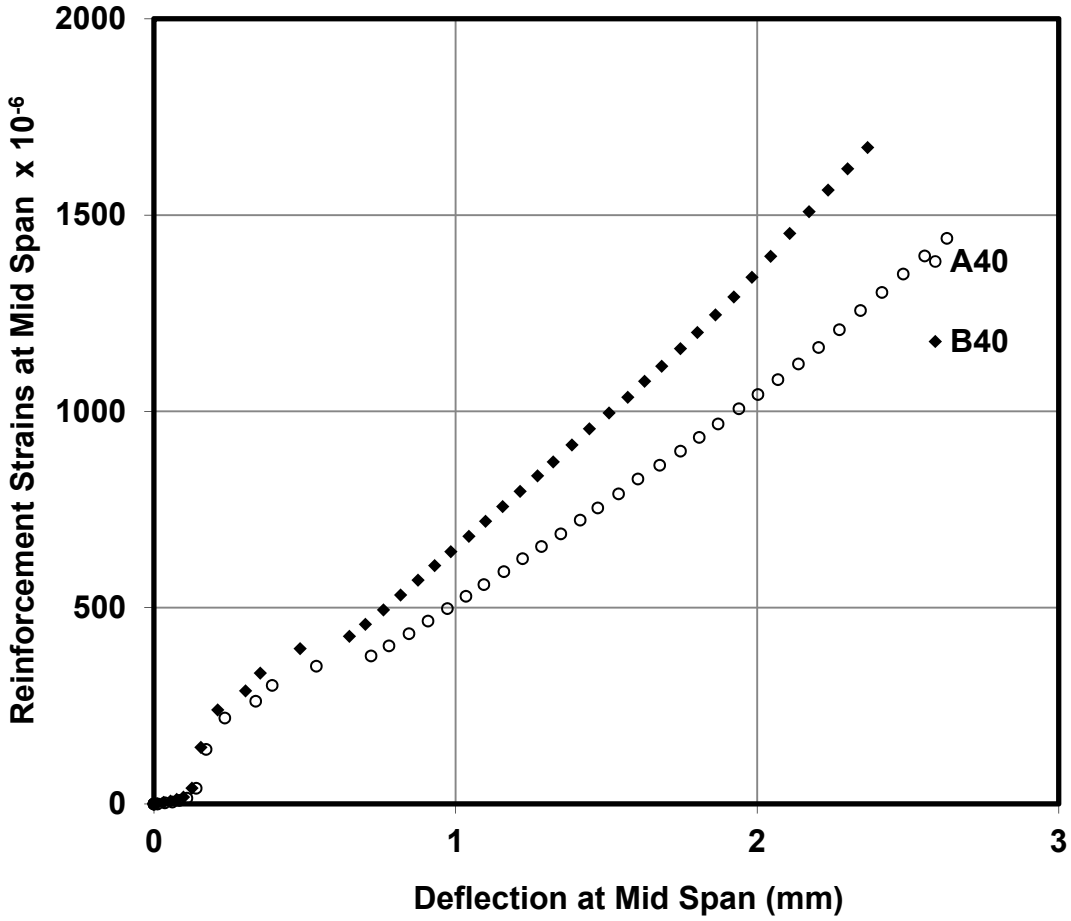

Figure 6.11: Strain in tensile reinforcement at mid span vs mid span deflection curve for A40 and B40 beams.

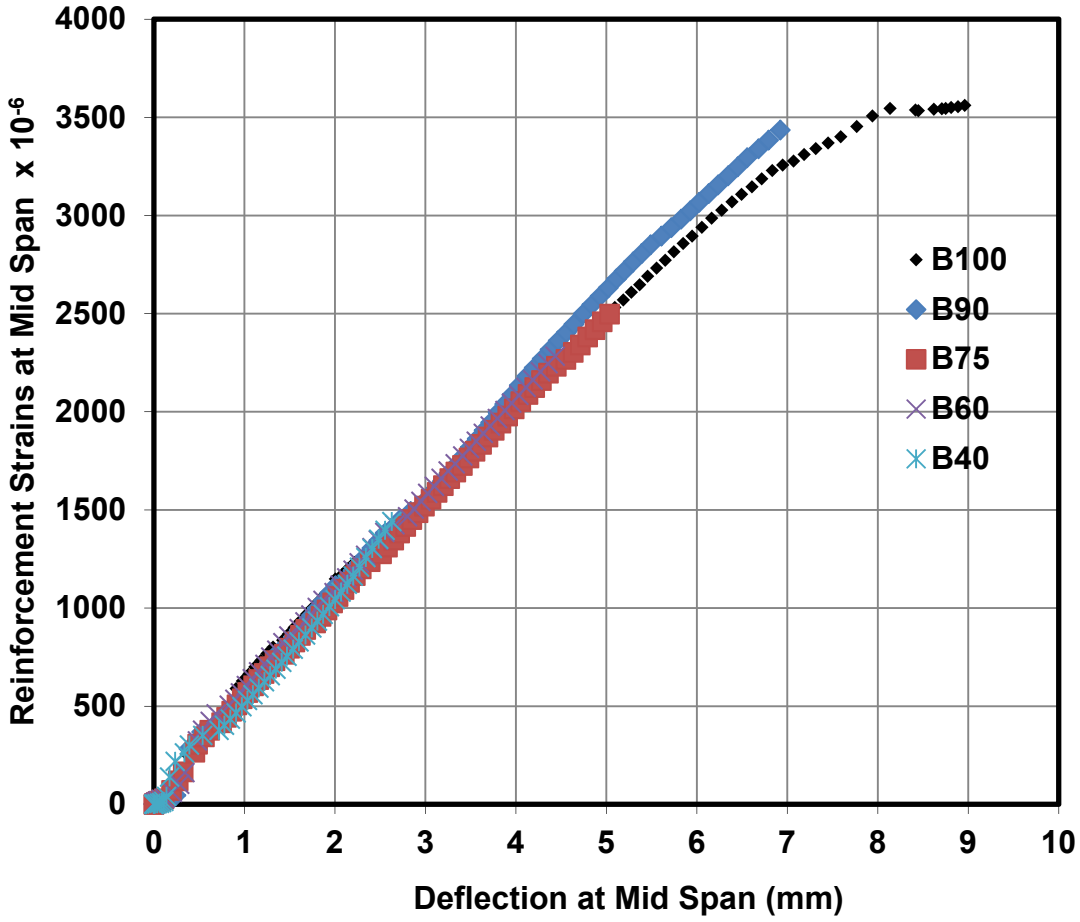

Figure 6.12: Strain in reinforcement vs mid span deflection curve for 40%, 60%, 75%, 90% and 100% loading.

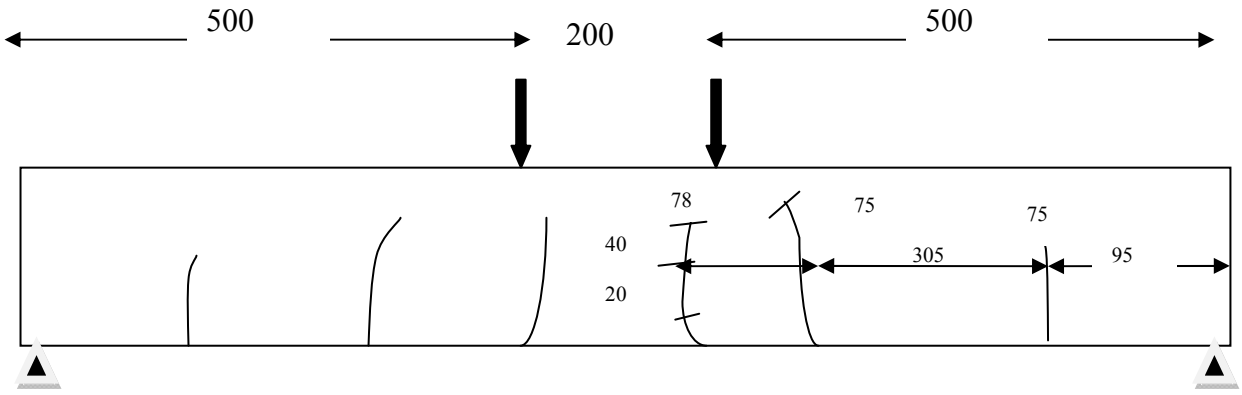

Figure 6.13: Cracking map of up to 100% loading.

Table 6.2: Chloride content in % by weight of concrete for undamaged and in the tensile zone of damaged RC beams.

Beam	**Depth, (mm)**	**2.25**	**7.25**	**12.25**	**17.25**	**22.25**
Undamaged Beam	C_f **%**	0.18	0.065	0.02	0.01	0.005
	C_t **%**	0.30	0.165	0.05	0.035	0.013
B40	C_f **%**	0.20	0.08	0.03	0.02	0.005
	C_t **%**	0.28	0.165	0.09	0.035	0.013
B60	C_f **%**	0.23	0.10	0.05	0.03	0.01
	C_t **%**	0.36	0.23	0.12	0.05	0.01
B75	C_f **%**	0.26	0.165	0.09	0.035	0.013
	C_t **%**	0.38	0.30	0.17	0.11	0.05
B90	C_f **%**	0.26	0.22	0.14	0.05	0.01
	C_t **%**	0.41	0.32	0.23	0.08	0.023

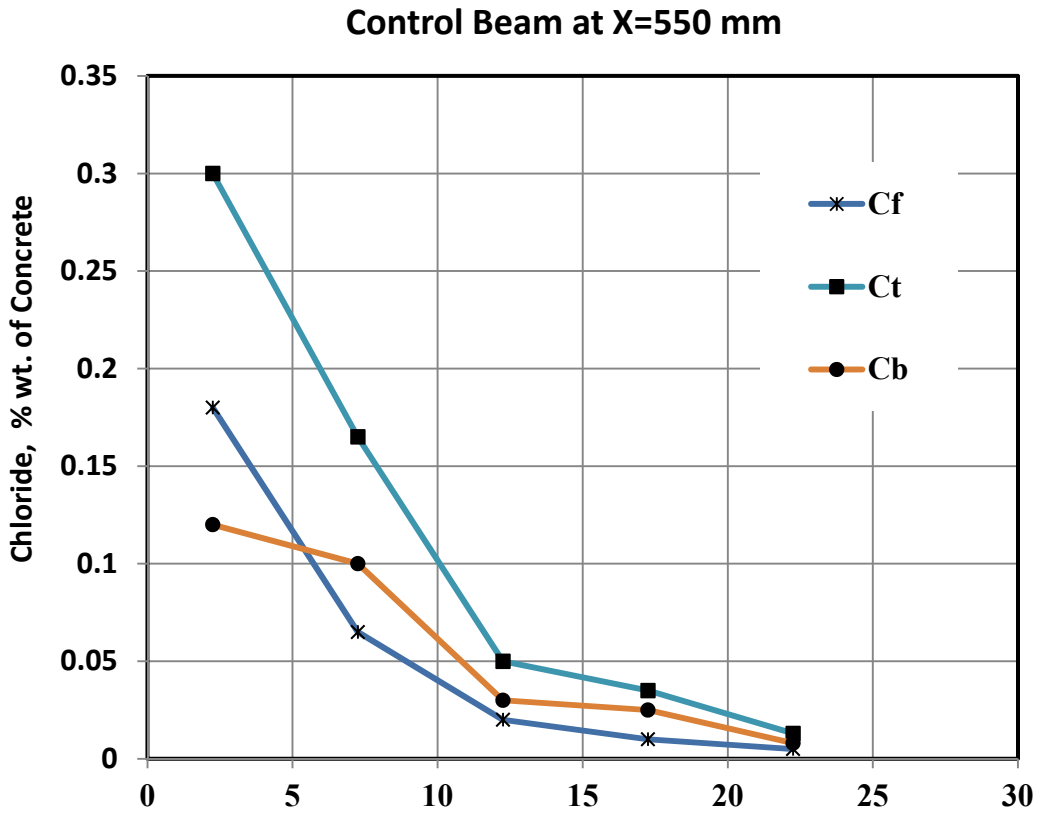

Figure 6.14: Total, bound and free chloride penetration in undamaged RC beams.

The total, bound and free chloride profiles for RC beam subjected to 40% of ultimate flexural loading after 90 days of exposure to 8% of NaCl are presented in Figure 6.15 where the free chloride was found to be 0.20% by weight of concrete, while the total and bound chloride were 0.28% and 0.08% by weight of concrete, respectively. Theses values decrease to a range below 0.02% by weight of concrete. With increasing the flexural loading, the chloride contents tend to increase as shown in Figure 6.16, where the chloride profiles for total, bound and free chloride contents are presented for RC beams subjected to 60% of its ultimate flexural loading. From Figure 6.16, the total chloride content increases up to 0.36% by weight of concrete and the fee chloride was found to be 0.23% while the bound chloride stable at a level of 0.13% by weight of concrete.

The total, bound and free chloride profile for RC beam subjected to 75% of ultimate flexural loading after 90 days of exposure to 8% of NaCl is presented in Figure 6.17 where the free chloride was found to be 0.26% by weight of concrete, while the total and bound chloride were 0.39% and 0.13% by weight of concrete, respectively. These values decrease to a range below 0.05% by weight of concrete. Figure 6.18 shows the chloride profiles for total, bound and free chloride contents for RC beams subjected to 90% of its ultimate flexural loading. From Figure 6.18, the total chloride content increased up to 0.42% by weight of concrete and the fee chloride was found to be 0.26% while the bound chloride was at a level of 0.16% by weight of concrete. From these figures, it can be noted that the measured free and total chloride percentages increase with the increase of the tensile stress.

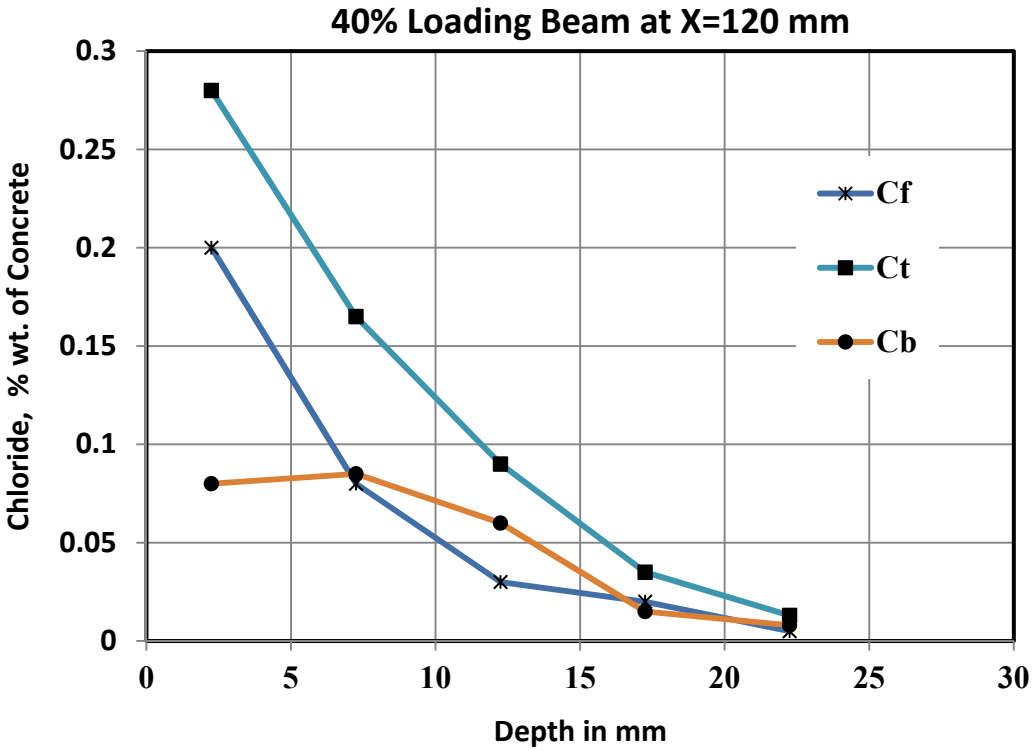

Figure 6.15: Total, bound and free chloride penetration in the tensile zone of 40% loaded RC beam.

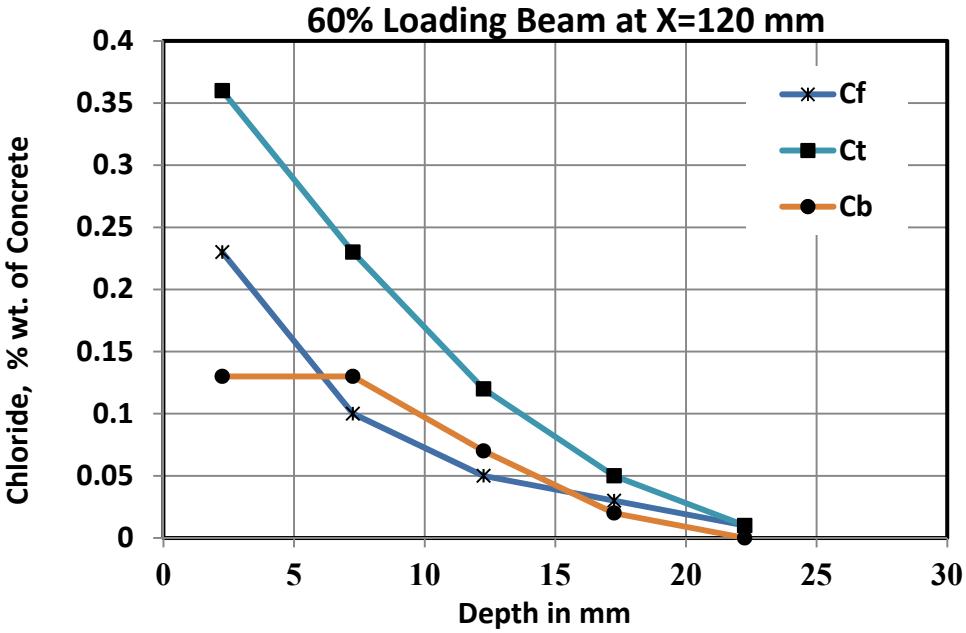

Figure 6.16: Total, bound and free chloride penetration in the tensile zone of 60% loaded RC beam.

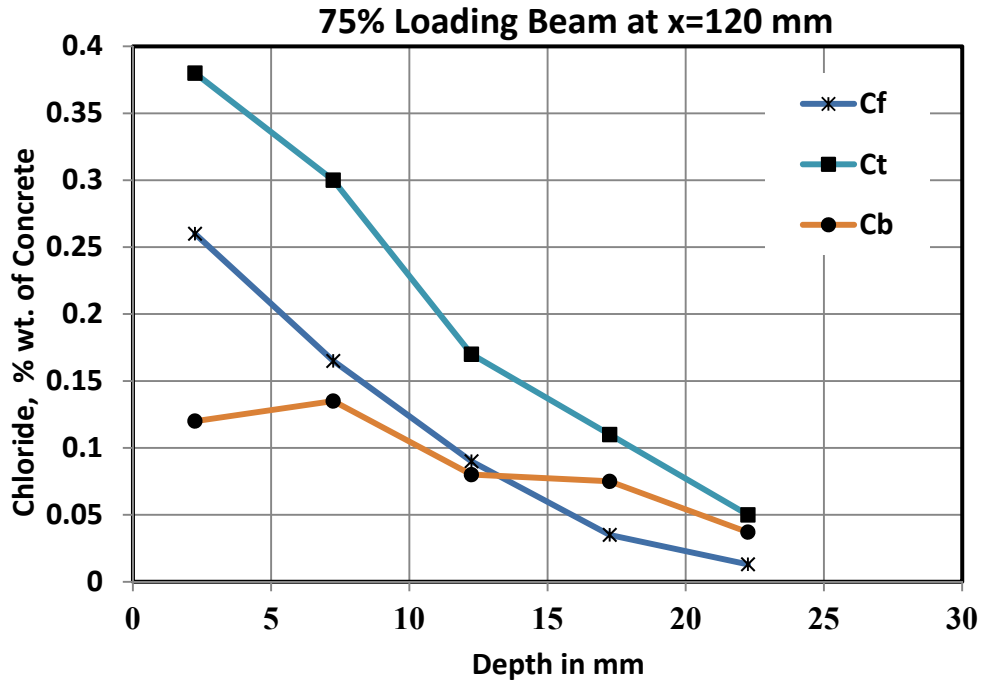

Figure 6.17: Total, bound and free chloride penetration in the tensile zone of 75% loaded RC beam.

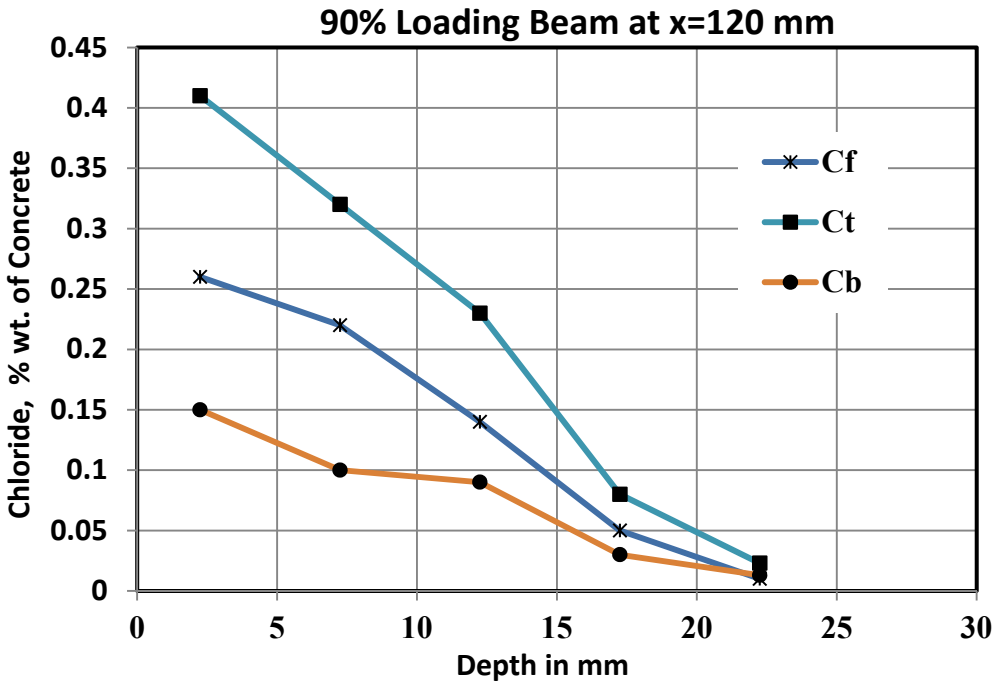

Figure 6.18: Total, bound and free chloride penetration in the tensile zone of 90% loaded RC beam.

A comparison between free, total and bond chlorides for undamaged and damaged RC beams is shown in Figures 6.19 through 6.20. From Figure 6.19 and Figure 6.20, it can be noted that with increasing the tensile stress, there is significant increase in the free and total chlorides. From Figure 6.19, it is observed that the free chloride content increases from 0.18% by weight of concrete for undamaged concrete at a depth of 2.5 mm up to 0.20%, 0.23% and 0.26% by weight of concrete for 40%, 60%, and 90% loaded RC beams.

Tables 6.3 summarize the correlation between the damage influence function F_d and the effective diffusion coefficients in damaged concrete subjected to tensile stresses. For undamaged concrete, D_{effd} (D_d F_{cb}) was 2.1×10^{-6} mm^2/s and for the tensile damaged concrete corresponding to stress levels of 40%, 60%, 75% and 90% of the ultimate flexural loading, the effective diffusion coefficient D_{effd} was computed as $7.4\text{x}10^{-6}$, $1.7\text{x}10^{-5}$, $2.1\ \text{x}10^{-5}$ and 2.2×10^{-5} mm^2/s, respectively as shown in Table 6.3. This indicates significant increase of diffusivity in the tensile zone of about 3.0, 6.7, 8.3, 8.7 times the chloride diffusion coefficients in undamaged, when the RC beams loaded up to 40%, 60%,75% and 90% of its ultimate flexural load, respectively. Similar conclusions was reported by Gerard and Marchand (2000), in which the presence of continues cracks tends to markedly modify the transport coefficient of the solid while the diffusivity of the concrete can be increased by a factor ranging from 2 to 10. Experimental results reported by He and Gong [2005] and Xing et al. [2005] showed significant increase in the chloride diffusivity of concrete up to two times the chloride diffusion in sound concrete.

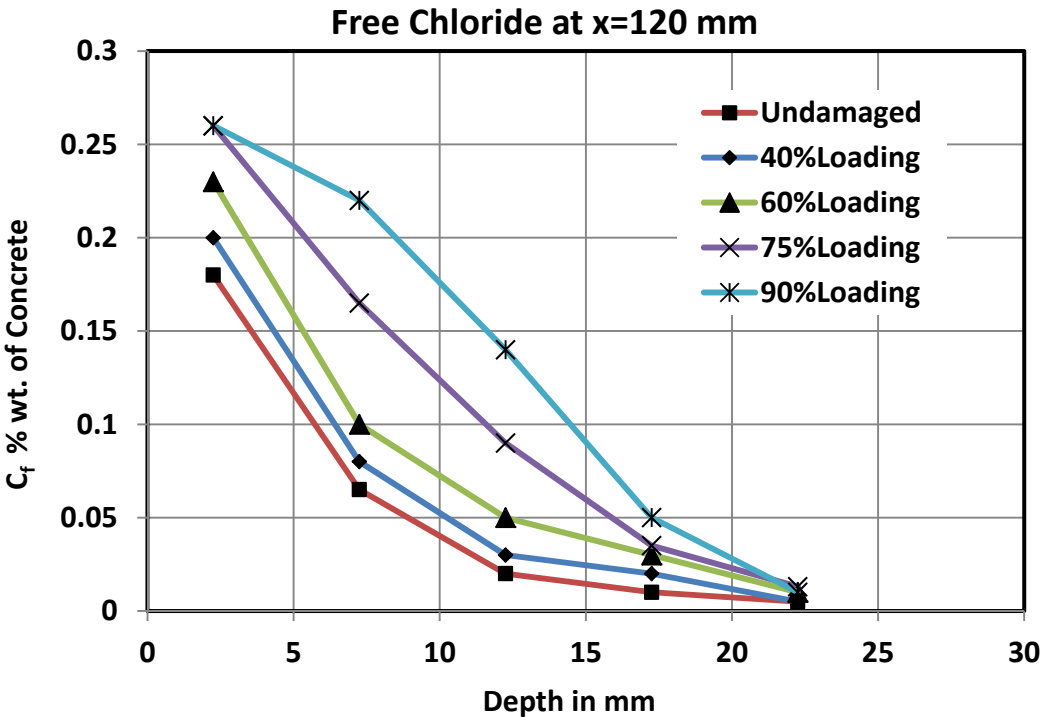

Figure 6.19: Free chloride profile in sound and in the tensile zone of damaged RC beam.

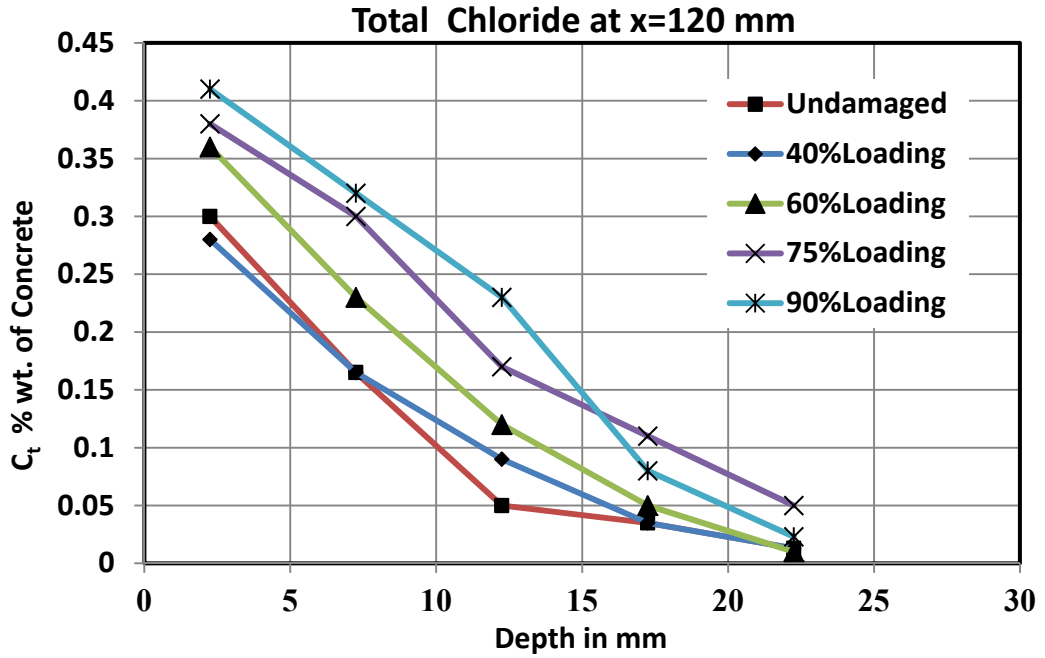

Figure 6.20: Total chloride profile in sound and in the tensile zone of damaged RC beam.

Table 6.3: Correlation between damage function F_d and chloride diffusivity at various tensile stress levels

level of loading	***d***	D_{effd} (mm^2/s)	$F_d=D_{effd}/(D_d \times F_{cb})$
0	0	2.1×10^{-6}	1.0
40	0.62	7.4×10^{-6}	3.0
60	0.74	1.7×10^{-5}	6.7
75	0.95	$2.1\text{x}10^{-5}$	8.3
90	0.98	$2.2\text{x}10^{-5}$	8.7

6.2.2 Effect of Compressive Stresses on Chloride Diffusion in RC Beams

Figure 6.21 and Figure 6.22 show the total and free chloride profiles in sound and damaged RC beams subjected to different flexural loading after 90 days of exposure to 0.3% of free chloride at a distance of 550 mm from the edge of the beam and from the top of the RC beams. All experimental results for chloride content in the compressive zone for different damaged beams are presented in Table 6.4.

From Figure 6.21 and Figure 6.22, it can be noted that there is insignificant increase of chloride diffusivity up to 60% of ultimate flexural loading. From Figure 6.21, it is observed that the free chloride content increases from 0.18% by weight of concrete for undamaged concrete at a depth of 2.5 mm up to 0.20% and 0.22% by weight of concrete for 75%, and 90% loaded RC beams.

For damaged concrete in compressive zone, the chloride diffusion coefficients in concrete is presented on Table 6.5 for the compressive damaged concrete corresponding to stress levels of 60%, 75% and 90% of the ultimate flexural loading. Whereby the effective diffusion coefficient D_{effd} was computed as $2.9\text{x}10^{-6}$, $3.1\text{x}10^{-6}$ and 3.6×10^{-6} mm^2/s, respectively. It was noted that up to 60% of ultimate flexural loading, the chloride diffusion coefficient did not increase while at higher level of compressive stress there was increase in the chloride diffusivity up to 50% more than the chloride diffusivity in sound concrete.

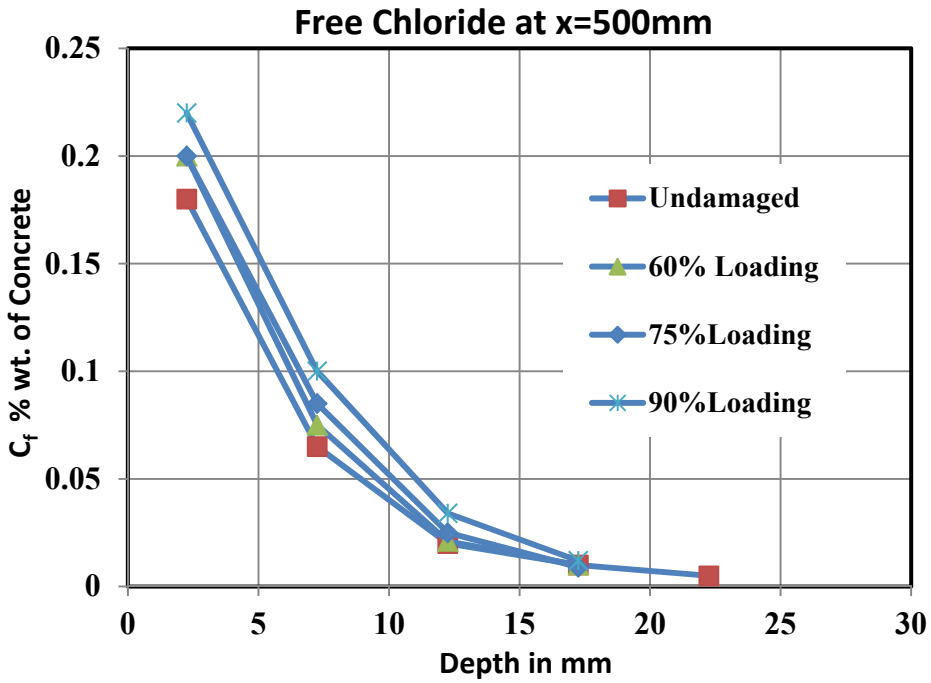

Figure 6.21: Free chloride profile in sound and in the compressive zone of damaged RC beam.

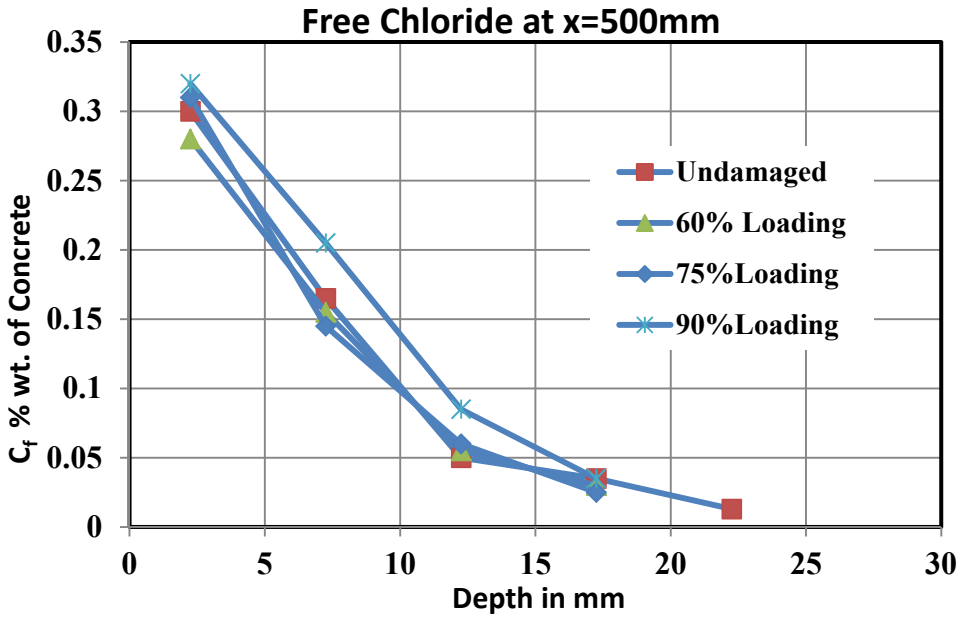

Figure 6.22: Total chloride profile in sound and in the compressive zone of damaged RC beam.

Table 6.4: Chloride content in % by weight of concrete for undamaged and in the compressive zone of damaged RC beams.

Beam	Depth, (mm)	2.25	7.25	12.25	17.25	22.25
B60	C_f %	0.200	0.075	0.021	0.010	0.200
	C_t %	0.280	0.155	0.055	0.030	0.280
B75	C_f %	0.200	0.085	0.025	0.009	0.200
	C_t %	0.310	0.145	0.060	0.025	0.310
B90	C_f %	0.220	0.100	0.034	0.012	0.220
	C_t %	0.320	0.205	0.085	0.035	0.320

Table 6.5: Correlation between damage function F_d and chloride diffusivity at various compressive stress levels.

level of loading	d	D_{effd} (mm^2/s)	$F_d=D_{effd}/(D_d*F_{cb})$
0	0	2.1×10^{-6}	1.00
60	0.10	2.9×10^{-6}	1.15
75	0.15	3.1×10^{-6}	1.23
90	0.40	3.6×10^{-6}	1.43

Similar experimental observations have been reported by several researchers. Wang et al. (2008) concluded that the chloride diffusivity of concrete under compression and tension increases rapidly when the applied stress surpasses a certain threshold value. Sakoi and Horiguchi (2006) studied the loading effects on chloride penetration in fiber reinforced concrete and they reported that for concrete samples subjected to compressive stress up to 80% of ultimate strength there was about 70% increase in the chloride diffusion coefficient compared to sound concrete samples.

Chatzigeorgiou et al., [2005] investigated the coupled problem of mechanical damage and the permeability of concrete and concluded that the permeability of concrete increases drastically when the load is very close to the ultimate strength of the material, where the increase of applied compressive stress will lead to the formation of microcrack networks and the density of distribution of these cracks will increase as the applied compressive stress increases (Pijaudier-Cabot et al [2009]). Kamaran et al. [1998] conducted an experimental study to evaluate development of microcracks in concrete subjected to compressive loading. Scanning electron micrescopic (SEM) images showed that in undamaged concrete the interfacial transition zone is mostly a collection of interconnected pores, and once the load is applied these pores connect to form microcracks and they propagate to connect with the microcraks generated in the cement paste matrix. Based on the damage model and the ratio of diffusion coefficient of damaged and undamaged samples ($D_{effm}/ D_d. F_{cb}$), the damage influence function F_d was established as follows (see Figure 6.23):

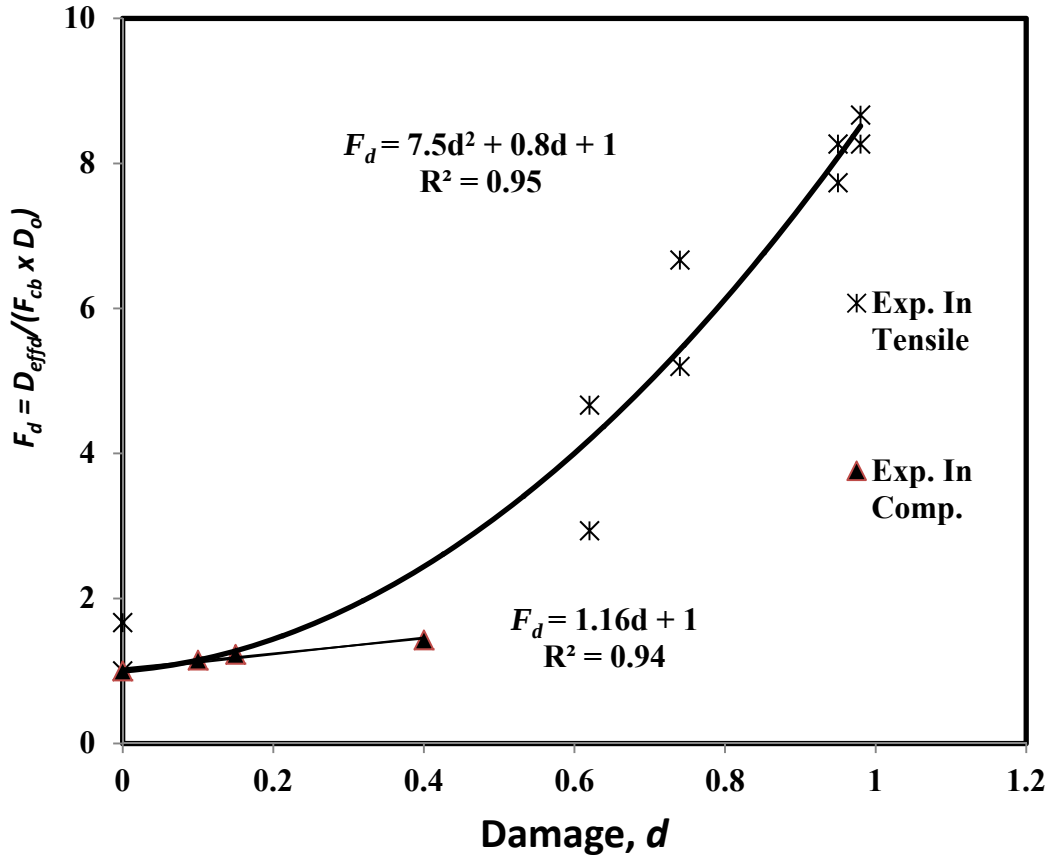

Figure 6.23: Relationship between mechanical damage and D_{effd}.

For the tensile zone: $F_d = D_{effm} / (D_d \,.\, F_{cb}) = 7.5\, d^2 + 0.8\, d + 1$ [6.1a]

For the compressive zone: $F_d = D_{effm} / (D_d \,.\, F_{cb}) = 1.16 d + 1$ [6.1b]

6.2.3 Chloride Binding Isotherm

The results of free and bound chlorides for different RC beams were presented in Figure 6.24. As expected, it can be noticed that increasing the free chloride leads to increase of bound chloride up to a limit state. From the experimental results, a Langmuir isotherm model was found to be the best fit and the model parameters were found as 2.39 for α and 15.6 for β. These parameters are used in the binding capacity influence function F_{cb} as defined in equation [3.13]. The Langmuir isotherm model is then described as:

$$C_b = \frac{2.39 C_f}{1 + 15.6 C_f} \qquad [6.2]$$

$$F_{cb} = \frac{1}{\left(1 + \frac{2.39}{\left(1 + 15.6 C_f\right)^2}\right)} \qquad [6.3]$$

6.2.4 Effect of Crack widths on chloride diffusivity in RC beams Subjected to Flexural Loading.

Several studies were conducted in the last decade to investigate the transport properties of concrete. Pijaudier-Cabot et al. (2009) suggested a formula describing the evolution of permeability with damage which matches consistently two extreme configurations: the first one when the permeability as a function of distributed diffuse damage and second one when it is govern by the crack opening. Two zones were applied; when the scalar

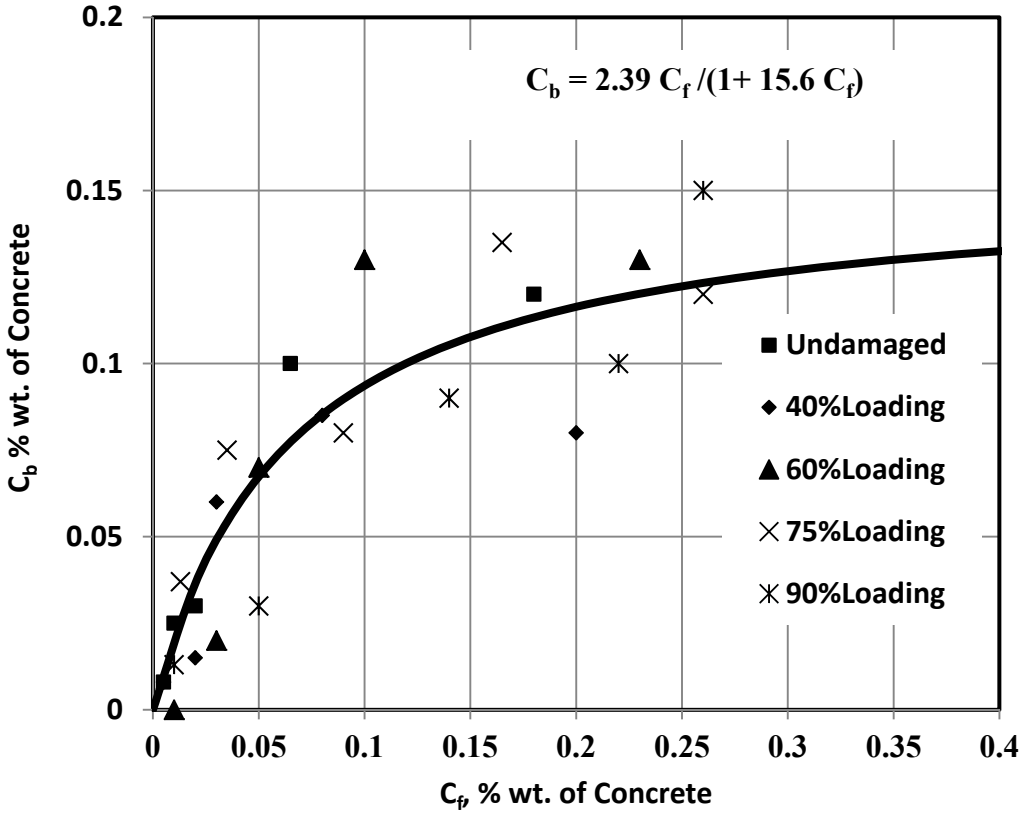

Figure 6.24: Relationship between free and bound chloride.

damage is close to zero then the first concept is used, and when the scalar damage is close to one the crack opening parameter is used.

Following the same approach, the chloride profile was measured in the maximum crack widths for different loaded RC beams. Table 6.6 and Figure 6.25 show the free chloride profile along the crack wall with different crack widths ranging from 0.25 to 1 mm in damaged RC beams. In the location of the maximum crack width which is located under the point loading, the powder samples were taken for the depth of 40 mm. from Figure 6.25, it could be noted that although there is an increase in the chloride content with increasing the crack width, the effect of the crack width was reduced as the depth of the crack increased.

Same conclusion was reported by Kato et al. (2005), where in their study; they reported that the chloride content in cracked zone in concrete increased with the increase in the crack width up to 0.075 mm. Kato et, al (2005) also concluded that the chloride content in the cracked zone decreased with the increase in the depth from the exposed surface. Ishida et.al (2009) developed chloride transport model for sound and cracked concrete with crack widths up to 0.3 mm. They concluded that the chloride transport is very rapid along and cross the crack boundaries. Using the chloride profile in Figure 6.25, the chloride diffusion coefficients along the crack could be calculated. Table 6.7 shows the correlation between crack with and chloride diffusion coefficients at various crack widths, from the data in Table 6.7, the chloride diffusion coefficient increased by 104 times chloride

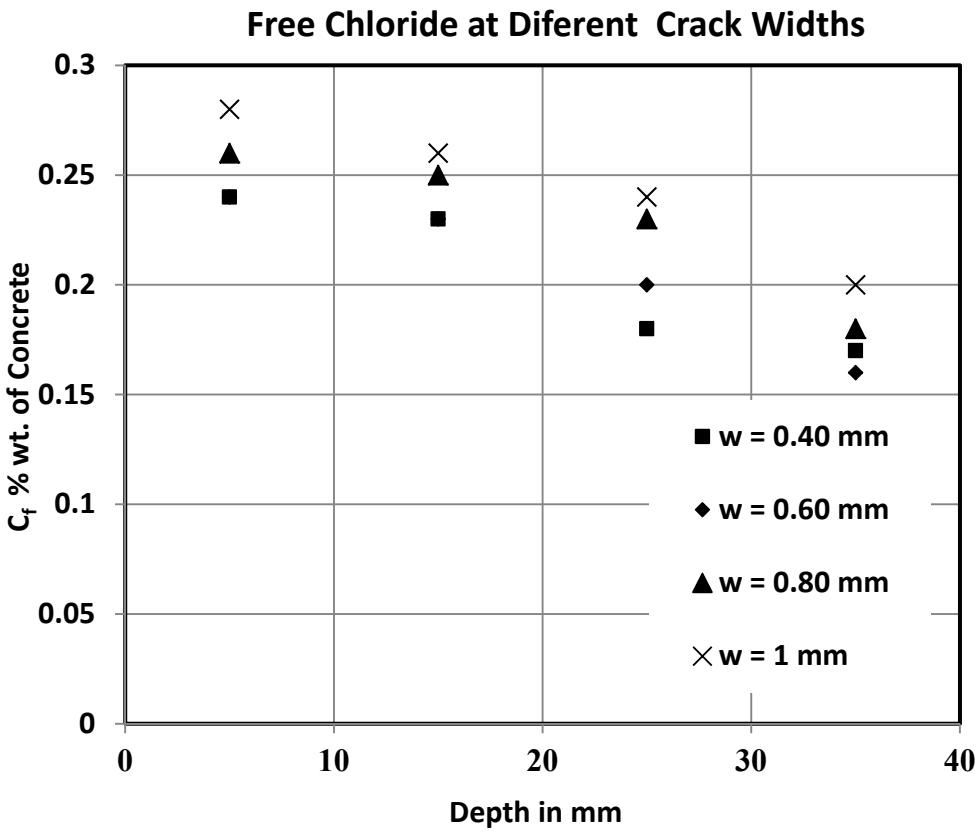

Figure 6.25: Free Chloride Profile a long crack walls with different crack widths.

Table 6.6: Free chloride content as % by weight of concrete along cracks with different widths.

Crack Width (mm)	**Depth in (mm)**			
	5	**15**	**25**	**35**
0.40	0.24	0.23	0.18	0.17
0.60	0.24	0.23	0.2	0.16
0.80	0.26	0.25	0.23	0.18
1	0.28	0.26	0.24	0.20

Table 6.7: Correlation between crack function F_w and chloride diffusivity at various crack widths

Crack width in mm	D_{cr} **(mm^2/s)**	$F_w = D_{cr}/D_o$
Undamaged Beam	3.4×10^{-6}	1.0
0.25	3.5×10^{-4}	104
0.4	3.8×10^{-4}	113
0.6	3.9×10^{-4}	116
0.8	3.9×10^{-4}	115
1	4.2×10^{-4}	126

diffusion coefficient of sound concrete for a crack width equal to 0.25 mm and tends to increase up to 126 times the chloride diffusion coefficients of sound concrete with crack widths of 1 mm. Sahmaran [2007] studied the relationship between the crack width and chloride diffusivity. He reported that the flexural load was introduced to generate cracks of width ranging between 29 and 390 μm. As the crack width was increased, the effective diffusion coefficient was also increased, thus reducing the initiation period of corrosion process. For cracks with widths less than 135 μm, the effect of crack widths on the effective diffusion coefficient of mortar was found to be marginal, whereas for crack widths higher than 135 μm the effective diffusion coefficient increased rapidly.

To establish the crack influence function F_w, a relationship between the crack width (w) and the ratio of chloride diffusion coefficient in the crack (D_{cr}) to the chloride diffusion coefficient in sound concrete D_o was established as shown in Figure 6.26, where two zones are distinguished as follows:

$$\left.\begin{array}{ll} F_w = 120 & \text{for } w > 0.25 \\ F_w = 476\ w+1 & \text{for } 0 < w < 0.25 \end{array}\right\} \qquad [6.4]$$

These functions agreed with the conclusion reported by Jang et al, (2011), who concluded that the diffusion of coefficients of concrete do not increase with increasing the crack widths up to so-called "threshold crack width" while, over this threshold value, the diffusion coefficient starts to increase.

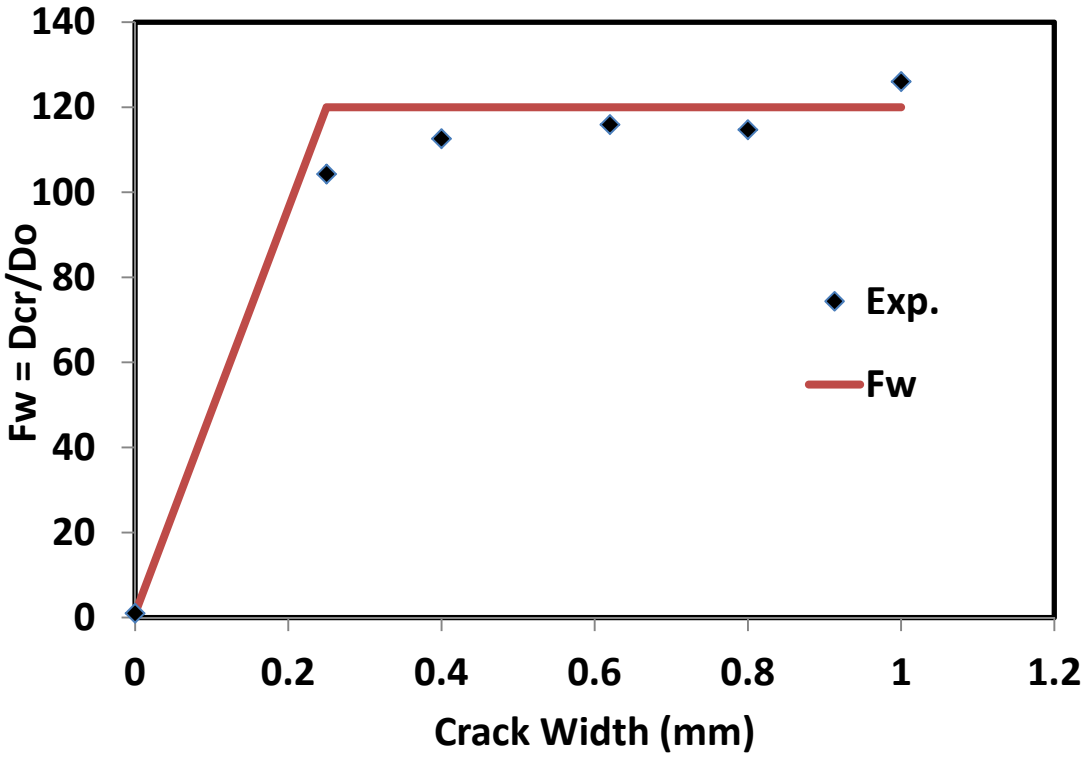

Figure 6.26: Effect of crack widths on chloride diffusion coefficients.

6.3 COMSOL Simulation of Chloride Diffusion in RC beams Subjected to Flexural Induced Damage

6.3.1 COMSOL Modeling, Subdomains Physics and Boundary Conditions

COMSOL finite element software was used to simulate the chloride diffusion in concrete taking into consideration the effect of stress induced damage. The coupled problem of mechanically induced damage and chloride binding capacity on chloride diffusivity in concrete was solved using two multi physics problem involving:

- The structural damage mechanics embodied in equations [3.15] to [3.21]; and
- The chloride diffusion with binding in equations [3.9], [3.10] and [3.11].

The scalar damage as defined in equation [6.1] is based on the total normal strain in concrete ε_x which could be calculated by solving the 2-D structural mechanics using the Drucker-Prager yield criterion for concrete together with Von Mises material model for the reinforcing steel which describes the ductile behavior of the RC beams.

The 2-D structural mechanics using the Drucker-Prager yield criterion was first used to describe the ductile behavior of the RC beams where the Drucker-Prager yield criterion can be written as:

$$f\ (I, \sqrt{J}) = \sqrt{J} + \alpha I = k \qquad [6.5]$$

In which $I = \sigma_{kk}$ is the hydrostatic component of the stress tensor, $J = \frac{1}{2} S_{ij} S_{ji}$ is the deviatoric stress tensor invariant, α and k are materials constant which can be related to

the friction angle *(φ)* and cohesion (c) of the Mohr-Coulomb criterion in several ways. For plane stress, the relation between the parameters are as follows:

$$\alpha = \frac{\sin\varphi}{\sqrt{3}} \; ; \quad k = \frac{2}{\sqrt{3}} \, c \, \cos\varphi \qquad [6.6]$$

In this study, c was 4.8 MPa and the friction angle φ was 53°, where these material parameters were found by calibration to match the experimentally determined P-Δ curve. Thereafter, the chloride transport problem was used to advance the solution of the coupled problem upon diffusion and binding of chloride.

Von Mises material model was used for the steel reinforcement in which E_s and F_{ys} was 19000 MPa and 560 MPa, respectively. Figure 6.27 shows the finite element modeling including dimensions and boundary conditions of the RC beams. The steel reinforcement was modeled as a plate representing the area of reinforcement in the beam with the same thickness of the concrete section.

Table 6.8 shows the parameters used in COMSOL model, in which the coefficient of chloride diffusion parameter *(D_d)* was taken as 3.35×10^{-6} mm^2/s, the free chloride concentration *(C_f)* at the boundary was 0.30% per weight of concrete. Initial chloride content in the sample, C_i, was assumed to be zero.

Figure 6.28 shows the flow chart for the simulation of coupled problem of chloride diffusivity in damaged RC beam subjected to flexural loading. As shown in Figure 6.28,

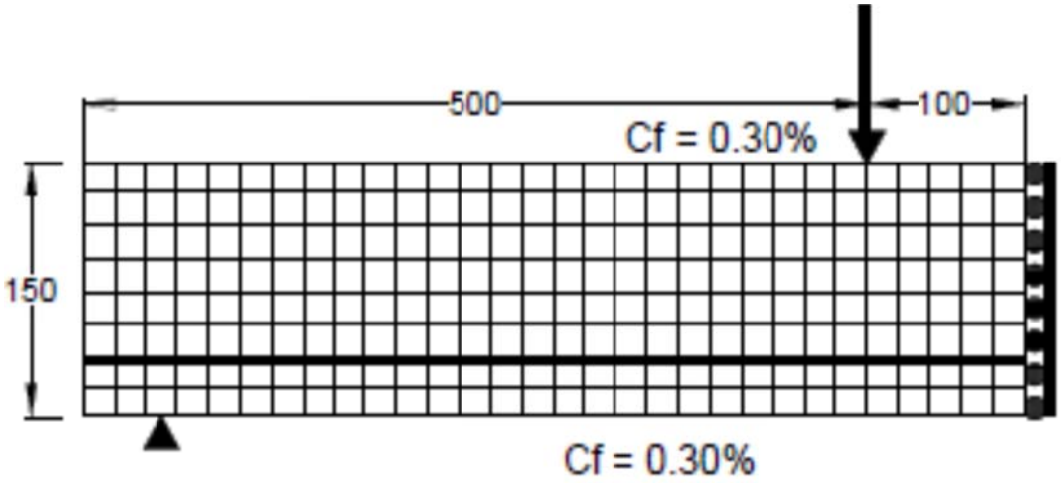

Figure 6.27: Finite Element Modeling of the RC Beams Subjected to Flexural Loading and Exposed to 0.30% Free Chloride.

Table 6.8: COMSOL model parameters.

COMSOL Commands	**COMSOL Expression/Parameters**	**Value**
Boundary Setting	C_o	C_f=0.30% by weight. Of concrete
Constants	m_t	1.46
	m_c	3.45
	f_{cr}	4 Mpa
	f_u	50 Mpa
	ε_{cr}	1.55e-4
	ε_u	2.3e-3
	F_{ys}	560 Mpa
	α	2.39
	β	15.6
Scalar Expression	F_d	$7.5\ d^2 + 0.8\ d + 1$ *for Tension* $1.15\ d + 1$ *for Compression*
	F_{cb}	$1/(1+\alpha/(1+\beta*C))$
	C_b	$\alpha\ C/(1+\beta*C)$
	C_t	C_b+C

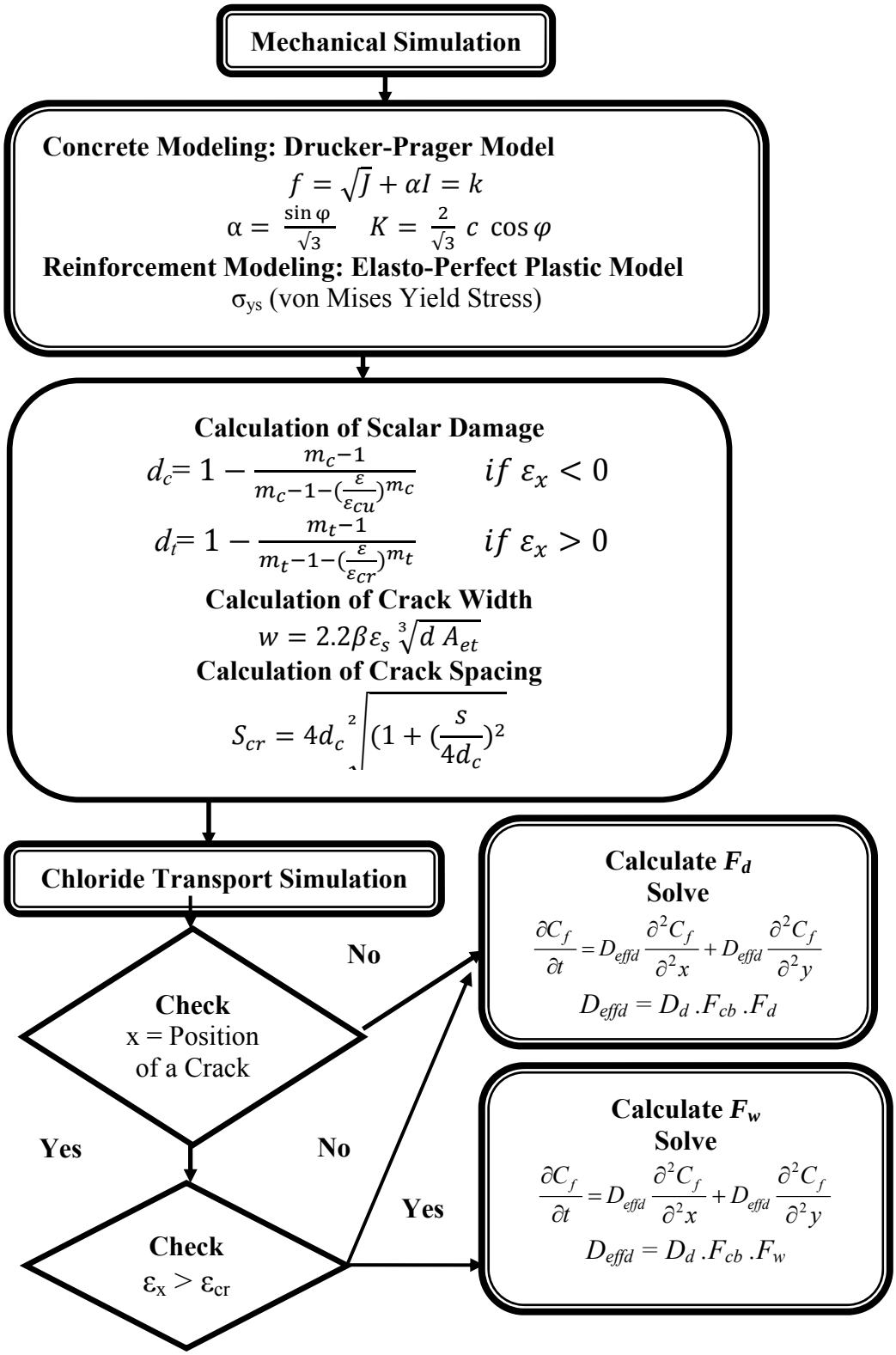

Figure 6.28: Flow chart for the simulation of effect of mechanical damage on chloride diffusivity in RC beams.

the simulation was conducted using COMSOL multiphysics finite element software using two modes: First, the structural mechanics mode, in which the plane stress using static analysis was chosen to simulate the mechanical behavior of the RC beams. Secondly, the diffusion mode, in which the transient analysis was chosen to solve the chloride diffusion problem.

The RC beam was modeled according to the following steps:

1- From **Draw** command in COMSOL commands menu, the RC beam was drawn using three rectangles which represent the concrete cover domain with 30 x 600 mm, the reinforcement steel domain with dimensions of 2.7 x 600 mm and the concrete beam domain with 117.3 x 600 mm long. The total depth of the three domains is 150 mm as shown in Figure 6.27.

2- Using **Physics** command, the materials model, and the material parameters, such as Young's modulus, Poisson's ratio and thickness, should be added for each subdomain. As mentioned previously. Full details for input parameters are presented in Table 6.9. The Drucker-Prager model for the concrete was used in the elasto-plastic material settings commands and a defined yield function (*f)* and the yield stress *(k)* were added as defined in equation [6.5].

Table 6.9: COMSOL Plan Stress Mode Input Parameters.

Subdomain	**Material Model**	**Young's Modulus [MPa]**	**Poisson;s Ratio**	**Thickness [mm]**
Concrete	Druker-Prager	29000	0.15	150
Reinforcement Steel	Von Miese	190000	0.33	150

3- From **Options** command, the scalar damage function, the crack width (w) the crack spacing, were added in the scalar expressions commands, details of these function are shown in Figure 6.28 and Table 6.8.

Using the Gergely-Lutz equation [6.7], we can estimate the maximum width of cracks in the concrete in the tension faces of flexural members. The maximum width of cracks is given by (Gergely and Lutz, 1968):

$$w = 2.2\ \beta x\ \varepsilon_s\ \sqrt{d_c\ x\ A} \qquad [6.7]$$

where:

w is the estimated crack width, (in); β is ratio of the distance to the neutral axis from the extreme tension concrete fiber to the distance from the neutral axis to the centroid of the tensile steel; ε_s is the strain in the steel; A (in^2) is the effective tension area of concrete around the main reinforcement (having the same centroid as the reinforcement) divided by the number of bars (n).

The crack spacing (S_{cr}) was calculated according to ACI 224R, (2001), where:

$$S_{cr} = 4\ x\ d_c\ \sqrt{1 + \left(\frac{s}{4d_c}\right)^2} \qquad [6.8]$$

d_c is the distance of the bar to extreme tension fiber and s is the bar spacing, Details of the calculation are in Appendix B. Details of the crack calculation are in Appendix B.

4- From **Solve** command, the solving parameter was used to solve the plane stress problem with incremental loading steps to assure the convergence of the solution.

5- Using **Solver Manager** command in **Solve**, all solutions for each load step was stored. By the end of this step, all the required information needed for the chloride diffusion problem is stored. This information included the crack widths, the crack spacing, and the damage in the concrete domain.

6- To simulate the transport of chlorides, the COMSOL diffusion mode is started, where it will check the position for each crack in the RC beam. If the element under solution is not in a crack position then the chloride transport problem will be solved using the damage influence function F_d and the chloride binding influence function F_{cb}. Otherwise, if the element under consideration then the software will check if the normal strain (ε_x) along the crack position is more than the cracking strain in concrete (ε_{cr}). If this is true then the cracking influence function will be combined with the chloride binding influence function to solve the chloride transport problem. Once the normal strain in the crack path is less than the cracking strain in concrete ε_{cr} then the software will replace the cracking influence function with the damage influence function reflecting that the crack reached its depth in the RC beam.

6.3.2 Finite Element Simulation of the Mechanical Behavior of RC Beams Subjected to Flexural-Induced Damage

a- Load-deflection curves

Figures 6.29 and 6.30 shows the experimental and numerical results of load-deflection curve and reinforcement strain vs. mid span deflection up to failure loading. From data in Figure 6.29, it can be noted that the first cracking load was at 7.5 kN after that the beam approached to the cracking section up an average to ultimate load of 95 kN. These results match well with the cracking load calculated using ACI approach (ACI 224R-01, 2001) and COMSOL where it was found to be about 7 and 7.25 kN, respectively. While both ACI and COMSOL show more stiffened behavior than the experimental results after the cracking load, the numerical simulation predicted well the behavior of reinforced concrete beam when approaching to the ultimate load where the predicted ultimate load was 93 kN which about 3% less than the actual ultimate load. Figure 6.30 shows the experimental and numerical results of reinforcement strain vs. mid span deflection up to failure loading. From Figure 6.30, it can be noted that the maximum strain in tensile reinforcement was found to be 3500 μm at the maximum mid-span deflection of about 8 mm.

Figures 6.31 through 6.35 show the deflection curves, obtained from COMSOL model, of RC beams subjected to different flexural loading levels up to 90% of its ultimate flexural load. From these figures, the deflection at mid span was about 2, 3.6, 5.2, and 7.4 mm for 40%, 60%, 75%, and 90% of ultimate flexural loading, these results match well the experimental test.

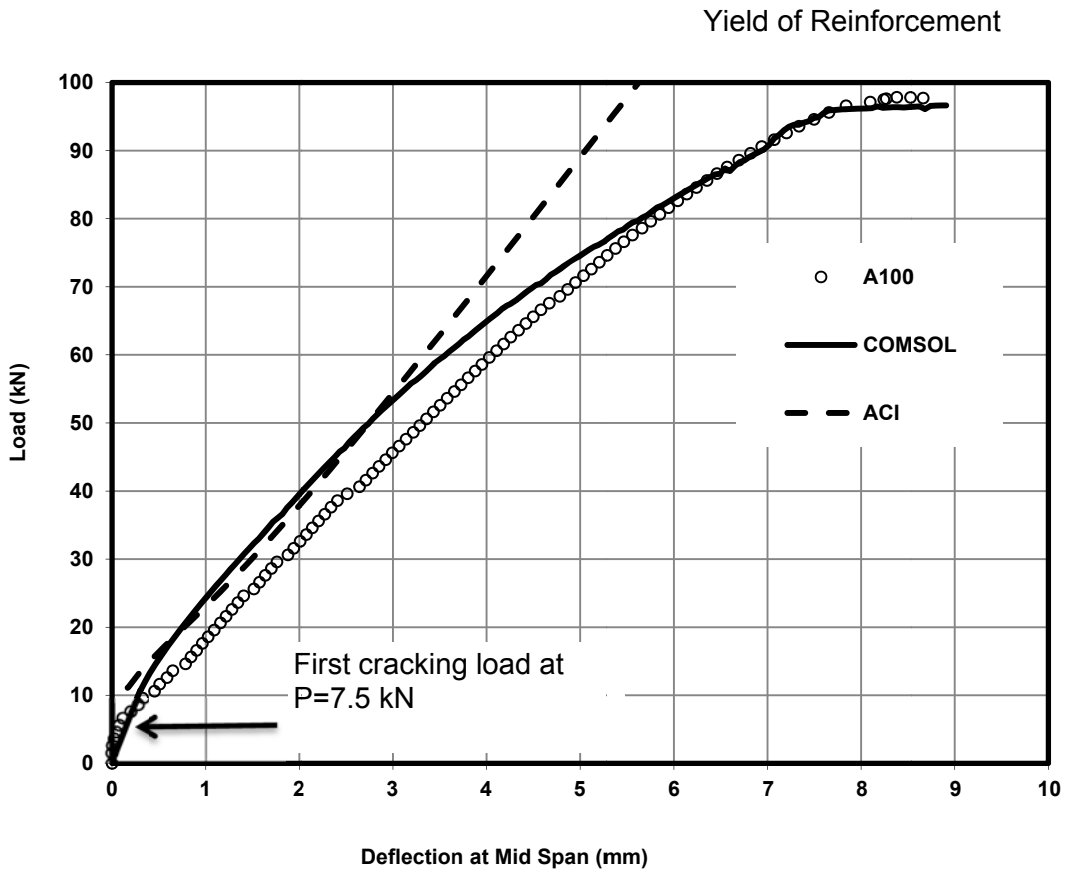

Figure 6.29: Experimental load-mid span deflection curve vs ACI and COMSOL simulation.

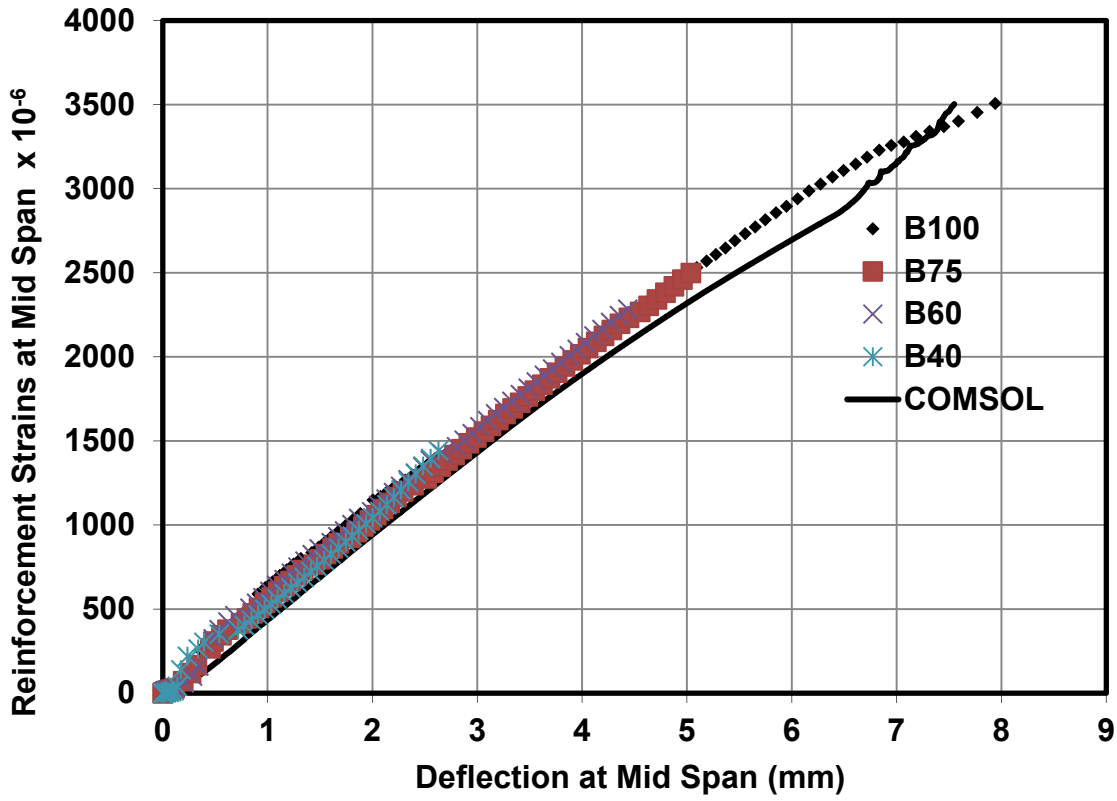

Figure 6.30: Experimental reinforcement strain-mid span deflection curve vs COMSOL simulation for 40%, 60%, 75% and 100% loading beams.

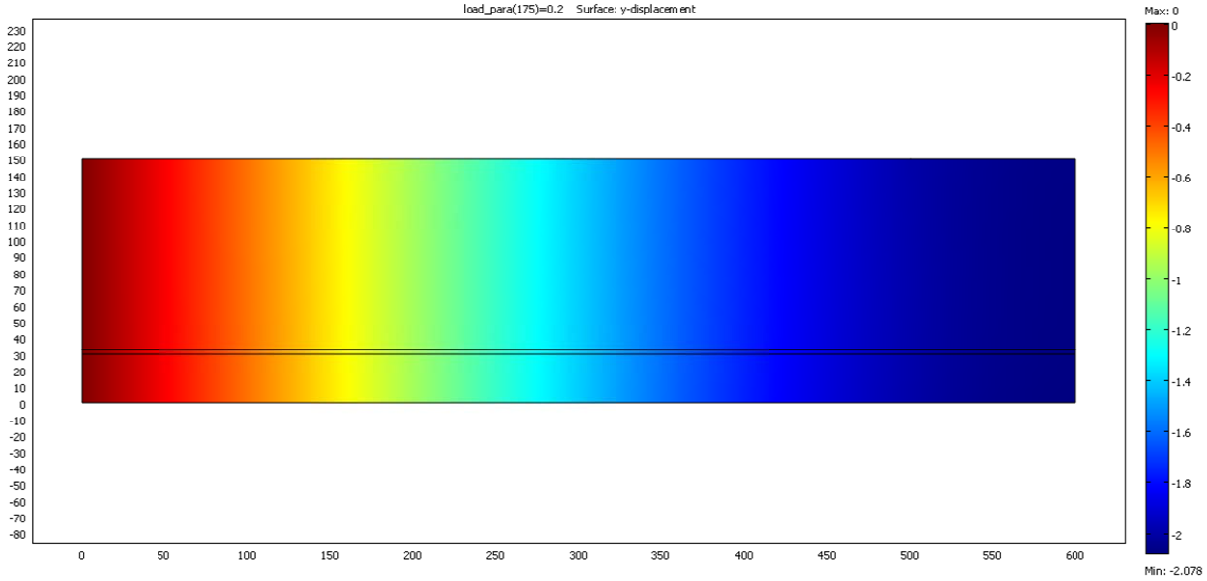

Figure 6.31: Deflection curve vs for 40% loading beam.

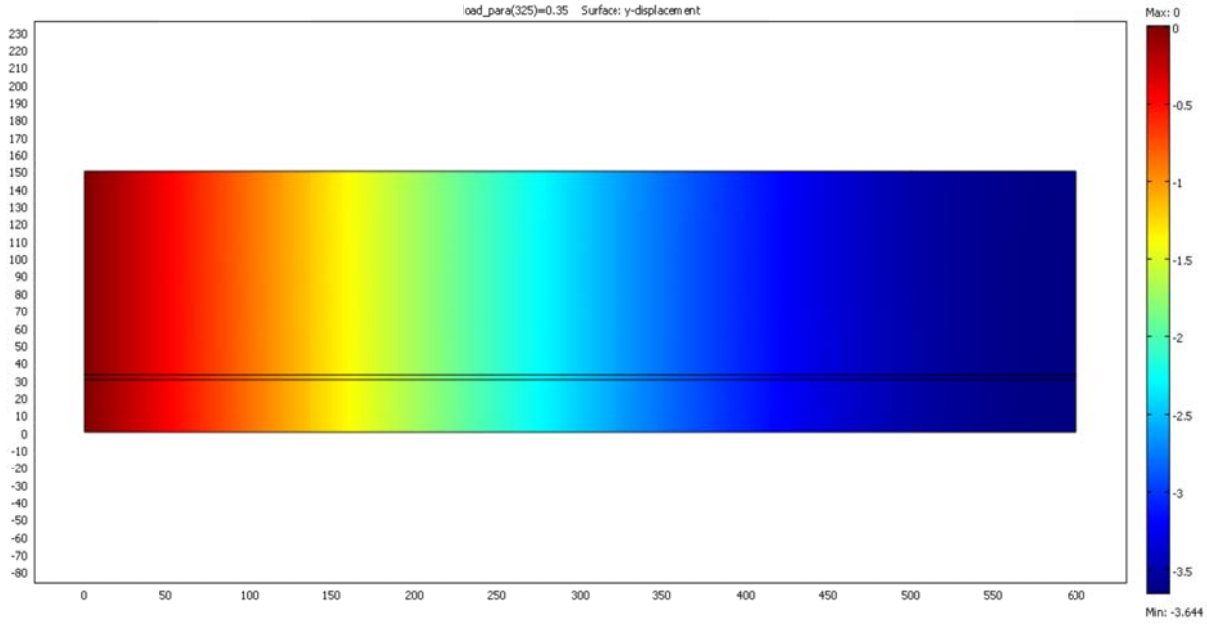

Figure 6.32: Deflection curve vs for 60% loading beam.

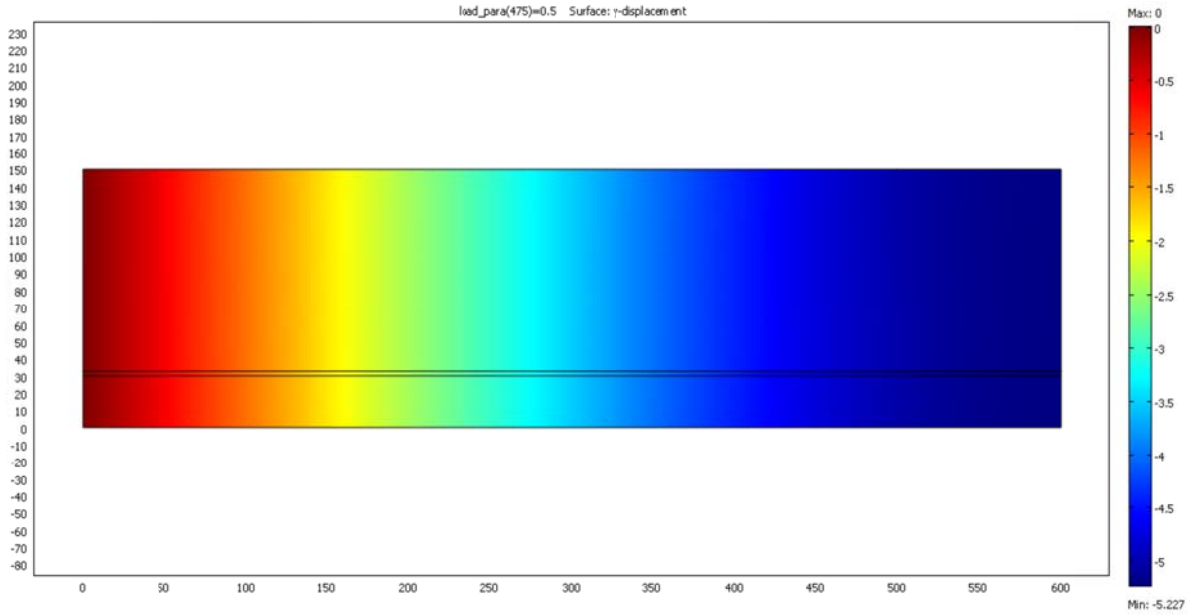

Figure 6.33: Deflection curve vs for 75% loading beam.

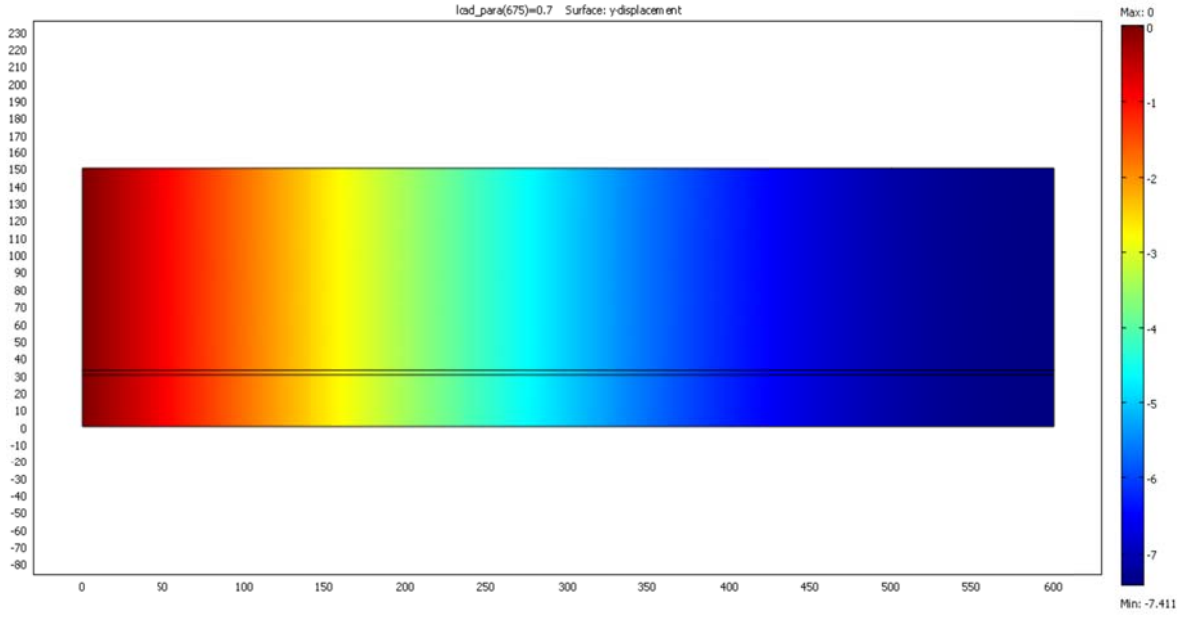

Figure 6.34: Deflection curve vs for 90% loading beam.

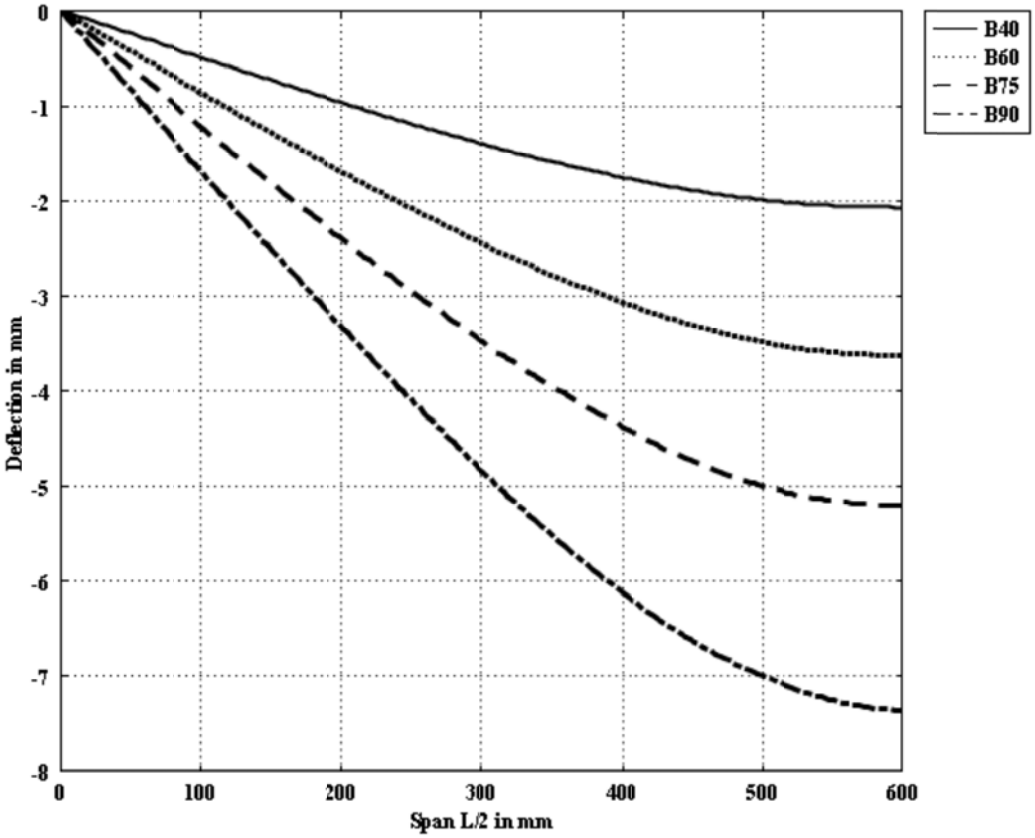

Figure 6.35: Deflection curves for all loaded beams for span of L/2.

b- Normal Stress S_x

To verify the ability of COMSOL model to simulate the mechanical behavior of the RC beams, two dimensional stress and strain results were plotted at different loading cases. Figure 6.36 shows the normal stress distribution (S_x) along the RC beam subjected to 40% of ultimate flexural loading. From Figure 6.36, it can be observed that the tensile stress in the reinforcement was about 180 MPa which means it was in the elastic state. All normal stress (S_x) decreases to approach zero at the support of the RC beam.

More details could be found in Figure 6.37 where the normal stress distribution (S_x) along the RC beam subjected to 40% of ultimate flexural loading at mid span is presented. From Figure 6.37, it can be noted that the concrete in the compressive zone was in the elastic state and the maximum compressive stress was 25 MPa. Besides, it can be observed that the neutral axis was about 60 mm from the top of the RC beam and after that the section was subjected to constant tensile stress of about 3.5 MPa which represent the tensile strength of concrete as calculated using Drucker-Prager tension cutoff model.

Figure 6.38 shows the normal stress distribution (S_x) along the RC beam subjected to 60% of ultimate flexural loading. From Figure 6.38, it can be observed that the maximum tensile stress in the reinforcement was about 300 MPa which is less than the yield stress of about 560 MPa. The normal stress distribution (S_x) along the cross section of the RC beam is shown in Figure 6.39 and the nonlinear behavior of the concrete can be observed in the compressive zone with a maximum compressive stress of about 30 MPa .

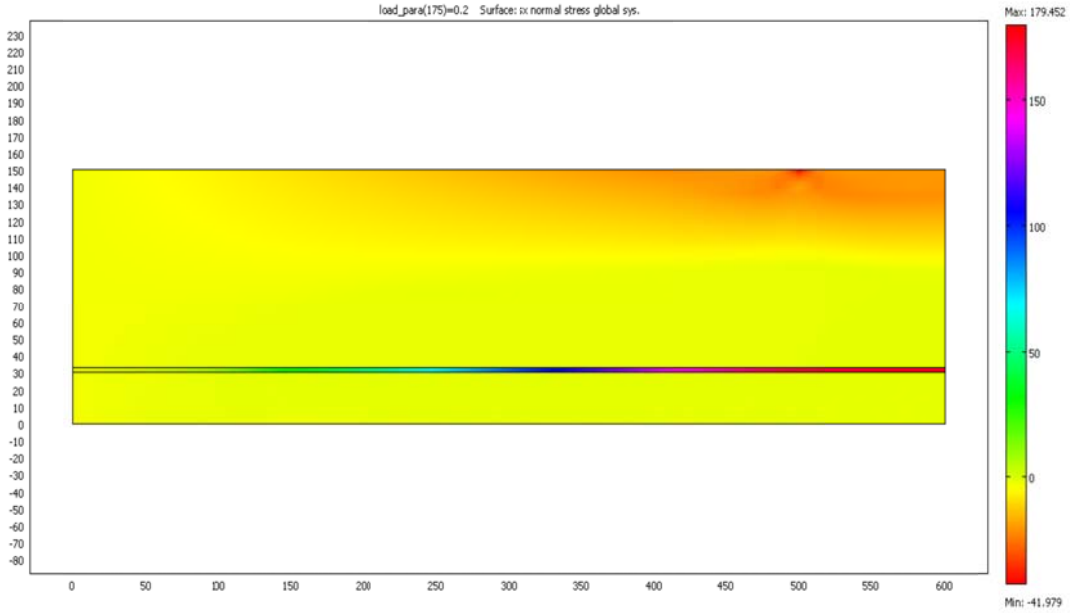

Figure 6.36: Normal Stress S_x for B40.

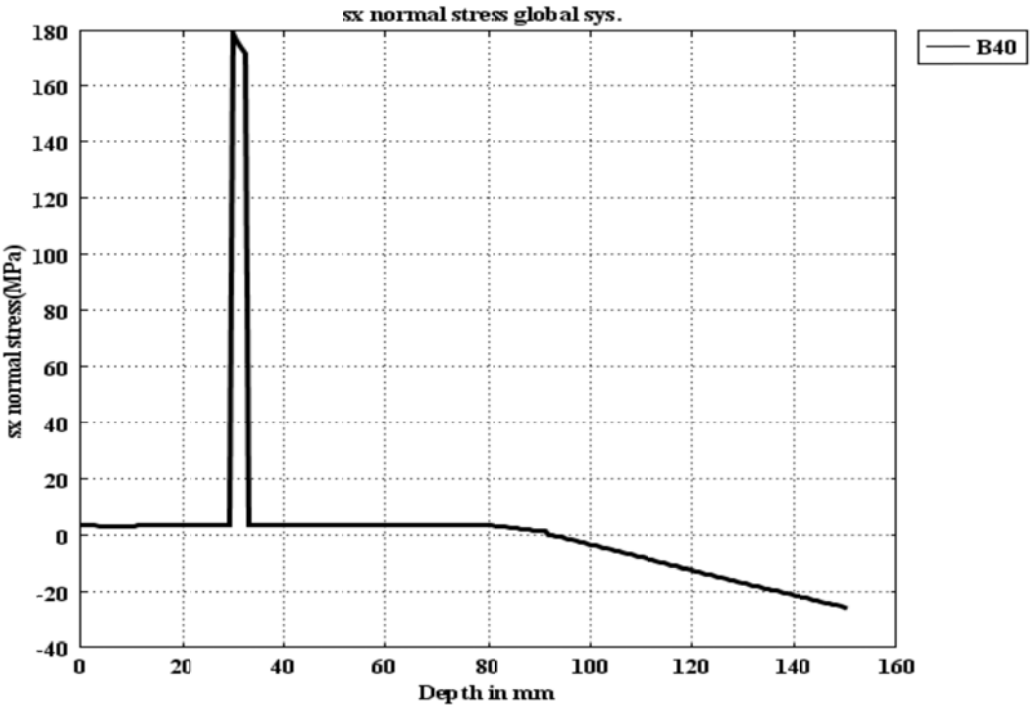

Figure 6.37: Normal Stress S_x Distribution at Constant Moment Zone (x=550 mm from Support) for B40.

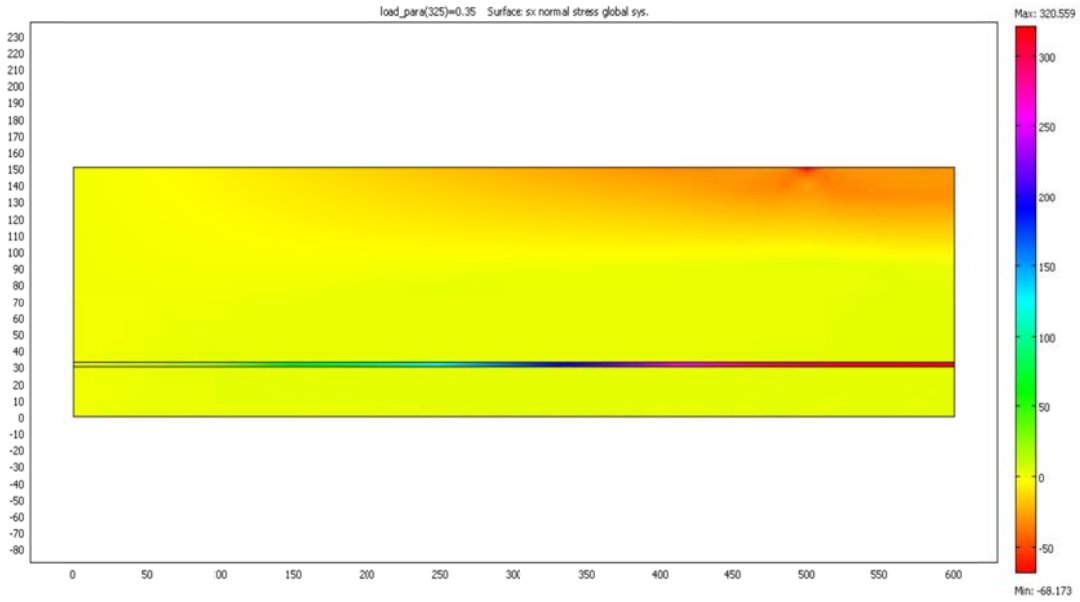

Figure 6.38: Normal Stress S_x for B60.

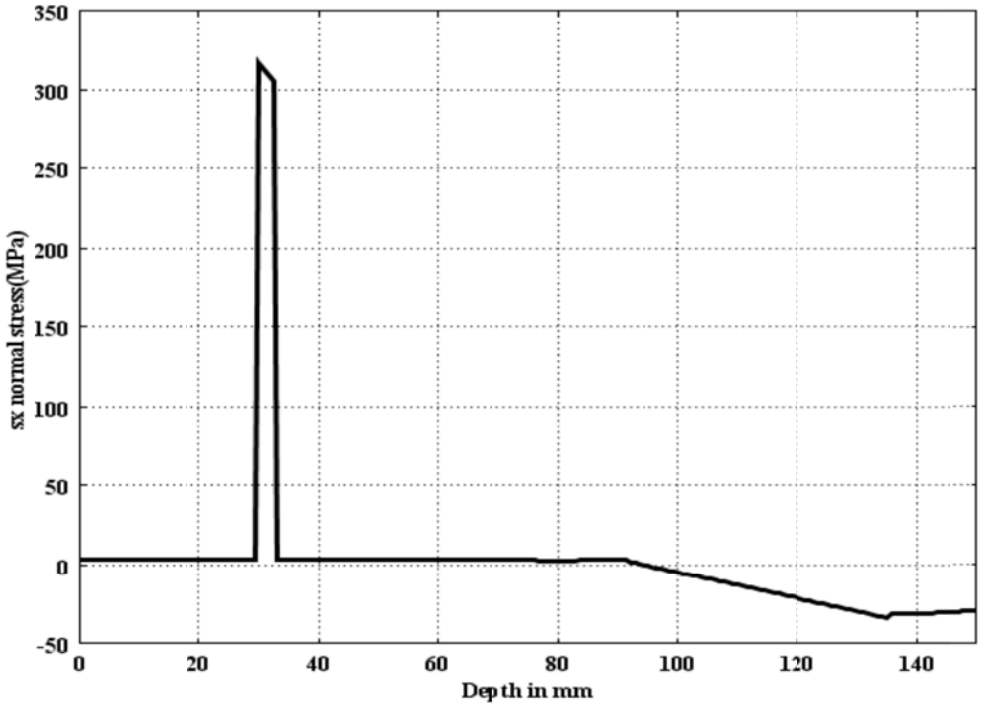

Figure 6.39: Normal Stress S_x Distribution at Constant Moment Zone (x=550 mm from Support) for B60.

Upon the increase of flexural loading, there was an increase in the nonlinearity behavior of concrete in the compressive zone as well as in the tensile stress in the reinforcement steel. Figure 6.40 shows the normal stress distribution (S_x) along the RC beam subjected to 75% of ultimate flexural loading.

From Figure 6.40, t can be observed that the maximum tensile stress in the reinforcement was about 450 MPa which less than the yields stress of the reinforcement of about 560 MPa. The normal stress distribution (S_x) along the cross section of the RC beam is shown in Figure 6.41, and it can noted the nonlinear behavior of the concrete in the compressive zone at a depth of 30 mm from the top of the beam and the maximum compressive stress was more than 35 MPa.

Figure 6.42 shows the normal stress distribution (S_x) along the RC beam subjected to 90% of ultimate flexural loading. As expected, at this level of flexural loading which approached the failure load of the beam, the maximum compressive stress was about 50 MPa and the tensile stress in the reinforcement was about 560 MPa which means that the reinforcement reached its yielding state. More details could be observed in Figure 6.43, where the normal stress distribution (S_x) along the cross section of the RC beam is presented, and it can be noted the compressive zone fixed at a distance of 60 mm from the top of the RC beam.

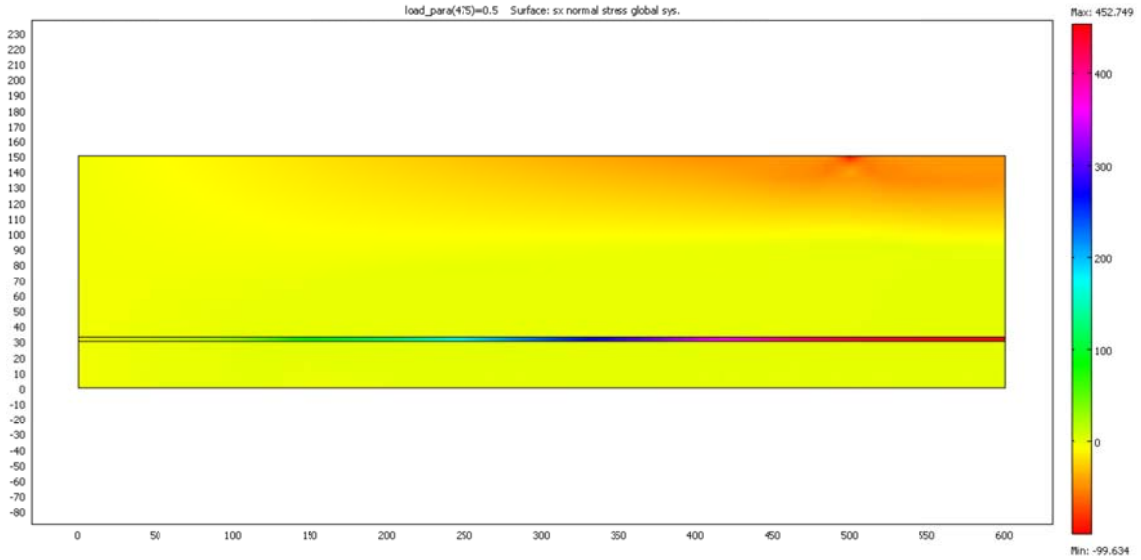

Figure 6.40: Normal Stress (S_x) for B75.

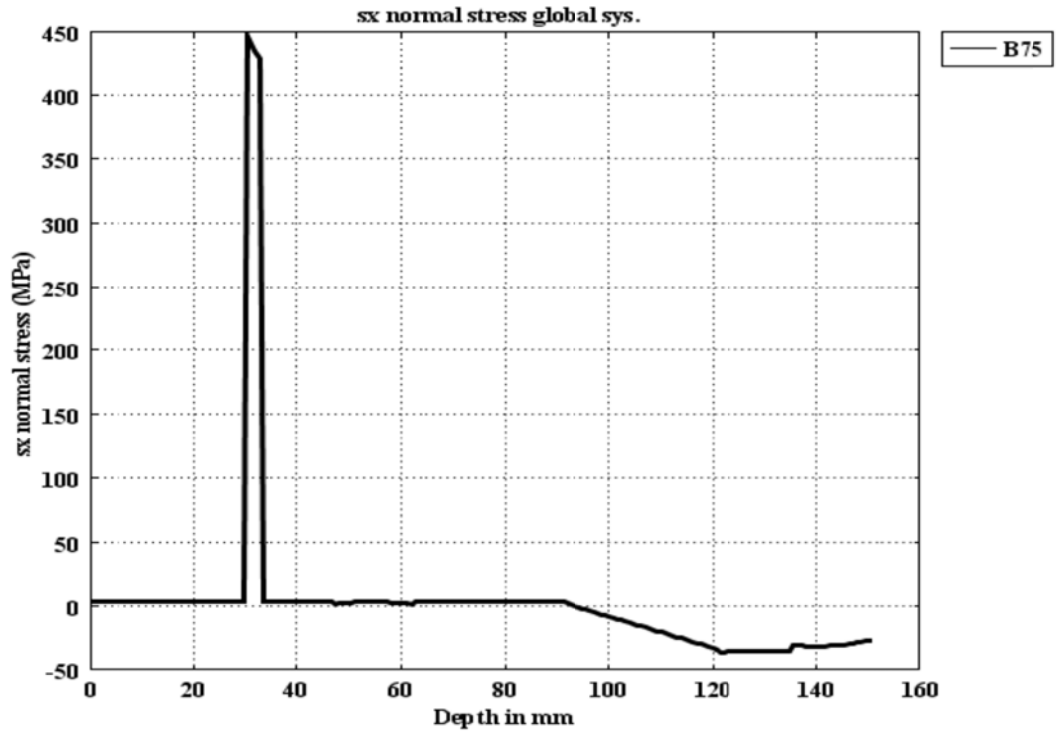

Figure 6.41: Normal Stress (S_x) Distribution at Constant Moment Zone (x=550 mm from Support for) B75.

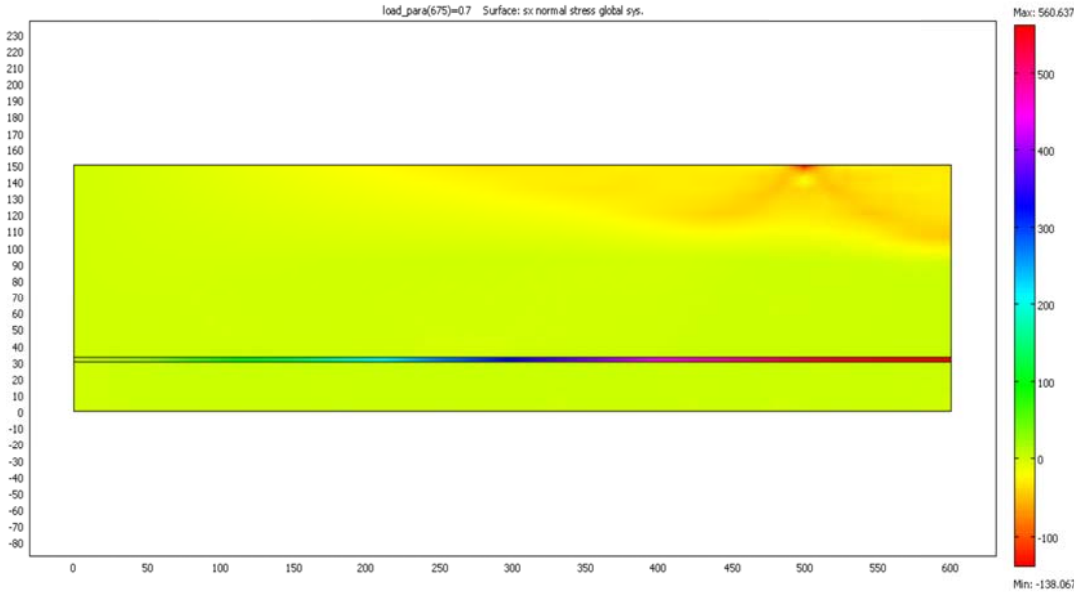

Figure 6.42: Normal Stress (S_x) for B90.

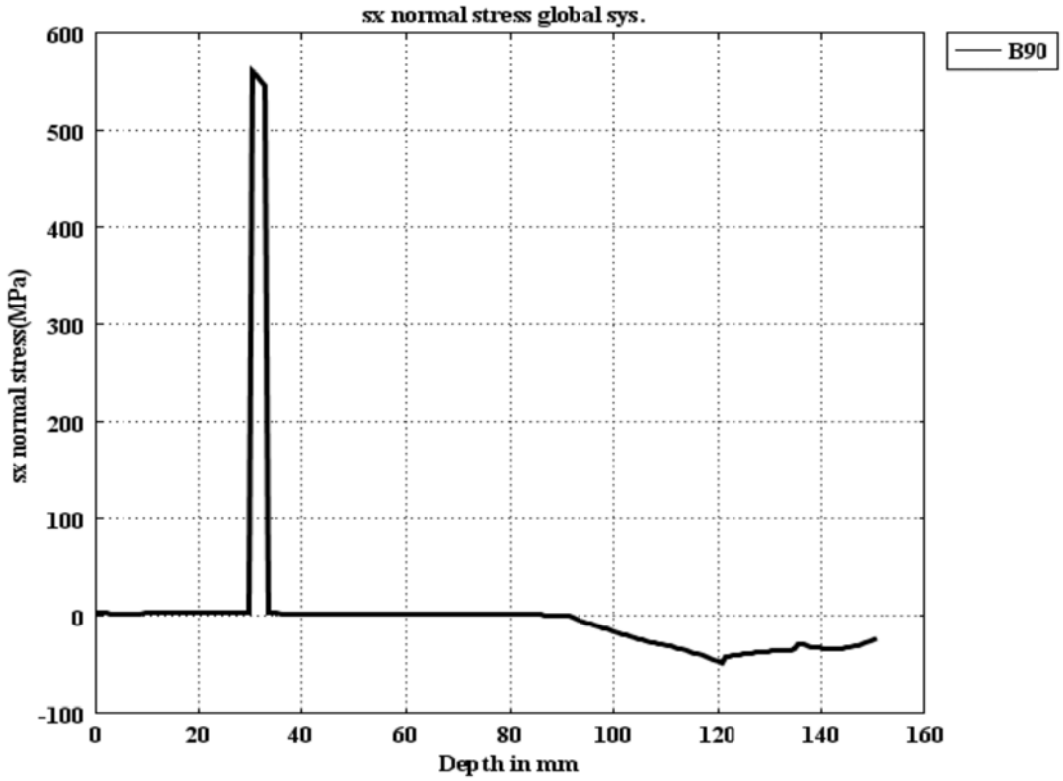

Figure 6.43: Normal Stress (S_x) Distribution at Constant Moment Zone (x=550 mm from Support) for B90.

b- Normal Strain ε_x

Two dimensional simulation using COMSOL model was conducted for normal strain **(ε_x)** and the results were plotted for different loading cases and presented in Figures 6.44 through 6.51. Figure 6.44 and Figure 6.45 show the normal strain distribution **(ε_x)** along the RC beam subjected to 40% of ultimate flexural loading.

From Figure 6.44, it can be observed that the maximum normal strain was about 8×10^{-4}, while the maximum normal strain **(ε_x)** in the reinforcement was about 1×10^{-3} and these results match well with the reinforcement strain experimental results as shown in Figure 6.11 where the average measured strain in the reinforcement was found to be 1.25×10^{-3} which means that the COMSOL model predicted accurately the mechanical behavior of the RC beams.

Figure 6.46 and Figure 6.47 show the normal strain distribution **(ε_x)** along the RC beam subjected to 60% of ultimate flexural loading. From Figure 6.46, it can be observed that the maximum compressive strain in concrete was about be 1.5×10^{-3} and the tensile strain in the reinforcement was about 1.75×10^{-3} which match well when compared with the value of 2×10^{-3} measured for the strain in the reinforcement as shown in Figure 6.10 From Figure 6.47, it can be noted that at the constant moment zone, the normal strain **(ε_x)** was exceeding the crack strain ε_{cr} (1.55×10^{-3}), which means that this zone under severe cracking condition.

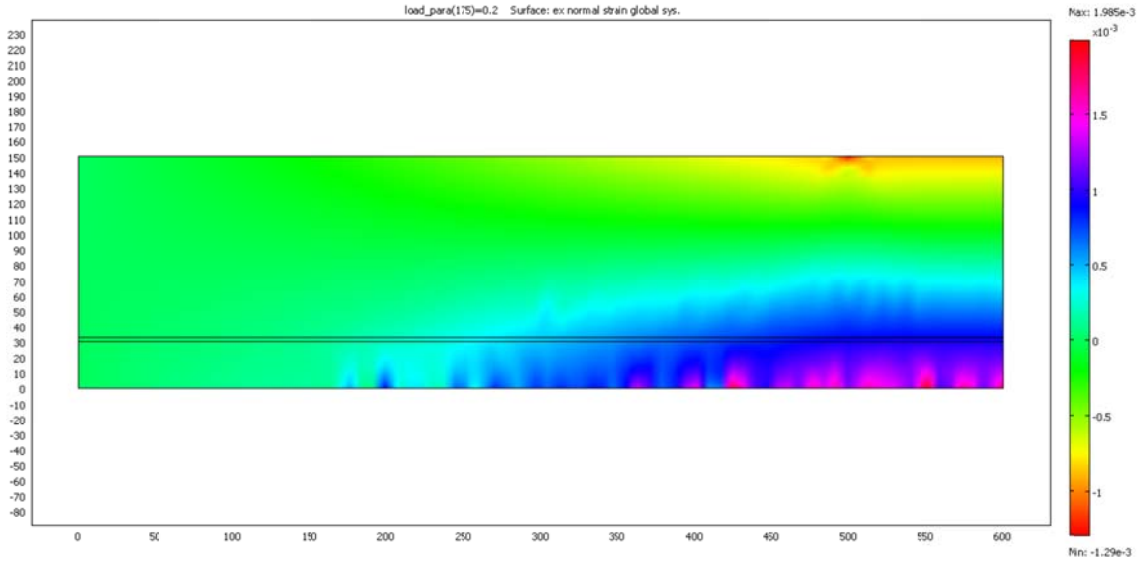

Figure 6.44: Normal Strain ε_x for B40.

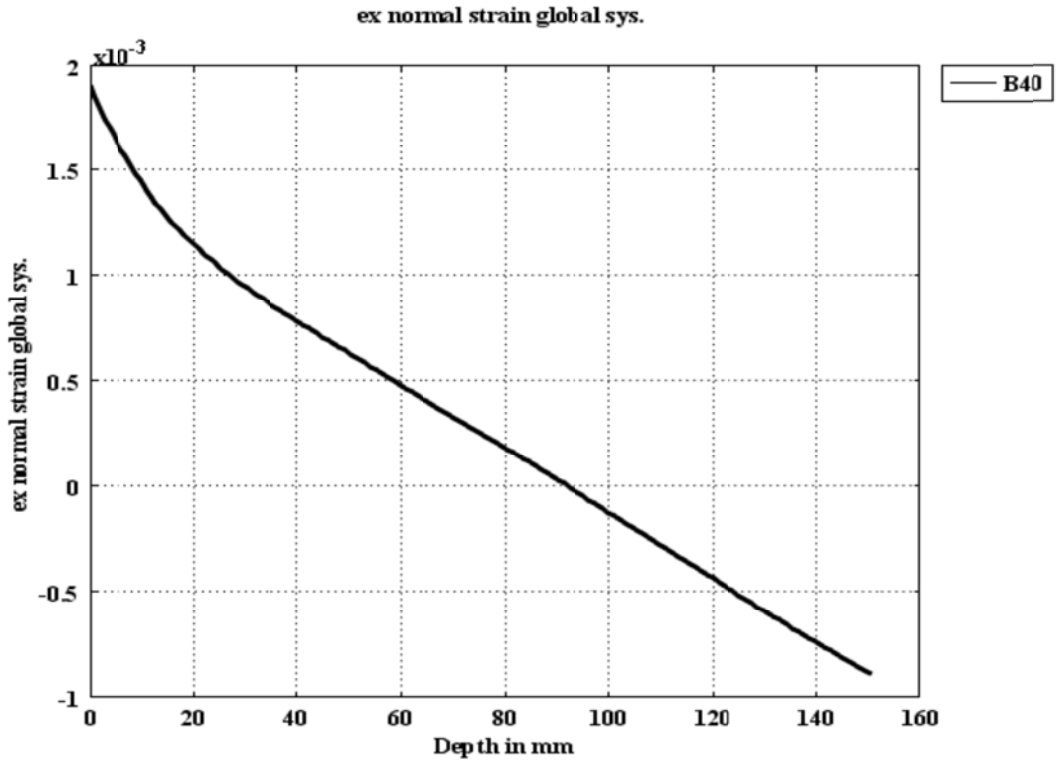

Figure 6.45: Normal Strain ε_x Distribution at Constant Moment Zone (x=550 mm from Support) for B40.

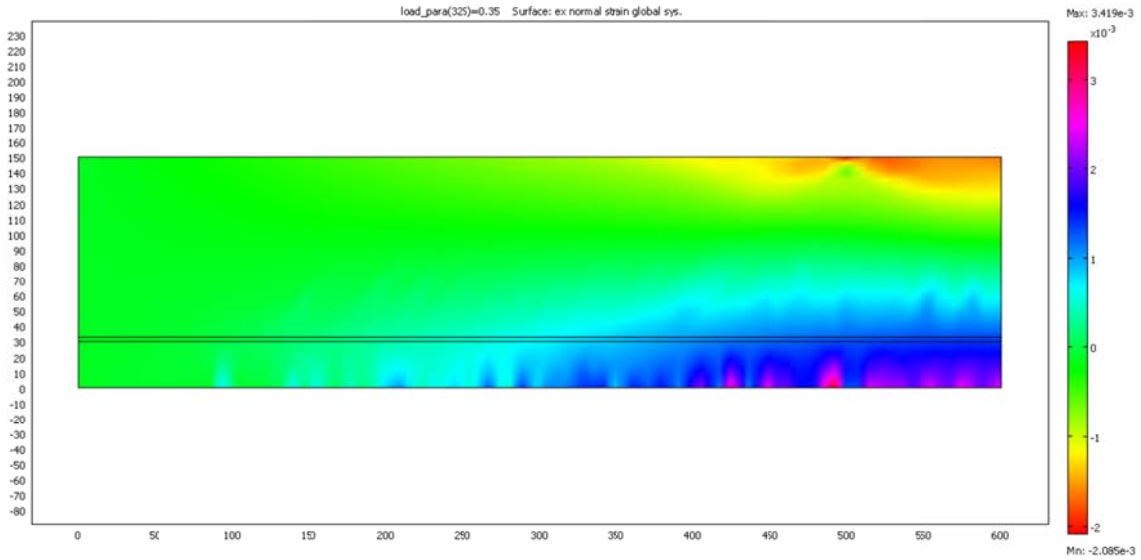

Figure 6.46: Normal Strain ε_x for B60.

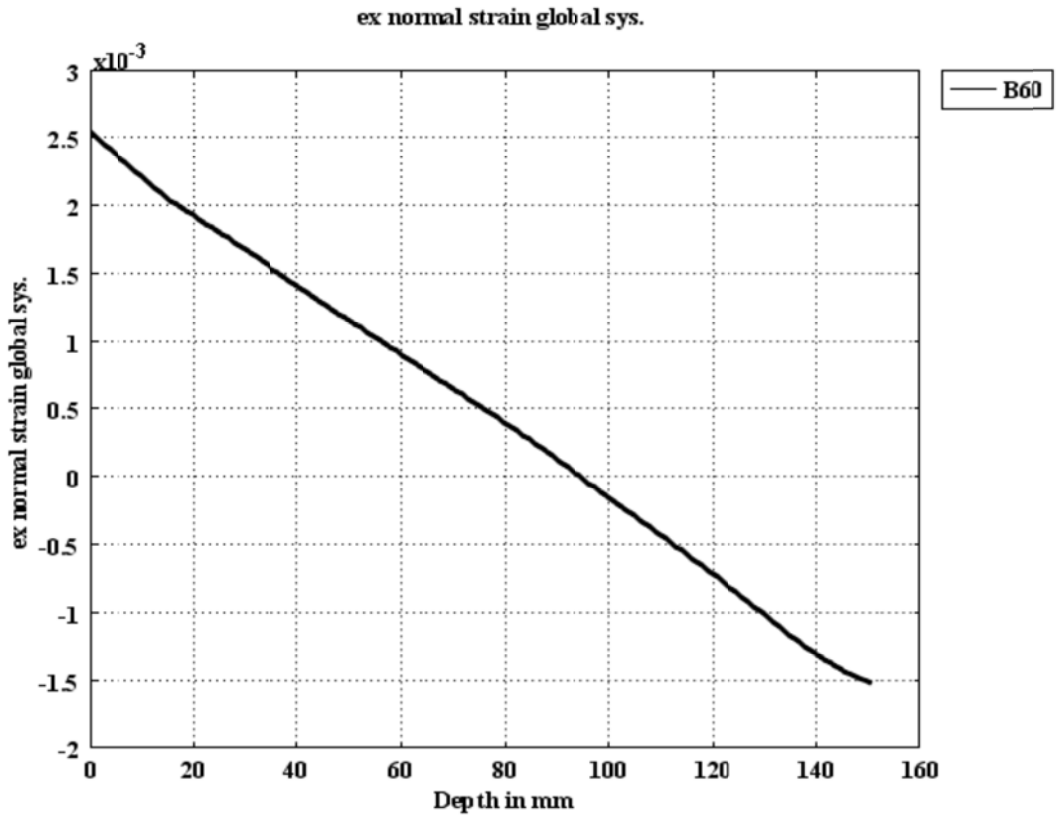

Figure 6.47: Normal Strain ε_x Distribution at Constant Moment Zone (x=550 mm from Support) for B60.

The tensile normal strain **(ε_x)** in the reinforcement increases to 2.5 x 10^{-3} as the RC beam loaded up to 75% of its ultimate flexural loading as shown in Figure 6.48 and Figure 6.49 and this value is very close to the measured strain in the reinforcement at the same level of loading which was 2.3 x 10^{-3} as shown in Figure 6.9. From Figure 6.49, it can be noted that the strain in the concrete reached a value of 2.3 x 10^{-3} and the nonlinear behavior of the concrete was found to be about 10 mm from the top of the beam and the tensile zone was found to be about 90 mm from the bottom of the RC beam.

When the RC beam was loaded up to 90% of its flexural loading, the normal strain in the compressive zone in the concrete approached to a value of 3.5 x 10^{-3} as shown in Figures 6.50 and 6.51, which is very close to the ultimate concrete values suggested by ACI. The normal strain in the reinforcement increases as more flexural load applied on the RC beam and reached a value of 3 x 10^{-3} which matches well with the experimental results for the normal strain in the reinforcement at the 90% of flexural loading which was about 3.5 x 10^{-3} as shown in Figure 6.8.

6.3.3 Finite Element Simulation of the Flexural-Induced Damage in RC Beams

Figures 6.52 through 6.56 show the two dimensional damage distribution in half of the reinforced concrete beam span (L/2 = 600 mm). From these figures, it can be noted that the development of the stress induced damage related to compressive and tensile stresses for the beams under flexural loading at first crack load, 40%, 60% and 100% of ultimate

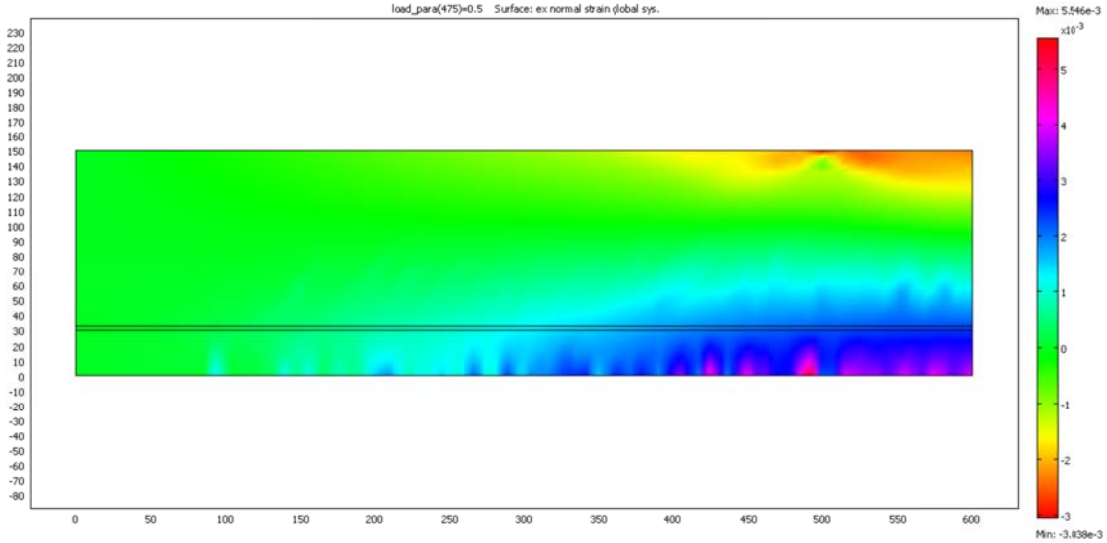

Figure 6.48: Normal Strain ε_x for B75.

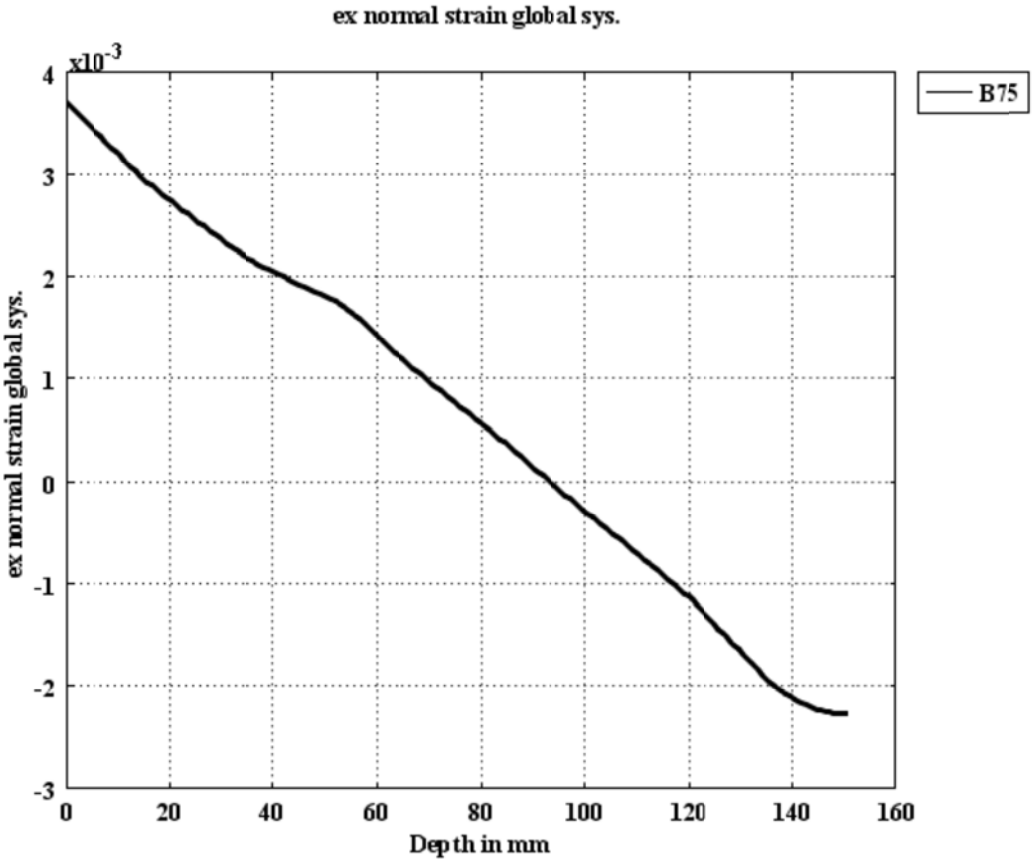

Figure 6.49: Normal Strain ε_x Distribution at Constant Moment Zone (x=550 mm from Support) for B75.

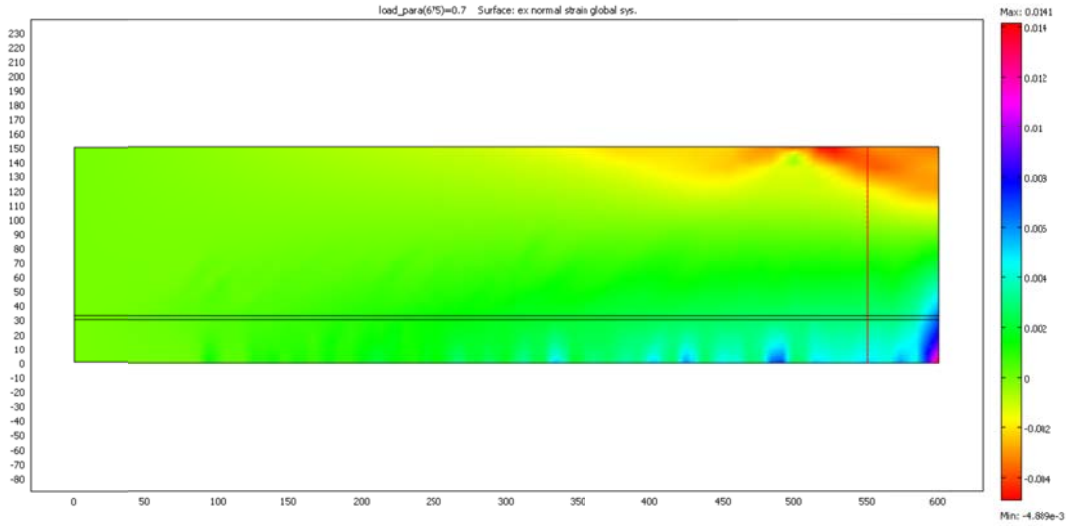

Figure 6.50: Normal Strain ε_x for B90.

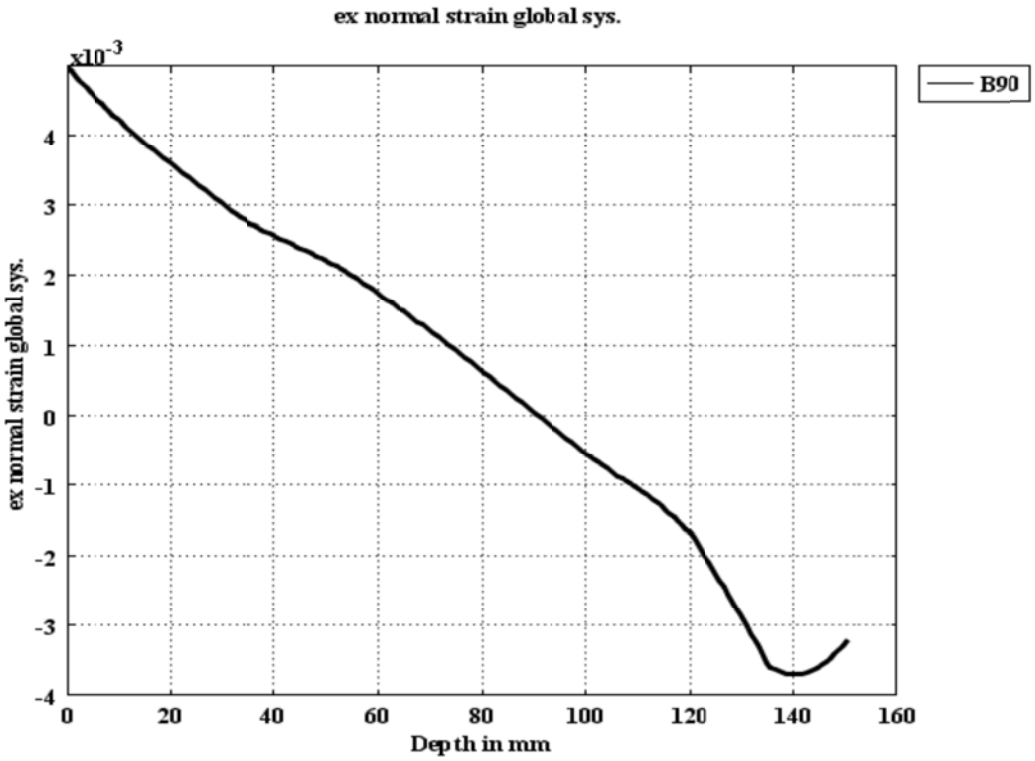

Figure 6.51: Normal Strain ε_x Distribution at Constant Moment Zone (x=550 mm from Support) for B90.

loading. For more details, damage distribution along the cross section of the RC beam subjected to different levels of flexural loading is sown in Figures 6.57 through 6.59.

Figure 6.52 shows the mechanical damage distribution in RC beam subjected to 40% of its ultimate flexural loading. It can be noted from Figure 6.52 that in the tensile zone, there is severe damage up to 0.90 due to applied flexural loading which increase the tensile stress in this region. The tensile damage extended about 80 mm in the cross section of the beam from the bottom. No damage was detected in the compressive zone at this state of loading.

The damage distribution for RC beam subjected to 60% of its ultimate flexural loading is shown in Figure 6.53. No damage was developed in the compression zone, while the damage in the tensile zone was extended along the beam toward the support. The depth of the damage increased from 80 mm in 40% loaded RC beam to about 90 mm for 90% loaded beam. With the increases of the flexural load up to 75% of ultimate flexural loading of the RC beam, the damage in compressive zone as shown in Figure 6.54 started to develop in the constant moment zone of about 550 mm from the edge of the RC beam and this compressive damage was extended about 20 mm from the top of the with scalar damage range from 0 to 0.20 as shown in Figure 6.52 and Figure 6.56. The tensile zone was subjected to stable damage as in RC beam subjected to 60% and the extent of this damage is about 90 mm from the bottom of the cross section at the constant moment zone. Figure 6.55 shows the damage distribution in RC beam subjected to 90% of

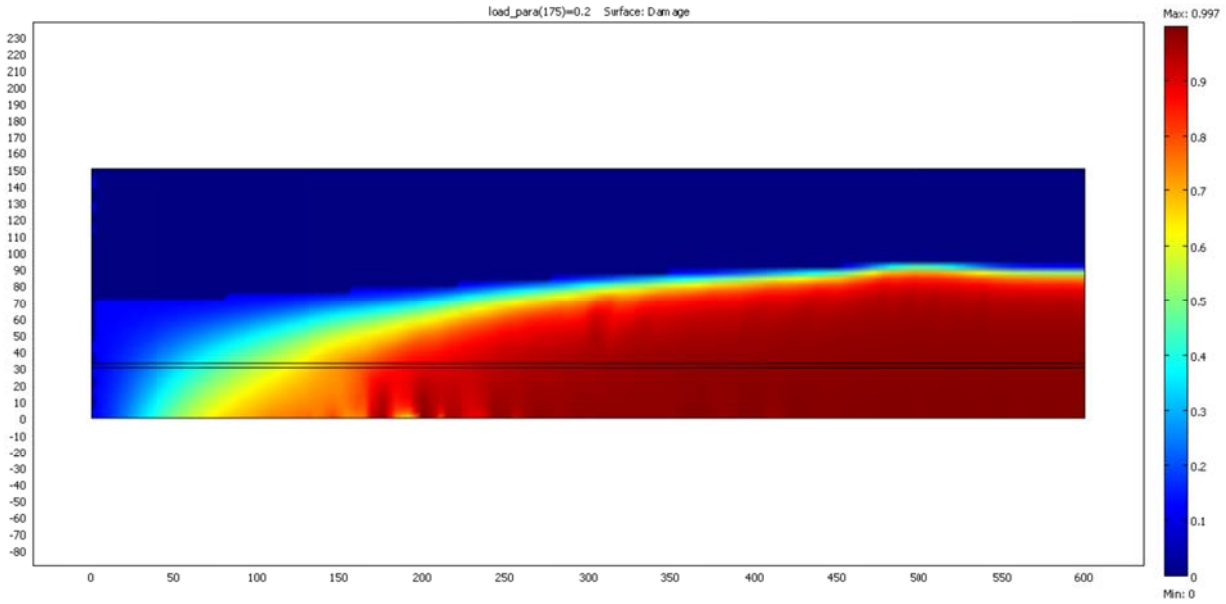

Figure 6.52: Scalar Damage *d* at 40% Loading Beam B40.

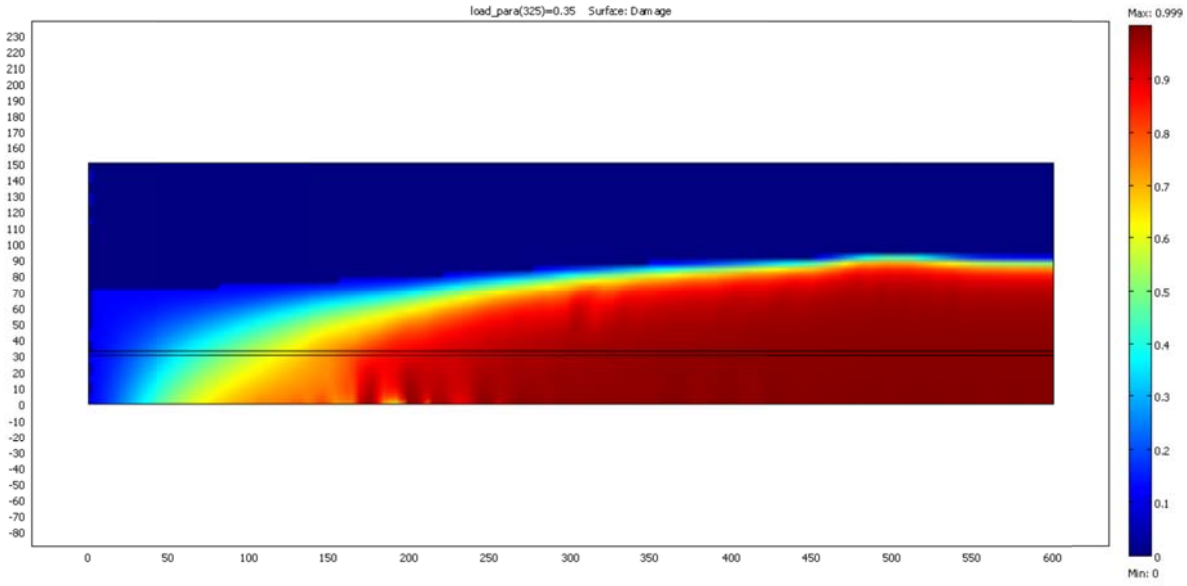

Figure 6.53: Scalar Damage *d* at 60% Loading Beam B60.

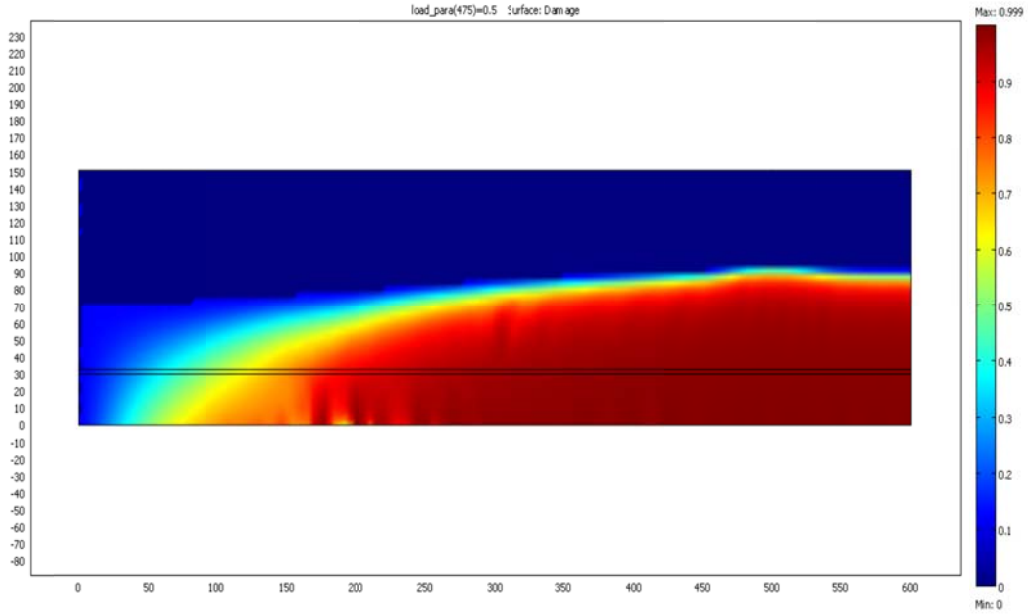

Figure 6.54: Scalar Damage *d* at 75% Loading Beam B75.

its ultimate flexural loading. From Figure 6.55, it can be observed that a significant increase in compressive damage with about 0.90 was developed under the point loading and these values decreased to 0.65 at constant moment zone. In tensile zone, it can be noted more development in tensile damage especially towards the support because of the increase of the tensile stress with the increase of the applied flexural loading and the depth of the damage increased up to 90 mm from the region between 150 from the support up to the mid span of the RC beam.

At failure load, the compressive damage increased up to 0.90 with a depth of 50 mm while the damage in the tensile zone was up to 0.90 for 90 mm depth from the bottom of the RC beam which indicates the development of full crack in the RC beam at failure as shown in Figure 6.56. More details about the development of mechanical damage along the cross section of the RC beam is shown in Figures 6.57 through 6.59, where the scalar damage *d* was plotted along the cross section at constant moment zone, at a distance of 100, 150 mm from the support for RC beams subjected to different flexural loading states.

Form Figure 6.57, it can be noted that at the constant moment zone, the tensile damage is more than 0.90 up to a depth of 80 mm for all damaged RC beams due to higher tensile stress in this region. Besides, the compressive damage was initiated when the RC beams subjected to 75% of its ultimate flexural loading and this indicates that the compressive damage propagated at lower rate compared with the tensile damage due to the fact that concrete sustained more compressive stress than tensile. The same behavior could be

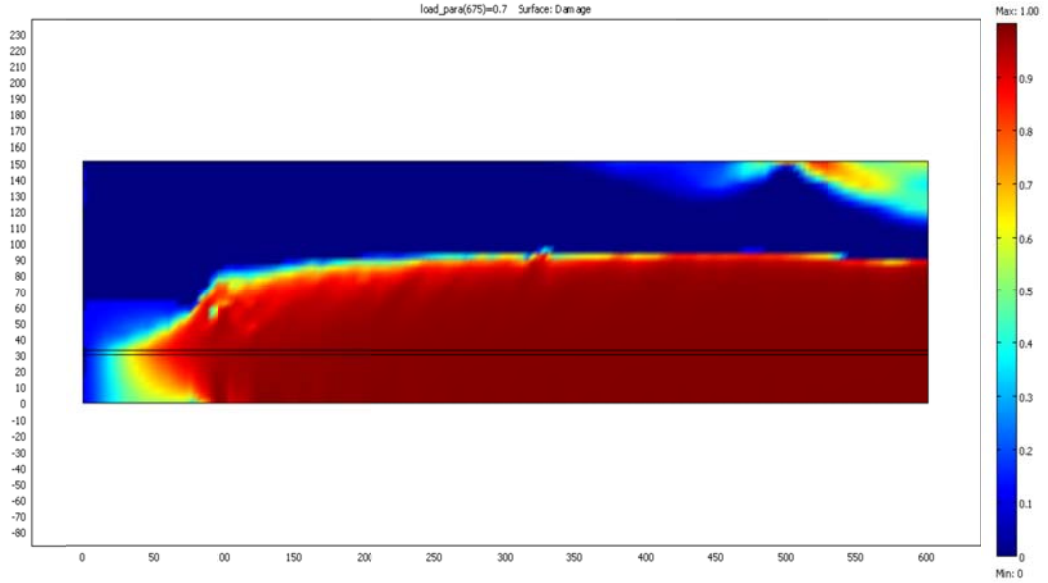

Figure 6.55: Scalar Damage *d* at 90% Loading Beam B90.

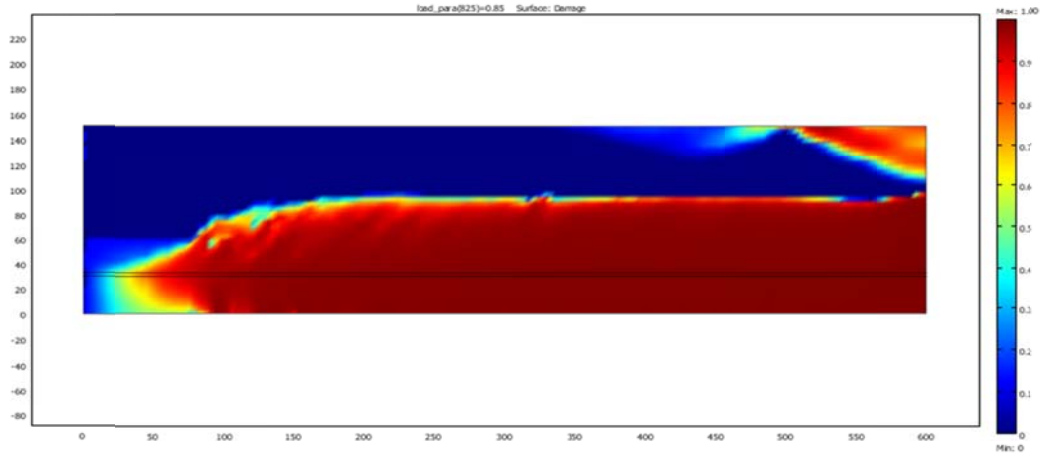

Figure 6.56: Scalar Damage *d* at Failure Loading.

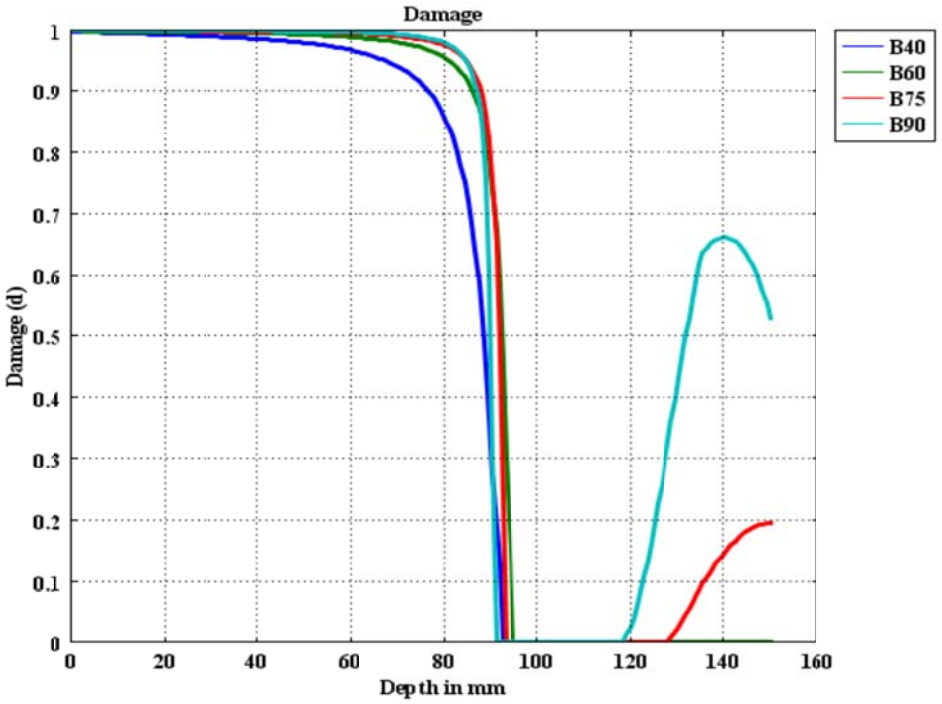

Figure 6.57: Damage Distribution across the Beam Section at Mid Span (Constant Moment Zone, x=550 mm).

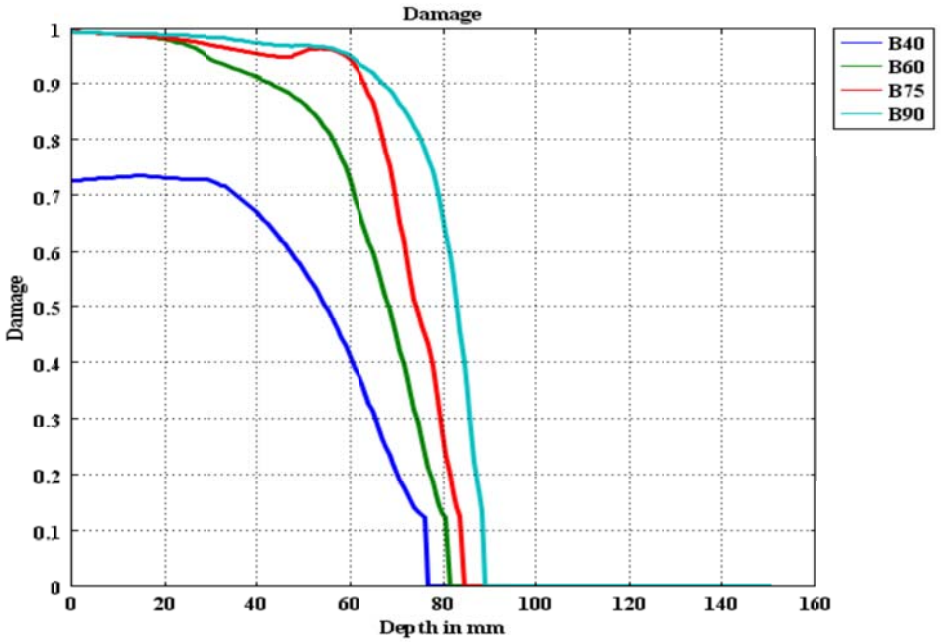

Figure 6.58: Damage Distribution across the Beam Section at distance of 150 mm from the support.

observed in the section at a distance of 100 mm from the support of the RC beam as shown in Figure 6.59. The tensile damage was varied in sections at distances of 150 and 100 mm from the support of the RC beams as shown in Figure 6.58 and Figure 6.59. From Figure 6.58, the compressive damage ranged between 0.10 and 0.72 for 40% loaded RC beam while the maximum limit of this range increases to almost 1 for beams subjected to 60%, 75% and 90% of ultimate flexural load. Besides, with more loading, it can be observed that there was extension in the depth of the damage which varied from 75 to 82, 85, and 90 mm for 40%, 60%, 75%, and 90% loaded RC beams.

To verify the COMSOL model with experimental results at crack positions in RC beams with different loading levels, the axial strain (ε_x) was plotted at crack positions in the RC beams as shown in Figures 6.60 through 6.63. It was assumed that the crack will propagate when (ε_x) is more than the crack normal strain ($\varepsilon_{cr} = 1.55 \times 10^{-3}$). Figure 6.60 shows the normal strain (ε_x) along the position of cracks at distance of 400 and 530 mm from the support in RC beams subjected to 40% of its ultimate flexural loading. From Figure 6.60, it can be noted that the crack depths were found to be about 75 and 85 mm at distances of 400 and 530 mm, respectively, and these results match well with experimental crack maps shown in Figure 6.13.

The number of cracks and the crack depths increase with the increase the applied flexural loading. As shown in Figure 6.61, the crack depths were increased as the applied flexural loading increased up to 60% of ultimate loading and were about 82 and 90 mm from crack

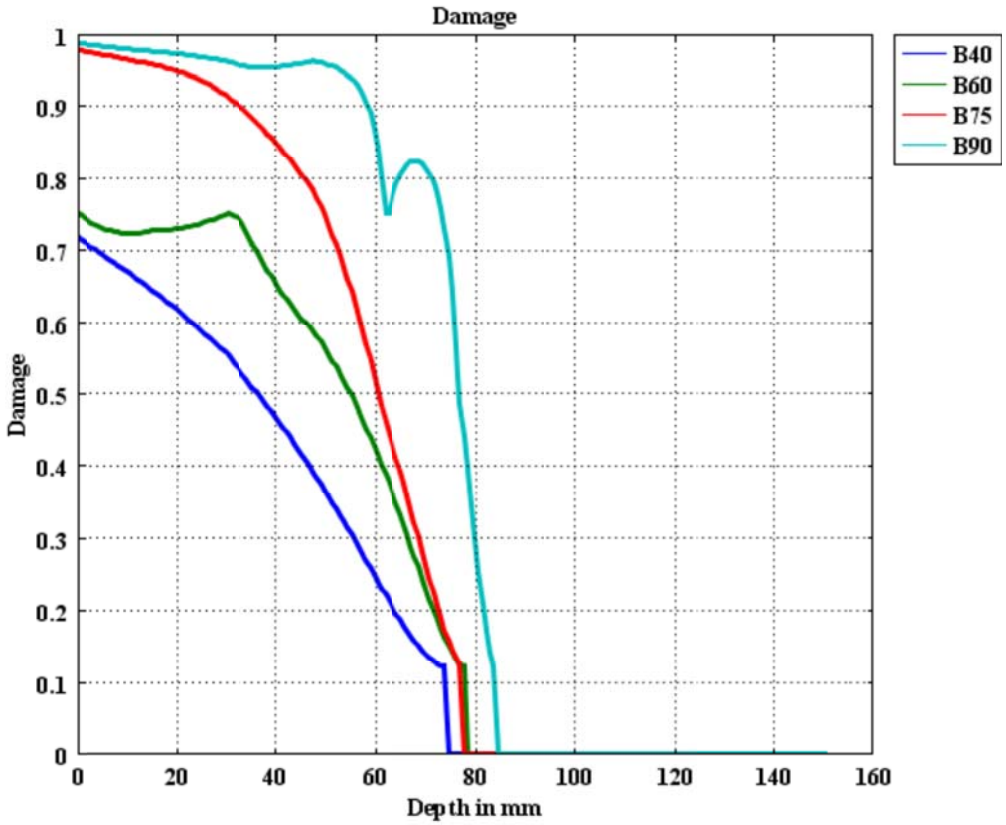

Figure 6.59: Damage Distribution across the Beam Section at distance of 100 mm from the support.

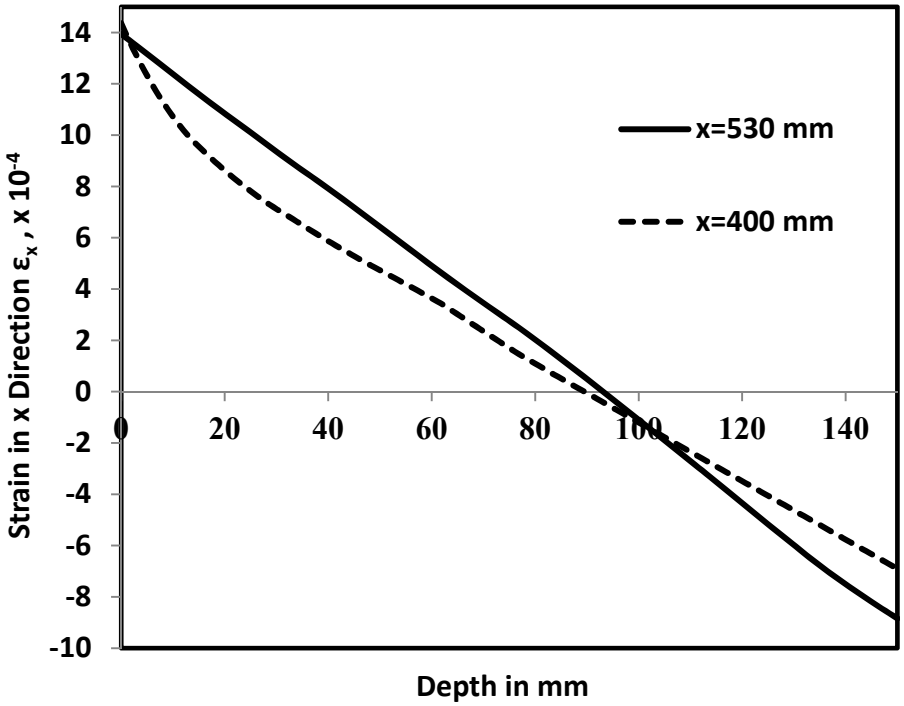

Figure 6.60: Axial Strain ε_x at Cracks in x=530 mm and x= 400 mm for B40.

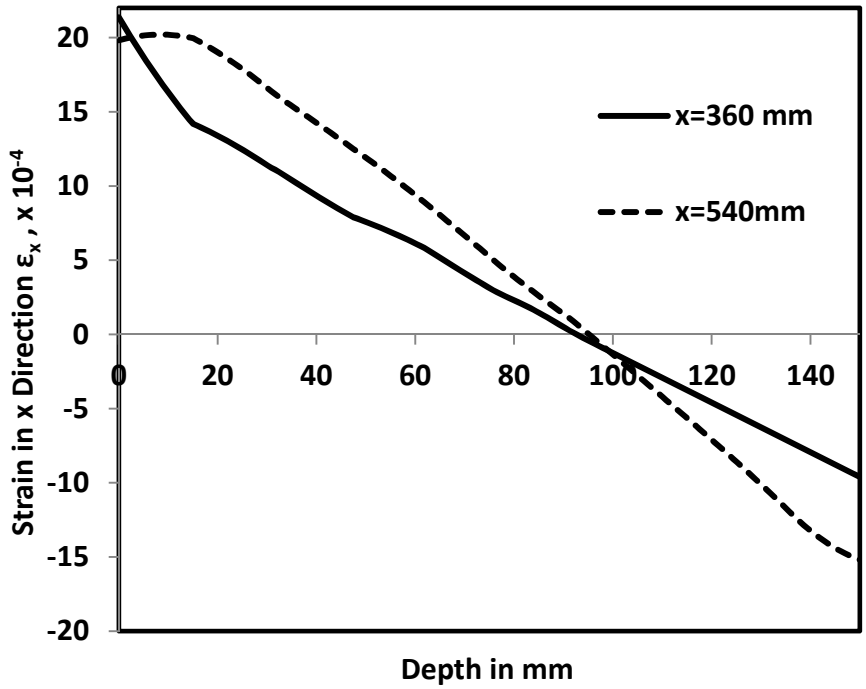

Figure 6.61: Axial Strain ε_x at Cracks in x=540 mm and x=360 mm for B60.

positions at distance of 360 and 540 mm for the support of the RC beam. One more crack was developed when the RC beams loaded up to 75% of its flexural loading as shown in Figure 6.62, the crack depths were found to be 50, 85, and 90 mm for cracks at distances of 95, 400 and 520 mm, respectively, from the support of the RC beam.

Figure 6.63 shows the normal strain (ε_x) at RC beams subjected to 90% flexural loading and it can be noted that the crack depths were 70, 87 and 90 mm for cracks at distances of 100, 400, and 550 mm, respectively.

6.3.4 Finite Element Simulation of Chloride Diffusion in RC Beams Subjected to Flexural-Induced Damage

Two-dimensional numerical simulation was conducted using COMSOL software to be compared with the experimental results obtained after 90 days chloride exposure period. Figures 6.64 through 6.71 show two dimensional free chloride distribution in the undamaged RC beams, at first cracking load, 10 kN, 40 kN, 65 kN and 90 kN flexural loading.

From these Figures, the two zones of chloride diffusion could be noted while the distribution of mechanical damage was used in the zones between cracks to evaluate the chloride diffusion; the crack width influence function controlled the transport of the chloride along the crack depth. The damage influence functions as described in equation [6.1], the chloride binding influence function as in equation [6.3], and the crack width

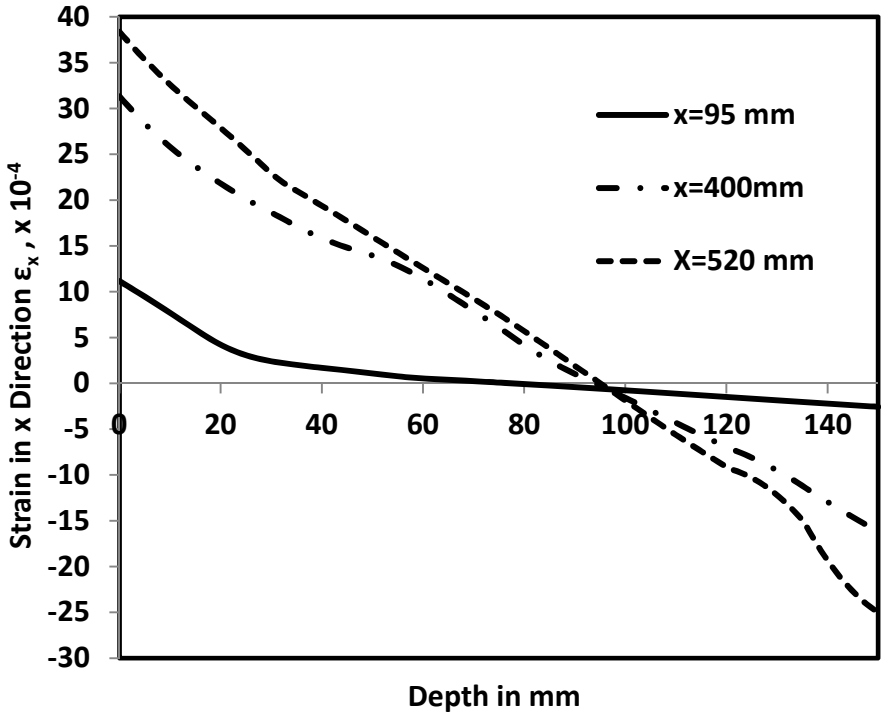

Figure 6.62: Axial Strain ε_x at Cracks in x=95, 400 and 520 mm for B75.

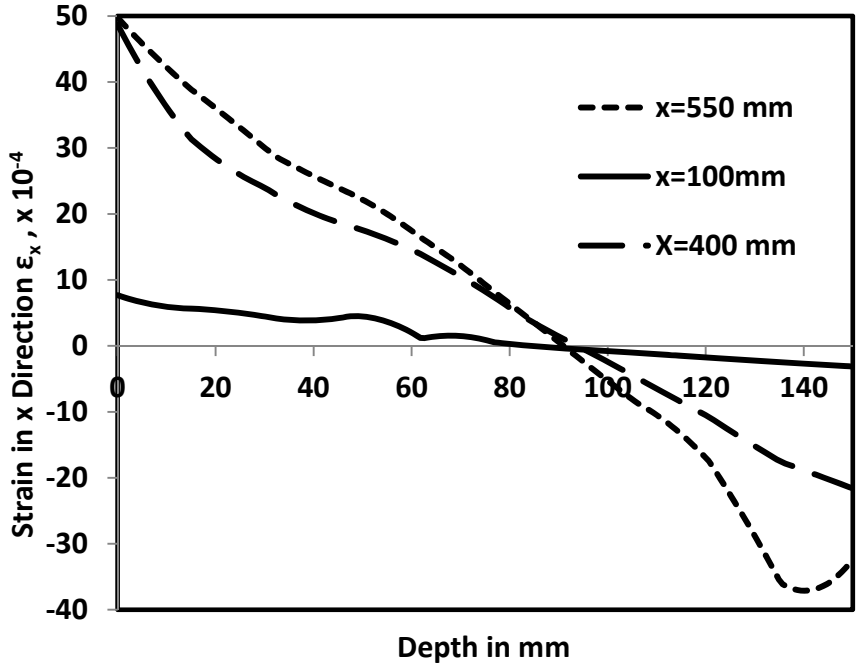

Figure 6.63: Axial Strain ε_x at Cracks in x=100, 400 and 550 mm for B90.

influence function as in equation [6.4] were used to simulate the chloride diffusion in damaged RC beams. As expected, increasing the mechanical damage in both compressive and tensile zone will increase the chloride penetration into concrete, and the influence of tensile damage is higher than the compressive damage. As mentioned in the experimental results in section 6.1, the effect of mechanical damage could be explained due to the creation of microcracks in the cement paste as well as on the transition zone between the coarse aggregate and the cement past.

Figure 6.64 shows the free chloride distribution in undamaged RC beam, where the chloride diffusion coefficient was found to be D_{effd} (D_d F_{cb}) 2.1×10^{-6} mm^2/s and for the tensile damaged concrete corresponding to stress levels of 40%, 60%, 75% and 90% of the ultimate flexural loading, the effective diffusion coefficient D_{effd} was computed as $7.4x10^{-6}$, $1.7x10^{-5}$, $2.1\ x10^{-5}$ and 2.2×10^{-5} mm^2/s, respectively. Figure 6.65 shows the free chloride distribution in RC beam subjected to first crack loading at 7.5 kN. From Figure 6.65, it can be observed that there is no significant change in the chloride penetration in the compressive zone as the compressive damage is till not initiated, while in tensile damage zone, it can be noted that there is an increase in the free chloride penetration towards the constant moment zone. Besides, at the first crack position, the chloride penetrated up to a depth of 30 mm with free chloride concentration of a bout 0.12% by weight of concrete.

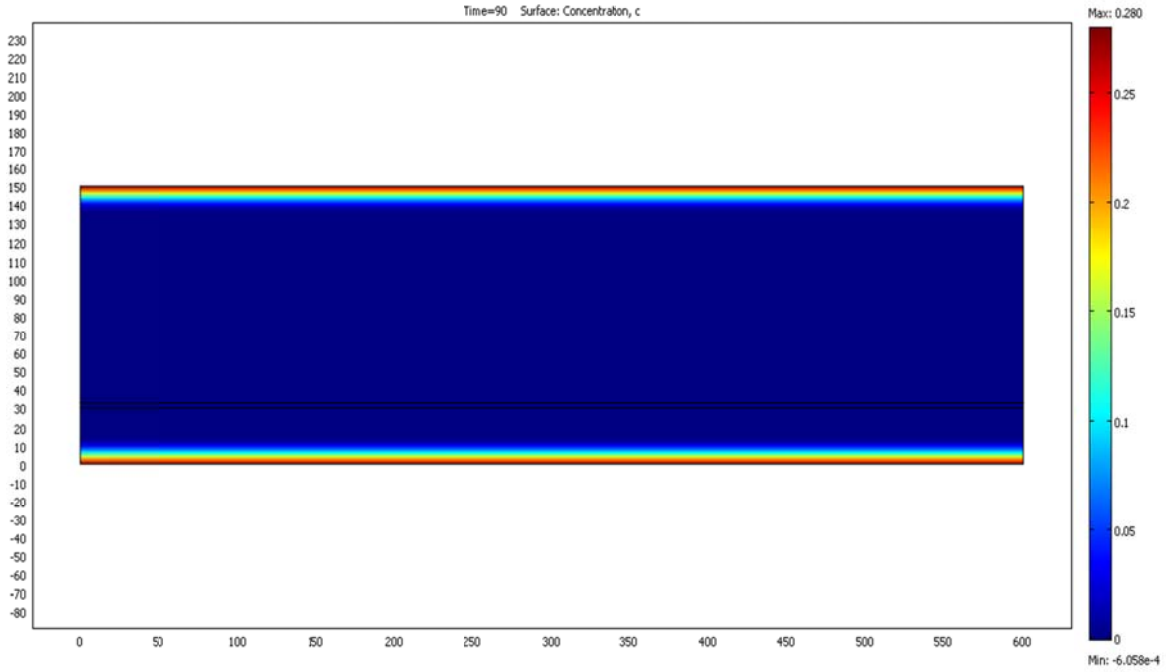

Figure 6.64: Free Chloride Distribution in Undamaged RC Beam.

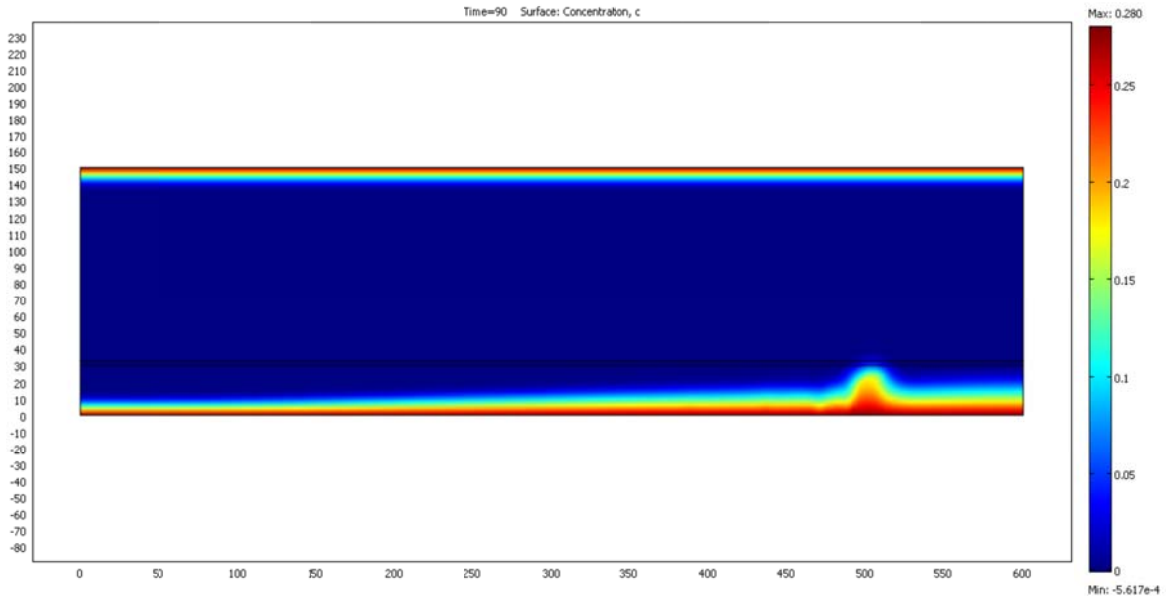

Figure 6.65: Free Chloride Distribution at First Cracking Load P= 7.5 kN.

Due to the increase of flexural loading up to 10 kN, the first crack depth increases up to 50 mm with a chloride content about of 0.15% by weight of concrete at the level of the reinforcement steel. A second crack was initiated with crack depth of 28 mm and chloride content about 0.075% by weight of concrete as well as shown in Figure 6.66.

Figure 6.67 shows the free chloride distribution in RC beam subjected to first crack loading at 20 kN. From Figure 6.67, it can be observed there is no significant change in the chloride penetration in the compressive zone as the compressive damage is till not initiated, while in the tensile damage zone, it can be noted an increase in the free chloride penetration towards the constant moment zone.

Due to the increase of flexural loading up to 20 kN, the first crack depth increases up to 70 mm with a chloride content about of 0.18% by weight of concrete at the level of the reinforcement steel. A third crack was initiated with crack depth of 28 mm and chloride content about 0.10% by weight of concrete as well as shown in Figure 6.67

The same trend could be observed in Figure 6.68 and Figure 6.69, where with the increase of the applied flexural loading up to 40, 60 kN, there was no significant increase in the chloride penetration in compressive zone, while it can be noted the increase in the chloride penetration in tensile damaged zone as well as in the crack positions and the free chloride content reached values of 0.20% by weight of concrete at the level of the reinforcement at 40 kN loading.

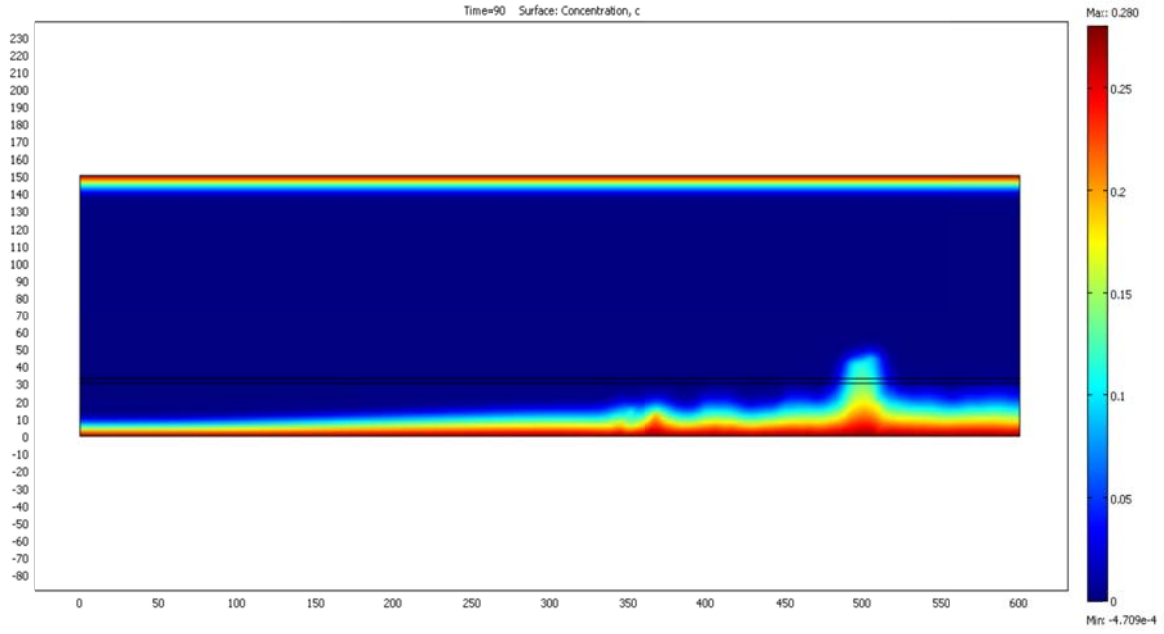

Figure 6.66: Free Chloride Distribution at First Cracking Load P= 10 Kn.

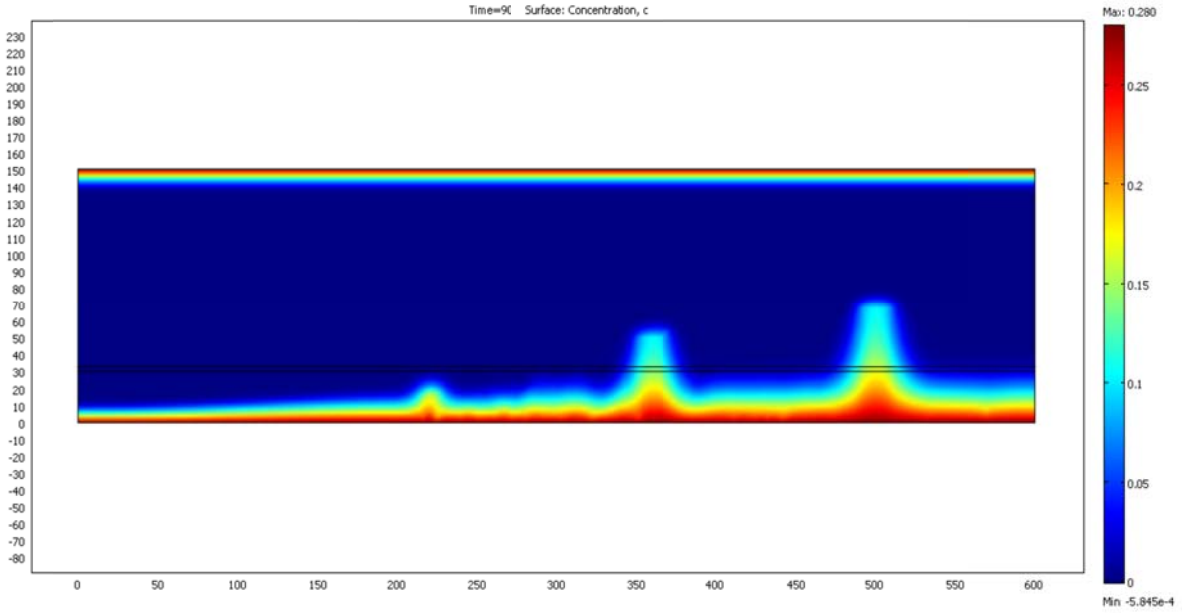

Figure 6.67: Free Chloride Distribution at First Cracking Load P= 20 kN.

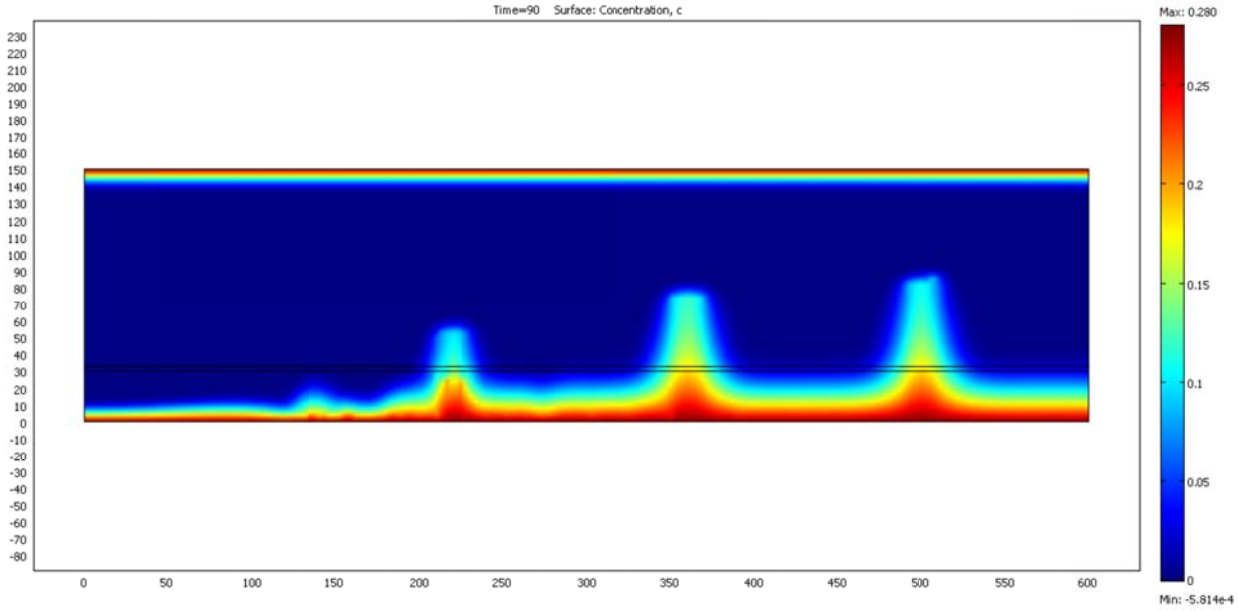

Figure 6.68: Free Chloride Distribution at First Cracking Load P= 40 kN.

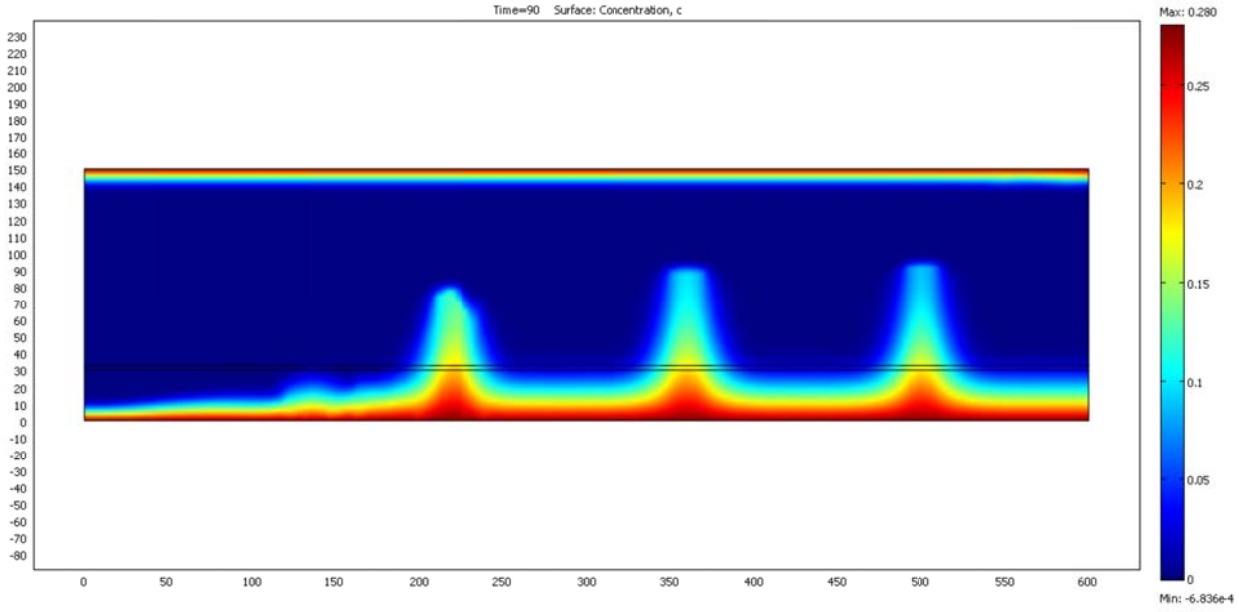

Figure 6.69: Free Chloride Distribution at First Cracking Load P= 60 kN.

The effect of compressive damage started to be significant when the RC beams subjected to 75% flexural loading as shown in Figure 6.70 and Figure 6.71, where it can be noted that the increase in the chloride penetration in the constant moment zone at the top of the RC beams. The free chloride content in compressive damage zone was found to be 0.10% at depth of 10 mm as shown in Figure 6.70, while at the tensile zone with the same depth of 10 mm the free chloride content reached a value of 0.25% by weight of concrete.

A comparison between the experimental and numerical results of free, total, and bound chloride profiles at a distance of 120 mm from the support is shown in Figure 6.72, Figure 6.73 and Figure 6.74, respectively. It can be noted that the proposed COMSOL model is predicting accurately the chloride profile contents for sound and damaged concrete.

To compare the experimental and the numerical results along the crack depth, a one dimensional chloride profile was plotted in Figure 6.75 at the position of maximum crack width of about 500 mm from the edge of the RC beam. From Figure 6.75, it can be noted that the finite element simulation matched well with the experimental results. The chloride diffusion coefficient in the crack positions with crack widths more than 0.40 mm was found to be about 2.0×10^{-4} about 100 times the chloride diffusion coefficient in undamaged concrete.

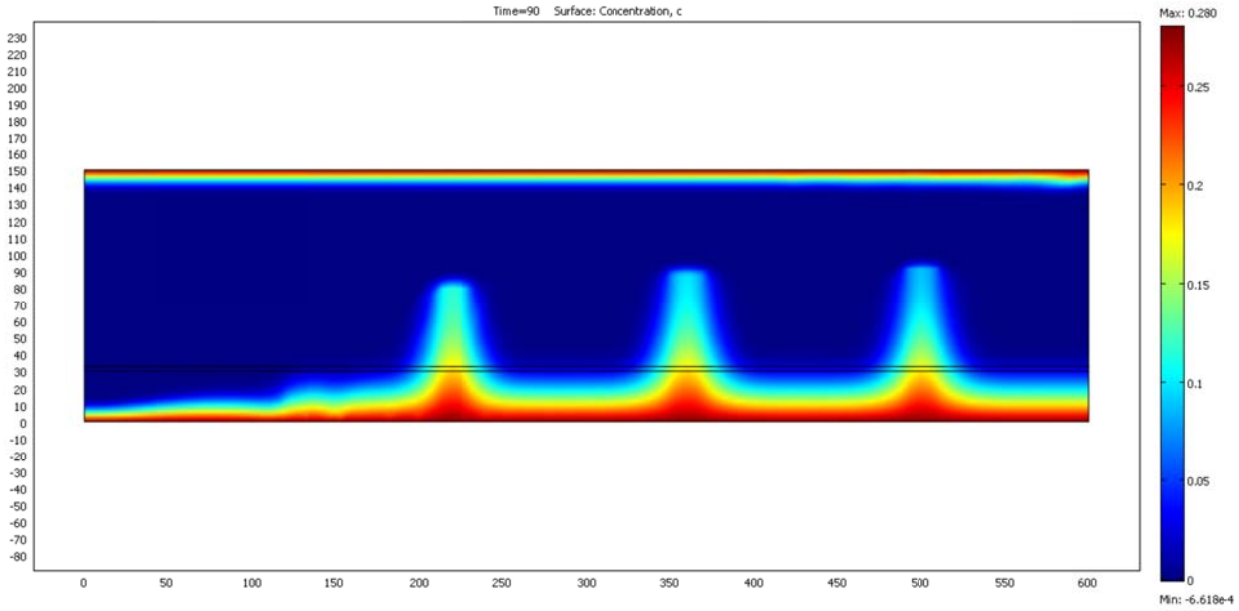

Figure 6.70: Free Chloride Distribution at First Cracking Load P= 75 kN.

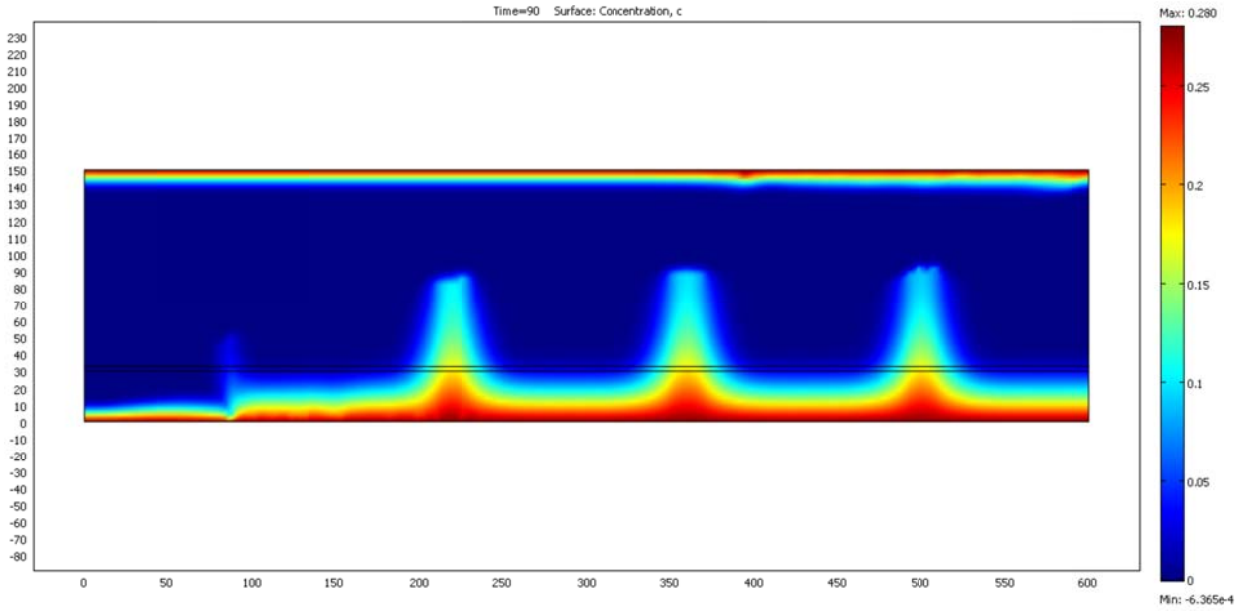

Figure 6.71: Free Chloride Distribution at First Cracking Load P= 90 kN.

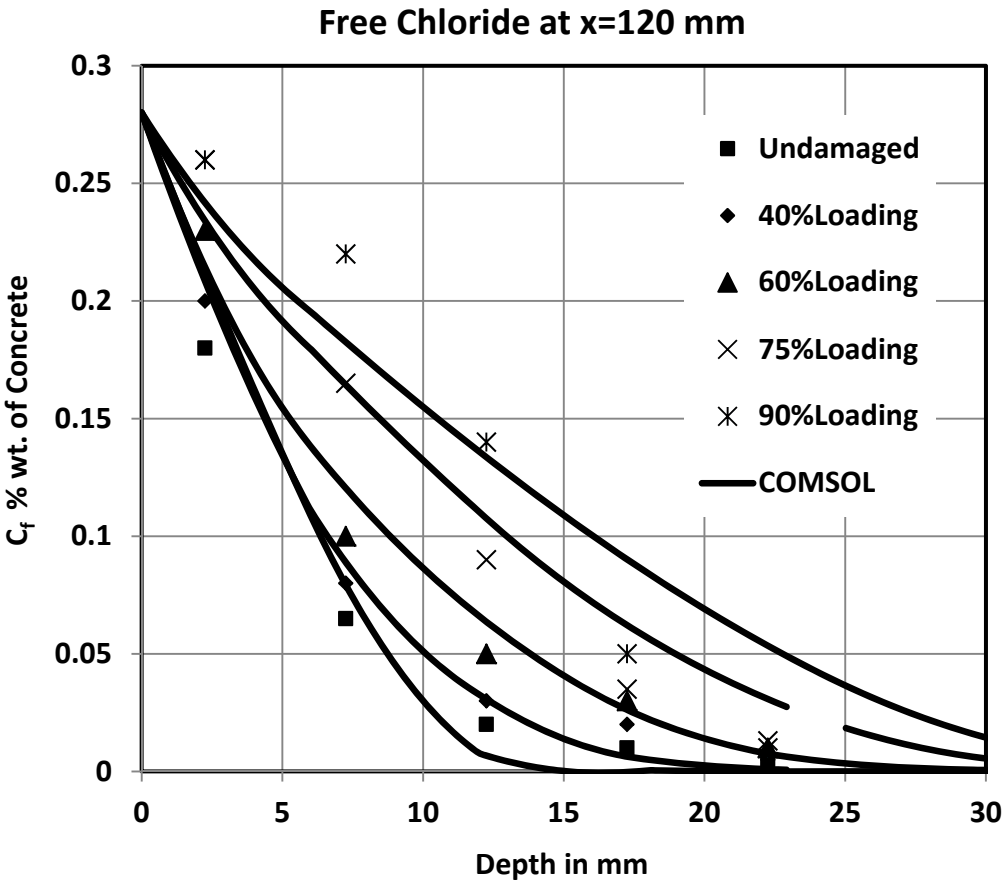

Figure 6.72: Experimental vs. numerical free chloride profile in sound and damaged concrete.

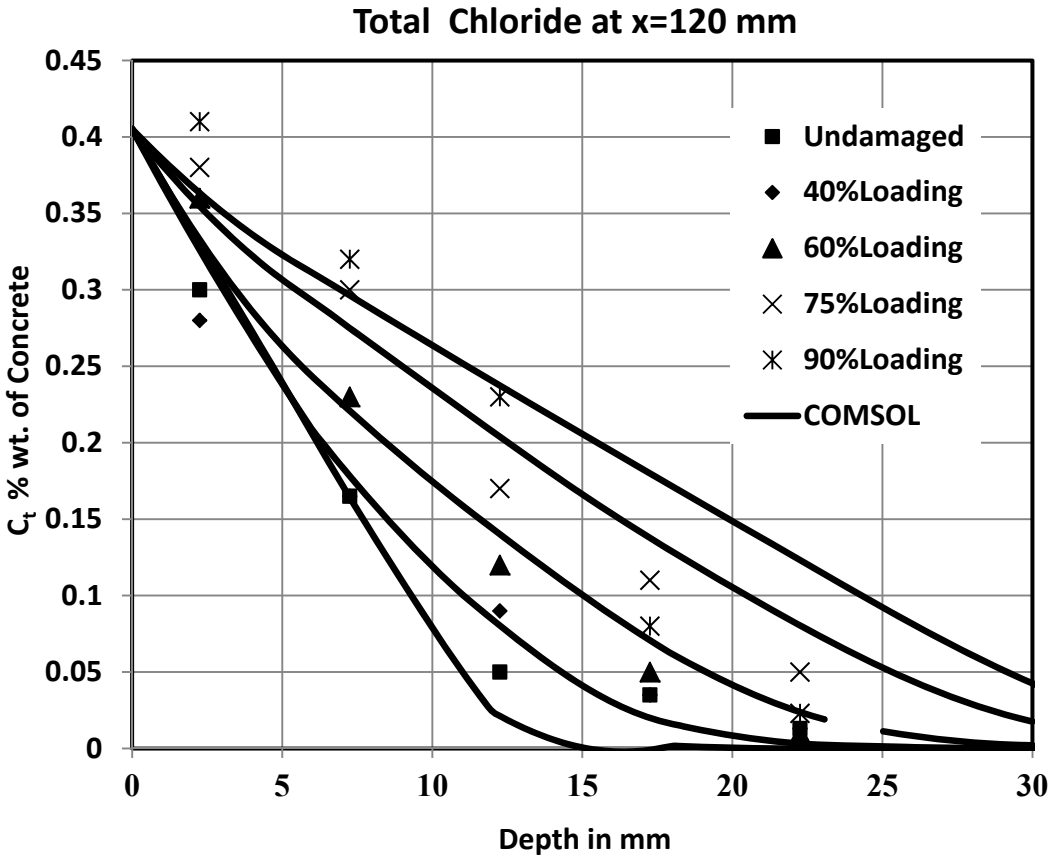

Figure 6.73: Experimental vs. numerical total chloride profile in sound and damaged concrete.

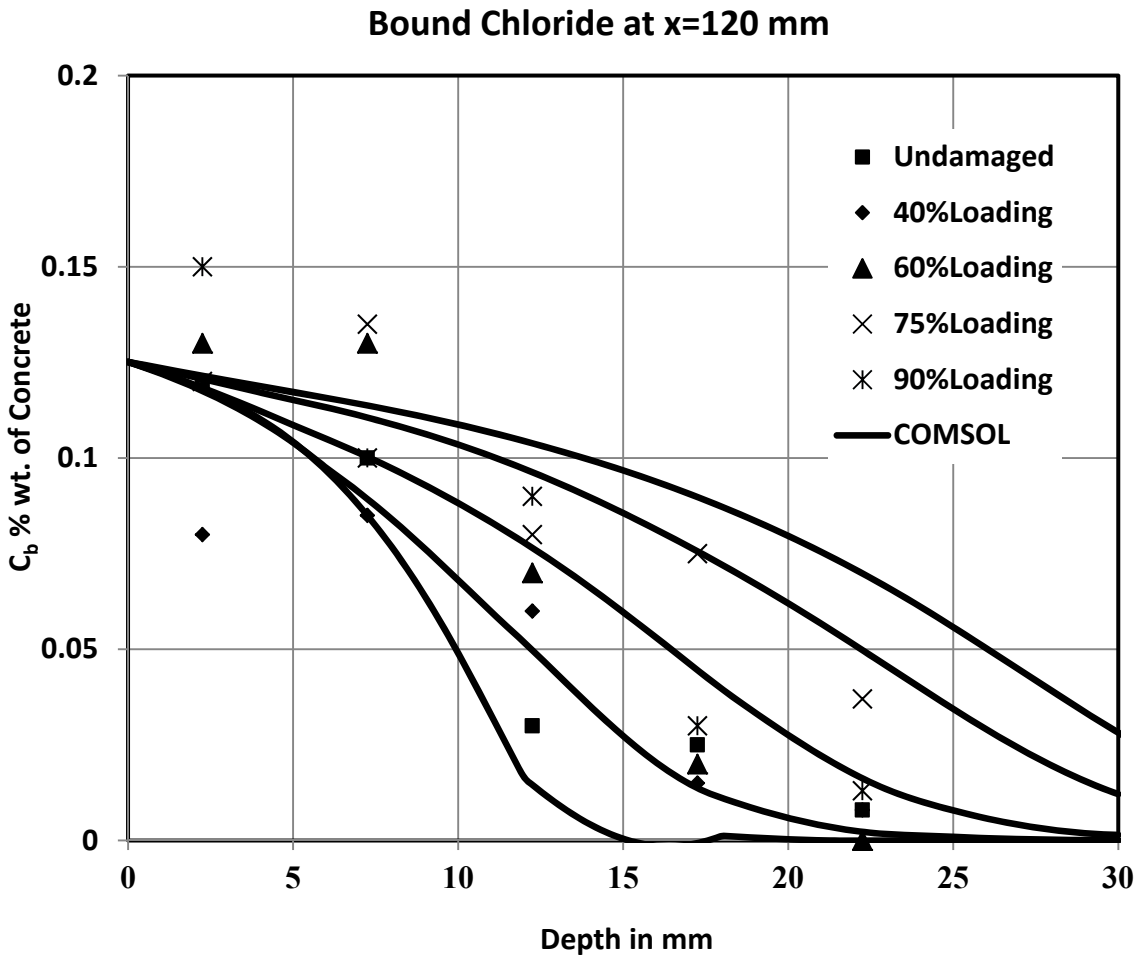

Figure 6.74: Experimental vs. numerical bound chloride profile in sound and damaged concrete.

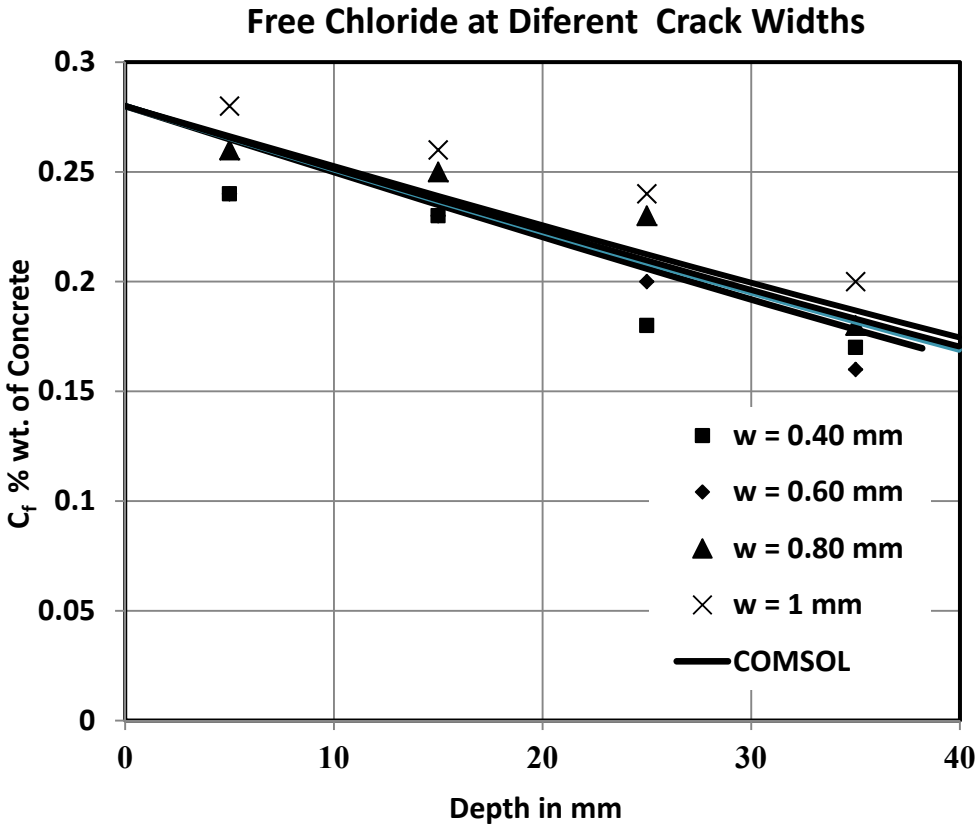

Figure 6.75: Experimental Vs. numerical free chloride profile along cracks with various crack widths.

To verify the proposed model, experimental results reported by Sakoi and Horiguchi [2006], He and Gong [2005] and Xing et al. [2005] were compared with the same level of stress obtained from the COMSOL model at a distance of 100 mm from the edge of the RC beams as shown in Figure 6.76 where it can be noted that the proposed model is matching well up to 80% of the tensile strength of concrete. The crack width influence function will take the residual effect of any tensile stress more than 80% if tensile strength of concrete which indicates that the proposed model could be used to predict the service life of the reinforced concrete structures subjected to tensile and compressive service stress.

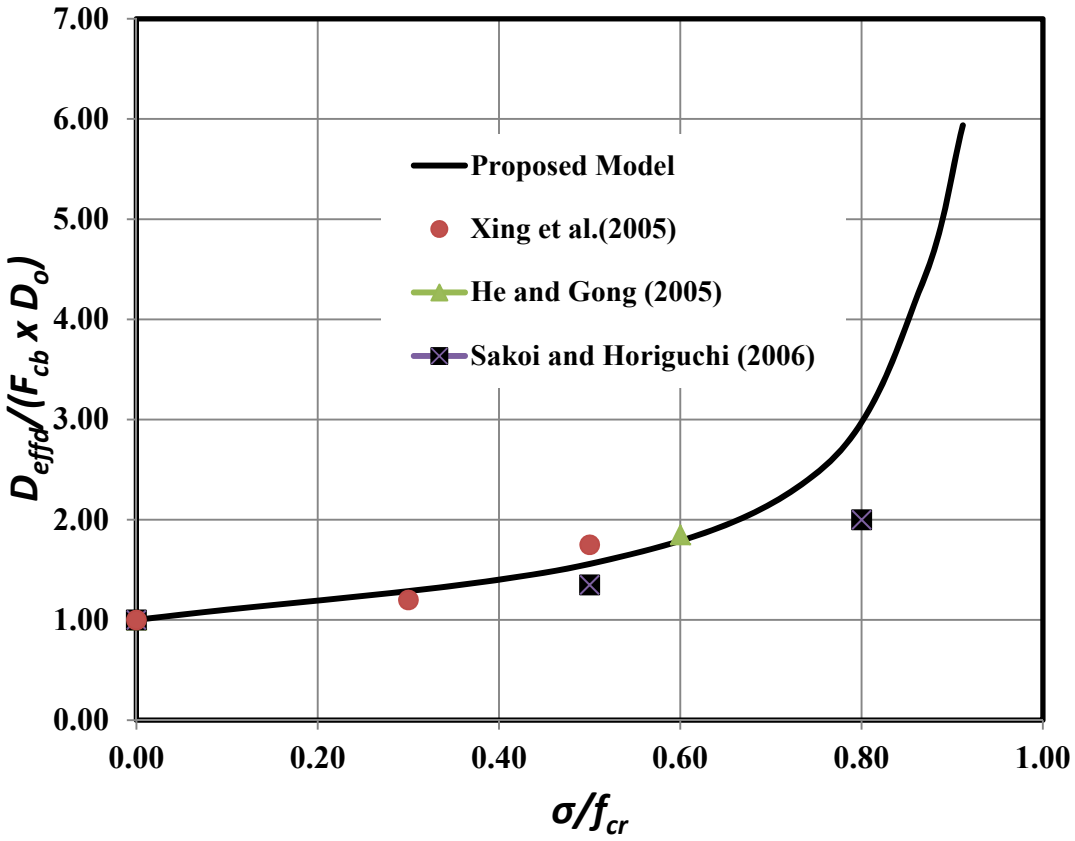

Figure 6.76: Comparison between the proposed model and other experimental results.

CHAPTER 7

CONCLUSIONS AND RECOMMENDATIONS

7.1 Conclusions

Experimental and numerical studies of chloride penetration in concrete samples damaged with high levels of compressive stress and exposed to 10% NaCl in NT BUILD 492 test were conducted. Besides, RC beams damaged in flexure with 40%, 60%, 75%, and 90% of ultimate flexural loading and exposed to 8% NaCl solution for 90 days were conducted. A phenomenological damage model and Langmuir chloride binding hypothesis coupled with chloride diffusion and chloride migration governing equations using Nernst Planck equation were used to assess chloride transport in damaged concrete. Empirical relations between both mechanical damage and crack width were established to simulate the transport of chloride in damaged concrete.

- For undamaged self-compacting concrete samples, D_{effm} was 4×10^{-5} mm^2/s while for the damaged concrete with damage levels corresponding to 40%, 75% and 90% of the compressive strength of the concrete, the effective migration coefficient D_{effm} was determined to be 4.5, 7.5 and 12×10^{-5} mm^2/s, respectively. These values indicate an increase of diffusivity of up to three times in damaged concrete subjected to a compressive loading corresponding up to 90% of the compressive strength.

- It is noted that the influence of binding phenomena on chloride migration opposes that of damage by inducing a reduction of about 20% of chloride migration diffusivity in self-compacting concrete.

- For undamaged concrete, D_{effd} was 2.1×10^{-6} mm^2/s while for the damaged concrete with tensile damage levels corresponding to 40%, 75% and 90% of the ultimate flexural loading of the concrete, the ratio of damaged to sound effective diffusion coefficient $D_{effd}/(D_d x\ F_{cb})$ was determined to be 3, 6.7, 8.3 and 8.7, respectively, these values indicate an increase of diffusivity of up to nine times in damaged concrete.

- In compressive damage zone, these ratios are 1.15, 1.23 and 1.43 corresponding to 60%, 75% and 90% of ultimate flexural loading. It is noted that the influence of binding phenomena on chloride diffusion opposes that of damage by inducing a reduction of about 25% of chloride diffusivity in concrete. Using the approach

outlined in this research, the impact of damage coupled with chloride transport may be used for predicting the reduced service life of reinforced concrete structures subjected mainly to flexural stress fields.

- The effect of crack widths on the chloride diffusivity in RC beams subjected to flexural loading was investigated for crack ranges from 0.25 to 1 mm in damaged RC beams. The chloride diffusion coefficient increased by 104 times the chloride diffusion coefficient of sound concrete for crack width equal to 0.25 mm and tends to increase up to 126 times the chloride diffusion coefficients of sound concrete with crack width of 1 mm.

- It was noted that the chloride binding in concrete has un upper limit value of about 50% of free chloride, and the effect of binding capacity on chloride diffusivity decreased by about 25 to 35% of the chloride diffusion coefficient.

7.2 Recommendations for Further Studies

- This research could be extended to predict the service life of concrete structures under environmental and mechanical loading.

- There is a need to conduct further research on the assessment of the migration of chloride using NT BUILD 492 to study the effect of surface chloride

concentration, the applied electrical current and adding mineral admixture such as fly ash and silica fume.

- The chloride binding capacity in concrete is a transient process, and there is a need to investigate the chloride binding with respect to both time and mechanical damage. Nano-scale investigation is needed to find out the effect of mechanical damage on binding chloride as well as its affect on the hydrated cement paste.

- More investigation could be conducted in the transport of chloride in concrete structure in unsaturated or in wetting and drying conditions.

- This research was conducted using RC beams subjected to flexural loading, more research is needed to simulate the chloride transport in concrete structure subjected to different loading cases such as columns which are subjected to compression or other type of concrete structures such bridges which subjected to cyclic loading.

- Similar simulation could be conducted to study the effect of mechanical induced damage on other transport properties such as thermal conductivity and permeability in concrete and other heterogeneous materials.

NOMENCLATURE

C_t : Total Chloride in g chloride per g of concrete.

C_f : Free Chloride in g chloride per g of concrete.

C_b : Bound Chloride in g chloride per g of concrete.

D_d : Chloride diffusion coefficient in undamaged concrete in mm^2/s.

D_{effd} : Effective chloride diffusion coefficient mm^2/s.

F_d : Mechanical damage influence function.

F_{cb} : Chloride binding influence function.

α & β: Chloride binding isotherm parameters.

σ: Uniaxial stress in MPa.

ε: Uniaxial strain in mm/mm.

E: Damage secant modulus in MPa.

E_o: Undamage secant modulus in MPa.

d: Scalar damage.

σ_u : Peak stress in MPa.

ε_u : Peak stain in mm/mm.

m : Material parameter.

d_c: Compressive scalar damage.

d_t: Tensile scalar damage.

ε_{cr}: Tensile cracking stain in mm/mm.

m_c: Material parameter for compression damage.

m_t : Material parameter for tensile damage.

I : Hydrostatic component of the stress tensor.

J : Deviatoric stress tensor invariant.

φ: the friction angle (Degree).

c: cohesion in MPa.

E_s: Young's modulus of reinforcement steel in MPa.

F_{ys}: Yield Stress of reinforcement steel in MPa.

APPENDIX A

Calculation of Cracking Load (P_{cr})

Section Properties:

t = 150 mm, b = 150 mm

d = 120 mm

Ig = 42187500 mm^4

As = 402 mm^2

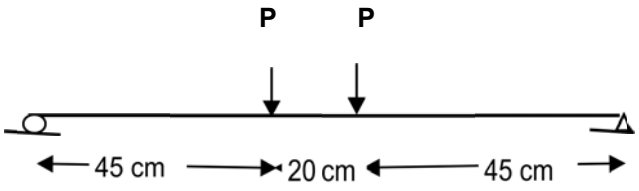

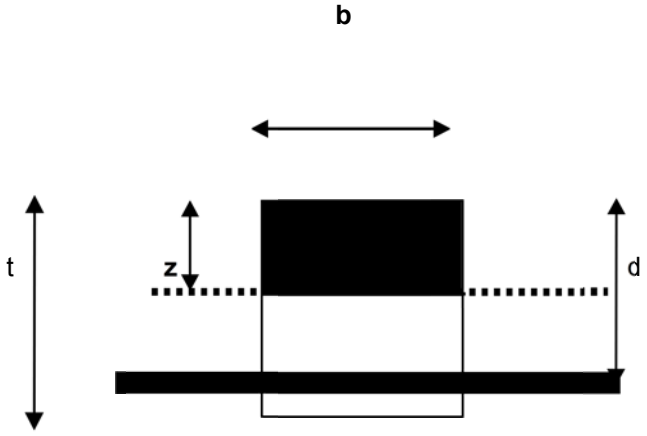

Materials Propreties:

Fc = 50 MPa , Fy = 560 MPa

E_c = 29000 MPa

E_s = 190000 Mpa

Fcr = 7.6 $\sqrt{fc}$ in (psi)

Fcr = 4.5 MPa

$$Mcr = \frac{Fcr \cdot \frac{t}{2}}{Ig} = \frac{4.5\ x\ 75}{42187500} = 3.14\ kN.m$$

$$Mcr = 3.14 = Pcr\ x\ 0.45$$

$$\boldsymbol{Pcr = \frac{3.14}{0.45} = 7\ kN}$$

Compared to average calculated from COMSOL ***Pcr* = 7.25 kN** ; Error = 3.5%

2.0 Calculation of Ultimate Load *Pu*

$$C = \frac{\alpha \times Fc \times 0.8z \times b}{\gamma c} = \frac{0.85 \times 50 \times 0.8z \times 150}{1.5} = 3400\ z\ N$$

$$T = As \times \frac{Fy}{\gamma s} = 402 \times \frac{560}{1.15} = 195756\ N$$

$$C = T = \frac{3400\ z}{195756}\ get\ z = 57.6\ mm$$

$$\frac{\varepsilon}{d - z} = \frac{\varepsilon u}{z}$$

$$\varepsilon = \frac{0.0035 \times (120 - 57.6)}{57.6} = 0.003795$$

$$\varepsilon y = \frac{fy}{Es} = \frac{560}{190000} = 0.002947$$

ε > εy → The Reinforcement Steel is yielding at ultimate loading

$$Mu = T\ (d - x) + C\ (0.67\ x)$$

$$= 195756\ (120 - 57.6) + 3400 \times 57.6 \times 0.67(57.6)$$

= 19.77 kN. m

$$Mu = Pu * 0.45$$

Get *Pu = 43.93 kN total Pu = 2 x 43.93 =* ***88 kN***

Compared to ultimate load computed by COMSOL *Pu =* ***94 kN***

Error = 6%

APPENDIX B

Calculation of Crack width and Spacing

1. Calculation of Crack Width (w)

Using the Gergely-Lutz equation, we can estimate the maximum width of cracks in the concrete in the tension faces of flexural members. The maximum width of cracks is given by (Gergely and Lutz, 1968):

$$w = 2.2\ \beta x\ \varepsilon_s\ \sqrt{d_c\ x\ A}$$

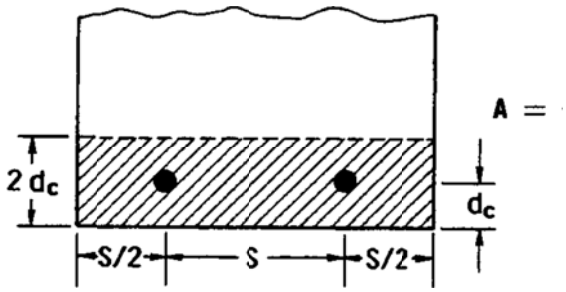

where:

w is the estimated crack width, (in);

β is ratio of the distance to the neutral axis from the extreme tension concrete fiber to the distance from the neutral axis to the centroid of the tensile steel;

β = (d-z)/(t-z) = (150-57.6)/(120-57.6) = 1.5

ε_s is the strain in the steel;

A (in^2) is the effective tension area of concrete around the main reinforcement (having the same centroid as the reinforcement) divided by the number of bars (n),

$A = 2 \; x \; dc \; x \; b/n = 2 \text{ x } 1.5 \text{ x } 6/2 = 9 \text{ in}^2$

Table A shows comparison between calculated and measured crack widths.

Table A: Comparison between calculated and measured crack widths.

Measured\calculated	**% of Ultimate Flexural Loading**			
	40	**60**	**75**	**90**
ε_s (Measured)	1500	2350	2600	3400
***w* calculated(mm)**	0.3	0.5	0.6	0.7
***w* measured(mm)**	0.4	0.6	0.8	1

2. Calculation of Crack Spacing (S_{cr})

The crack spacing (S_{cr}) was calculated according to ACI 224R-01, where:

$$S_{cr} = 4 \; x \; d_c \; \sqrt{1 + \left(\frac{s}{4d_c}\right)^2}$$

d_c is the distance of the bar to extreme tension fiber, (in) = 1.2 in

s is the bar spacing, (in) = 3 in

$$S_{cr} = 4 \; x \; 1.2 \; \sqrt{1 + \left(\frac{3}{4x1.2}\right)^2}$$

$$S_{cr} = 5.66 \; in = 143 \; mm$$

REFERENCES

Al-Amoudi O.S.B., Rasheeduzzafar, M. Maslehuddin, and S.N. Abduljauwad, (1991) "Influence of Sulfate Ions on Chloride-Induced Reinforcement Corrosion in Portland and Blended Cement Concretes", *Cement, Concrete and Aggregates,* **16**(**1**), pp. 3-11.

Al-Amoudi, O.S.B., Abduljauwad, S.N., Rasheeduzzafar, and Maslehuddin, M. (1992), Effect of Chloride and Sulfate Contamination in Soils on Corrosion of Steel and Concrete, *Transportation Research Record 1345,* pp. 67-73.

Alexander M.G.,(2003), "Towards a Performance Specification for Reinforced Concrete, Based on Durability Indexes", *Proc. International Conference on Performance of Construction Materials in the New Millennium – A New Era of Building,* Vol. 2, eds. A.S. El-Dieb, M.M.R. Taha, and S.L. Lissel, Elmaarefa Printing House, Cairo, Egypt, pp. 837-846.

Al-Gahtani, A. S., (1981), "An Investigation of Corrosion of Reinforcement in Concrete in the Eastern Province of Saudi Arabia", M. S. Thesis, King Fahd University of Petroleum and Minerals, Dhahran.

American Concrete Institute, (2001), "Guide to Durable Concrete, ACI 201.2R-01", A*CI World Headquarters*, 38800 Country Club Drive, Farmington Hills, MI, USA.

ACI 224R-01. 2001. Control of Cracking in Concrete Structures. *American Concrete Institute (ACI)*, 38800 Country Club Drive, Farmington Hills, MI 48331, USA.

Andrade C., (1993),"Calculation of chloride diffusion coefficients in concrete from ionic migration measurements", *Cement and Concrete Research, 23 (3)*, 724– 742, 1993.

Antoni, Horiguchi, T. and Saekin, N., (2003),"Influence of Stress on Chloride Penetration into FRC", *Proceedings of the JCI*, v.25, pp.779-784.

Arya C, Buenfeld NR, Newman JB. (1990),"Factors influencing chloride binding in concrete", Cem Concr Res, 20(2):291–300.

ASTM P214 “Test Method for Accelerated Deleterious Expansion of Mortar Bars Due to Alkali-Silica Reaction”.

Ayman Ababneh1; Farid Benboudjema2; and Yunping Xi, (2003),"Chloride Penetration in Nonsaturated Concrete" *Journal of Materials in Civil Engineering*, Vol. 15, No. 2.

Azad, A.K., Alfarabi, S.,Navaz, M., Loughlin, K., (1997)," Chloride Diffusion Coefficient of Concrete in the Arabian Gulf Environment", The Arabian journal for science and engineering , Vol. 22, No. 2B, pp.169

Baluch M.H., M.K. Rahman, and A.H. Al-Gadhib, (2002), “Risks of Cracking and Delamination in Patch Repair”, *Journal of Materials in Civil Engineering, ASCE,* 14(4), pp. 294-302.

Bamforth PB . (1999), "The derivation of input data for modeling chloride ingress from eight-years UK coastal exposure trials", Mag Concrete Res 1999; 51:87–96.

Baroghel-Bouny, Patrick Belin, Matthias Maultzsch , Dominique Henry, (2007),"AgNO3 spray tests: advantages, weaknesses, and various applications to quantify chloride ingress into concrete. Part 2: Non-steady-state migration tests and chloride diffusion coefficients", Materials and Structures ,40:783–799.

Basheer P.A.M., S. Chidiac, and A.E. Long, (1984), “Predictive Models for Deterioration of Concrete Structures”, *Construction and Building Materials,* 10(1), pp. 27-36.

Bazant, Z. P., and Najjar, L. J. (1972). Nonlinear Water diffusion in Non-Saturated Concrete. *Materials and Structures*; Vol. 5, No. 25, pp. 3-20

Bentz EC, Evans CM, Thomas MDA. Chloride diffusion modeling for marine exposed concretes. In: Page CL, Bamforth PB, Figg JW, editors. Corrosion of reinforcement in concrete construction. Cambridge,

Berman HA. (1972), Determination of chloride in hardened portland cement paste, mortar, and concrete. J Mater; 7(3):330–5.

Blunk G, Gunkel P, Smolczyk HG. (1986)," On the distribution of chloride between the hardening cement paste and its pore solution. In: Proceedings of the 8th international congress on the chemistry of cement; p. 85–90.

Breysse, D. and Gerard, B., (1997),” Transport of Fluids in Cracked Media, Penetration and Permeability of Concrete: Barriers to Organic and Contaminating Liquids, *RILEM Report 16, E&FN Spon*, London, 1997.pp.123-153.

Byfors, K., (1987), "Influence of Silica Fume and Fly Ash on Chloride Diffusion and pH Values in Cement Paste, Cement and Concrete Research, Vol. 17, pp. 115-130.

Castel A., R. François, G. Arliguie , (1998), ” Effect of loading on carbonation penetration in reinforced concrete elements”, *Complesce Scientifique de Rangueil, I.N.S.A.—U.P.S. Genie Civil, Laboratoire Matériaux et durabilité des constructions (L.M.D.C.), 31077 Toulouse Cedex 4, France* Manuscript received 5 August 1998; accepted manuscript 20 January 1999.

Castellote M, Andrade C, Alonso C. (1999), "Chloride binding isotherms in concrete submitted to non-steady-state migration experiments. Cem Concr Res , Vol. 29, pp.1799–806.

Chatzigeorgiou G., Picandet V., Khelidj A., and Pijaudier-Cabot G., (2005), “Coupling between progressive damage and permeability of concrete: analysis with a discrete model” *Int. J. Numer. Anal. Meth. Geomech*.,; pp.1005–1018.

Chiang C.T., C.C. Yang, (2007)," Relation between the diffusion characteristic of concrete from Salt ponding test and accelerated chloride migration test", Materials Chemistry and Physics 106 , 240–246.

Christensen, R. M. (1979). *Mechanics of composite materials.* Wiley-Interscience, New York.

Collepardi, M., (1995), “Quick Method to Determine Free and Bound Chlorides in Concrete”, Chloride Penetration into Concrete, *Proceedings of the RILEM International Workshop,* France, Edited by L.O. Nilsson and J.P. Ollivier, pp. 10-16.

Crank J. ,(1975), *The Mathematics of Diffusion,* 2nd edn. Oxford: Clarendon Press.

Delagrave Anik, Marchand Jacques, Olliver Jean-Pierre, Julien Simone, Hazrati Kati., (1997), " Chloride binding capacity of various hydrated cement systems", Adv Cem-Based Mater 1997(6):28–35.

Dhir RK, El-Mohr MAK, Dyer TD. (1997), " Developing chloride resisting concrete using PFA. Cem Concr Res , 27(11):1633–9.

Dhir RK, Jones MR, McCarthy MJ. (1994), " PFA concrete: chloride-induced reinforcement corrosion. Mag Concr Res , 46(169):269–77.

Dong Chen, (2006),” Computational Framework for Durability Assessment of Reinforced Concrete Structures Under Coupled Deterioration Processes”, *PhD Dissertation*, Vanderbilt University, Nashville, Tennessee, USA, 2006.

Elsener, B., Zimmermann, D., Fluckiger, D., Burchler, D., Bohni, H., (1995), “Chloride Penetration- non Destructive Determination of the Free Chloride Content in Mortar and Concrete”, Chloride Penetration into Concrete, *Proceedings of the RILEM International Workshop,* France, Edited by L.O. Nilsson and J.P. Ollivier, pp. 17-26

Evardsen C (1999) *ACI Mater J* 96(4):448

Frederiksen, J., Nilsson, L., Sandberg, P., Pousen, E., Tang, L., and Andersen, A., (1997),”System for Estimation of Chloride Ingress into Concrete. Theoretical Background, *HETEK Report No. 83. The Danish Road Directorate*, .

Friedmann H., O. Amiri, A. A. Mokhtar, P. Dumargue, (2004)," A direct method for determining chloride diffusion coefficient by using migration test", Cement and Concrete Research 34, 1967–1973.

Gerard B, Reinhardt HW, Breysse D (1997) In: Reinhardt HW (ed) Measured transport in cracked concrete, penetration and permeability of concrete. RILEM, France, Report 16, pp 123–153.

Gerard B., J. Marchand, (2000), “Influence of cracking on the diffusion properties of cement-based materials Part I: Influence of continuous cracks on the steady-state regime”, *Cement & Concrete Composites,* 30, pp. 37-43.

Gergely, P. and Lutz, L.A. (1968). “Maximum Crack Width in Reinforced Flexural Members, Causes, Mechanisms and Control of Cracking in Concrete.”SP-20, Detroit, *American Concrete Institute*, PP: 87-117.

He, S.Q. and Gong, J.X. (2005)."Influence of Flexural Loading on permeability of Chloride Ion in Concrete." J. of Building Materials, Vol. 8, No. 2, pp. 134-138.

Kachanov, L. M. , (1958), "Time of the rupture process under creep conditions." *Izv. Akad. Nauk.,* S. S. R. Otd. Tekh. Nauk., 8, 26.

Kamran, M., Monteiro, P., and Neville, G., (1998)," A new Method for Studing Stress-Induced Microcraks in Concrete" *Journal of Materials in Civil Engineering,* Vol. 10, No. 3, pp.128-134.

Khan A. R., A.H. Al-Gadhib, and M.H. Baluch, (1998), “Elasto-Damage Constitutive Model for High Strength Concrete”, *Proc., EURO-C 1998*

Conference on Computational Modeling of Concrete Structures, Austria, , 133-142.

Kong, J.S., Ababneh, A.N., Frangopol, D.M., and Xi, Y. (2002) Reliability analysis of chloride penetration in saturated concrete, *Probabilistic Engineering Mechanics*, Vol. 17, No. 3, pp. 305-315.

Krajcinovic, D. and Lemaitre, J., (1986). "Continuum damage mechanics – theory and applications". Springer-Verlag, Berlin.

Kropp, J., Hilsdorf, H.K., Grube, H., Andrade, C., and Nilsson, L. O., (1995), "Transport Mechanisms and Definitions", *RILEM Report 12*, Performance Criteria for ConcreteDurability, London, E&FN Spon, pp. 5-14.

Larsson J. (1995), The enrichment of chlorides in expressed concrete pore solution submerged in saline solution. In: Proceedings of the Nordic seminar on field studies of chloride initiated reinforcement corrosion in concrete, Lund University of Technology, Report TVBM-3064; pp. 171–6.

Lemaitre, J. and Mazars, J., (1982). "Application de la theorie de l'endommagement au comportement non linearie et a la rupture de beton de structure". Annales de l'ITBTP, 401

Leung C., F. Ulm, Y. Xi, G.P. Cabot, and S. Sture, (2000),"Editorial", *Journal of Engineering Mechanics,* ASCE, **126**(**3**).

Long A.E., G.D. Henderson, and F.R. Montgomery, (2000), "Why Assess the Properties of Near-surface Concrete?", *Fifth CANMET/ACI International Conference on Durability of Concrete,* ed. P.A.M. Basheer, *Proceedings of a Special Technical Session on Near-Surface Testing for Strength and Durability of Concrete,* Barcelona, Spain, pp. 1-31.

M.A. Shazali, W.A. Al-Kutti, M.K. Rahman, A.H. Al-Gadhib, M.H. Baluch, (2009) " COMSOL Multiphysics Modeling of Chloride Binding in Diffusive Transport of Chlorides in Concrete", *COMSOL Users Conference in Dhahran*, Khobar, Saudi Arabia.

Maage, M., (1996), " Service Life Prediction of Existing Concrete Structures Exposed to Marine Environments, ACI Materials Journal, Nov.-Dec., pp. 603-608.

Marsavina L., K. Audenaer, G. De Schutter, N. Faur, D. Marsavina , (2008)," Experimental and Numerical Determination of Chloride Penetration in Cracked Concrete", Construction *and Building Materials*.

Marta Choinska a, Abdelhafid Khelidj b, George Chatzigeorgiou c, Gilles Pijaudier-Cabot, (2007),” Effects and interactions of temperature and stress-level related damage on permeability of concrete”, *Cement and Concrete Research* 37, pp. 79–88.

Martin-Perez, B., Zibara, H., Hooton, R.D., and Thomas, M.D.A. (2000) A study of The effect of chloride binding on service life prediction, *Cement and Concrete Research*, Vol. 30, No. 8, pp. 1215-1223.

Mazars J., G. Pijaudier-Cabot, (1989), “Continuum damage theory. Application to concrete”, *J. Engrg. Mech*. *ASCE 115, 345–365*.

McGrath Patrick F., (1996), ' Development of test methods for predicting chloride penetration into high performance concrete. PhD thesis, Department of Civil Engineering, University of Toronto, Canada.

Mehta, P.K., (1986), 'Concrete: Structures, Properties and Materials, Prentic. hall Inc.

Michael D.A. Thomas and Phil B. Bamforth, (1999), " Modelling chloride diffusion in concrete Effect of fly ash and slag", Cement and Concrete Research 29,pp. 487–495

Mustafa Sahmaran, (2007), “Effect of flexure induced transverse crack and self-healing on chloride diffusivity of reinforced mortar”, *Journal of Materials Science*, v 42, n 22, November, pp 9131-9136.

Nagataki S, Otsuki N, Wee TH, Nakashita K. (1993), 'Condensation of chloride ion in hardened cement matrix materials and on embedded steel bars. ACI Mater J; 90(4):323–32.

Neubauer, C. M., Bergstrom, T. B., Sujata, K., Xi, Y., Garboczi, E. J., and Jennings, H. M. (1997). ‘‘Drying shrinkage of cement paste as measured in an ESEM and comparison with microstructural models.’’ *J. Mat. Sci.*, 32, 6415–6427.

Neville A., (1995), “Chloride Attack of Reinforced Concrete: An Overview”, *Materials and Structures,* **28**, pp. 63-70.

Ollivier JP, Arsenault J, Truc O, Marchand J., (1997), 'Determination of chloride binding isotherms from migration tests. In: Mario Collepardi symposium on advances in concrete science and technology, Rome; pp. 198–217.

Page C.L. and O. Vennesland, (1983), "Pore Solution Composition and Chloride Binding Capacity of Silica Fume Cement Pastes", *Material and Structures,* 16(91), pp. 19-25.

Page CL, Lambert P, Vassie PRW, (1991)," Investigations of reinforcement corrosion. 1. The pore electrolyte phase in chloride-contaminated concrete. Mater Struct; 24(142):243–52.

Page, C. E., Nagala, V. T., Parrot,L. J., and Yu., S. W., (1995), " Diffusion in Cementitious Materials :Further Investigations of Chloride and Oxygen Diffusion in Well-Cured OPC and OPC/30% FA Pastes, Cement and Concrete Research, Vol. 25, No. 4, pp. 819-826.

Persson, B., (2004), "Cloride Migration Coefficient in Self -Compacting Concrete", Materials and Structures, Vol. 37, pp.82-91.

Pijaudier-Cabot, G., Dufour, F., Choinska, M., (2009), " Permeability due to the increase of Damage in concrete:from diffuse to localized damage distributions", *Journal of Engineering Mechanics*, Vol. 135, No. 9, pp. 1022-1028.

Qiang Yuan a, Caijun Shi , Geert De Schutter , Katrien Audenaert , Dehua Deng , (2009), "Chloride binding of cement-based materials subjected to external chloride environment – A review Construction and Building Materials 23 , pp. 1–13.

Raharinaivo A, Brevet P, Grimaldi G, Pannier G (1986) In: Relationship between concrete deterioration and reinforcing-steel corrosion. *Durability of building materials*, vol 4, pp 97–112.

Rahman M.K., M.H. Baluch, and A.H. Al-Gadhib, (1999), "Modeling of Shrinkage and Creep Stresses in Concrete Repair", *ACI Materials Journal,* , pp. 542-550.

Rahman M.K., M.H. Baluch, and A.H. Al-Gadhib, (2000),"Simulation of Shrinkage Distress and Creep Relief in Concrete Repair", *Composites: Part B: Engineering,* **31**, (2000), pp. 541-553.

Ramachandran VS. ,(1971), " Possible states of chloride in the hydration of tricalcium silicate in the presence of calcium chloride. Mater Struct ,4(1):3–12.

Rasheeduzzafar DFH, Al-Saadoun SS, Al-Fahtani AS, Dakhil FH. , (1990), "Effect of tricalcium alumina content of cement on corrosion of reinforcing steel in concrete. Cem Concr Res; 20(5):723–38.

Rasheeduzzafar DFH. (1992), "Influence of cement composition on concrete durability. ACI Mater J; 89(6):574–85.

Rasheeduzzafar, Al Gahtani, A.S., and Al-Saadoun, S.S., (1989), "Influence of Construction Practices on Concrete Durability, *ACI Materials Journal*, Vol. 86, No. 6, pp. 566-575.

Rasheeduzzafar, S.E. Hussain, and S.S. Al-Saadoun, (1991),"Effect of Cement Composition on Chloride Binding and Corrosion of Reinforcing Steel in Concrete", *Cement and Concrete Research,* **21**(**1**), pp. 777-794.

Reinhardt HW, Jooss M (2003) J Cement Concrete Res 33(7):981

Roberts MH. Effect of calcium chloride on the durability of pretensioned wire in prestressed concrete. Mag Concr Res 1962; 14(42): 143–54.

Rodriguez OG, Hooton RD (2003) ACI Mater J 100(2):120.

Saetta, A., Scotta, R., and Vitaliani, R. (1998). "Mechanical behavior of concrete under physical-chemical attacks". *ASCE J. Eng. Mech.,* 124(10), pp.1100–1109.

Sakoi, Y., and Horiguchi, T. (2006). "Loading effects on chloride penetration of fiber reinforced concrete." *Proc., the 2nd Int. Fib Congress,* Naples, Italy.

Samson E., Marchand J., (2007), "Modeling the Transport of Ions in Unsaturated Cement-Based Materials", *Computers and Structures*, vol. 85, p.1740-1756.

Sandberg P, Larsson J. Chloride binding in cement pastes in equilibrium with synthetic pore solutions. Chloride penetration into concrete structures. Nordic Miniseminar, Goteborg; Jan 1993. p. 98–107.

Saricimen , H., Concrete Durability Problems in the Arabian Gulf region -A Review, Proc. 4th International Conference Deterioration and Repair of Reinforced Concrete in the Arabian Gulf, V. 2,Bahrain ,1993.

Saricimen H., A.J. Al-Tayyib, M. Maslehuddin, and M. Shamim, "Concrete Deterioration High Chloride and Sulfate Environment and Repair Strategies", *ACI Publ. SP-128,* (1991), pp. 19-33.

Shazali, M. A., Al-Kutti, W. A., Rahman, M. K., Al-Gadhib, A. H., and Baluch, M. H. (2009). "COMSOL multiphysics modeling of chloride binding in diffusive transport of chlorides in concrete." *COMSOL Users Conf.,* Dhahran.

Snyder K.A. (2001) Validation and Modification of the 4SIGHT Computer Program, *NISTIR 6747*.

Sujata, K., Xi, Y., and Jennings, H. M. (1996). ‘‘Interfacial shrinkage cracks and the mechanisms.’’ *Proc., Mat. Conf. in 1996 ASCE Convention*, ASCE, Reston, Va.

Taher S., M.H. Baluch, A.H. Al-Gadhib.”Towards a Cononical Elastoplatic Damage Model”, *Engineering Fracture Mechanics*, Vol.48, No.2, pp, 151-166, 1994.

Tang L, Nilsson LO (2001) Ionic migration and its relation to diffusion. In: Hooton RD, Thomas MDA, Marchand J, Beaudoin JJ, Skalny JP (eds) Materials science of concrete Special volume: Ion and mass transport in cement-based materials. American Ceramic Society, pp 81–96.

Tang L. Chloride transport in concrete – measurement and prediction. PhD thesis, Department of Building Materials, Chalmers University of Technology, Goteborg, Sweden; 1996.

Tang L., L.O. Nilsson, Rapid determination of the chloride diffusivity in concrete by applying an electrical field, *ACI Mater. J*. 49 (1), 49– 53, 1992 (Technical Paper).

Tang L., and L.-O. Nilsson, “Service Life Prediction for Concrete Structures Under Sea Water by a Numerical Approach”, *Durability of Building Materials and Components,* ed. C. Sjostrom, **7**(**1**), pp. 97-106. London: E&FN Spon, 1996.

Tang, L., Nilsson, O., (1995)," Chloride Binding Isotherms- An approach by applying the modeified BET equation, Proceedings of the RILEM International Workshop on Chloride Penetration into Concrete, St. Remy-le-Chvreuse, pp. 15-18.

Tang, L., Sorensen, H.E," Precision of the Nordic test methods for measuring the chloride diffusion/migration coefficients of concrete", *Materials and Structures,* Vol. 34, October 2001, pp 479-485.

Tognazzi C, Ollivier J-P, Carcasses M, Torrenti J-M (1998) In: Petit Ch, Pijaudier-Cabot G, Reynouard JM (eds) Couplage Fissuration- De´gradation Chimique des Mate´riaux Cimentaires: Premiers Re´sultats sur les Proprie´te´s de Transfert, Ouvrages, ge´omate´riaux et interactions. Herme’s, Paris, pp 69–84.

Tritthart J. Chloride binding in cement II. The influence of the hydroxide concentration in the pore solution of hardened cement paste on chloride binding. Cem Concr Res 1989;19(5):683–91.

Tuutti K., (1982), "Corrosion of Steel in Concrete", Swedish Cement and Concrete Research Institute, Stockholm.

Voyiadjis, G. Z. and Abu Lebdeh, T. M., 1993. "Damage model for concrete using bounding surface concept". *J. Eng. Mech.,* 119(9), 1865-1885.

Wiens U, Schiessl P. Chloride binding of cement paste containing fly ash. In: Justnes H, editor, Proceedings of the 10th ICCC, Goteborg, Sweden; 1997. p. 4–10.

Winslow, D. N., Cohen, M. D., Bentz, D. P., Snyder, K. A., and Graboczi, E. J. (1994). ''Percolation and pores structure in mortars and concrete.'' *Cement and Concrete Res.*, 24, 25–37.

Wischers, G. (1978). "Application of effects of compressive loads on concrete." *Betontech. Ber,* Nos. 2 and 3, Duesseldorf.

Xing, F.,Lemg, F.G. and Feng, N.Q. (2005)." The Influence of Long-Term Load on the Chloride Permeability in Reinforced Concrete." In: T. Zhao, F.H.Wittmann and T. Ueda, Eds., Proc. of an International Workshop on Durability of Reinforced Concrete Under Combined Mechanical and Climate Loads (CMCL), Qingdao, Oct. 2005, China. Freiburg: Adeificatio Publishers, pp.139-147.

Yunping Xi, Ammar Nakhi, "Composite Damage Models for Diffusivity of Distressed Materials", *Journal of Materials in Civil Engineering*, ASCE, 17(3), (2005), pp. 286-295.

Zibara Hassan. Binding of external chloride by cement pastes. PhD thesis, Department of Building Materials, University of Toronto, Canada; 2001.

VITA

Name: Walid Abubaker Salem Al-Kutti

Birth: 22 Nov, 1972, Aden, Yemen

Nationality: Yemeni

Present Address: BLDG. 1816, KFUPM, Dhahran, Saudi Arabia

Permanent Address: BLDG 97, Aden, Yemen

Email: al_kutti@hotmail.com

Tel: +9672232849

Education: **Ph.D.** (Civil Engineering), King Fahd University of Petroleum and Minerals, Dhahran, Saudi Arabia, 2011.

Ph.D. Dissertation: *Simulation of Chloride Transport in Concrete with Stress Induced Damage*

M.S. (Civil Engineering), King Fahd University of Petroleum and Minerals, Dhahran, Saudi Arabia, 2005.

M.S. Thesis: *Compliance Criteria for Quality Concrete*

B.S. (Civil Engineering), Cairo University, Egypt, 1998.

Project: Structural Design of High-Rise Building (Distinction).

Summary:

Walid Abubaker Al-Kutti is a Lecturer at KFUPM, where he has been involved in the research activities in the Department of Civil Engineering and the Research Institute.

From 2005 to 2011, he was working towards his PhD in concrete durability in Saudi Arabia and his PhD research focussed on simulation of chloride transport in concrete with stress-induced damage where experimental and numerical research was conducted to evaluate the transport properties of damaged concrete structures. Moreover, he was involved in the strengthening of existing structures using CFRP which is one of the latest techniques used in Saudi Arabia and the Gulf region to improve the capacity of concrete structure, specially the precast slab panels.

From 1998-2003, he was working as a Graduate Assistant in the Department of Civil Engineering at Aden University, in which he gained academic experience and worked as an instructor of the following undergraduate courses: Concrete Materials I, Structural Analysis II, Design of Reinforced Concrete Structures I and Design of Steel Structures I.